Biochemical Characterization of Murine Calprotectin and the Host-Pathogen Competition for Manganese

by

Rose Currier Hadley

B.S. Chemistry
B.S. Neuroscience
University of New Hampshire, 2014

Submitted to the Department of Chemistry in Partial Fulfillment of the Requirements of the Degree of

DOCTOR OF PHILOSOPHY IN CHEMISTRY

at the
Massachusetts Institute of Technology

June 2019

Signature of Author: Signature redacted
Department of Chemistry
May 10, 2019

Certified by: Signature redacted
Elizabeth M. Nolan
Associate Professor of Chemistry
Thesis Supervisor

Accepted by: Signature redacted
Robert W. Field
Haslam and Dewey Professor of Chemistry
Chairman, Departmental Committee for Graduate Students

This doctoral thesis has been examined by a committee of the Department of Chemistry as follows:

Signature redacted

Daniel L. M. Suess
Assistant Professor of Chemistry
Committee Chairperson

Signature redacted

Elizabeth M. Nolan
Associate Professor of Chemistry
Thesis Supervisor

Signature redacted

Mircea Dincă
Associate Professor of Chemistry
Committee Member

Biochemical Characterization of Murine Calprotectin and the Host-Pathogen Competition for Manganese

by

Rose Currier Hadley

Submitted to the Department of Chemistry
on 05/10/2019 in Partial Fulfillment of the
Requirements of the Degree of
Doctor of Philosophy in Chemistry

ABSTRACT

Microorganisms need to acquire metal ion nutrients when they attempt to colonize the host milieu. The competition for transition metal ions between a host and an invading pathogen constitutes an important aspect of innate immunity and microbial pathogenesis. The host deploys the metal-sequestering antimicrobial protein calprotectin (CP) to sites of infection to withhold transition metal ions. The goals of this thesis are to characterize the biochemical, and Mn(II)-binding properties of the murine orthologue of calprotectin (mCP) as well as to evaluate the molecular details of the competition for Mn(II) between calprotectin and Mn(II) transport proteins from pathogenic bacteria. In the first part of this thesis, we provide initial biochemical characterization of mCP, supporting a role of this protein in transition metal sequestration and antibacterial activity. We demonstrate that this protein is a heterodimer than can undergo Ca(II)-induced tetramerization. We further show that mCP can bind a range of first row transition metal ions and displays antibacterial species against a panel of bacterial species. In the second part of this thesis, we characterize the Mn(II)-binding properties of mCP, revealing Ca(II)-dependent Mn(II) affinity at a hexahistidine site that bears a remarkable resemblance to the Mn(II)-sequestering site in human CP (hCP). We use biochemical assays and electron paramagnetic resonance (EPR) spectroscopy to elucidate the Mn(II)-coordinating residues of mCP. Altogether, we find that mCP possesses a much lower Ca(II) sensitivity than human CP, a fact that may have consequences *in vivo*. In the final portion of this thesis, we use biochemical assays and EPR spectroscopy to monitor the competition for Mn(II) between hCP and the bacterial Mn(II) transport proteins MntC and PsaA. We show that in the presence of excess Ca(II), hCP rapidly outcompetes these proteins for Mn(II), revealing the notably high Mn(II) affinity of hCP and giving molecular credence to the role of CP in sequestering Mn(II) *in vivo*.

Thesis Supervisor: Elizabeth M. Nolan
Title: Associate Professor of Chemistry

Abstracts

Chapter 1: Innate Immunity and Bacterial Manganese Import Systems

The innate immune system is responsible for maintaining proper homeostasis, which includes fighting off invading pathogens. Neutrophils are enlisted as the first line of defense against such insult and enact many antibacterial strategies. Calprotectin (CP) is released by neutrophils at infection sites and, in addition to other biological roles, acts to sequester transition metal ions to prevent pathogens from accessing these nutrients. The structure and metal-chelating properties of human calprotectin are well characterized. However, murine models are often used to study the host-pathogen interaction, including investigation that probe the role of CP in biology. Besides the numerous differences between human and murine innate immunity that include differences in neutrophil composition and function, rigorous biochemical characterization of the murine orthologue of CP is lacking, which represents an important gap in current knowledge. This paucity extends to the competition between murine CP and microbes for metal ions, including manganese. Microbes utilize manganese import systems to acquire manganese, and this process is often critical for virulence. The molecular details of the competition between CP and bacterial manganese acquisition machinery is not well understood. Shedding light on the molecular details of manganese sequestration by CP and the host-pathogen competition for manganese has implications for the future development of antibacterial strategies.

Chapter 2: Initial Biochemical and Functional Evaluation of Murine Calprotectin Reveals Ca(II)-Dependence and Its Ability to Chelate Multiple Nutrient Transition Metal Ions

Calprotectin (CP) is an abundant host-defense protein that contributes to the metal-withholding innate immune response by sequestering nutrient metal ions from microbial pathogens in the extracellular space. Over the past decade, murine models of infectious disease have advanced understanding of the physiological functions of CP and its ability to compete with microbes for essential metal nutrients. Despite this extensive work, murine CP (mCP) has not been biochemically evaluated, and structural and biophysical understanding of CP is currently limited to the human orthologue. We present the reconstitution, purification, and characterization of mCP as well as the cysteine-null variant mCP-Ser. Apo mCP is a mS100A8/mS100A9 heterodimer and Ca(II) binding causes two heterodimers to self-associate and form a heterotetramer. Initial metal-depletion studies demonstrate that mCP depletes multiple first-row transition metal ions, including Mn, Fe, Ni, Cu and Zn, from complex microbial growth medium, indicating that mCP binds multiple nutrient metals with high affinity. Moreover, antibacterial activity assays show that mCP inhibits the growth of a variety of bacterial species. The metal-depletion and antibacterial activity studies also provide evidence that Ca(II) ions enhance these functional properties of mCP. This contribution provides the groundwork for understanding the similarities and differences between the human and murine orthologues of CP, and for further elucidation of its biological coordination chemistry.

Chapter 3: Murine Calprotectin Coordinates Mn(II) at a Hexahistidine Site with Ca(II)-dependent Affinity

Manganese is an essential metal ion that bacterial pathogens need to acquire from the vertebrate host during infection. In the mammalian nutritional immunity strategy to combat bacterial infection, the host restricts access to Mn(II) by sequestering this metal nutrient using the protein calprotectin (CP). The role of murine calprotectin (mCP) in Mn(II) sequestration has been demonstrated *in vivo*, but the molecular basis of this function has not been evaluated. Herein, biochemical assays and electron paramagnetic resonance (EPR) spectroscopy are employed to characterize the Mn(II)-binding properties of mCP. We report that mCP has one high-affinity Mn(II)-binding site. This site is a His_6 site composed of His17 and His27 of mS100A8 and His92, His97, His105 and His107 of mS100A9. Similar to the human orthologue, Ca(II) binding to the EF-hand domains of mCP enhances the Mn(II) affinity of the protein; however, this effect requires ~10-fold more Ca(II) than what was previously observed for hCP. Mn(II) coordination to the His_6 site also promotes self-association of two mCP heterodimers to form a heterotetramer. Low-temperature X-band EPR spectroscopy revealed a nearly octahedral Mn(II) coordination sphere for the Mn(II)-His_6 site characterized by zero-field splitting (ZFS) parameters D = 525 MHz and E/D = 0.3. Further electron-nuclear double resonance (ENDOR) studies with globally ^{15}N-labeled mCP provided hyperfine couplings from the coordinating ε-nitrogen atoms of the His ligands (a_{iso} = 4.3 MHz) as well as the distal δ-nitrogen atoms (a_{iso} = 0.25 MHz). Mn(II)-competition assays between mCP and the bacterial Mn(II)-transport proteins staphylococcal MntC and streptococcal PsaA showed that mCP outcompetes both proteins for Mn(II) under conditions of excess Ca(II). In total, this work provides the first coordination chemistry study of mCP and reveals

striking similarities in the Mn(II) coordination sphere as well as notable differences in Ca(II) sensitivity and oligomerization behavior between hCP and mCP.

Chapter 4: Biochemical and Spectroscopic Observation of Mn(II) Transfer Between Bacterial Mn(II) Transport Machinery and Calprotectin

Human calprotectin (CP, S100A8/S100A9 oligomer) is a metal-sequestering host-defense protein that prevents bacterial acquisition of Mn(II). In this work, we investigate Mn(II) competition between CP and two solute-binding proteins that *Staphylococcus aureus* and *Streptococcus pneumoniae*, Gram-positive bacterial pathogens of significant clinical concern, use to obtain Mn(II) when infecting a host. Biochemical and electron paramagnetic resonance (EPR) spectroscopic analyses demonstrate that CP outcompetes staphylococcal MntC and streptococcal PsaA for Mn(II). This behavior requires the presence of excess Ca(II) ions, which enhance the Mn(II) affinity of CP. This report presents new spectroscopic evaluation of two Mn(II) proteins important for bacterial pathogenesis, direct observation of Mn(II) transfer from bacterial Mn(II) acquisition proteins to CP, and molecular insight into the extracellular battle for metal nutrients that occurs during infection.

Appendix A: High–field EPR Spectroscopic Characterization of Mn(II) Bound to the Bacterial Solute-binding Proteins MntC and PsaA

During infection, the bacterial pathogens *Staphylococcus aureus* and *Streptococcus pneumoniae* employ ATP-binding cassette (ABC) transporters to acquire Mn(II), an essential nutrient, from the host environment. Staphylococcal MntABC and

streptococcal PsaABC attract the attention of the biophysical and bacterial pathogenesis communities because of their established importance during infection. Previous biophysical examination of Mn(II)-MntC and Mn(II)-PsaA using continuous-wave (≈9 GHz) electron paramagnetic resonance (EPR) spectroscopy revealed broad, difficult-to-interpret spectra (Hadley *et al. J. Am. Chem. Soc.* **2018**, *140*, 110-113; Chapter 4). Herein, we employ high-frequency (>90 GHz), high-field (>3 T) EPR spectroscopy to investigate the Mn(II)-binding sites of these proteins and determine the Spin Hamiltonian parameters. Our analyses demonstrate that the zero-field splitting (ZFS) is large for Mn(II)-MntC and Mn(II)-PsaA at 2.72 and 2.87 GHz, respectively. The measured ^{55}Mn hyperfine coupling values for Mn(II)-MntC and Mn(II)-PsaA of 241 and 236 MHz, respectively, demonstrate a more covalent interaction between Mn(II) and the protein compared to Mn(II) in aqueous solution (≈265 MHz). These studies indicate that MntC and PsaA bind Mn(II) in a similar coordination geometry. Comparison of the ZFS values determined herein with those ascertained for other Mn(II) proteins suggests that the Mn(II)-MntC and Mn(II)-PsaA coordination spheres are not five coordinate in solution.

Appendix B: Preparation and Iron Redox Speciation Study of the Fe(II)-binding Antimicrobial Protein Calprotectin

Calprotectin (CP, S100A8/S100A9 heterooligomer) is an abundant metal-sequestering host-defense protein expressed by neutrophils, other white blood cells, and epithelial cells. The apo protein is a S100A8/S100A9 heterodimer that contains two sites for transition-metal binding at the S100A8/S100A9 interface: a His_3Asp motif (site 1) and a His_6 motif (site 2). In this chapter, we provide a step-by-step protocol for the overexpression and purification of the human and murine orthologues of CP that affords

each apo heterodimer in high yield and purity. In these procedures, the S100A8 and S100A9 subunits are overexpressed in *Escherichia. coli* BL21(DE3), and each apo heterodimer is obtained following cell lysis, folding, column chromatography, and dialysis against Chelex resin to reduce metal contamination. Recent studies demonstrated that human CP coordinates Fe(II) and that the protein affects the redox speciation of Fe in solution. An Fe redox speciation assay that employs ferrozine is described that demonstrates the ability of both human and murine CP to shift the redox speciation of Fe from the ferric to the ferrous oxidation state over time.

For Mom and Dad

Acknowledgments

I am sincerely grateful for my experience at MIT. I came to graduate school wanting to make the best future for myself that I could, both in awe of and intimidated by the outstanding prospect of enrolling in the Chemistry PhD program at MIT. I experienced a steep learning curve in my early years in the program. My subsequent commitment to improve myself marked a turning point in my life and career that would not have been possible without the generous support of my advisor Professor Elizabeth M. Nolan. Graduate school has been a very challenging and rewarding journey that has pushed me beyond what I thought possible for myself and has been central to my personal growth over the last five years. I recognize in myself greater capability, organization, scientific understanding, and communication skills than when I began and for these positive changes, among others, I am extremely grateful to Liz. I feel very lucky to have learned from such an excellent scientist.

I have also been fortunate to work with wonderful colleagues who helped me to grow as a scientist. In addition to scientific advice and suggestions, I appreciate all the help with my oral exams, writing, and presentations. Toshiki and Fabien trained me early on in protein biochemistry and peptide synthesis. Jules and Lisa taught me experimental techniques and answered many of my questions over the years. I would like to thank the rest of the lab as well for all of their help and advice and for making lab a positive place: Wilma, Tim, Claire, Phoom, Megan, Julie, Fangting, Anmol, Haritha, Emily, Chuchu, Artur, Aaron, Abraham, and Tomer. Additionally, there are two undergraduates whom I had the pleasure of working with: Yu (Vicky) Gu and Ravalika Damerla. Vicky and Rav were great people to work with and both showed impressive skill levels and commitment to research.

I am also very thankful for the advice and support of my past and present thesis committee members Professor Daniel Suess, Professor Mircea Dincă, and Professor Stephen Lippard. I have furthermore been very fortunate to have excellent collaborators. I learned a great deal about EPR spectroscopy from Professor R. D. Britt, Dr. Derek Gagnon, and Dr. Andrew Ozarowski. I had fun visiting the Britt Lab as well as the National High Magnetic Field Lab and I am very thankful for all of their help and guidance. In addition, I would like to thank my undergraduate professors at the University of New Hampshire for their kindness and support throughout my undergraduate experience. Their excellent teaching of courses provided me with the foundation for my graduate studies. I am especially grateful for all of the guidance and support of my undergraduate advisor Professor Roy P. Planalp. He introduced me to bioinorganic chemistry and helped me tremendously in achieving my goal of attending graduate school.

Finally, I am incredibly thankful for my family and partner who helped me to keep moving forward in graduate school and encouraged me to "just do my best." Mom and Dad: I am eternally grateful for your love, support, and encouragement that have helped me to become the person I am today and I dedicate this thesis to you. Neal: thank you for always driving me places, providing great support, and always finding a way to make me laugh. To my partner Hark: thank you for being my rock, pushing me to be better, and always putting a smile on my face. I'll never forget all the times you waited for me to get out of lab so we could go home together. I can't imagine where I would be without you.

Table of Contents

List of Figures

Chapter 1

Chapter 2

Chapter 3

Chapter 4

Appendix A

Appendix B

List of Tables

Chapter 2

Chapter 3

Chapter 4

Appendix A

Abbreviations

ABC	ATP-binding cassette
AMA	antimicrobial activity
ATCC	American Type Culture Collection
BHI	brain heart infusion medium
BME	beta-mercaptoethanol
BPEOIA	biotin polyethyleneoxide iodoacetamide
CbpA	calprotectin-binding protein A
CP	calprotectin
hCP	human calprotectin (including hCP-Ser, the Cys→Ser variant)
mCP	murine calprotectin (including mCP-Ser, the Cys→Ser variant)
CD	circular dichroism *or* cluster of differentiation receptor family
CFU	colony forming units
CV	column volumes
CW	continuous wave
DAMPS	damage-associated molecular patterns
DMSO	dimethylsulfoxide
DNA	deoxyribonucleic acid
DTT	dithiothreitol
EDTA	Ethylenediaminetetraacetic acid
ENDOR	electron nuclear double resonance
EPR	electron paramagnetic resonance
FPLC	fast protein liquid chromatography
GE	General Electric
Gu-HCl	guanidinium hydrochloride
HEPES	4-(2-hydroxyethyl)-1-piperazineethanesulfonic acid
HNP	Human neutrophil peptide
ICP-MS	inductive-coupled plasma mass spectrometry
IPTG	isopropyl β-D-1-thiogalactopyranoside
LB	Luria-Bertani medium
LC-MS	liquid chromatography mass spectrometry
LD_{50}	lethal dose that kills 50% of sample
LDPE	low-density polyethylene
MES	2-(*N*-morpholino)ethanesulfonic acid
MRS	De Man, Rogosa, and Sharpe medium
MWCO	molecular weight cutoff
NARSA	Network on Antimicrobial Resistance in *Staphylococcus aureus*
NBD	nucleotide-binding domain
NCBI	National Center of Biotechnology Information
NET	neutrophil extracellular trap
NHMFL	National High Magnetic Field Laboratory
NRAMP	natural resistance-associated macrophage protein
OD_{600}	optical density at 600 nm
PCR	polymerase chain reaction

PDB	Protein Data Bank
PMSF	phenylmethylsulfonylfluoride
PQ	precision quartz
ROS	reactive oxygen species
SBP	solute-binding protein
SDS-PAGE	sodium dodecylsulfate-polyacrylamide gel electrophoresis
SEC	size exclusion chromatography
SOD	superoxide dismutase
TCEP	tris(2-carboxyethyl)phosphine
TLR	toll-like receptor
TM	transmembrane
Tris	tris(hydroxymethyl)aminomethane
TSB	tryptic soy broth medium
ZFS	zero-field splitting
ZP1	Zinpyr-1

Chapter 1: Innate Immunity and Bacterial Manganese Import Systems

1.1 Innate Immunity

The innate immune system responds to bodily harm or danger, including alarm signals from distressed or injured cells as well as those from invading pathogenic microorganisms.[1, 2] Generally regarded as the first line of defense during infection, the innate immune system detects and responds to infection before the adaptive immune response is initiated through signaling mechanisms.[2] When the adaptive immune system is activated, it orchestrates the fastidious production of novel receptors for specific antigens as well as antibodies, creating and saving unique immune system "memories" in the organism that serve its continued survival.[3]

1.1.1 Neutrophils in the Innate Immune Response

As the first responders in the innate immune system, neutrophils are major players in innate immunity. These white blood cells are derived from bone marrow and exist in circulating plasma at low levels.[4] They are produced in quantities of $\approx 10^{11}$ per day in adult humans.[5] The lifespan of neutrophils may be between hours and days, with inflammation extending the lifespan.[6-8] Upon sensing danger signals, neutrophils accumulate at the appropriate locus to perform effector functions. Neutrophils are important for immune response mediation as well, as they are able to signal to other neutrophils, macrophages, and T-cells.[5] Furthermore, these fascinating cells continue to be players as the adaptive arm of the immune response is elaborated.[9]

During microbial infection, neutrophils are well known to enact degranulation, phagocytosis, and release of neutrophil extracellular traps (NETs).[4] Degranulation involves the deployment of granules, which consist of proteins packaged into

compartments within the cell.[5] There are three main types of granules: those containing myeloperoxidase, lactoferrin, and gelatinase protein, respectively.[5] Another typical process by which neutrophils combat pathogens is by phagocytosing them and treating them with antimicrobial agents within a phagocytic vacuole.[5] Finally, NET-osis consists of a coordinated release of decondensed DNA, cytosolic proteins, granule contents, and histones.[5] Reactive oxygen species (ROS) play a key role in the antimicrobial tactics of neutrophils as well. NADPH oxidase is present in the neutrophil membrane and generates superoxide radicals, characterizing the neutrophil oxidative burst.[10] The superoxide then dismutates to hydrogen peroxide, which is utilized by myeloperoxidase to produce many reactive products, including the toxic hypochlorous and hypothiocyanous acids.[10]

In contrast to the prior dogma that neutrophils are a homogenous group of cells with a specific function, recent work is uncovering the bountiful phenotypic and functional diversity that these cells develop.[4, 11] Indeed, as a function of aging or as a response to environmental stimuli, neutrophils display divergent phenotypes that are characterized by transcriptional changes, changes in expression of surface molecules, and changes in activity.[4, 11] For instance, in aberrant metabolic states such as hyperglycemia and hypercholesterolemia, neutrophils become primed for NETosis or display increased ROS generation and myeloperoxidase release, respectively.[12, 13] Additionally, during methicillin-resistant *Staphylococcus aureus* infection, murine neutrophils develop subpopulations with differential expression of cell surface proteins, including those of the toll-like receptor (TLR) and cluster of differentiation (CD) families.[14] These cellular subgroups display different cytokine production and macrophage activation potentials.[14] Molecules derived from the microbiota can also drive neutrophil diversity in mice by

priming the neutrophils for greater antimicrobial activity as well as altering their lifespan.[15, 16] Remarkably, neutrophil priming by peptidoglycan from the microbiota enhances the neutrophil-mediated killing of *Streptococcus pneumoniae* and *S. aureus*.[16] Cumulatively, the rich diversity of neutrophils generated in a plethora of biological contexts makes these special cells a promising subject of future discoveries.

1.1.2. Innate Immunity in Mice Versus Humans

Humans and mice diverged from a common ancestor ≈65-75 million years ago.[17] Though the species have much in common genetically, sharing over 90% of the same genes, their innate immune systems are notably different.[18] Indeed, immune systems are in general are especially vulnerable to evolutionary change.[2] In mice, this change may have arisen from environmental pressures such as pathogen coevolution as well as the increased evolution manifested as a result of a significantly shorter generation time.[2] In a comparative analysis of human and mouse genes, it was shown that the most divergent family of proteins are those involved in host defense.[19] These proteins were ~35% divergent based on the amino acid sequences and around 3-fold more divergent compared to the average proteins in the analysis.[19] It is now clear that there are numerous intricate differences in the composition and function of innate immune factors used by humans and mice that undoubtedly influence the nature of their innate immune responses.[2, 17, 20] A plethora of differences are present with respect to the secreted peptides and proteins, cytokines and chemokines, as well as toll-like receptors (TLRs), nod-like receptors, and cytokine receptors that exist in mice and humans.[2] For example,

TLR11, TLR12, and TLR13 are present in mice but not humans; these receptors mediate sensing of various pathogenic substances.[2]

The degrees of similarities and differences between mice and humans, particularly in relation to innate immunity, are important to consider because mouse models are utilized to study diseases and infections, which naturally involve innate immune response activation. Mice (species *mus musculus*) represent the most common animal models in biomedical research.[18] As model organisms that are easy to maintain and manipulate genetically while possessing great genetic similarity to humans, mice have been indispensable for decades worth of discoveries in biomedicine and immunology.[18] Mouse models have been generated to study a range of innate immune functions and diseases and seen notable success; thus, there is a definite power and utility in the application of mouse model systems to understand immune functions.[18] An associated immunotherapy breakthrough, which relied on murine models, was the discovery of the role of inhibitory receptors in checkpoint blockade.[21]

However, the numerous deficiencies of murine models in imitating human biology often limit the translational ability of mouse model systems to human disease.[22] This includes, for example, mouse models failing to recapitulate the immune aspects of human tumor evolution in cancer.[23] As is typical for mouse model systems, this disparity stems from intrinsic biological differences between mice and humans as well as the fact that the mice studied are inbred, genetically homogenous, and sometimes raised under sterile, pathogen-free conditions that are far from capturing the natural state of humans.[23] In fact, there is a greater disparity in immune system function between humans and inbred specific pathogen-free laboratory mice compared to wild mice.[24] Such limitations have

spurred ongoing efforts to improve mouse model systems to increase their similarity to adult human immune systems. These efforts include consideration of bystander infections to further develop the immune systems of mice before they are used in studies as well as the development of humanized mouse strains that are engineered to have greater immune system similarity to humans.[25]

1.1.2.1 Antimicrobial Arsenals within Neutrophils

There are extensive differences between neutrophils from humans and mice. Strikingly, the relative amounts of neutrophils circulating in mice and humans differs drastically; whereas white blood cells in human blood are composed of 50-70% neutrophils, in mice, neutrophils compose only 10-25% of the white blood cells.[17] The pathways by which ROS are generated in neutrophils differ between humans and mice as well.[26] Among numerous other differences, mice lack the FcαRI receptor for IgA on neutrophils, which is important for effector functions such as the oxidative burst, cytokine release, and NETosis in humans.[27, 28]

Furthermore, the antimicrobial repertoires and regulation differ within human and murine neutrophils. For instance, a single lysozyme enzyme, an antimicrobial enzyme packaged within neutrophil granules, is present in humans, whereas two lysozyme genes exist in mice.[29] Human neutrophils harbor antimicrobial defensin peptides (HNP1-4), whereas mouse neutrophils do not.[23] Additionally, the activities of multiple granule enzymes, including myeloperoxidase and lysozyme, are higher in human neutrophils relative to mouse neutrophils.[30] Arginase-1, an enzyme with fungicidal activity, is a

constitutive component of human azurophil granules, but is only inducibly expressed in mouse neutrophils.[31]

There are additionally notable differences in the antimicrobial S100 proteins deployed during innate immune responses between humans and mice. Humans possess S100A8, S100A9, and S100A12 in neutrophils. S100A8 and S100A9, which heterooligomerize to form calprotectin, are abundant in human neutrophils and compose ≈40% of the neutrophil cytoplasmic protein while S100A12 composes ≈5% of the cytosolic protein.[32, 33] S100A8, S100A9 and S100A12 have intracellular roles related to migration and cytoskeletal modulation.[34] These proteins are released during NETosis and are significant components of NETs.[35] Extracellularly, these S100's also act as damage-associated molecular patterns (DAMPS; also referred to as endokines or alarmins) and can activate immune cells and vascular endothelial cells.[34] S100A8/S100A9 activates TLR4 whereas S100A12 is a ligand for the receptor for advanced glycation end products.[34, 36]

Mice contain S100A8 and S100A9 homologues and these proteins are abundant in murine neutrophils; these proteins have each been detected in excess of 5 mg/mL.[37] However, the amino acid identities of human and murine S100A8 and S100A9 are only ~56%. Compared to the average protein identity of ~85% identified in a comparative study of over 1,100 human and murine protein sequences, the identity between the S100A8 and S100A9 orthologues is relatively low.[38] Indeed, the value fits within the lowest quartile of proteins analyzed by Makalowski *et al.* in terms of amino acid identity.[38] Consistent with prior work by Murphy *et al.* identifying high divergence of host-defense proteins between mice and humans, S100A8 and S100A9 share this lowest quartile with other

antimicrobial host-defense proteins identified by Makalowski *et al.,* including multiple interleukins and interferons.[19, 38] In addition to these differences, mice completely lack a S100A12 orthologue.[39] Murine S100A8 has been shown to be chemotactic like human S100A12, whereas human S100A8 lacks chemotactic properties.[40] Together, these differences may contribute to the differing neutrophil responses and capabilities between humans and mice, including during microbial infection.

1.1.3. Nutritional Immunity

Nutritional immunity involves the withholding of essential metal ions by host proteins in order to deprive pathogens of these nutrients.[41] This process was first recognized as a factor in the host-pathogen competition for Fe(III).[41] The host maintains rigorous high-affinity chelation of Fe by proteins including ferritin, transferrin, hemoglobin, and myoglobin, which restricts available Fe to exceedingly low levels.[42] In more recent years, Zn(II) and Mn(II) sequestration became recognized as important in nutritional immunity. The host protein CP has been implicated in Mn(II) and Zn(II) sequestration *in vivo*.[43] Laser-ablation inductively-coupled plasma mass spectrometry has been used to show that murine tissue abscesses from *S. aureus* infection are relatively devoid of Zn and Mn despite an adequate abundance of these metals in surrounding healthy tissues.[43] Restriction of Cu in tissue abscesses has since been noted.[44] Furthermore, a recent report highlighted the heterogeneity of metal distributions between abscesses within the same tissue, providing more nuance to host-mediated nutritional immunity.[44] *In vitro* studies have illuminated the fact that the host protein CP (see section 1.1.3.1) is able to

sequester a range of transition metal ions, including Mn(II), Fe(II), Ni(II), and Zn(II), and the host protein S100A12 can sequester Zn(II).[45, 46]

Nevertheless, pathogens can often foil this host metal-withholding strategy by employing metal acquisition systems. For Fe(III) uptake, this includes siderophores, heme acquisition systems, and transferrin/lactoferrin receptors.[42] Mn(II) and Zn(II) are secured through the use of high-affinity metal uptake systems.[47] One ingenious pathogen, *Neisseria* sp, has the ability to bind CP using the aptly named calprotectin-binding protein A (CbpA; in *Neisseria meningitidis*).[48, 49] This outer membrane protein can facilitate the uptake of Zn(II) by *Neisseria*.[48] Though the nature of this interaction is not yet clear, this example represents a novel adaptive tactic to combat host-mediated metal limitation.

1.1.3.1. Structure and Function of Human Calprotectin

Calprotectin is a member of the S100 family of Ca(II)-binding proteins and a major contributor to the metal-withholding innate immune response.[45, 50] CP is a cytoplasmic protein expressed in neutrophils, macrophages, monocytes, and epithelial cells. Human calprotectin (hCP) is a heterooligomer of the S100 proteins S100A8 and S100A9 (**Figure 1.1**).[51-54] S100A8 and S100A9 each harbor two EF-hand domains, with a non-canonical EF-hand in the N-terminal region of the polypeptide and a canonical EF-hand near the C-terminus.[55] In the absence of Ca(II) and transition metal ions, hCP exists as a heterodimer.[51] The protein has two transition-metal-binding sites, both present at the S100A8/S100A9 dimer interface, and designated site 1 and site 2.[54, 56, 57] Site 1 is a His_3Asp motif composed of (A8)His83, (A8)His87, (A9)His20 and (A9)Asp30.[54] Site 2 is a His_6 site composed of (A8)His17, (A8)His27, (A9)His91, (A9)His95, (A9)His103 and

(A9)His105 (**Figure 1.1**).[58-60] The His_6 site of hCP is of particular interest because it can sequester a number of divalent first-row transition metal ions including Mn(II), Fe(II), Zn(II) and Ni(II).[45, 59-64] Recent work indicated CP can bind Cu, but the details of this interaction are not yet clearly defined.[65]

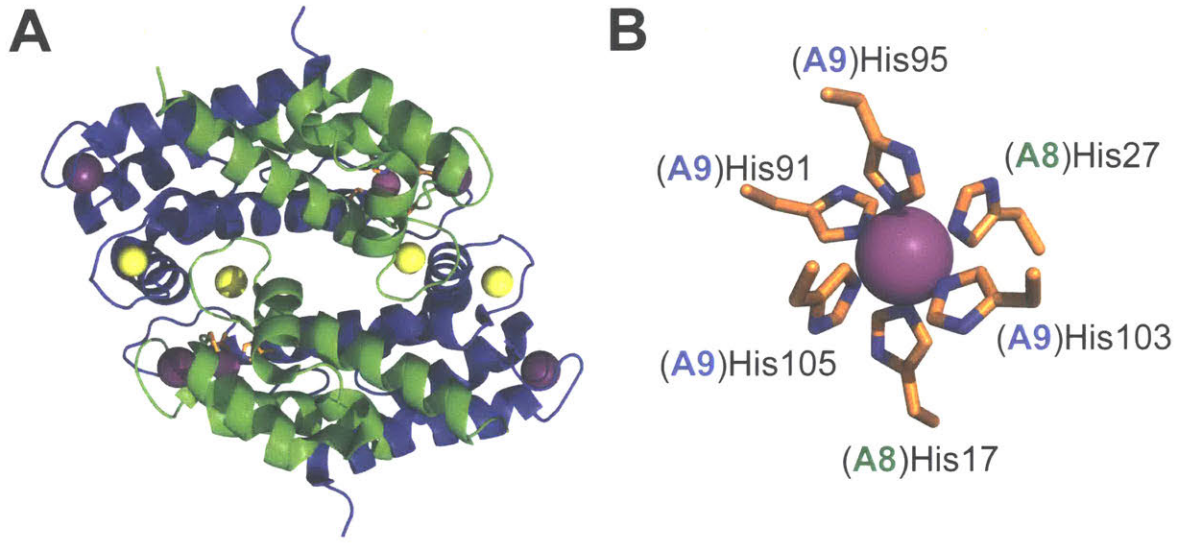

Figure 1.1. Crystal structure of the Mn(II)-, Ca(II)-, and Na(I)-bound human calprotectin heterotetramer (**A**) and composition of the Mn-His_6 site (**B**). S100A8 is shown in green and the S100A9 subunit in blue. Metal ions are shown as spheres: Mn (magenta), Ca (yellow), and Na (purple) (PDB: 4XJK). Na(I) derived from the crystallization buffer is shown occupying the non-canonical EF-hand domains.

The working model has been informed by extensive studies of this protein. It has been known for some time that Ca(II) binding by CP causes association of two heterodimers to generate a heterotetramer.[52, 53] Beyond promoting tetramerization, Ca(II) binding increases the transition-metal-ion affinities, antimicrobial activity, and proteolytic stability of hCP.[45, 57, 66] Thus, a working model has been put forth wherein CP senses the high extracellular Ca(II) concentration (≈2 mM) at an infection site and becomes a

tetramer with enhanced transition metal affinities, enabling effective metal sequestration.[45, 57] It is this high-affinity metal sequestration in the extracellular space that allows CP to limit microbial growth by competing with microbes for metal nutrients (**Figure 1.2**)

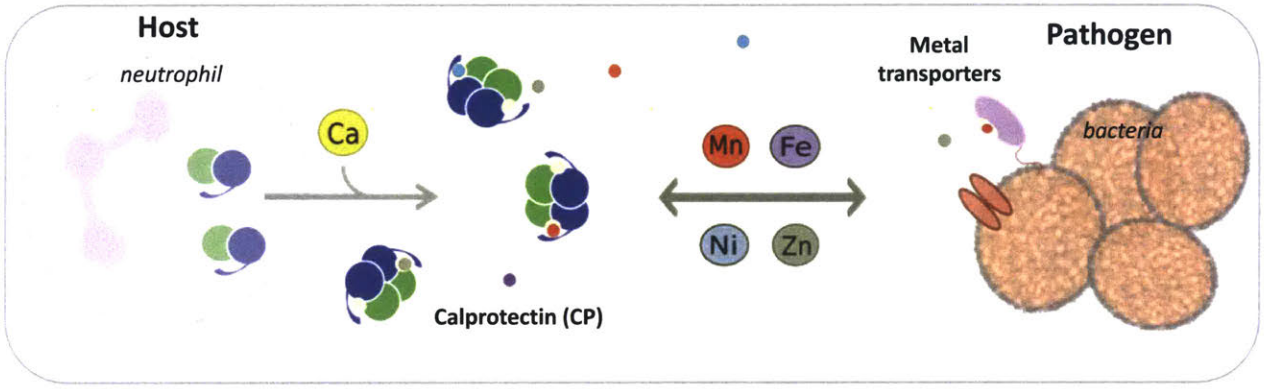

Figure 1.2. Depiction of a nutritional immunity scenario in which calprotectin (CP) competes with pathogenic bacterial metal importers for transition metal ions.

1.1.3.2. Manganese-binding Properties of Human Calprotectin

A 2008 report identified a role for CP in sequestration of Mn(II) in a murine tissue abscess model of *S. aureus* infection.[43] This work represented an exciting discovery; prior to that report, only Zn(II) sequestration by CP was recognized.[67] Subsequently, the molecular characteristics of Mn(II) binding to hCP were explored. In 2013, robust biochemical and structural data were reported that elucidated the Ca(II)-modulated Mn(II) affinity and biologically unique hexahistidine Mn(II) coordination sphere of CP (**Figure 1.1**).[58, 60, 61] Characterization by advanced EPR spectroscopy followed soon after, shedding more light on the highly symmetric Mn(II)-binding site.[59] In Chapter 4, competition between human CP and bacterial Mn transport proteins is described that reveals a sub-nanomolar Mn(II) affinity for CP.

1.1.3.3. The Function of Calprotectin: *S100A9*$^{-/-}$ Mice as Infection Models

S100A9$^{-/-}$ mice have been generated to study the impact of this protein, or the associated S100A8/S100A9 protein complex CP, on various immune functions.[68, 69] Notably, S100A8$^{-/-}$ mice cannot be generated because the mutation is embryonic lethal.[70] In fact, S100A8 plays a pivotal and non-redundant role in the absence of its S100A9 partner in the developing mouse embryo.[70] Neutrophils from S100A9$^{-/-}$ mice are relatively similar to those from wildtype mice, but have some differences.[71-73] While the S100A9$^{-/-}$ cells have normal morphology, they do display a somewhat polarized shape and show observable defects in Ca(II)-related signaling.[71-73] Despite these drawbacks, S100A9$^{-/-}$ mice have been useful for understanding the role of this protein in a number of inflammation-related scenarios, from arthritis to bacterial infections.[69]

These CP-deficient mice have been used in infection models of a number of microbial pathogens, including the bacterial pathogens *S. aureus, Acinetobacter baumannii*, *Streptococcus pneumoniae*, *Klebsiella pneumoniae*, *Helicobacter pylori*, and *Salmonella* as well as the fungal pathogens *Aspergillus fumigatus* and *Candida albicans*.[35, 43, 65, 74-83] These models have provided many insights into the antimicrobial function of CP. For example, the absence of CP leads to a greater bacterial burden in the lungs and livers of mice infected with *A. baumannii*.[74] However, the consequence of S100A9 deficiency is often multi-faceted and context-dependent. For instance, animal models of *S. aureus* infection show that CP inhibits *S. aureus* growth in the murine liver, does not alter bacterial growth in the kidney, and can actually promote bacterial colonization of the heart.[43, 84, 85] The presence of CP can also promote bacterial growth in *S. pneumoniae* and *Salmonella* infections, which may stem from CP relieving the Zn(II)

toxicity experienced by these species.[78, 80] Furthermore, CP can modulate interactions between the pathogens *Pseudomonas aeruginosa* and *S. aureus*.[86] Therefore, the complex roles that CP plays in infectious disease, and the molecular mechanisms behind them, warrant continued investigation.

1.1.3.4. Competition for Manganese Between Murine Calprotectin and *Staphylococcus aureus*

The competition for Mn(II) between CP and bacterial proteins has been exemplified in studies involving mice infected with *S. aureus*.[43, 85] *S. aureus* has two Mn(II) import systems, MntABC and MntH, that contribute to infection.[85] These systems are necessary for full virulence in wildtype mice but not S100A9$^{-/-}$ mice. In the presence of CP, a defect in Mn(II) transport translates to lower bacterial burdens in murine liver and kidney tissue.[85] However, in the absence of CP, defects in Mn(II) transport do not impact the bacterial burden of organ tissues.[85] The molecular details of these observations are explored in Chapters 3 and 4 of this thesis.

1.1.3.5 The Gap in Knowledge Between Human and Murine Calprotectin

Our current understanding of the function of CP is predominately informed by mouse models of infectious disease[43, 74, 80, 83, 86, 87], including studies that involve the S100A9$^{-/-}$, CP-deficient, mouse strain noted above[68], and molecular characterization of the human orthologue.[51, 54, 57-63, 88] A biochemical assessment of mCP is fundamentally important to understand the function of this protein at the molecular level. Studies in this vein will serve to inform mouse models of infectious disease in addition to providing a

biochemical comparison to the human CP orthologue. Amino acid sequence alignment of the human and murine S100A8 and S100A9 polypeptides indicates, among other things, that the His_3Asp and His_6 sites are conserved. In an effort to supplement this gap in knowledge, the heterologous expression and purification of mCP is described along with initial metal binding and antibacterial activity studies in Chapters 2 and 3 of this thesis.

1.2. Manganese in Biology

Manganese composes ~0.085% of the earth's crust.[89] The redox properties of manganese govern its solubility and therefore bioavailability; Mn(II) is soluble, whereas the Mn(III)/Mn(IV) oxides are relatively insoluble.[90] Manganese is present in seawater at approximately low nanomolar concentrations.[90, 91] Since early times, life forms have concentrated metal ions in their cells at concentrations exceeding those in natural environments, such as the sea water from which life arose.[91] This observation gave an early clue as to the biological importance of metal ions by suggesting active uptake and retention within cells. Manganese concentrations in human plasma are slightly higher than seawater, in the nanomolar range.[91, 92] Bacterial species maintain varying Mn concentrations within their cells. For instance, *Escherichia coli* cells contain micromolar levels of Mn, with the exact content depending on growth conditions.[93, 94] In contrast, *Lactobacilli* sp. can accumulate millimolar intracellular Mn concentrations.[95] Recent work with *Streptococcus sanguinis* noted variable Mn concentrations even within different strains of the same species.[96]

1.2.1. Identification of Manganese as an Essential Nutrient: an Historical Perspective

Manganese was identified as a component of soil and plants as early as 1774.[97] By 1892, manganese was identified in mollusk blood, with studies and hypotheses of the element's importance in mollusks extending into the 20th-century.[98] In 1922, the necessity of Mn in plant growth was established, and the role of Mn as a nutrient in mammals subsequently began to be illuminated.[97] Studies in the 1920's and 1930's revealed that supplementation of Mn in the rations of animals was beneficial for growth, and conversely that too much was toxic.[99-102] Researchers first revealed the importance of Mn in mice and rats, and later work reported the requirement of Mn in childhood development.[100, 101, 103]

The concept that Mn is essential in biology was strengthened through the 20th century as the molecular details of Mn utilization in biology were elucidated. In the mid-20th century, the importance of Mn in photosynthesis and role as a component of photosystem II were becoming apparent through studies regarding the effect of Mn-deficiency on photosynthesis and oxygen evolution.[104-106] Enzymes that could be active with added Mn, including arginase, were identified.[107] In 1966, pyruvate carboxylase, isolated from chicken liver mitochondria, was the first enzyme reported to contain bound Mn(II).[108] Multiple lines of evidence, including *in vivo* incorporation of ^{54}Mn and the effect of Mn-bound enzyme on the proton relaxation rate as measured by nuclear magnetic resonance supported the conclusion.[108] A jack-bean globulin, called concanavalin A, was found to contain bound Mn.[109] An electron paramagnetic resonance spectroscopy (EPR) study was then undertaken to characterize the Mn-protein complex and assess the

observation that "immobilized" Mn bound to proteins was not detectable by EPR.[110] The EPR characterization revealed a Mn-coordination sphere with near-cubic symmetry.[110]

The subsequent discovery of high-affinity Mn import systems and Mn-dependent enzymes in various microorganisms suggested an important role for this element in bacterial physiology. A high-affinity Mn uptake system in *E. coli* was discovered in 1969, suggesting that Mn was a crucial nutrient.[111, 112] The landmark discovery of a Mn-utilizing superoxide dismutase (SOD) from *E. coli* followed in 1970.[113] This work established a function for Mn in *E. coli* and represented the identification of a new type of SOD that bore little resemblance to the previously characterized mammalian Cu,Zn-SOD.[113] Elucidation of Mn as the required cofactor hinged on characterization of Mn(II) released from the denatured enzyme by EPR spectroscopy.[113]

Subsequently, high-affinity, active Mn transport was verified in other species, including *Bacillus subtilis*, *Rhodopseudomonas capsulata*, and *S. aureus*.[114-116] A Mn-requiring ribonucleotide reductase was discovered in some species of Gram-positive bacteria in 1981, adding a third type on top of the already-discovered Fe-dependent varieties.[117] The Mn-requiring, non-heme "pseudocatalase" was isolated and characterized from *Lactobacillus plantarum* two years later.[118] *L. plantarum* is an unusual bacterium that can accumulate intracellular concentrations of Mn in excess of 30 millimolar. In the absence of an SOD, this Mn acts to scavenge the superoxide radical anion.[119] An active transport system for Mn was characterized in this organism in 1984.[119]

The requirement of Mn as a micronutrient in pathogens portends its relevance in virulence. Indeed, for pathogens to survive in a hostile host environment, they must successfully acquire essential elements (see section 1.1.3). The roles of the bacterial Mn-

SOD in the virulence of both *S. pneumoniae* and *Haemophilus influenzae* in murine infection models were reported by 2000.[120, 121] The Mn-dependent transcriptional repressor PerR was determined to be essential for full virulence in a murine skin abscess model of *S. aureus* infection.[122] In addition, Mn-uptake systems were being discovered and established as virulence determinants. Mn(II) acquisition systems were found to be important in the virulence of *Salmonella, Yersinia pestis, Enterococcus faecalis, Streptococcus mutans,* and *S. pneumoniae* by 2002.[123-128] As elucidation of the role of Mn in bacterial pathogenesis and virulence has unfolded in the years since, understanding and appreciation of the role that Mn import systems play in these processes has blossomed.

1.2.2. Manganese Import Systems in Bacteria

Due to the low propensity for passive diffusion of Mn across cell membranes, bacteria utilize energy-powered transport systems to acquire this ion.[129] One type of Mn importers in bacteria are homologs of the eukaryotic NRAMP (Natural resistance-associated macrophage protein) transporters. The bacterial proteins are referred to as MntH transporters, in reference to their proton(H)-dependent Mn transport function.[130] There are three primary groups of prokaryotic MntH transporters (A, B, and C) that diverged from each other over evolution and display relatively low amino acid sequence identity of <30%.[130] Group A MntH transporters are present in Gram-positive organisms such as *Bacillus subtilis* and *Mycobacterium tuberculosis*, as well as the Gram-negative organisms *E. coli*, *Salmonella typhimurium*, *Yersinia pestis*, and *Deinococcus radiodurans*, among others.[130] Of note, group A MntH transporters are the type utilized

by intracellular pathogens and group C MntH transporters are the most similar to eukaryotic NRAMP proteins. Group C proteins are present in strains such as *S. aureus*, *Enterococcus faecalis*, and *Pseudomonas aeruginosa*.[130] Representative transporters from both group A and group C have been structurally and functionally characterized from the organisms *D. radiodurans* and *Staphylococcus capitis*, respectively.[131, 132]

ABC-type transporters are a second type of Mn transport system. ABC transporters can be divided into Types I, II, and III that are defined by structural determinants.[133] They are composed of three types of subunits: a nucleotide-binding domain (NBD), a trans-membrane permease (TM), and a solute (or substrate)-binding protein (SBP). The nucleotide-binding domain and permease each form homodimers, where the permease is in the membrane (inner membrane for Gram-negative bacteria) and the NBDs are in the cytoplasm associated with the TM. Each of these architectures requires a single SBP that scavenges the substrate from the extracellular space in Gram-positive bacteria, or the periplasm in Gram-negative bacteria. For transition-metal-importing ABC transporters, recognition of the metal ion occurs by the SBP.[129] The SBP is thought to confer specificity to the transport system by way of providing the highest affinity binding of substrate in the system.[129] For instance, in the case of the *E. coli* vitamin B12-importing BtuCD-F, the permease lacks the high-affinity substrate binding that characterizes the SBP and thus successful transport requires the presence of the cognate SBP.[129, 134] Though this property has not been stringently evaluated for Mn(II)-specific ABC transporters, the high affinities (~nM K_d) reported for Mn-binding SBPs are consistent with this conclusion.[135-137] The paucity of information regarding the molecular-

level structural and functional properties of Mn(II)-specific ABC transport systems presents a rich area for future exploration.

1.2.3. Manganese Import Systems in Virulence

Maintaining a sufficient Mn supply is often important for virulence. Manganese importers have been extensively linked to virulence in a variety of pathogens, though the relative importance of a given system in a given organism is variable.[138] For instance, the putative Mn(II) import system MntABC of *Bacillus anthracis* is crucial for virulence; a 10^4-fold decrease in the LD_{50} (lethal dose at which there a 50% reduction in viability) was observed in a guinea pig infection model.[139] Mn(II) import, specifically through ABC transport systems, is also critical for streptococcal virulence.[140] Mn(II) import proteins have been identified as important virulence factors in a number of streptococci, including *S. pyogenes, S. suis, S. uberis, and S. pneumoniae*.[128, 141-143] In the case of *S. aureus* and *Y. pestis*, the involvement of Mn(II) acquisition systems in virulence is more nuanced. Though important in liver abscesses, the requirement for Mn(II) importers is nullified during heart colonization of *S. aureus* when there is excess dietary Mn.[43, 84] For *Y. pestis*, The Mn(II) import systems Yfe and MntH were important for virulence in the bubonic plague model of disease but not in the pneumonic plague model, emphasizing that the location and type of infection can be important factors.[125, 144]

1.2.4. MntABC of *Staphylococcus aureus*

S. aureus is a commensal bacterium that can become a dangerous pathogen, causing diseases that include bacteremia, pneumonia, cellulitis, and osteomyelitis,

sepsis, and death.[145] *S. aureus* is one of the most common causes of bacterial infections and is a significant contributor to bacteria-induced morbidity and mortality.[145] Distressingly, this pathogen has developed multi-drug resistance, and is able to withstand treatment with drugs including β-lactams and vancomycin.[145] Furthermore, *S. aureus* possesses conniving strategies to circumvent the host innate immune responses. One such trick involves the modulation of neutrophil function; after phagocytosis, *S. aureus* can cause neutrophil necrosis such that the bacterium is released from the host cell.[145] According to the World Health Organization, *S. aureus* is a high-priority pathogen for which new antibiotics are desperately needed.

1.2.4.1. MntABC is a Manganese Import System that is Important for Growth and Virulence

Manganese uptake plays a role in the growth and virulence of *S. aureus*. This bacterium has two types of Mn import systems: MntABC and MntH. In MntABC, MntA is the ATP-binding protein, MntB is the permease, and MntC is the solute-binding protein. Studies with mutant *S. aureus* strains implicated these systems in Mn(II) uptake.[146] The mutant strains were defective in growth and Mn(II) uptake while also showing sensitivity toward reactive oxygen species, as compared to the wildtype strain.[146] An *mntC* mutant was also found to have reduced SOD activity.[147] Furthermore, *mntC* mutant cells were more susceptible to killing by human neutrophils.[148]

MntABC plays an important role in the virulence of *S. aureus*. In a model of murine systemic infection with methicillin-resistant *S .aureus*, MntC was found to be expressed in a kidney abscess *in vivo*.[149] Similarly, a murine bacteremia model found that MntC was

expressed within 1-4 hours after infection.[150] Furthermore, deletion of *mntC* caused a dramatic ~10^4 decrease in bacterial loads from infected kidneys that was likewise observed when *mntA* or *mntB* was mutated.[149] Mutation of *mntC* was also shown to significantly increase survival of infected mice relative to infection with the wildtype strain.[149] In a murine sepsis model, again mutation of *mntC* led to decreased virulence and longer survival time for infected mice.[147] However, as mentioned earlier, *mntC* is not uniformly required for *S. aureus* infection. For example, increased dietary Mn can render the manganese import systems less important for successful infection.[84] Lastly, the importance of the manganese transport systems MntABC and MntH has been shown to be related to the competition with the host metal-sequestering protein calprotectin for Mn.[85]

1.2.4.2. Structure and Manganese-binding Properties of MntC

MntC from *S. aureus* is a lipoprotein composed of 312 amino acids and has a molecular weight of 35.1 kDa. The N-terminal 25 amino acids correspond to the signal peptide portion. This region includes the residue Cys18 that can be modified following proteolysis in order to attach a lipid moiety for anchoring MntC on the extracellular face of the cell membrane.[151] The crystal structure of metal-bound MntC with a resolution of 2.2 Å was reported in 2013 (**Figure 1.3**).[135] This protein possesses a bilobal structure with an extended backbone alpha-helix, similar to that of *S. pneumoniae* PsaA (**Figure 1.4**), with a metal-ion binding site at the domain interface.[135] MntC is classified as a Cluster A (Class III) solute binding protein, a family of proteins that collectively transport

metal ions and metal chelates.[152] The defining feature of this class is the extended alpha-helix that connects the two domains of the protein.[152]

In the MntC structure, the metal-binding site was occupied and assigned as Mn(II), though the identity of the metal(s) was not confirmed.[135] In any case, the coordination sphere was shown to be a $His_2AspGlu$ motif. The ligating residues (numbered based on a soluble construct of MntC) with corresponding metal-ligand distances are as follows: His50 (Nε2, 2.1 Å), His123 (Nε2, 2.1 Å), Glu189 (Oε1, 2.3 Å; Oε2, 2.8 Å), and Asp264 (Oδ1, 2.2 Å; Oδ2, 2.3 Å) (**Figure 1.3**; ligand numbering refers to the truncated protein used in ref 135).[135] The noticeably longer metal-ligand distance associated with Oε2 of Glu189 has led to the idea that the metal ion, tentatively assigned as Mn(II), was in a motif that could be described as 5-coordinate.[153] A 1.17-Å resolution structure of Zn(II)-MntC has been reported as well.[154] The Zn(II)-bound structure displays metal-ligand distances of 2.1 Å for His67(Nε2), His140(Nε2), Glu206(Oε1), and Asp281(Oδ1), 2.5 Å for Glu206(Oε2), and 2.6 Å for Asp281(Oδ1) (ligand numbering refers to the full-length MntC protein).[154]

The Mn(II) binding properties of MntC have been examined as well. The Mn(II) affinity of MntC was assessed using isothermal titration calorimetry and the value was found to be rather high: ~4 nM K_D.[135] However, as with other SBPs, including *S. pneumoniae* PsaA, MntC can bind other metal ions. Similar to other SBPs, purification of the apo-protein is a recurring challenge.[135] Notably, MntC forms a stable complex with

Zn(II) that, similar to results reported about *S. pneumoniae* PsaA, is not readily dissociable.[135, 136]

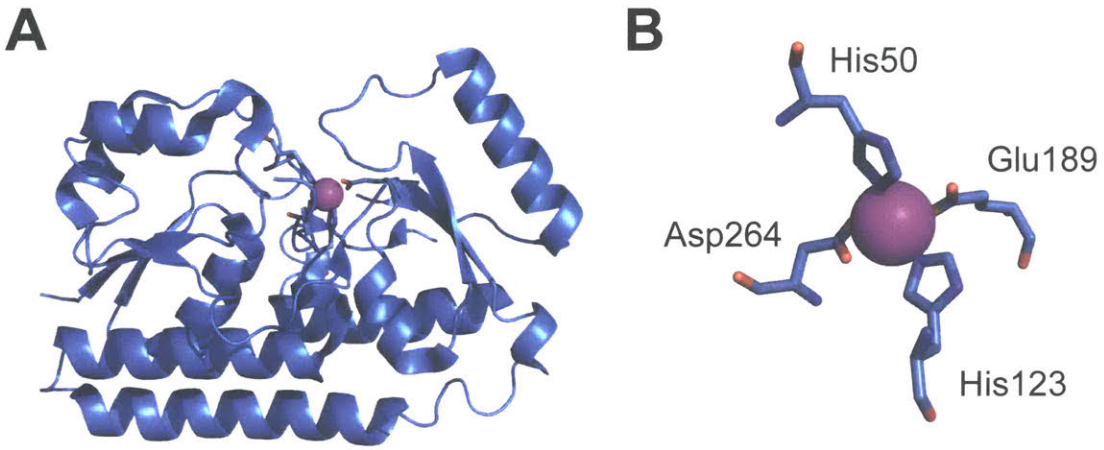

Figure 1.3. Crystal structure of Mn-MntC (**A**) and depiction of Mn-binding ligands (**B**) with the Mn ion shown in magenta (PDB: 4K3V). Ligand numbering refers to the truncated protein used in ref 135.[135]

1.2.4.3. MntC as a Vaccine Candidate

Because of its surface expression during infection and its importance for *S. aureus* virulence along with its high conservation among *S. aureus* isolates, MntC has been explored as a vaccine candidate. In a mouse bacteremia model, vaccination of mice with MntC decreased the bacterial burden in the mice, demonstrating the vaccine potential of this protein.[150] When anti-MntC antibodies were recovered, three interference groups were identified that represented three binding modes for antibody-MntC interactions.[150] Importantly, immunization of young rats with any subgroup of the anti-MntC monoclonal antibodies successfully reduced subsequent bacterial burden.[155] Overall, this work has strengthened the idea that MntC can be both immunogenic and that the antibodies generated from MntC exposure can serve a protective role upon *S. aureus* infection.[150] Additionally, Pfizer has created a multicomponent vaccine that includes MntC.[155]

1.2.5. PsaABC of *Streptococcus pneumoniae*

S. pneumoniae is an opportunistic human pathogen of serious concern. The organism can maintain a commensal relationship with the host and colonizes the upper reparatory tract, leading to asymptomatic carriage and transmission.[156] However, it can turn pathogenic, causing multiple types of infections, including otitis media, pneumonia, meningitis, and sepsis.[156] The difficulty in controlling the incidence of *S. pneumoniae* infection lies in its ability to adapt. Its natural competence allows it to take up exogenous DNA and modify its genome to overcome antibiotic challenge and vaccine-related immunity.[156] This bacteria is therefore an ongoing health concern, listed in 2017 as one of the World Health Organization's twelve priority pathogens for which the development of new antibiotics is urgently sought. Efforts to understanding and manipulate its many virulence factors for vaccine and therapeutic development may lead to significant future advances in preventing and treating these infections.

1.2.5.1. PsaABC is a Manganese Import System that is Important for Growth and Virulence

S. pneumoniae harbors an ABC Mn(II)-import system named PsaABC that includes the SBP PsaA, the ATP-binding protein PsaB, and the transmembrane permease PsaC.[157] The importance of each of PsaA, PsaB, and PsaC in Mn(II) uptake has been rigorously established. In 1997, Dintilhac *et al.* observed that a *psaA* mutant required Mn(II) for growth, suggesting that PsaABC is an ABC Mn(II) transporter.[157] Further work showed that mutating any one of the *psa* genes caused a greater requirement of Mn(II) for growth in addition to lower intracellular Mn content and a greater

sensitivity to ROS.[158] Together, the results provided compelling evidence that PsaABC is a Mn(II)-import system.[158]

Manganese homeostasis is a major factor in the virulence of *S. pneumoniae*. Both the PsaABC Mn(II) importer as well as the MntE Mn(II) exporter have been implicated in virulence in mouse models of infection, suggesting the necessity of a careful intracellular balancing act in the homeostasis of this ion during infection.[128, 159] The role of PsaABC in infection has been extensively studied in a number of infection models. It was demonstrated in 1996 that disruption of the *psaA* gene in *S. pneumoniae* attenuated the virulence in both intranasal and intraperitoneal mouse models of infection.[160] Following this work, several animal models of infection confirmed the role of PsaABC in virulence.[128] The results showed that the *psa* promoter was induced ~10-fold in an intraperitoneal murine infection model.[128] Furthermore, *psaA* and psaB mutant strains did not colonize the lungs or the blood in a murine respiratory tract infection model, in contrast to the significant 10^6-10^8 colony forming units (cfu) per milliliter of solution concentrations isolated from mice infected with the wildtype D39 strain of *S. pneumoniae*.[128] This dramatic attenuation in growth was further observed in a murine intraperitoneal infection model, and, remarkably, addition of Mn(II) to the bacteria in the intraperitoneal chamber implant restored growth of all *psa* mutants to the high (~10^8 cfu mL^{-1}) wildtype levels.[128] This study demonstrated that loss of *psaABC* function results in a severe, Mn(II)-dependent reduction in growth and virulence. The importance of Mn(II) in virulence of this pathogen perhaps makes sense given that there are at least seven Mn(II)-utilizing enzymes in this organism.[161]

1.2.5.2. Structure and Manganese-binding Properties of PsaA

The solute-binding protein PsaA is a 34.6 kDa polypeptide composed of 309 amino acids. Following the N-terminal signal sequence, residues 17-20 are LVAC and compose the LX_1X_2C motif that is characteristic of solute-binding lipoproteins, where X_1 and X_2 are variable amino acids.[162] Lipid attachment to Cys20 followed by proteolytic cleavage of the protein between Ala19 and Cys20 results in a lipidated N-terminal Cys residue that facilitates membrane anchoring of this protein to the bacterial surface.[162] Though the fully reconstituted PsaABC transport system has not been well characterized, the structure and metal-binding properties of PsaA have been reported. The first crystal structure of PsaA, which had bound Zn(II), was solved in 1998, representing the first molecular characterization of this protein.[162] PsaA possesses twofold pseudosymmetry resulting from two $(\beta/\alpha)_4$ domains linked by a backbone alpha helix.[162] The N-terminal region of PsaA was disordered in the structure and proposed to be a flexible tether linking the protein to the membrane.[162]

Like *S. aureus* MntC, PsaA is classified as a Cluster A (Class III) solute binding protein.[152] PsaA additionally possesses particular structural similarities to other Mn(II)-binding SBPs, including MntA (*Bacillus anthracis*), MntC (*S. aureus*), and MtsA (*Streptococcus pyogenes*) that include conserved metal binding residues as well as conservation in the surrounding regions that may interact with the permease.[163] Vigonsky *et al.* identified conserved proline residues present on each lobe of the SBP on the putative SBP-permease interface and proposed that they play a role in protein-protein interaction during metal transport.[163] Future work is necessary to delineate the precise molecular interactions involved in metal transport for this class of SBPs.

The metal-binding site of PsaA exists between the two lobes and is composed of a $His_2AspGlu$ motif. A crystal structure of Mn(II)-PsaA has been reported (**Figure 1.4**).[136] The following residues coordinate Mn(II) with the Mn(II)-ligand distances indicated: His67 (Nε2, 2.1 Å), His139 (Nε2, 2.1 Å), Glu205 (Oε1, 2.1 Å; Oε2, 2.4 Å), and Asp280 (Oδ1, 2.1 Å; Oδ2, 2.4 Å) (**Figure 1.4**).[136] The Mn(II) coordination sphere has been described as tetrahedral, though the bond lengths make the nature of Mn(II) coordination rather ambiguous. Furthermore, the nature of Mn(II) coordination in solution is not clear. There is also a crystal structure of Zn(II)-PsaA that displays similar metal-ligand distances.[162]

The Mn(II) affinity of PsaA is high: ≤ 10 nM.[136] However, this protein can bind other metal ions, most notably Zn(II). Zn(II) binds to PsaA with high affinity and irreversibly, whereas Mn(II) binding is more labile.[136] This discrepancy suggests that Mn transport can occur but has led to the idea that Zn(II) binding "poisons" the transport system via irreversible Zn(II) binding locking the SBP.[136] Similar effects of Zn(II) and Mn(II) binding have been observed in studies of the analogous proteins MntA and SitA, from *Bacillus anthracis* and *Staphylococcus pseudointermedius*, respectively.[137, 163]

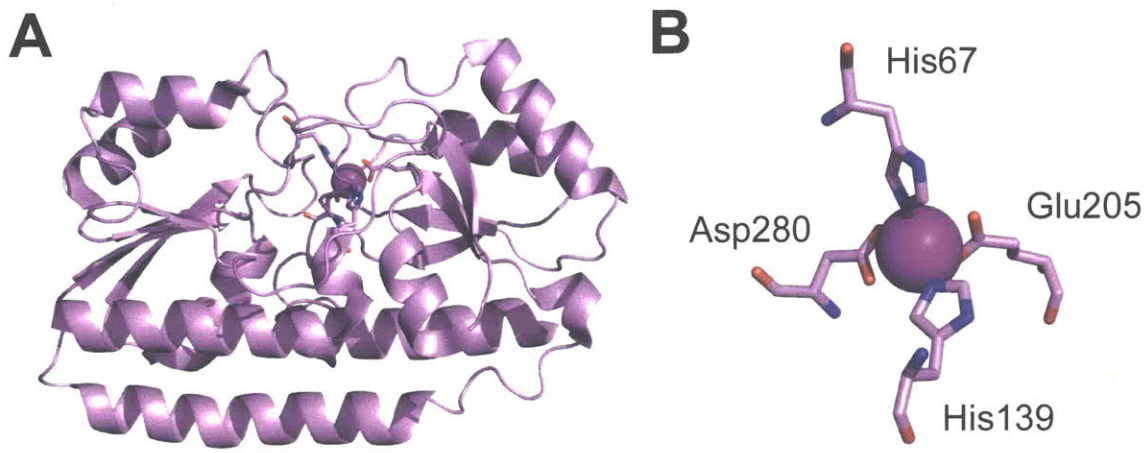

Figure 1.4. Crystal structure of Mn(II)-PsaA (**A**) and depiction of Mn(II)-binding ligands (**B**) with the Mn ion shown in magenta (PDB: 3ZTT).

1.2.5.3. PsaA as a Vaccine Candidate

The application of PsaA in vaccine strategies against *S. pneumoniae* has been given much attention. The wide conservation of the surface-exposed lipoprotein PsaA in pneumococcal serotypes makes it potentially useful as a vaccine.[164] This observation encouraged further investigation into its ability to be immunogenic and protective, factors that together would make it a promising vaccine candidate. In 1996, immunization of mice with PsaA was found to be protective against infection.[165] Anti-PsaA antibodies were later detected in the saliva of children carrying *S. pneumoniae*, suggesting that this protein can be effectively recognized by the immune system.[166] In later work, a multivalent vaccine that included PsaA was found to be effective in a phase I trial.[167] Generating a greater understanding of the molecular details of PsaA function and role in virulence can help to move this effort forward for potentially profound societal benefits.

1.3 Summary of Thesis

The primary goal of this thesis is to bridge the gap in knowledge between studies of human CP (hCP) and murine models of infection by providing a purification protocol as well as biochemical characterization of murine calprotectin (mCP). In Chapter 2, we utilize various techniques to evaluate the oligomeric properties, metal-binding properties, and antibacterial activity of mCP and report that it possesses properties consistent with a role in nutritional immunity. We utilize the Cys-null mutant in parallel and observe that, while this variant can bind metal ions and displays antibacterial activity, its properties are not identical to those of mCP. Therefore, it appears that at least one of the four total Cys residues is necessary for full function. Furthermore, when mCP is compared to human CP, it is revealed that mCP requires much more Ca(II) for tetramerization, a striking result given the importance of Ca(II) in the working model.

CP is the only known host protein that sequesters Mn(II) during infection and a mouse model of *S. aureus* infection was used to discover this in 2008.[43] In Chapter 3, we look in depth at the Mn(II)-chelating ability of mCP to provide molecular details about how mCP sequesters Mn(II). We utilize size exclusion chromatography and Mn(II)-binding assays to ascertain the Mn(II)-coordinating resides of mCP and to deduce the Ca(II)-dependence of the Mn(II) affinity. Similar to our results from Chapter 2, a high Ca(II) concentration is required for high-affinity Mn(II) binding by mCP that is about one order of magnitude greater than that required by hCP for similar function. In a collaboration with the laboratory of Professor R. David Britt at UC Davis, we employ EPR spectroscopy and further confirm the residues associated with Mn(II) chelation and ascertain that the Mn(II) coordination sphere is highly symmetric and very similar to that of hCP. Finally, we show

that in the presence of excess Ca(II), mCP is able to outcompete bacterial Mn(II) transport proteins MntC and PsaA for Mn(II). In total, this work demonstrates that mCP is a high-affinity Mn(II)-sequestering protein, consistent with *in vivo* observations.

CP has been implicated in the competition between the host and *S. aureus* of nutrient Mn(II). The secondary goal of this thesis is to characterize this competition for Mn(II) on a molecular level. In Chapter 4, evaluation of the competition between the bacterial SBPs MntC and PsaA and hCP for Mn(II) is described. Pull-down assays are used to identify the Mn(II) speciation during a competition assay. Furthermore, the Mn(II)-SBPs are characterized by low-temperature X-band EPR spectroscopy. The broad spectra exhibited by Mn(II)-SBPs is in contrast to the sharp resonance exhibited by Mn(II)-hCP, and so low-temperature EPR spectroscopy is used to differentiate the metalation state of each of these proteins prepared in a mixture to ascertain which has higher affinity. The results reveal that in the presence of excess Ca(II), hCP has higher affinity for Mn(II) than both SBPs and furthermore that it can rapidly sequester Mn(II) from a preformed Mn(II)-SBP complex.

1.4 References

1. Matzinger, P. The danger model: a renewed sense of self. *Science* **2002,** *296*, 301-305.

2. Kapetanovic, R.; Ariffin, J. K.; Sweet, M. J. In *Evolutionary Biology: Genome Evolution, Speciation, Coevolution and Origin of Life*; Pontarotti, P., Ed.; Springer International Publishing: Switzerland, 2014; Chapter 6, pp 115-155.

3. Bonilla, F. A.; Oettgen, H. C. Adaptive immunity. *J. Allergy Clin. Immunol.* **2010,** *125*, S33-S40.

4. Rosales, C. Neutrophil: a cell with many roles in inflammation or several cell types? *Front. Physiol.* **2018,** *9*, 1-17.

5. Borregaard, N. Neutrophils, from marrow to microbes. *Immunity* **2010,** *33*, 657-670.

6. Cartwright, G. E.; Athens, J. W.; Wintrobe, M. M. The kinetics of granulopoiesis in normal man. *Blood* **1964,** *24*, 780-803.

7. Pillay, J.; den Braber, I.; Vrisekoop, N.; Kwast, L. M.; de Boer, R. J.; Borghans, J. A.; Tesselaar, K.; Koenderman, L. In vivo labeling with $^{2}H_2O$ reveals a human neutrophil lifespan of 5.4 days. *Blood* **2010,** *116*, 625-627.

8. Geering, B.; Stoeckle, C.; Conus, S.; Simon, H. U. Living and dying for inflammation: neutrophils, eosinophils, basophils. *Trends Immunol.* **2013,** *34*, 398-409.

9. Mantovani, A.; Cassatella, M. A.; Costantini, C.; Jaillon, S. Neutrophils in the activation and regulation of innate and adaptive immunity. *Nat. Rev. Immunol.* **2011,** *11*, 519-531.

10. Winterbourn, C. C.; Kettle, A. J.; Hampton, M. B. Reactive oxygen species and neutrophil function. *Annu. Rev. Biochem.* **2016,** *85*, 765-792.

11. Silvestre-Roig, C.; Hidalgo, A.; Soehnlein, O. Neutrophil heterogeneity: implications for homeostasis and pathogenesis. *Blood* **2016,** *127*, 2173-2181.

12. Wong, S. L.; Demers, M.; Martinod, K.; Gallant, M.; Wang, Y.; Goldfine, A. B.; Kahn, C. R.; Wagner, D. D. Diabetes primes neutrophils to undergo NETosis, which impairs wound healing. *Nat. Med.* **2015,** *21*, 815-819.

13. Mazor, R.; Shurtz-Swirski, R.; Farah, R.; Kristal, B.; Shapiro, G.; Dorlechter, F.; Cohen-Mazor, M.; Meilin, E.; Tamara, S.; Sela, S. Primed polymorphonuclear leukocytes constitute a possible link between inflammation and oxidative stress in hyperlipidemic patients. *Atherosclerosis* **2008,** *197*, 937-943.

14. Tsuda, Y.; Takahashi, H.; Kobayashi, M.; Hanafusa, T.; Herndon, D. N.; Suzuki, F. Three different neutrophil subsets exhibited in mice with different susceptibilities to infection by methicillin-resistant *Staphylococcus aureus*. *Immunity* **2004,** *21*, 215-226.

15. Hergott, C. B.; Roche, A. M.; Tamashiro, E.; Clarke, T. B.; Bailey, A. G.; Laughlin, A.; Bushman, F. D.; Weiser, J. N. Peptidoglycan from the gut microbiota governs the lifespan of circulating phagocytes at homeostasis. *Blood* **2016,** *127*, 2460-2471.

16. Clarke, T. B.; Davis, K. M.; Lysenko, E. S.; Zhou, A. Y.; Yu, Y.; Weiser, J. N. Recognition of peptidoglycan from the microbiota by Nod1 enhances systemic innate immunity. *Nat. Med.* **2010,** *16*, 228-231.

17. Mestas, J.; Hughes, C. C. W. Of mice and not men: differences between mouse and human immunology. *J. Immunol.* **2004,** *172*, 2731-2738.

18. Masopust, D.; Sivula, C. P.; Jameson, S. C. Of mice, dirty mice, and men: using mice to understand human immunology. *J. Immunol.* **2017,** *199*, 383-388.

19. Murphy, P. M. Molecular mimicry and the generation of host defense protein diversity. *Cell* **1993,** *72*, 823-826.

20. Zschaler, J.; Schlorke, D.; Arnhold, J. Differences in innate immune response between man and mouse. *Crit. Rev. Immunol.* **2014,** *34*, 433-454.

21. Sharma, P.; Allison, J. P. The future of immune checkpoint therapy. *Science* **2015,** *348*, 56-61.

22. Seok, J.; Warren, H. S.; Cuenca, A. G.; Mindrinos, M. N.; Baker, H. V.; Xu, W.; Richards, D. R.; McDonald-Smith, G. P.; Gao, H.; Hennessy, L.; Finnerty, C. C.; Lopez, C. M.; Honari, S.; Moore, E. E.; Minei, J. P.; Cuschieri, J.; Bankey, P. E.; Johnson, J. L.; Sperry, J.; Nathens, A. B.; Billiar, T. R.; West, M. A.; Jeschke, M. G.; Klein, M. B.; Gamelli, R. L.; Gibran, N. S.; Brownstein, B. H.; Miller-Graziano, C.; Calvano, S. E.; Mason, P. H.; Cobb, J. P.; Rahme, L. G.; Lowry, S. F.; Maier, R. V.; Moldawer, L. L.; Herndon, D. N.; Davis, R. W.; Xiao, W.; Tompkins, R. G. Genomic responses in mouse models poorly mimic human inflammatory diseases. *Proc. Natl. Acad. Sci.* **2013,** *110*, 3507-3512.

23. Eruslanov, E. B.; Singhal, S.; Albelda, S. M. Mouse versus human neutrophils in cancer: a major knowledge gap. *Trends Cancer* **2017,** *3*, 149-160.

24. Beura, L. K.; Hamilton, S. E.; Bi, K.; Schenkel, J. M.; Odumade, O. A.; Casey, K. A.; Thompson, E. A.; Fraser, K. A.; Rosato, P. C.; Filali-Mouhim, A.; Sekaly, R. P.; Jenkins, M. K.; Vezys, V.; Haining, W. N.; Jameson, S. C.; Masopust, D. Normalizing the environment recapitulates adult human immune traits in laboratory mice. *Nature* **2016,** *532*, 512-516.

25. Tao, L.; Reese, T. A. Making mouse models that reflect human immune responses. *Trends Immunol.* **2017,** *38*, 181-193.

26. Bagaitkar, J.; Matute, J. D.; Austin, A.; Arias, A. A.; Dinauer, M. C. Activation of neutrophil respiratory burst by fungal particles requires phosphatidylinositol 3-phosphate binding to $p40^{phox}$ in humans but not in mice. *Blood* **2012,** *120*, 3385-3387.

27. Martin, A. M.; Kulski, J. K.; Witt, C.; Pontarotti, P.; Christiansen, F. T. Leukocyte Ig-like receptor complex (LRC) in mice and men. *Trends Immunol.* **2002,** *23*, 81-88.

28. Aleyd, E.; Heineke, M. H.; van Egmond, M. The era of the immunoglobulin A Fc receptor FcaRI; its function and potential as target in disease. *Immunol. Rev.* **2015,** *268*, 123-138.

29. Yeh, T. C.; Wilson, A. C.; Irwin, D. M. Evolution of rodent lysozymes: isolation and sequence of the rat lysozyme genes. *Mol. Phylogenetics Evol.* **1993,** *2*, 65-75.

30. Rausch, P. G.; Moore, T. G. Granule enzymes of polymorphonuclear neutrophils: a phylogenetic comparison. *Blood* **1975,** *46*, 913-919.

31. Munder, M.; Mollinedo, F.; Calafat, J.; Canchado, J.; Gil-Lamaignere, C.; Fuentes, J. M.; Luckner, C.; Doschko, G.; Soler, G.; Eichmann, K.; Muller, F.; Ho, A. D.; Goerner, M.; Modolell, M. Arginase I is constitutively expressed in human granulocytes and participates in fungicidal activity. *Blood* **2005,** *105*, 2549-2556.

32. Edgeworth, J.; Gorman, M.; Bennett, R.; Freemont, P.; Hogg, N. Identification of p8,14 as a highly abundant heterodimeric calcium binding protein complex of myeloid cell. *J. Biol. Chem.* **1991,** *266*, 7706-7713.

33. Guignard, F.; Mauel, J.; Markert, M. Identification and characterization of a novel human neutrophil protein related to the S100 family. *Biochem. J.* **1995,** *309*, 395-401.

34. Foell, D.; Wittkowski, H.; Vogl, T.; Roth, J. S100 proteins expressed in phagocytes: a novel group of damage-associated molecular pattern molecules. *J. Leukoc. Biol.* **2007,** *81*, 28-37.

35. Urban, C. F.; Ermert, D.; Schmid, M.; Abu-Abed, U.; Goosmann, C.; Nacken, W.; Brinkmann, V.; Jungblut, P. R.; Zychlinsky, A. Neutrophil extracellular traps contain calprotectin, a cytosolic protein complex involved in host defense against Candida albicans. *PLoS Pathog.* **2009,** *5*, e1000639.

36. Vogl, T.; Tenbrock, K.; Ludwig, S.; Leukert, N.; Ehrhardt, C.; van Zoelen, M. A.; Nacken, W.; Foell, D.; van der Poll, T.; Sorg, C.; Roth, J. Mrp8 and Mrp14 are endogenous activators of Toll-like receptor 4, promoting lethal, endotoxin-induced shock. *Nat. Med.* **2007,** *13*, 1042-1049.

37. Kocher, M.; Kenny, P. A.; Farram, E.; Abdul Majid, K. B.; Finlay-Jones, J. J.; Geczy, C. L. Functional chemotactic factor CP-10 and MRP-14 are abundant in murine abscesses. *Infect. Immun.* **1996,** *64*, 1342-1350.

38. Makalowski, W.; Zhang, J.; Boguski, M. S. Comparative analysis of 1196 orthologous mouse and human full-length mRNA and protein sequences. *Genome Res.* **1996,** *6*, 846-857.

39. Fuellen, G.; Foell, D.; Nacken, W.; Sorg, C.; Kerkhoff, C. Absence of S100A12 in mouse: implications for RAGE–S100A12 interaction. *Trends Immunol.* **2003,** *24*, 622-624.

40. Ravasi, T.; Hsu, K.; Goyette, J.; Schroder, K.; Yang, Z.; Rahimi, F.; Miranda, L. P.; Alewood, P. F.; Hume, D. A.; Geczy, C. Probing the S100 protein family through genomic and functional analysis. *Genomics* **2004,** *84*, 10-22.

41. Weinberg, E. D. Nutritional immunity: host's attempt to withhold iron from microbial invaders. *J. Am. Med. Assoc.* **1975,** *231*, 39–41.

42. Skaar, E. P. The battle for iron between bacterial pathogens and their vertebrate hosts. *Plos Pathog.* **2010,** *6*, e1000949.

43. Corbin, B. D.; Seeley, E. H.; Raab, A.; Feldmann, J.; Miller, M. R.; Torres, V. J.; Anderson, K. L.; Dattilo, B. M.; Dunman, P. M.; Gerads, R.; Caprioli, R. M.; Nacken, W.; Chazin, W. J.; Skaar, E. P. Metal chelation and inhibition of bacterial growth in tissue abscesses. *Science* **2008,** *319*, 962-965.

44. Cassat, J. E.; Moore, J. L.; Wilson, K. J.; Stark, Z.; Prentice, B. M.; Van de Plas, R.; Perry, W. J.; Zhang, Y.; Virostko, J.; Colvin, D. C.; Rose, K. L.; Judd, A. M.; Reyzer, M. L.; Spraggins, J. M.; Grunenwald, C. M.; Gore, J. C.; Caprioli, R. M.; Skaar, E. P. Integrated molecular imaging reveals tissue heterogeneity driving host-pathogen interactions. *Sci. Transl. Med.* **2018,** *10*, 1-14.

45. Zygiel, E. M.; Nolan, E. M. Transition metal sequestration by host-defense protein calprotectin. *Ann. Rev. Biochem.* **2018,** *87*, 621-643.

46. Cunden, L. S.; Gaillard, A.; Nolan, E. M. Calcium ions tune the zinc-sequestering properties and antimicrobial activity of human S100A12. *Chem. Sci.* **2016,** *7*, 1338-1348.

47. Kehl-Fie, T. E.; Skaar, E. P. Nutritional immunity beyond iron: a role for manganese and zinc. *Curr. Opin. Chem. Biol.* **2010,** *14*, 218-224.

48. Stork, M.; Grijpstra, J.; Bos, M. P.; Manas Torres, C.; Devos, N.; Poolman, J. T.; Chazin, W. J.; Tommassen, J. Zinc piracy as a mechanism of *Neisseria meningitidis* for evasion of nutritional immunity. *PLoS Pathog.* **2013,** *9*, e1003733.

49. Jean, S.; Juneau, R. A.; Criss, A. K.; Cornelissen, C. N. *Neisseria gonorrhoeae* evades calprotectin-mediated nutritional immunity and survives neutrophil extracellular traps by production of TdfH. *Infect. Immun.* **2016,** *84*, 2982-2994.

50. Hood, M. I.; Skaar, E. P. Nutritional immunity: transition metals at the pathogen-host interface. *Nat. Rev. Microbiol.* **2012,** *10*, 525-537.

51. Hunter, M. J.; Chazin, W. J. High level expression and dimer characterization of the S100 EF-hand proteins, migration inhibitory factor-related proteins 8 and 14. *J. Biol. Chem.* **1998,** *273*, 12427-12435.

52. Vogl, T.; Roth, J.; Sorg, C.; Hillenkamp, F.; Strupat, K. Calcium-induced noncovalently linked tetramers of MRP8 and MRP14 detected by ultraviolet matrix-assisted laser desorption/ionization mass spectrometry. *J. Am. Soc. Mass Spectrom.* **1999,** *10*, 1124-1130.

53. Strupat, K.; Rogniaux, H.; Van Dorsselaer, A.; Roth, J.; Vogl, T. Calcium-induced noncovalently linked tetramers of MRP8 and MRP14 are confirmed by electrospray ionization-mass analysis. *J. Am. Soc. Mass Spectrom.* **2000,** *11*, 780-788.

54. Korndörfer, I. P.; Brueckner, F.; Skerra, A. The crystal structure of the human $(S100A8/S100A9)_2$ heterotetramer, calprotectin, illustrates how conformational changes of interacting α-helices can determine specific association of two EF-hand proteins. *J. Mol. Biol.* **2007,** *370*, 887-898.

55. Gifford, J. L.; Walsh, M. P.; Vogel, H. J. Structures and metal-ion-binding properties of the Ca^{2+}-binding helix-loop-helix EF-hand motifs. *Biochem. J.* **2007,** *405*, 199-221.

56. Kehl-Fie, T. E.; Chitayat, S.; Hood, M. I.; Damo, S.; Restrepo, N.; Garcia, C.; Munro, K. A.; Chazin, W. J.; Skaar, E. P. Nutrient metal sequestration by calprotectin inhibits bacterial superoxide defense, enhancing neutrophil killing of *Staphylococcus aureus*. *Cell Host Microbe* **2011,** *10*, 158-164.

57. Brophy, M. B.; Hayden, J. A.; Nolan, E. M. Calcium ion gradients modulate the zinc affinity and antibacterial activity of human calprotectin. *J. Am. Chem. Soc.* **2012,** *134*, 18089-18100.

58. Brophy, M. B.; Nakashige, T. G.; Gaillard, A.; Nolan, E. M. Contributions of the S100A9 C-terminal tail to high-affinity Mn(II) chelation by the host-defense protein human calprotectin. *J. Am. Chem. Soc.* **2013,** *135*, 17804-17817.

59. Gagnon, D. M.; Brophy, M. B.; Bowman, S. E.; Stich, T. A.; Drennan, C. L.; Britt, R. D.; Nolan, E. M. Manganese binding properties of human calprotectin under conditions of high and low calcium: X-ray crystallographic and advanced electron paramagnetic resonance spectroscopic analysis. *J. Am. Chem. Soc.* **2015,** *137*, 3004-3016.

60. Damo, S. M.; Kehl-Fie, T. E.; Sugitani, N.; Holt, M. E.; Rathi, S.; Murphy, W. J.; Zhang, Y.; Betz, C.; Hench, L.; Fritz, G.; Skaar, E. P.; Chazin, W. J. Molecular basis for manganese sequestration by calprotectin and roles in the innate immune response to invading bacterial pathogens. *Proc. Natl. Acad. Sci.* **2013,** *110*, 3841-3846.

61. Hayden, J. A.; Brophy, M. B.; Cunden, L. S.; Nolan, E. M. High-affinity manganese coordination by human calprotectin is calcium-dependent and requires the histidine-rich site formed at the dimer interface. *J. Am. Chem. Soc.* **2013,** *135*, 775-787.

62. Nakashige, T. G.; Zhang, B.; Krebs, C.; Nolan, E. M. Human calprotectin is an iron-sequestering host-defense protein. *Nat. Chem. Biol.* **2015,** *11*, 765-771.

63. Nakashige, T. G.; Stephan, J. R.; Cunden, L. S.; Brophy, M. B.; Wommack, A. J.; Keegan, B. C.; Shearer, J. M.; Nolan, E. M. The hexahistidine motif of host-defense protein human calprotectin contributes to zinc withholding and its functional versatility. *J. Am. Chem. Soc.* **2016,** *138*, 12243-12251.

64. Nakashige, T. G.; Zygiel, E. M.; Drennan, C. L.; Nolan, E. M. Nickel sequestration by the host-defense protein human calprotectin. *J. Am. Chem. Soc.* **2017,** *139*, 8828-8836.

65. Besold, A. N.; Gilston, B. A.; Radin, J. N.; Ramsoomair, C.; Culbertson, E. M.; Li, C. X.; Cormack, B. P.; Chazin, W. J.; Kehl-Fie, T. E.; Culotta, V. C. Role of calprotectin in withholding zinc and copper from *Candida albicans*. *Infect. Immun.* **2017,** *86*, e00779-17.

66. Stephan, J. R.; Nolan, E. M. Calcium-induced tetramerization and zinc chelation shield human calprotectin from degradation by host and bacterial extracellular proteases. *Chem. Sci.* **2016,** *7*, 1962-1975.

67. Sohnle, P. G.; Collins-Lech, C.; Wiessner, J. H. The zinc-reversible antimicrobial activity of neutrophil lysates and abscess fluid supernatants. *J. Infect. Dis.* **1991,** *164*, 137-142.

68. Hobbs, J. A. R.; May, R.; Tanousis, K.; McNeill, E.; Mathies, M.; Gebhardt, C.; Henderson, R.; Robinson, M. J.; Hogg, N. Myeloid cell function in MRP-14 (S100A9) null mice. *Mol. Cell. Biol.* **2003,** *23*, 2564-2576.

69. Geczy, C. L.; Tessier, P. A.; Gomes, L. In *The Neutrophils: New Outlook for Old Cells*; 3 ed.; Gabrilovich, D., Ed.; Imperial College Press: 2013; Chapter 8, pp 310-377.

70. Passey, R. J.; Williams, E.; Lichanska, A. M.; Wells, C.; Hu, S.; Geczy, C. L.; Little, M. H.; Hume, D. A. A null mutation in the inflammation-associated S100 protein S100A8 causes early resorption of the mouse embryo. *J. Immunol.* **1999,** *163*, 2209-2216.

71. Manitz, M. P.; Horst, B.; Seeliger, S.; Strey, A.; Skryabin, B. V.; Gunzer, M.; Frings, W.; Schonlau, F.; Roth, J.; Sorg, C.; Nacken, W. Loss of S100A9 (MRP14) results in reduced interleukin-8-induced CD11b surface expression, a polarized microfilament system, and diminished responsiveness to chemoattractants *in vitro*. *Mol. Cell. Biol.* **2003,** *23*, 1034-1043.

72. McNeill, E.; Conway, S. J.; Roderick, H. L.; Bootman, M. D.; Hogg, N. Defective chemoattractant-induced calcium signalling in S100A9 null neutrophils. *Cell Calcium* **2007,** *41*, 107-121.

73. Nacken, W.; Mooren, F. C.; Manitz, M. P.; Bode, G.; Sorg, C.; Kerkhoff, C. S100A9 deficiency alters adenosine-5'-triphosphate induced calcium signalling but does not generally interfere with calcium and zinc homeostasis in murine neutrophils. *Int. J. Biochem. Cell. Biol.* **2005,** *37*, 1241-1253.

74. Hood, M. I.; Mortensen, B. L.; Moore, J. L.; Zhang, Y.; Kehl-Fie, T. E.; Sugitani, N.; Chazin, W. J.; Caprioli, R. M.; Skaar, E. P. Identification of an *Acinetobacter baumannii* zinc acquisition system that facilitates resistance to calprotectin-mediated zinc sequestration. *PLoS Pathog.* **2012,** *8*, e1003068.

75. Mortensen, B. L.; Rathi, S.; Chazin, W. J.; Skaar, E. P. *Acinetobacter baumannii* response to host-mediated zinc limitation requires the transcriptional regulator Zur. *J. Bacteriol.* **2014,** *196*, 2616-2626.

76. Juttukonda, L. J.; Chazin, W. J.; Skaar, E. P. *Acinetobacter baumannii* coordinates urea metabolism with metal import to resist host-mediated metal limitation. *mBio* **2016,** *7*, e01475-16.

77. Nairn, B. L.; Lonergan, Z. R.; Wang, J.; Braymer, J. J.; Zhang, Y.; Calcutt, M. W.; Lisher, J. P.; Gilston, B. A.; Chazin, W. J.; de Crecy-Lagard, V.; Giedroc, D. P.; Skaar, E. P. The response of *Acinetobacter baumannii* to zinc starvation. *Cell Host Microbe* **2016,** *19*, 826-836.

78. Achouiti, A.; Vogl, T.; Endeman, H.; Mortensen, B. L.; Laterre, P. F.; Wittebole, X.; van Zoelen, M. A.; Zhang, Y.; Hoogerwerf, J. J.; Florquin, S.; Schultz, M. J.; Grutters, J. C.; Biesma, D. H.; Roth, J.; Skaar, E. P.; van 't Veer, C.; de Vos, A. F.; van der Poll, T. Myeloid-related protein-8/14 facilitates bacterial growth during pneumococcal pneumonia. *Thorax* **2014,** *69*, 1034-1042.

79. Achouiti, A.; Vogl, T.; Urban, C. F.; Rohm, M.; Hommes, T. J.; van Zoelen, M. A.; Florquin, S.; Roth, J.; van 't Veer, C.; de Vos, A. F.; van der Poll, T. Myeloid-related protein-14 contributes to protective immunity in Gram-negative pneumonia derived sepsis. *PLoS Pathog.* **2012,** *8*, e1002987.

80. Liu, J. Z.; Jellbauer, S.; Poe, A. J.; Ton, V.; Pesciaroli, M.; Kehl-Fie, T. E.; Restrepo, N. A.; Hosking, M. P.; Edwards, R. A.; Battistoni, A.; Pasquali, P.; Lane, T. E.; Chazin, W. J.; Vogl, T.; Roth, J.; Skaar, E. P.; Raffatellu, M. Zinc sequestration by the neutrophil protein calprotectin enhances *Salmonella* growth in the inflamed gut. *Cell Host Microbe* **2012,** *11*, 227-239.

81. Diaz-Ochoa, V. E.; Lam, D.; Lee, C. S.; Klaus, S.; Behnsen, J.; Liu, J. Z.; Chim, N.; Nuccio, S. P.; Rathi, S. G.; Mastroianni, J. R.; Edwards, R. A.; Jacobo, C. M.; Cerasi,

M.; Battistoni, A.; Ouellette, A. J.; Goulding, C. W.; Chazin, W. J.; Skaar, E. P.; Raffatellu, M. *Salmonella* mitigates oxidative stress and thrives in the inflamed gut by evading calprotectin-mediated manganese sequestration. *Cell Host Microbe* **2016,** *19*, 814-825.

82. Gaddy, J. A.; Radin, J. N.; Loh, J. T.; Piazuelo, M. B.; Kehl-Fie, T. E.; Delgado, A. G.; Ilca, F. T.; Peek, R. M.; Cover, T. L.; Chazin, W. J.; Skaar, E. P.; Algood, H. M. S. The host protein calprotectin modulates the *Helicobacter pylori cag* type IV secretion system via zinc sequestration. *PLoS Pathog.* **2014,** *10*, e1004450.

83. Clark, H. L.; Jhingran, A.; Sun, Y.; Vareechon, C.; de Jesus Carrion, S.; Skaar, E. P.; Chazin, W. J.; Calera, J. A.; Hohl, T. M.; Pearlman, E. Zinc and manganese chelation by neutrophil S100A8/A9 (calprotectin) limits extracellular *Aspergillus fumigatus* hyphal growth and corneal infection. *J. Immunol.* **2016,** *196*, 336-344.

84. Juttukonda, L. J.; Berends, E. T. M.; Zackular, J. P.; Moore, J. L.; Stier, M. T.; Zhang, Y.; Schmitz, J. E.; Beavers, W. N.; Wijers, C. D.; Gilston, B. A.; Kehl-Fie, T. E.; Atkinson, J.; Washington, M. K.; Peebles, R. S.; Chazin, W. J.; Torres, V. J.; Caprioli, R. M.; Skaar, E. P. Dietary manganese promotes Staphylococcal infection of the heart. *Cell Host Microbe* **2017,** *22*, 531-545.

85. Kehl-Fie, T. E.; Zhang, Y.; Moore, J. L.; Farrand, A. J.; Hood, M. I.; Rathi, S.; Chazin, W. J.; Caprioli, R. M.; Skaar, E. P. MntABC and MntH contribute to systemic *Staphylococcus aureus* infection by competing with calprotectin for nutrient manganese. *Infect. Immun.* **2013,** *81*, 3395-3405.

86. Wakeman, C. A.; Moore, J. L.; Noto, M. J.; Zhang, Y.; Singleton, M. D.; Prentice, B. M.; Gilston, B. A.; Doster, R. S.; Gaddy, J. A.; Chazin, W. J.; Caprioli, R. M.; Skaar, E.

P. The innate immune protein calprotectin promotes *Pseudomonas aeruginosa* and *Staphylococcus aureus* interaction. *Nat. Commun.* **2016,** *7*, 11951.

87. De Jong, H. K.; Achouiti, A.; Koh, G. C.; Parry, C. M.; Baker, S.; Faiz, M. A.; van Dissel, J. T.; Vollaard, A. M.; van Leeuwen, E. M.; Roelofs, J. J.; de Vos, A. F.; Roth, J.; van der Poll, T.; Vogl, T.; Wiersinga, W. J. Expression and function of S100A8/A9 (calprotectin) in human typhoid fever and the murine *Salmonella* model. *PLoS Negl. Trop. Dis.* **2015,** *9*, e0003663.

88. Nakashige, T. G.; Nolan, E. M. Human calprotectin affects the redox speciation of iron. *Metallomics* **2017,** *9*, 1086-1095.

89. Reed, G. H. In *Manganese in metabolism and enzyme function*; Schramm, V. L., Wedler, F. C., Ed.; Academic Press, Inc: Orlando, FL, 1986; Chapter 17, pp 313-325.

90. Vedamati, J.; Chan, C.; Moffett, J. W. Distribution of dissolved manganese in the Peruvian upwelling and oxygen minimum zone. *Geochim. Cosmochim. Acta* **2015,** *156*, 222-240.

91. Bertini, I.; Gray, H. B.; Lippard, S. J.; Valentine, J. S. *Bioinorganic Chemistry*. University Science Books: Mill Valley, CA, 1994; p 611.

92. Rükgauer, M.; Klein, J.; Kruse-Jarres, J. D. Reference values for the trace elements copper, manganese, selenium, and zinc in the serum / plasma of children, adolescents, and adults. *J.Trace Elem. Med. Biol.* **1997,** *11*, 92-98.

93. Anjem, A.; Varghese, S.; Imlay, J. A. Manganese import is a key element of the OxyR response to hydrogen peroxide in *Escherichia coli*. *Mol. Microbiol.* **2009,** *72*, 844-858.

94. Outten, C. E.; O'Halloran, T. V. Femtomolar sensitivity of metalloregulatory proteins controlling zinc homeostasis. *Science* **2001,** *292*, 2488-2492.

95. Archibald, F. S.; Fridovich, I. Manganese, superoxide dismutase, and oxygen tolerance in some lactic acid bacteria. *J. Bacteriol.* **1981,** *146*, 928-936.

96. Baker, S. P.; Nulton, T. J.; Kitten, T. Genomic, phenotypic, and virulence analysis of *Streptococcus sanguinis* oral and infective-endocarditis isolates. *Infect. Immun.* **2019,** *87*, e00703-18.

97. McHargue, J. S. The role of manganese in plants. *J. Am. Chem. Soc.* **1922,** *44*, 1592-1598.

98. Bradley, H. C. Manganese of the Lamellibranchs. *Biol. Bull.* **1910,** *19*, 161-166.

99. Peterson, W. H.; Skinner, J. T. Distribution of manganese in foods. *J. Nutr.* **1931,** *4*, 419-426.

100. Skinner, J. T.; Peterson, W. H.; Steenbock, H. The manganese metabolism of the rat. *J. Biol. Chem.* **1931,** *90*, 60-85.

101. Kemmerer, A. R.; Elvehjem, C. A.; Hart, E. B. Studies on the relation of manganese to the nutrition of the mouse. *J. Biol. Chem.* **1931,** *92*, 623-630.

102. Daniels, A. L.; Everson, G. J. The relation of manganese to congenital debility. *J. Nutr.* **1935,** *9*, 191-203.

103. Everson, G. J.; Daniels, A. L. A study of manganese retentions in children. *J. Nutr.* **1934,** *8*, 497-502.

104. Pirson, A.; Bergmann, L. Manganese requirement and carbon source in *Chlorella*. *Nature* **1945,** *176*, 209-210.

105. Cheniae, G. M.; Martin, I. F. Site of manganese function in photosynthesis. *Biochim. Biophys. Acta.* **1968,** *153*, 819-837.

106. Pirson, A. Sixty years in algal physiology and photosynthesis. *Photosyn. Res.* **1994,** *40*, 207-221.

107. Anderson, A. B. The activation of jack-bean arginase by cobalt, manganese, and iron. *Biochem. J.* **1945,** *39*, 139-142.

108. Scrutton, M. C.; Utter, M. F.; Mildvan, A. S. Pyruvate carboxylase: the presence of tightly bound manganese. *J. Biol. Chem.* **1966,** *241*, 3480-3487.

109. Agrawal, B. B. L.; Goldstein, I. J. Physical and chemical studies on concanavalin A, the hemagglutinin of the jack bean. *Arch. Biochem. Biophys.* **1968,** *124*, 218-229.

110. Reed, G. H.; Cohn, M. Electron paramagnetic resonance spectra of manganese(II)-protein complexes: manganese(II)-concanavalin A. *J. Biol. Chem.* **1970,** *245*, 662-667.

111. Silver, S.; Kralovic, M. L. Manganese accumulation by *Escherichia coli*: evidence for a specific transport system. *Biochem. Biophys. Res. Commun.* **1969,** *34*, 640-645.

112. Silver, S.; Johnseine, P.; King, K. Manganese active transport in *Escherichia coli*. *J. Bacteriol.* **1970,** *104*, 1299-1306.

113. Keele, J., B. B.; McCord, J. M.; Fridovich, I. Superoxide dismutase from *Escherichia coli* B: A new manganese-containing enzyme. *J. Biol. Chem.* **1970,** *245*, 6176-6181.

114. Eisenstadt, E.; Fisher, S.; Der, C. L.; Silver, S. Manganese transport in *Bacillus subtilis* W23 during growth and sporulation. *J. Bacteriol.* **1973,** *113*, 1363-1372.

115. Jasper, P.; Silver, S. Divalent cation transport systems of *Rhodopseudomonas*

capsulata. *J. Bacteriol.* **1978,** *133*, 1323-1328.

116. Perry, R. D.; Silver, S. Cadmium and manganese transport in *Staphylococcus aureus* membrane vesicles. *J. Bacteriol.* **1982,** *150*, 973-976.

117. Schimpff-Weiland, G.; Follmann, H.; Auling, G. A new manganese-activated ribonucelotide reductase found In Gram-positive bacteria. *Biochem. Biophys. Res. Commun.* **1981,** *102*, 1276-1282.

118. Kono, Y.; Fridovich, I. Isolation and characterization of the pseudocatalase of *Lactobacillus plantarum*. *J. Biol. Chem.* **1983,** *258*, 6015-6019.

119. Archibald, F. S.; Duong, M. N. Manganese acquisition by *Lactobacillus plantarum*. *J. Bacteriol.* **1984,** *158*, 1-8.

120. Yesilkaya, H.; Kadioglu, A.; Gingles, N.; Alexander, J. E.; Mitchell, T. J.; Andrew, P. W. Role of manganese-containing superoxide dismutase in oxidative stress and virulence of *Streptococcus pneumoniae*. *Infect. Immun.* **2000,** *68*, 2819-2826.

121. D'Mello, R. A.; Langford, P. R.; Kroll, J. S. Role of bacterial Mn-cofactored superoxide dismutase in oxidative stress responses, nasopharyngeal colonization, and sustained bacteremia caused by *Haemophilus influenzae* Type b. *Infect. Immun.* **1997,** *65*, 2700-2706.

122. Horsburgh, M. J.; Clements, M. O.; Crossley, H.; Ingham, E.; Foster, S. J. PerR controls oxidative stress resistance and iron storage proteins and is required for virulence in *Staphylococcus aureus*. *Infect. Immun.* **2001,** *69*, 3744-3754.

123. Boyer, E.; Bergevin, I.; Malo, D.; Gros, P.; Cellier, M. F. M. Acquisition of Mn(II) in addition to Fe(II) Is required for full virulence of *Salmonella enterica* serovar Typhimurium. *Infect. Immun.* **2002,** *70*, 6032-6042.

124. Janakiraman, A.; Slauch, J. M. The putative iron transport system SitABCD encoded on SPI1 is required for full virulence of *Salmonella typhimurium*. *Mol. Microbiol.* **2000,** *35*, 1146-1155.

125. Bearden, S. W.; Perry, R. D. The Yfe system of *Yersinia pestis* transports iron and manganese and is required for full virulence of plague. *Mol. Microbiol.* **1999,** *32*, 403-414.

126. Singh, K. V.; Qin, X.; Weinstock, G. M.; Murray, B. E. Generation and testing of mutants of *Enterococcus faecalis* in a mouse peritonitis model. *J. Infect. Dis.* **1998,** *178*, 1416-1420.

127. Kitten, T.; Munro, C. L.; Michalek, S. M.; Macrina, F. L. Genetic characterization of a *Streptococcus mutans* LraI family operon and role in virulence. *Infect. Immun.* **2000,** *68*, 4441-4451.

128. Marra, A.; Lawson, S.; Asundi, J. S.; Brigham, D.; Hromockyj, A. E. *In vivo* characterization of the *psa* genes from *Streptococcus pneumoniae* in multiple models of infection. *Microbiology* **2002,** *148*, 1483-1491.

129. Klein, J. S.; Lewinson, O. Bacterial ATP-driven transporters of transition metals: physiological roles, mechanisms of action, and roles in bacterial virulence. *Metallomics* **2011,** *3*, 1098-1108.

130. Cellier, M. F. M.; Bergevin, I.; Boyer, E.; Richer, E. Polyphyletic origins of bacterial Nramp transporters. *Trends Genet.* **2001,** *17*, 365-370.

131. Bozzi, A. T.; Bane, L. B.; Weihofen, W. A.; Singharoy, A.; Guillen, E. R.; Ploegh, H. L.; Schulten, K.; Gaudet, R. Crystal structure and conformational change mechanism of a bacterial Nramp-family divalent metal transporter. *Structure* **2016,** *24*, 2102-2114.

132. Ehrnstorfer, I. A.; Geertsma, E. R.; Pardon, E.; Steyaert, J.; Dutzler, R. Crystal structure of a SLC11 (NRAMP) transporter reveals the basis for transition-metal ion transport. *Nat. Struct. Mol. Biol.* **2014,** *21*, 990-996.

133. Lewinson, O.; Livnat-Levanon, N. Mechanism of action of ABC importers: conservation, divergence, and physiological adaptations. *J. Mol. Biol.* **2017,** *429*, 606-619.

134. Borths, E. L.; Poolman, B.; Hvorup, R. N.; Locher, K. P.; Rees, D. C. *In vitro* functional characterization of BtuCD-F, the *Escherichia coli* ABC transporter for vitamin B12 Uptake. *Biochemistry* **2005,** *44*, 16301-16309.

135. Gribenko, A.; Mosyak, L.; Ghosh, S.; Parris, K.; Svenson, K.; Moran, J.; Chu, L.; Li, S.; Liu, T.; Woods, V. L., Jr.; Jansen, K. U.; Green, B. A.; Anderson, A. S.; Matsuka, Y. V. Three-dimensional structure and biophysical characterization of *Staphylococcus aureus* cell surface antigen-manganese transporter MntC. *J. Mol. Biol.* **2013,** *425*, 3429-3445.

136. McDevitt, C. A.; Ogunniyi, A. D.; Valkov, E.; Lawrence, M. C.; Kobe, B.; McEwan, A. G.; Paton, J. C. A molecular mechanism for bacterial susceptibility to zinc. *PLoS Pathog.* **2011,** *7*, e1002357.

137. Abate, F.; Malito, E.; Cozzi, R.; Lo Surdo, P.; Maione, D.; Bottomley, M. J. Apo, Zn^{2+}-bound and Mn^{2+}-bound structures reveal ligand-binding properties of SitA from the pathogen *Staphylococcus pseudintermedius*. *Biosci. Rep.* **2014,** *34*, e00154.

138. Papp-Wallace, K. M.; Maguire, M. E. Manganese transport and the role of manganese in virulence. *Annu. Rev. Microbiol.* **2006,** *60*, 187-209.

139. Gat, O.; Mendelson, I.; Chitlaru, T.; Ariel, N.; Altboum, Z.; Levy, H.; Weiss, S.; Grosfeld, H.; Cohen, S.; Shafferman, A. The solute-binding component of a putative Mn(II) ABC transporter (MntA) is a novel *Bacillus anthracis* virulence determinant. *Mol. Microbiol.* **2005,** *58*, 533-551.

140. Eijkelkamp, B. A.; McDevitt, C. A.; Kitten, T. Manganese uptake and streptococcal virulence. *Biometals* **2015,** *28*, 491-508.

141. Janulczyk, R.; Ricci, S.; Bjorck, L. MtsABC Is important for manganese and iron transport, oxidative stress resistance, and virulence of *Streptococcus pyogenes*. *Infect. Immun.* **2003,** *71*, 2656-2664.

142. Schreur, P. J. W.; Rebel, J. M.; Smits, M. A.; van Putten, J. P.; Smith, H. E. TroA of *Streptococcus suis* is required for manganese acquisition and full virulence. *J. Bacteriol.* **2011,** *193*, 5073-5080.

143. Smith, A. J.; Ward, P. N.; Field, T. R.; Jones, C. L.; Lincoln, R. A.; Leigh, J. A. MtuA, a lipoprotein receptor antigen from *Streptococcus uberis*, Is responsible for acquisition of manganese during growth in milk and is essential for infection of the lactating bovine mammary gland. *Infect. Immun.* **2003,** *71*, 4842-4849.

144. Perry, R. D.; Craig, S. K.; Abney, J.; Bobrov, A. G.; Kirillina, O.; Mier, I., Jr.; Truszczynska, H.; Fetherston, J. D. Manganese transporters Yfe and MntH are Fur-regulated and important for the virulence of *Yersinia pestis*. *Microbiology* **2012,** *158*, 804-815.

145. Kobayashi, S. D.; Malachowa, N.; DeLeo, F. R. Pathogenesis of *Staphylococcus aureus* abscesses. *Am. J. Pathol.* **2015,** *185*, 1518-1527.

146. Horsburgh, M. J.; Wharton, S. J.; Cox, A. G.; Ingham, E.; Peacock, S.; Foster, S. J. MntR modulates expression of the PerR regulon and superoxide resistance in *Staphylococcus aureus* through control of manganese uptake. *Mol. Microbiol.* **2002,** *44*, 1269-1286.

147. Handke, L. D.; Gribenko, A. V.; Timofeyeva, Y.; Scully, I. L.; Anderson, A. S. MntC-dependent manganese transport is essential for *Staphylococcus aureus* oxidative stress resistance and virulence. *mSphere* **2018,** *3*, e00336-18.

148. Coady, A.; Xu, M.; Phung, Q.; Cheung, T. K.; Bakalarski, C.; Alexander, M. K.; Lehar, S. M.; Kim, J.; Park, S.; Tan, M. W.; Nishiyama, M. The *Staphylococcus aureus* ABC-Type manganese transporter MntABC is critical for reinitiation of bacterial replication following exposure to phagocytic oxidative burst. *PLoS One* **2015,** *10*, e0138350.

149. Diep, B. A.; Phung, Q.; Date, S.; Arnott, D.; Bakalarski, C.; Xu, M.; Nakamura, G.; Swem, D. L.; Alexander, M. K.; Le, H. N.; Mai, T. T.; Tan, M. W.; Brown, E. J.; Nishiyama, M. Identifying potential therapeutic targets of methicillin-resistant *Staphylococcus aureus* through *in vivo* proteomic analysis. *J. Infect. Dis.* **2014,** *209*, 1533-1541.

150. Anderson, A. S.; Scully, I. L.; Timofeyeva, Y.; Murphy, E.; McNeil, L. K.; Mininni, T.; Nunez, L.; Carriere, M.; Singer, C.; Dilts, D. A.; Jansen, K. U. *Staphylococcus aureus* manganese transport protein C is a highly conserved cell surface protein that elicits protective immunity against *S. aureus* and *Staphylococcus epidermidis*. *J. Infect. Dis.* **2012,** *205*, 1688-1696.

151. Kovacs-Simon, A.; Titball, R. W.; Michell, S. L. Lipoproteins of bacterial pathogens. *Infect. Immun.* **2011,** *79*, 548-561.

152. Berntsson, R. P.; Smits, S. H.; Schmitt, L.; Slotboom, D. J.; Poolman, B. A structural classification of substrate-binding proteins. *FEBS Lett.* **2010,** *584*, 2606-2617.

153. Brophy, M. B.; Nolan, E. M. Manganese and microbial pathogenesis: sequestration by the Mammalian immune system and utilization by microorganisms. *ACS Chem. Biol.* **2015,** *10*, 641-651.

154. Ahuja, S.; Rouge, L.; Swem, D. L.; Sudhamsu, J.; Wu, P.; Russell, S. J.; Alexander, M. K.; Tam, C.; Nishiyama, M.; Starovasnik, M. A.; Koth, C. M. Structural analysis of bacterial ABC transporter inhibition by an antibody fragment. *Structure* **2015,** *23*, 713-723.

155. Anderson, A. S.; Miller, A. A.; Donald, R. G.; Scully, I. L.; Nanra, J. S.; Cooper, D.; Jansen, K. U. Development of a multicomponent *Staphylococcus aureus* vaccine designed to counter multiple bacterial virulence factors. *Hum. Vaccin. Immunother.* **2012,** *8*, 1585-1594.

156. Weiser, J. N.; Ferreira, D. M.; Paton, J. C. *Streptococcus pneumoniae*: transmission, colonization and invasion. *Nat. Rev. Microbiol.* **2018,** *16*, 355-367.

157. Dintilhac, A.; Alloing, G.; Granadel, C.; Claverys, J. Competence and virulence of *Streptococcus pneumoniae*: Adc and PsaA mutants exhibit a requirement for Zn and Mn resulting from inactivation of putative ABC metal permeases. *Mol. Microbiol.* **1997,** *25*, 727-739.

158. McAllister, L. J.; Tseng, H. J.; Ogunniyi, A. D.; Jennings, M. P.; McEwan, A. G.; Paton, J. C. Molecular analysis of the psa permease complex of *Streptococcus pneumoniae*. *Mol. Microbiol.* **2004,** *53*, 889-901.

159. Rosch, J. W.; Gao, G.; Ridout, G.; Wang, Y. D.; Tuomanen, E. I. Role of the manganese efflux system mntE for signalling and pathogenesis in *Streptococcus pneumoniae*. *Mol. Microbiol.* **2009,** *72*, 12-25.

160. Berry, A. M.; Paton, J. C. Sequence heterogeneity of PsaA, a 37-kilodalton putative adhesin essential for virulence of *Streptococcus pneumoniae*. *Infect. Immun.* **1996,** *64*, 5255-5262.

161. Martin, J. E.; Lisher, J. P.; Winkler, M. E.; Giedroc, D. P. Perturbation of manganese metabolism disrupts cell division in *Streptococcus pneumoniae*. *Mol. Microbiol.* **2017,** *104*, 334-348.

162. Lawrence, M. C.; Pilling, P.; Epa, V.; Berry, A.; Ogunniyi, A.; Paton, J. The crystal structure of pneumococcal surface antigen PsaA reveals a metal-binding site and a novel structure for a putative ABC-type binding protein. *Structure* **1998,** *6*, 1553-1561.

163. Vigonsky, E.; Fish, I.; Livnat-Levanon, N.; Ovcharenko, E.; Ben-Tal, N.; Lewinson, O. Metal binding spectrum and model structure of the *Bacillus anthracis* virulence determinant MntA. *Metallomics* **2015,** *7*, 1407-1419.

164. Sampson, J. S.; Furlow, Z.; Whitney, A. M.; Williams, D.; Facklam, R.; Carlone, G. M. Limited diversity of *Streptococcus pneumoniae* psaA among Pneumococcal vaccine serotypes. *Infect. Immun.* **1997,** *65*, 1967-1971.

165. Talkington, D. F.; Brown, B. G.; Tharpe, J. A.; Koenig, A.; Russell, H. Protection of mice against fatal pneumococcal challenge by immunization with pneumococcal surface adhesin A (PsaA). *Microb. Pathog.* **1996,** *21*, 17-22.

166. Simell, B.; Korkeila, M.; Pursiainen, H.; Kilpi, T. M.; Kayhty, H. Pneumococcal carriage and otitis media induce salivary antibodies to pneumococcal surface adhesin A,

pneumolysin, and pneumococcal surface protein A in children. *J. Infect. Dis.* **2001,** *183*, 887-896.

167. Schmid, P.; Selak, S.; Keller, M.; Luhan, B.; Magyarics, Z.; Seidel, S.; Schlick, P.; Reinisch, C.; Lingnau, K.; Nagy, E.; Grubeck-Loebenstein, B. Th17/Th1 biased immunity to the pneumococcal proteins PcsB, StkP and PsaA in adults of different age. *Vaccine* **2011,** *29*, 3982-3989.

Chapter 2: Initial Biochemical and Functional Evaluation of Murine Calprotectin Reveals Ca(II)-Dependence and Its Ability to Chelate Multiple Nutrient Transition Metal Ions

This Chapter is adapted from *Biochemistry* **2018**, 57 (19), 2846-2856.

2.1 Contributions

Yu (Vicky) Gu carried out the antimicrobial activity assays with some of the strains presented in this Chapter.

2.2 Introduction

S100 proteins serve important and diverse functions in the life processes of vertebrates, and share some distinguishing features.[1] These proteins are predominantly α-helical, have a propensity to self-associate and typically form homodimers, contain Ca(II)-binding EF-hand domains, and possess varying capacities for coordinating Ca(II) and divalent transition metal ions.[1, 2] Several S100 proteins, including human S100A7 (psoriasin), human S100A12, and the S100A8/S100A9 heterooligomer calprotectin (CP), contribute to the metal-withholding innate immune response and exhibit antimicrobial activity attributed to their ability to sequester transition metal ions from microbial pathogens in the extracellular space.[3-5]

CP is the most thoroughly evaluated metal-sequestering S100 protein. Both humans and mice express CP in epithelial and white blood cells, and our current understanding of its contributions to metal homeostasis and the innate immune response results from early clinical investigations and *ex vivo* analyses of human specimens, murine model studies of infectious disease, and chemical and biological studies of the human orthologue obtained by recombinant protein expression.[5] Murine infection model studies have leveraged *S100A9*$^{-/-}$ knockout mice, which are effectively CP deficient,[6] to provide insight into the role of murine CP (mCP) during acute bacterial and fungal infections. For instance, seminal studies using a *Staphylococcus aureus* infection model

in wild-type and *S100A9*$^{-/-}$ mice revealed that CP contributes to manganese withholding.[7] Since this work, *S100A9*$^{-/-}$ mice have been used to investigate the interplay between CP and a variety of microbial pathogens that include *Salmonella enterica* serovar Typhimurium,[8, 9] *Acinetobacter baumannii*,[10-13] *Streptococcus pneumoniae*,[14] *Helicobacter pylori*,[15] *Aspergillus fumigatus*,[16] and *Candida albicans*.[17, 18] Taken together, these studies illuminate that the contributions of mCP to metal availability and the host/pathogen interaction are varied and context dependent. For example, some pathogens like *Salmonella* and *S. pneumoniae* appear to benefit from mCP-mediated metal limitation,[8, 9, 14] and recent work indicates that the role of mCP in metal-withholding can be organ-specific.[19] In addition, mCP has been shown to modulate the composition of polymicrobial communities *in vivo*.[20]

The working model for the extracellular metal-sequestering function of CP begins with its release from white blood cells, especially neutrophils recruited to an infection site, and epithelial cells. Once in the extracellular space, CP competes with invading microbial pathogens for available transition metal nutrients. Studies of recombinant human CP (hCP) have informed our understanding of its competition with microbes for metal nutrients, including the molecular basis for this process. hCP is a heterooligomer of two S100 polypeptides, hS100A8 (α subunit, 10.8 kDa) and hS100A9 (β subunit, 13.2 kDa). Like other S100 polypeptides, each subunit harbors two Ca(II)-binding EF-hand domains.[2, 21] The C-terminal EF-hands, described as "canonical," bind Ca(II) in a heptadentate coordination geometry. The N-terminal EF-hands are considered "non-canonical" and bind Ca(II) with lower coordination number and lower affinity. Apo hCP, which we define as the species that does not have Ca(II) ions or transition metal ions

bound, is a hS100A8/hS100A9 heterodimer.[22] Each heterodimer unit harbors two sites for transition metals that form at the hS100A8/hS100A9 interface and are comprised of metal-chelating residues from both subunits.[21, 23] Site 1 is a His_3Asp motif formed by His83 and His87 of hS100A8, and His20 and Asp30 of hS100A9. Site 2 is an unusual His_6 motif formed by His17 and His27 of hS100A8, and His91, His95, His103 and His105 of hS100A9.[24, 25] Binding of Ca(II) ions at the EF-hands or a transition metal ion at the His_6 site causes self-association of two hCP heterodimers to form a heterotetramer.[26-29] The Ca(II)-bound heterotetramer exhibits enhanced transition metal affinities relative to the Ca(II)-free heterodimer, and this feature indicates that hCP morphs into its metal-sequestering form in the extracellular space where Ca(II) ion concentrations are ≈2 mM.[23, 30, 31] Along similar lines, Ca(II) ions enhance the antimicrobial activity of hCP against a variety of bacterial species.[7, 23, 32] Its growth inhibitory activity was originally attributed to Zn(II) and then also Mn(II) sequestration.[7, 33, 34] More recent work has demonstrated additional Fe(II)-, Ni(II)-, and Cu-sequestering properties of hCP, and affords a model of functional versatility in which hCP has the capacity to bind and entrap multiple divalent nutrient metal ions.[18, 31, 35]

This discussion highlights that classical biochemical and microbiology studies have focused on the human orthologue. Accordingly, results from biochemical and functional investigations of hCP are used to inform studies in murine model systems and vice versa with the apparent presumption that hCP and mCP behave similarly. To the best of our knowledge, little is known about the biochemical and biophysical properties of mCP, which presents a limitation in our current appreciation of the similarities and differences of CP orthologues. Although procedures to obtain recombinant mS100A8 and

recombinant mS100A9 have been reported,[36, 37] we are unaware of any work describing robust reconstitution of the mCP heterooligomer. Reports related to mCP include early investigations demonstrating the isolation of mS100A8 (originally named CP-10)[38] and mS100A9 (originally named murine MRP14)[39] from activated spleen cells. In the latter study, mS100A8 and mS100A9 were reported to co-purify by ion-exchange chromatography.[39] Moreover, analysis of murine abscess fluid revealed the presence of mS100A8/mS100A9 complexes as well as unassociated mS100A8 and mS100A9 species.[40] This study also reported that the abscesses contained high levels of mS100A8 (≈8 mg/mL, ≈780 μM monomer) and mS100A9 (≈6 mg/mL, ≈460 μM monomer).[40] Lastly, murine model systems are highly informative, but there are some caveats to their applicability to the host/pathogen interaction in humans because of inherent differences between the murine and human immune systems.[41] For these reasons, we concluded that mCP warrants biochemical consideration and that studies of this protein will improve our understanding of CP in metal withholding and other biological phenomena.

Amino acid sequence alignment provides a first point of comparison between human and murine CP (**Figure 2.1**). The human and murine forms of S100A8 share 52 identical amino acid residues (56% identity) and 15 similar amino acid residues (72% similarity), and the corresponding S100A9 polypeptides share 66 identical amino acid residues (57% identity) and 10 similar amino acids (66% similarity). The residues that comprise the His_3Asp and His_6 metal-binding sites of hCP are conserved in the murine polypeptides, suggesting that mCP employs the same metal-binding sites as hCP. Moreover, the Ca(II)-binding loops of the human and murine S100A8 and S100A9 subunits possess similar residues. Nevertheless, inspection of the amino acid sequences

reveals several intriguing differences between the human and murine polypeptides. In particular, the C-terminus of mS100A8 lacks the EESH motif of hS100A8, and the S100A9 C-terminal tail regions exhibit low sequence identity. The hS100A9 C-terminal tail is an important contributor to the His_6 metal-binding site because it provides two His residues that complete the octahedral coordination sphere and encapsulates the bound M(II) ion (M = Fe, Mn, Ni, Zn) at this site.[24, 25, 31, 35, 42, 43] Curiously, the mS100A9 tail contains an HxHxH motif (residues 103-107) rather than the HHH motif (residues 103-105) of hS100A9. We also note that hS100A8 and mS100A8 each contain one conserved Cys residue at position 42. In contrast, the quantity and locations of the Cys residues in hS100A9 and mS100A9 differ. Whereas hS100A9 contains one Cys residue at position 3, which is located before an alternative translation start site at position 5, mS100A9 contains three Cys residues at positions 80, 91 and 111.

In this work, we present initial biochemical and functional characterization of mCP and the cysteine-null variant mCP-Ser. The results demonstrate that apo mCP is a heterodimer and that the protein tetramerizes in the presence of Ca(II), binds various first-row transition metal ions, and displays broad-spectrum antibacterial activity. These properties are reminiscent of hCP; however, this study also reveals several differences between the human and murine orthologues. In particular, mCP appears to be less responsive to Ca(II) ions than hCP. Overall, this work provides a foundation for further investigations of mCP and informs prior and future studies of mCP in murine models of disease.

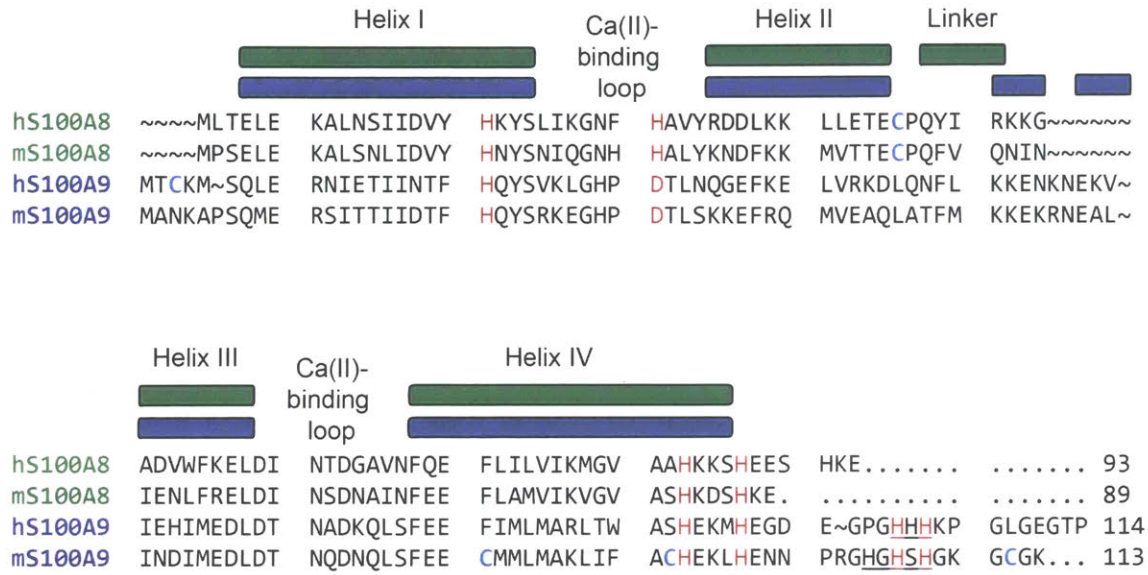

Figure 2.1. Amino acid sequence alignment of the S100A8 and S100A9 subunits of human (h) and murine (m) CP. Metal-binding residues of the human polypeptides and conserved murine residues are highlighted in red. Cys residues for all proteins are bolded and in blue. The C-terminal HHH and HxHxH motifs in the human and murine S100A9 subunits are underlined. The depictions of secondary structure are for the human orthologues.

2.3 Experimental

2.3.1 General Materials and Methods

All chemicals were acquired from commercial suppliers and used as received. All solutions were prepared using Milli-Q water (18.2 MΩ·cm). All buffer solutions were filtered (0.2 μm) before use. Stock solutions (1 M, 100 mL) of Ca(II) ($CaCl_2 \cdot 2H_2O$, Sigma, >99.0%) were prepared in acid-washed volumetric glassware and transferred to polypropylene tubes for storage. Working solutions of Ca(II) were prepared immediately before use by diluting the 1-M stock solution into Milli-Q water. ULTROL grade HEPES (Calbiochem) and BioXtra NaCl (>99.5%) were used to prepare buffers for analytical SEC to minimize metal ion contamination from the buffer. The hCP-Ser heterodimer was

prepared as previously described.[23] Protein aliquots were thawed only once, immediately prior to use. All concentrations were determined using calculated extinction coefficients (https://web.expasy.org/protparam/), and all reported concentration are for heterodimers or homodimers: murine S100A8/S100A9 heterodimer (ε_{280} = 5,960 $M^{-1}cm^{-1}$), human S100A8/S100A9 heterodimer (ε_{280} = 18,450 $M^{-1}cm^{-1}$).

2.3.2 Sub-cloning of mS100A8 and mS100A9

Synthetic genes containing the nucleotide sequences for mS100A8, mS100A9, and mS100A9(C80S)(C91S)(C111S) were codon-optimized for *Escherichia coli* expression, synthesized, and ligated into the *Nde*I and *Xho*I restriction sites of pET41a by DNA2.0 (currently ATUM). Each plasmid was transformed into chemically competent *E. coli* TOP10, isolated using a miniprep kit (Qiagen), and analyzed by DNA sequencing (Quintara Biosciences). The pET41a-*mS100A8(C42S)* plasmid was obtained by site-directed mutagenesis as described below. For protein expression, each plasmid was transformed into chemically competent *E. coli* BL21(DE3). Single colonies were grown to saturation in LB medium containing 50 μg/mL kanamycin (37 °C with agitation). Freezer stocks were prepared by diluting the culture 1:1 with 50% v/v glycerol in filter-sterilized Milli-Q water, frozen in liquid N_2, and stored at -80 °C.

Nucleotide sequence for ***Nde*I**-mS100A8-Stop-***Xho*I**:
CAT ATG CCG AGC GAA CTG GAG AAA GCA CTG AGC AAC CTG ATC GAC GTC TAC CAC AAC TAC AGC AAT ATT CAA GGT AAT CAT CAC GCT CTG TAC AAA AAT GAT TTC AAG AAG ATG GTT ACC ACG GAG TGC CCG CAG TTC GTG CAG AAT ATC AAC ATT GAA AAC CTG TTC CGT GAG CTG GAC ATC AAC TCC GAT AAT GCC ATT AAC TTT GAA GAG TTT TTG GCG ATG GTT ATC AAA GTG GGC GTC GCG AGC CAC AAG GAC TCT CAT AAA GAG **TAA** CTC GAG

Translated sequence for ***Nde*I**-mS100A8-Stop-***Xho*I**:
M P S E L E K A L S N L I D V Y H N Y S N I Q G N H H A L Y K N D F K K M V T T E
C P Q F V Q N I N I E N L F R E L D I N S D N A I N F E E F L A M V I K V G V A S H K
D S H K E Stop **L E**

Nucleotide sequence for ***Nde*I**-mS100A9-Stop-***Xho*I**:
CAT ATG GCG AAC AAA GCA CCT AGC CAA ATG GAA CGC AGC ATC ACT ACT
ATC ATC GAC ACT TTT CAT CAA TAC TCT CGT AAA GAG GGC CAC CCG GAT
ACG CTG TCC AAG AAA GAG TTC CGC CAG ATG GTT GAG GCC CAG CTG GCG
ACC TTT ATG AAG AAA GAA AAA CGT AAC GAG GCA CTG ATT AAC GAC ATT
ATG GAA GAT CTG GAC ACC AAT CAA GAT AAT CAG CTG AGC TTC GAA GAG
TGC ATG ATG CTG ATG GCG AAG TTG ATT TTC GCT TGC CAC GAG AAG CTG
CAT GAA AAC AAT CCG CGT GGT CAT GGT CAC AGC CAC GGT AAG GGT TGT
GGC AAA **TAA** CTC GAG

Translated sequence for ***Nde*I**-mS100A9-Stop-***Xho*I**:
M A N K A P S Q M E R S I T T I I D T F H Q Y S R K E G H P D T L S K K E F R Q M
V E A Q L A T F M K K E K R N E A L I N D I M E D L D T N Q D N Q L S F E E C M M
L M A K L I F A C H E K L H E N N P R G H G H S H G K G C G K Stop **L E**

Nucleotide sequence for ***Nde*I**-mS100A9(C80S)(C91S)(C111S)-Stop-***Xho*I**:
CAT ATG GCG AAC AAA GCA CCT AGC CAA ATG GAA CGC AGC ATC ACT ACT
ATC ATC GAC ACT TTT CAT CAA TAC TCT CGT AAA GAG GGC CAC CCG GAT
ACG CTG TCC AAG AAA GAG TTC CGC CAG ATG GTT GAG GCC CAG CTG GCG
ACC TTT ATG AAG AAA GAA AAA CGT AAC GAG GCA CTG ATT AAC GAC ATT
ATG GAA GAT CTG GAC ACC AAT CAA GAT AAT CAG CTG AGC TTC GAA GAG
AGC ATG ATG CTG ATG GCG AAG TTG ATT TTC GCT AGC CAC GAG AAG CTG
CAT GAA AAC AAT CCG CGT GGT CAT GGT CAC AGC CAC GGT AAG GGT AGT
GGC AAA **TAA** CTC GAG

Translated sequence for ***Nde*I**-mS100A9(C80S)(C91S)(C111S)-Stop-***Xho*I**:
M A N K A P S Q M E R S I T T I I D T F H Q Y S R K E G H P D T L S K K E F R Q M
V E A Q L A T F M K K E K R N E A L I N D I M E D L D T N Q D N Q L S F E E S M M
L M A K L I F A S H E K L H E N N P R G H G H S H G K G S G K Stop **L E**

Mutations are highlighted in yellow. A *Nde*I restriction site was placed at the 5' end and a stop codon and a *Xho*I restriction site was placed at the 3' end (underlined above).

Nucleotide sequences above are displayed from 5' to 3'.

2.3.3 Site-directed Mutagenesis

The oligonucleotide primers employed to prepare the mS100A8(C42S) variant by site-directed mutagenesis were synthesized by Integrated DNA Technologies (Coralville, IA). pET41a-*mS100A8(C42S)* was prepared using pET41a-*mS100A8* as a template and a modified Quick-Change site-directed mutagenesis protocol. The forward primer 5'-GATGGTTACCACGGAGAGCCCGCAGTTCGTGCAG-3' and the reverse primer 5'-CTGCACGAACTGCGGGCTCTCCGTGGTAACCATC-3' (mutation sites underlined) were used in PCR reactions with Pfu Turbo DNA polymerase. The PCR protocol was 95 °C for 30 sec; 95 °C for 30 sec, 60 °C for 1 min, 68 °C for 12 min (25x); 4 °C hold temperature. *Dpn*I (New England Biolabs) was used to degrade the template plasmid by adding a 0.75-μL aliquot to the sample, and incubating the sample at 37 °C for 3 h. A supplemental 0.75-μL aliquot of *Dpn*I was added at 1.5 h into the incubation. The resulting DNA was transformed into chemically-competent *E. coli* TOP10 and the cells were plated on agar containing 50 μg/mL kanamycin. Single colonies were inoculated into LB (5 mL, 50 μg/mL kanamycin) and grown overnight, and plasmids were obtained using a miniprep kit (Qiagen). The plasmids were analyzed by DNA sequencing (Quintara Biosciences) to confirm the presence of the desired mutation and then transformed into chemically competent *E. coli* BL21(DE3) for protein overexpression.

2.3.4 Overexpression of mS100A8 and mS100A9

For protein overexpression, overnight cultures in LB with 50 μg/mL kanamycin were inoculated from freezer stocks and grown to saturation (37 °C with agitation, ≈16 h) and used to inoculate 1 L of LB with 50 μg/mL kanamycin (1:100 dilution). These cultures

were grown at 37 °C with shaking at 150 rpm, induced with 100 μM IPTG at OD_{600} ~0.6-0.7, and then incubated for an additional ≈3.5-4 h at 37 °C with shaking at 150 rpm and pelleted by centrifugation (3,000 rpm, 15 min, 4 °C). The pellets were transferred to polypropylene tubes, flash frozen in liquid N_2, and stored at -80 °C. Typical cell pellets weighed ≈2-3 g / L culture. This overexpression procedure resulted in mS100A8 in the insoluble fraction and mS100A9 in the soluble fraction following cell lysis.

2.3.5 Reconstitution and Purification of mCP and mCP-Ser

All steps were performed on ice or in a 4 °C room. For reconstitution and purification of the mCP heterodimer, one mS100A8 and one mS100A9 cell pellet, each from a 1-L overexpression, were thawed on ice and each pellet was suspended in 30 mL lysis buffer A (50 mM Tris, 100 mM NaCl, 1 mM EDTA, 0.5% Triton X-100, pH 8.0) supplemented with 5 mM DTT and 1 mM PMSF (from a freshly prepared ≈1 mL solution in ethanol) immediately before use. The resuspended cell pellets were combined and sonicated (2.5 min, 30 sec on, 10 sec off, 40% amplitude) in a steel beaker on ice. The cell lysate was then clarified by centrifugation (14,000 rpm, 10 min, 4 °C). The supernatant, which contained soluble mS100A9, was transferred to a 250-mL glass beaker on ice and the cell pellets, which contained insoluble mS100A8, were combined in 60 mL of lysis buffer A and subjected to a second round of resuspension, sonication, and centrifugation. The resulting pellets containing mS100A8 were stored on ice, and the supernatant containing mS100A9 was treated with 60% ammonium sulfate to precipitate contaminating proteins (rapid stirring, ≈1 h, 4 °C). The resulting mixture was centrifuged (14,000 rpm, 20 min, 4 °C) and filtered. The filtered supernatant was collected and treated

with 100% ammonium sulfate to precipitate mS100A9 (rapid stirring, ≈1 h, 4 °C). The mixture was centrifuged (14,000 rpm, 20 min, 4 °C) and filtered, and the supernatant discarded, which afforded cell pellets containing mS100A9. At this point, the mS100A8 and mS100A9 cell pellets were combined and resuspended in 100 mL lysis buffer B (50 mM Tris, 100 mM NaCl, 4 M Gu-HCl, pH 8.0) supplemented with 5 mM DTT and the resulting mixture was sonicated (5 min, 30 sec on, 10 sec off, 40% amplitude) and centrifuged (14,000 rpm, 10 min, 4°C). The resulting supernatant containing denatured mS100A8 and denatured mS100A9 was transferred to a dialysis bag (SpectraPor, 3,500 kDa MWCO) and dialyzed against MonoQ buffer A (20 mM HEPES, pH 8.0) supplemented with 5 mM DTT (4 L, > 12 h, 3x, 4 °C). DTT powder was added to each dialysis buffer immediately before use.

Purification of the mCP heterodimer was performed by anion exchange chromatography and SEC on a ÄKTA Purifier HPLC system housed in a cold room (4 °C). After dialysis, the protein solution was centrifuged (14,000 rpm, 10 min, 4 °C), filtered (0.2 μm) and loaded onto a pre-equilibrated MonoQ 10/100 GL column (GE Life Sciences) using a Superloop (150 mL, GE Life Sciences). The anion exchange buffers were MonoQ buffer A (20 mM HEPES, pH 8.0) and MonoQ buffer B (20 mM HEPES, 1 M NaCl, pH 8.0), and both buffers were supplemented with 5 mM DTT and prepared immediately before use. The protein was eluted using a gradient of 0–15% B over 15 column volumes of MonoQ buffer B. The fractions containing mCP were combined, concentrated to ≈10 mL by spin filtration (Amicon, 10 kDa MWCO) and loaded onto a pre-equilibrated HiLoad 26/600 Superdex S75 column (GE Life Sciences) using S75 buffer (20 mM HEPES, 100 mM NaCl, pH 8.0) containing 5 mM DTT. The protein was eluted over 1 column volume

and dialyzed against 20 mM HEPES, 100 mM NaCl, pH 8.0, 5 mM DTT that contained ≈10 g Chelex resin (Biorad), typically overnight (>12 h) at 4°C before being filtered (0.2 μm) and concentrated by spin filtration (Amicon, 15-mL filter, 10 kDa MWCO), flash frozen in aliquots (50 μL), and stored at -80 °C. Typical yields of mCP were ≈45 mg / 2 L culture (1 L from each subunit overexpression). The mCP-Ser variant was prepared using the same procedures except that DTT was omitted from all buffers. Typical yields of mCP-Ser were ≈16 mg / 2 L of culture.

2.3.6 Electrospray Ionization Mass Spectrometry (ESI-MS)

A denaturing protocol was employed to analyze mCP and mCP-Ser by LC-MS. An Agilent 1260 series LC system outfitted with an Agilent Jetstream ESI source and an Agilent Poroshell 300SB-C18 column (5-μm pore size) was used for all analyses. Each protein was diluted in Milli-Q water to provide a final concentration of ≈5 μM. A 5-μL protein sample was injected onto the column, and the mS100A8 and mS100A9 subunits were eluted using a gradient of 10–90% B over 20 min with a flow rate of 0.2 mL/min (solvent A: 0.1% formic acid in water; solvent B: 0.1% formic acid in acetonitrile). The spectra were deconvoluted using the maximum entropy algorithm in the MassHunter software (Agilent).

2.3.7 Circular Dichroism Spectroscopy

A Jasco J-1500 circular dichroism (CD) spectrometer housed in the Biophysical Instrumentation Facility at MIT was used for all measurements. Proteins were buffer-exchanged into CD buffer (1 mM Tris-HCl, pH 7.5). The buffer was supplemented with 1

mM DTT for mCP. For samples that contained Ca(II), an aliquot from a 1-M Ca(II) stock solution was added to the protein solution to afford a final Ca(II) concentration of 3 mM. Each sample (10 μM protein, 300 μL) was transferred to a nitric acid-washed Hellma quartz cuvette (1-mm path length). Spectra were recorded from 195 to 260 nm using continuous scan mode (50 nm/min) and 1 nm bandwidth. All data represent averages of three replicate baseline-subtracted scans, where the baseline was obtained from a sample of CD buffer. For thermal denaturation experiments, the temperature was increased from 25–95 °C, at 1-°C intervals, and the CD intensity was recorded at 222 nm. Each thermal denaturation experiment was repeated on three independent samples and data from one representative experiment are shown.

2.3.8 Analytical Size Exclusion Chromatography

An ÄKTA Purifier FPLC system housed in a cold room (4 °C) and outfitted with a Superdex 75 10/300 GL SEC column was used for all analytical SEC. The running buffer was 75 mM HEPES, pH 7.0, 100 mM NaCl, 200 μM TCEP containing 0, 2, 5, 10 or 25 mM Ca(II). The column was calibrated with blue dextran and a low-molecular-weight protein mixture (GE Healthcare Life Sciences) consisting of ribonuclease A (13.7 kDa), carbonic anhydrase (29 kDa), ovalbumin (44 kDa), and conalbumin (75 kDa) prior to use. Proteins were buffer-exchanged (3x) into the running buffer using an Amicon spin filter (0.5 mL, 10 kDa MWCO). Samples (100 μM, 300 μL) were prepared and loaded into a 100-μL injection loop, and the FPLC system was programmed to inject 500 μL of sample onto the column. The samples were eluted over one column volume at a flow rate of 0.5

mL/min. At least two independent replicates were performed for each experiment, and representative data from one experiment are shown.

2.3.9 Metal-depletion Assay

The assay protocols were adapted from a reported procedure.[31] Antimicrobial activity (AMA) buffer (20 mM Tris-HCl, pH 7.5, 100 mM NaCl) was sterile filtered (0.22 μm) into sterile 50-mL polypropylene tubes (VWR). AMA medium (62:38 v/v ratio of AMA buffer and TSB; ± 3 mM BME, ± 2 mM Ca(II)) was then prepared. Proteins were buffer-exchanged into AMA buffer using 0.5-mL Amicon spin filters (10 kDa MWCO). Aliquots (1 mL) of AMA medium were placed into pre-sterilized 1.7-mL microcentrifuge tubes (VWR). Protein was then added from a concentrated stock solution to afford a final concentration of 250 μg/mL. The total volume change upon protein addition was ≤2%. The tubes were closed and incubated at 30 °C (150 rpm, 20 h). Subsequently, the samples were transferred by pipette to sterile 4-mL Amicon spin filters (10 kDa MWCO) and centrifuged (3700 rpm, 30 min, 4 °C). Samples for ICP-MS analyses were prepared by combining 700 μL of the filtrate with 700 μL of ≈3% nitric acid, and spiking the resulting mixture with 28 μL (2 ppb) of Terbium Internal Standard (Agilent part # 5190-8590).

2.3.10 Inductively-coupled Plasma Mass Spectrometry (ICP-MS)

Metal ion concentrations were quantified by using an Agilent 7900 ICP-MS housed in the Center for Environmental Health Sciences Bioanalytical Core Facility at MIT. The instrument was operated in helium mode. The instrument was calibrated before each analysis session using a series of five serially diluted (1:10 in ≈3% nitric acid) samples of

the Environmental Calibration Standard (Agilent, part # 5183-4688) as well as a nitric acid only standard. Each standard and sample was spiked with 2 ppb of the Tb internal standard described above.

2.3.11 Antimicrobial Activity Assays

Assays were performed by adapting a reported protocol.[23] Cultures were grown in TSB without dextrose for *Escherichia coli* CFT073, *Acinetobacter baumannii* ATCC 17961, and *Staphylococcus aureus* USA300 JE2. *Listeria monocytogenes* ATCC 19115 and *Staphylococcus epidermidis* NRS101 were grown in BHI broth, and *Lactobacillus plantarum* WCFS1 was grown in MRS medium. Protein aliquots were buffer-exchanged into AMA buffer (20 mM Tris-HCl, pH 7.5, 100 mM NaCl) using a 0.5-mL Amicon spin filter (Millipore, 10-kDa MWCO). The protein was then diluted in AMA media (62:38 v/v ratio of 20 mM Tris-HCl pH 7.5, 100 mM NaCl and TSB, BHI or MRS; ± 3 mM BME, ± 2 mM Ca(II)) to afford 10x stock solutions (1 mg/mL – 250 μg/mL). Overnight cultures were prepared from single colonies and grown in 5 mL of TSB, MRS, or BHI (37 °C, ≈16-20 h). The overnight cultures were diluted 1:100 into fresh TSB, BHI, or MRS and grown at 37 °C until the OD_{600} reached ≈0.6. Each culture was then diluted 1:500 into AMA medium and the assays were immediately set up in 96-well plates (Corning) using 90 μL of the diluted bacterial culture and 10 μL of the protein stocks (or no-protein control). Each condition was performed in triplicate in the assay plate. The plates were wrapped in moist paper towels and plastic wrap and incubated with shaking at 150 rpm at 37 °C. The OD_{600} was measured at 8 and 20 h. At least three independent replicates of each assay were performed and the resulting averages and standard deviations are reported.

Table 2.1. Bacterial strains used in this work.

Strain	Growth Medium[a]	Source
Escherichia coli CFT073	TSB	ATCC 700928
Acinetobacter baumannii	TSB	ATCC 17961
Staphylococcus aureus USA 300 JE2	TSB	NARSA repository
Staphylococcus epidermidis NRS101	BHI	NARSA repository
Listeria monocytogenes	BHI	ATCC 19115
Lactobacillus plantarum WCFS1	MRS	ATCC

[a] The medium used for culturing and diluted with AMA buffer for the AMA assays.

2.4 Results

2.4.1 Purification of mCP and mCP-Ser

Guided by procedures to obtain the hS100A8 and hS100A9 subunits of hCP,[23] the mCP subunits mS100A8 and mS100A9 were overexpressed separately in *E. coli* BL21(DE3) at 37 °C. SDS-PAGE of post-induction samples identified the mS100A8 subunit in the insoluble fraction, as observed for hS100A8 and hS100A9 expressed under the same conditions.[23] In contrast, the mS100A9 subunit was only identified in the soluble fraction. Thus, we took the different solubilities of mS100A8 and mS100A9 into account during the development and optimization of a purification procedure. We found that it was most efficient to combine the mS100A8 and mS100A9 cell pellets and lyse this mixture. Following centrifugation, the soluble fraction containing mS100A9 was decanted and stored on ice. The insoluble fraction, which contained mS100A8, was subjected to an additional round of resuspension, lysis and centrifugation to remove contaminating biomolecules. The soluble fraction containing mS100A9 was then treated with 60% ammonium sulfate to precipitate contaminating proteins, which were removed by centrifugation and filtration. The resulting supernatant was treated with 100% ammonium sulfate to precipitate mS100A9, which was pelleted by centrifugation. The resulting mS100A9 pellets were combined with the mS100A8 pellets in a solubilizing buffer

containing 4 M GuHCl, and, following sonication and centrifugation, the soluble denatured sample was dialyzed against HEPES buffer to allow protein folding to occur. Anion exchange chromatography of the dialyzed protein and SDS-PAGE of the resulting fractions revealed that folding resulted in a mixture that predominantly contained mCP (evidenced by comparable quantities of mS100A8 and mS100A9) with some mS100A9 homodimer, which were separated by this chromatographic method. Subsequent gel filtration chromatography of the mCP-containing fractions and dialysis against Chelex resin afforded purified mCP heterodimer in yields of ≈45 mg from 2 L culture. mCP-Ser was purified in the same manner; however, lower yields of ≈16 mg from 2 L culture were repeatedly obtained for this variant. In general, the anion-exchange chromatograms for mCP-Ser indicated that greater amounts of mS100A9-Ser homodimer formed during folding compared to the amounts of mS100A9 homodimer observed during mCP preparations.

The purified proteins were evaluated by SDS-PAGE, mass spectrometry, and ICP-MS (**Figure 2.2, Tables 2.2, 2.3**). These analyses confirmed protein identity and indicated high purity by SDS-PAGE and negligible metal contamination. Moreover, CD spectroscopy (**Figure 2.3**) and analytical SEC (**Figure 2.5, Table 2.4**) demonstrated that apo mCP and mCP-Ser were isolated as α-helical heterodimers as described further below.

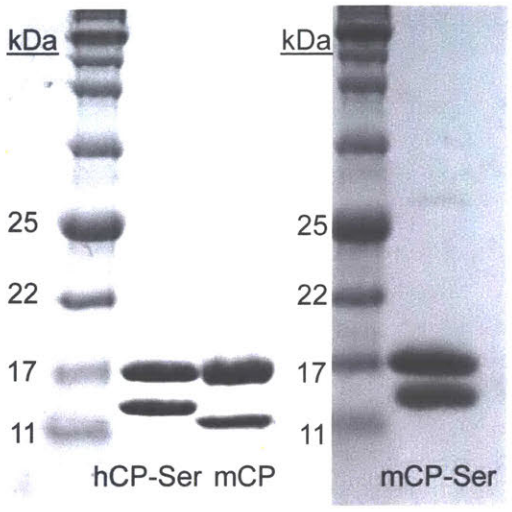

Figure 2.2. Purity of recombinant proteins by SDS-PAGE (15% Tris-glycine). The leftmost lane in each gel is a P7712S molecular weight ladder (New England Biolabs).

Table 2.2. Mass spectrometry analysis of mCP subunits.

Protein	mS100A8 Calculated Mass ± ^{N}Met (g/mol)[b]	mS100A8 Observed Mass (g/mol)[c]	mS100A9 Calculated Mass ± ^{N}Met (g/mol)[d]	mS100A9 Observed Mass (g/mol)
mCP	10294.59 10163.40	10294.71 10163.52	13048.86 12917.67	- 12917.78
mCP-Ser	10278.53 10147.34	10278.82 10147.60	13000.68 12869.49	- 12869.50

Table 2.3. Metal content of representative purified murine proteins.[a]

Metal	mCP (24 μM)[b]	mCP-Ser (7.7 μM)[b]
[Mn] (μM)	0.0025	0.00079
equivalents[c]	0.0001	0.0001
[Fe] (μM)	0.098	0.036
equivalents[c]	0.0041	0.0046
[Co] (μM)	0.00017	0.000
equivalents[c]	0.000	0.000
[Ni] (μM)	0.019	0.0094
equivalents[c]	0.0008	0.0012
[Cu] (μM)	0.018	0.0089
equivalents[c]	0.00075	0.0012
[Zn] (μM)	0.10	0.064
equivalents[c]	0.0042	0.0084

[a] Metal content was determined by ICP-MS.
[b] Concentration of protein in the sample.
[c] Equivalents of metal relative to the protein concentration.

2.4.2 mCP is α-Helical and Displays High Thermal Stability

The CD spectra of mCP and mCP-Ser displayed features characteristic of a predominantly α-helical protein in the presence and absence of Ca(II), as expected for S100 family members and consistent with the CD signatures of hCP and hCP-Ser (**Figure 2.3**).[22, 23] Thermal denaturation of 10 μM mCP at pH 7.5 afforded a melting temperature (T_m) of ≈76 °C that increased to ≈90 °C when 2 mM Ca(II) was added to the sample (**Figure 2.4**). mCP-Ser also displayed a Ca(II)-dependent increase in its T_m value from ≈63 °C to ≈77 °C in the absence and presence of 2 mM Ca(II), respectively. A comparison of the mCP and mCP-Ser data indicated that the Cys→Ser mutations that afford mCP-

Ser destabilized the protein fold to thermal denaturation. The observed Ca(II) dependence for both proteins is in general agreement with reported thermal denaturation and differential scanning calorimetry studies of the human orthologue.[23, 28] For instance, the presence of excess Ca(II) ions caused the T_m value of CP-Ser to increase from 59 to 79 °C.[23]

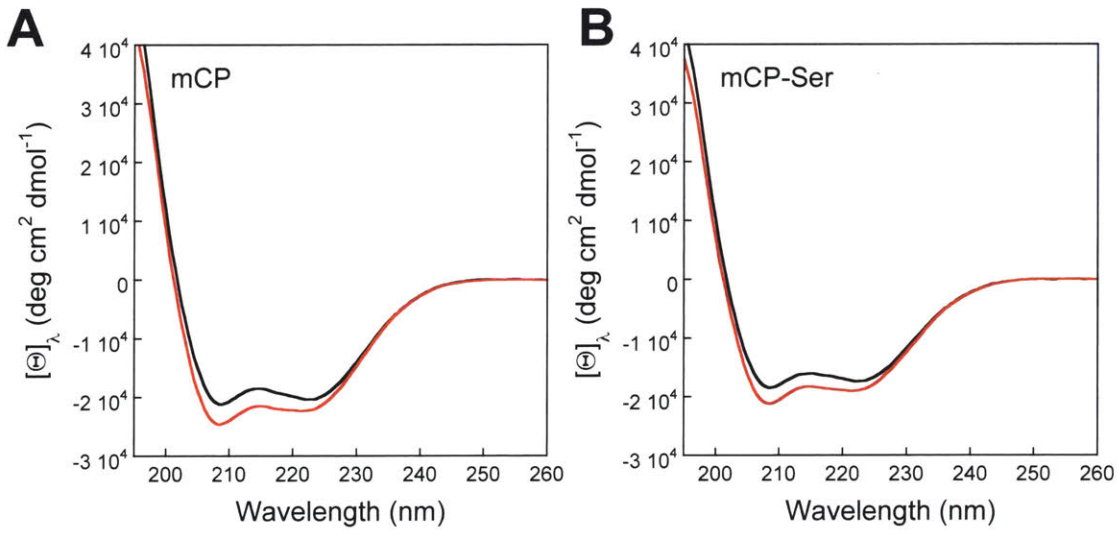

Figure 2.3. CD spectra of mCP (**A**) and mCP-Ser (**B**) in the absence (black) and presence (red) of 2 mM Ca(II) (1 mM Tris-HCl, pH 7.5, 25 °C).

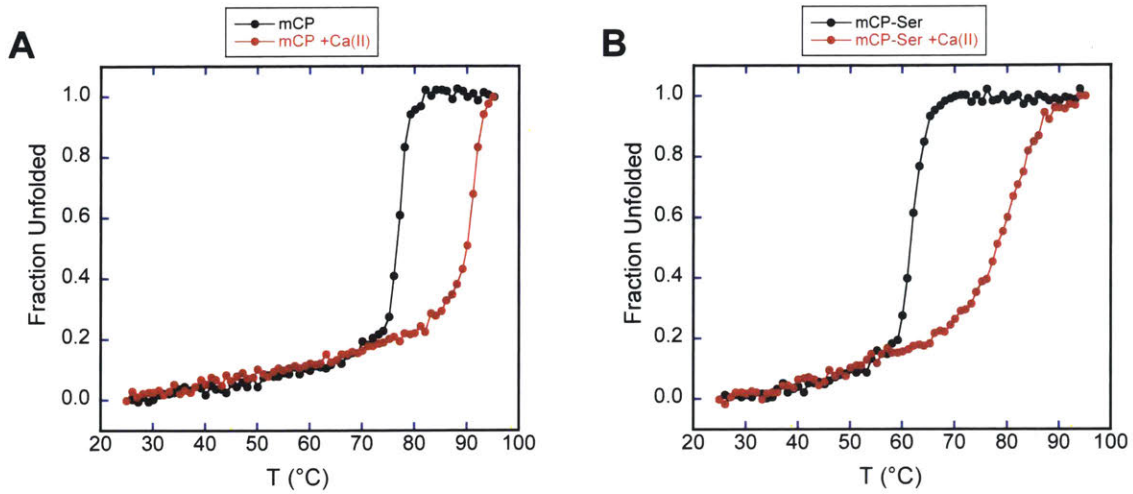

Figure 2.4. Representative thermal denaturation plots for 10 μM of mCP or mCP-Ser in the absence (black) and presence (red) of 3 mM Ca(II) (1 mM Tris-HCl, 1 mM DTT, pH 7.5). Each trace was normalized to the CD signal at 222 nm at 95 °C to obtain the fraction of unfolded protein.

2.4.3 mCP Exhibits Ca(II)-dependent Oligomerization

hCP exhibits Ca(II)-dependent oligomerization properties; the apo protein is a heterodimer and Ca(II) binding causes two heterodimers to self-associate and form a heterotetramer.[26-28] To evaluate whether mCP displays similar behavior, we investigated its oligomeric state in the absence and presence of Ca(II) ions using analytical SEC (**Figure 2.5, Table 2.4**). In the absence of added Ca(II) ions, mCP and mCP-Ser each exhibited an elution volume of ≈12.2 mL, which corresponds to a calculated molecular weight of 27 kDa and was assigned to the 23-kDa heterodimer. Next, we examined the elution profile of mCP and mCP-Ser in the presence of excess Ca(II) ions in the running buffer. At the highest Ca(II) concentration examined (25 mM, 250 equivalents), each protein exhibited an elution volume of ≈11.4 mL, which corresponds to a calculated molecular weight of 38 kDa and was assigned to the 46-kDa heterotetramer. Thus, similar to hCP, Ca(II) binding to the EF-hands of the mCP heterodimer causes formation of

heterotetramers. Nevertheless, the details of this self-association process appear to be markedly different for hCP and mCP. Our prior studies of hCP indicated that full conversion to the heterotetramer occurs when the protein is in the presence of ≈20 equivalents of Ca(II) ions.[23, 30, 31] The SEC results for mCP indicated that a mixture of heterodimers and heterotetramers exist under these conditions, and that >200 equivalents of Ca(II) are required for complete conversation to the heterotetramer.

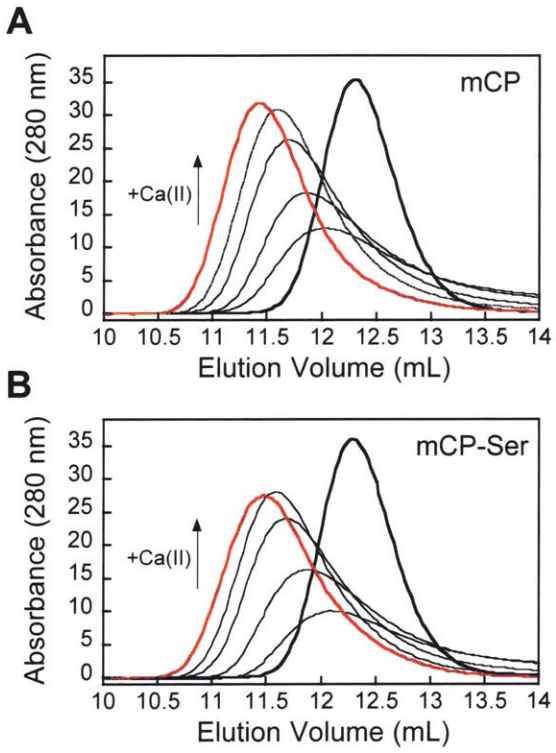

Figure 2.5. mCP displays Ca(II)-dependent heterotetramer formation. Analytical SEC chromatograms of 100 μM mCP (**A**) and mCP-Ser (**B**) in the absence (thick black trace) and presence of 1, 2, 5, 10, and 25 mM (thick red trace) Ca(II) (75 mM HEPES, 100 mM NaCl, pH 7.0, 200 μM TCEP) at 4 °C.

Table 2.4. Analytical SEC elution volume and calculated molecular weight of proteins.

Protein[a]	[Ca(II)] (mM)	V_e (mL)[b]	MW (kDa)
mCP	0	12.2	27.2
	1	11.9	30.5
	2	11.8	32.3
	5	11.6	34.6
	10	11.5	36.1
	25	11.4	37.6
mCP-Ser	0	12.2	27.8
	1	11.7	33.4
	2	11.6	34.5
	5	11.5	35.8
	10	11.4	37.6
	25	11.3	38.1

[a] The protein concentration was 100 μM. The running buffer was 75 mM HEPES, 100 mM NaCl, pH 7.0. The elution volume (V_e) corresponds to the maximum peak absorbance at 280 nm.

2.4.4 mCP Depletes Multiple Transition Metals from Microbial Growth Media

Because amino acid sequence alignment indicates that the transition-metal-binding residues in hCP are conserved in mCP (**Figure 2.1**), we hypothesized that mCP exhibits similar coordination chemistry to hCP – i.e. His_3Asp and His_6 sites with similar metal selectivity. In our prior studies of metal chelation by hCP, we designed a simple assay to ascertain which metal ions the protein depletes from microbial growth media,[31] and we later extended this experiment to S100A12 and S100A7.[44, 45] This metal-depletion assay delineates which transition metals a protein binds with sufficiently high affinity such that the metals remain bound to the protein during a spin filtration step. To obtain preliminary insights into the metal-sequestering repertoire of mCP, we evaluated the ability of mCP and mCP-Ser to deplete metal ions from the Tris:TSB AMA medium in the absence and presence of a ≈2 mM Ca(II) supplement. This Ca(II) concentration mimics extracellular Ca(II) levels.[46] Because the analytical SEC experiments detailed above indicated that mCP requires >200 equivalents of Ca(II) to fully convert to the

heterotetramer (**Figure 2.5**), we attempted to investigate metal depletion in the presence of 5 mM Ca(II) ions, but supplementation of Tris:TSB with this concentration of Ca(II) ions resulted in precipitation that confounded the analyses. We also evaluated the consequences of a ≈3 mM BME supplement because this reducing agent has been employed in antimicrobial activity assays with hCP,[7, 10, 23, 24] and it enhances the ability of hCP-Ser to deplete Fe from microbial growth medium.[31, 47]

The Tris:TSB medium employed in this work contained ≈3 μM Zn, ≈1.6 μM Fe, ≈0.5 μM Ni, and less than 150 nM of Mn, Co, and Cu. Treatment of Tris:TSB medium with 250 μg/mL (≈11 μM) mCP or mCP-Ser resulted in depletion of Mn, Fe, Ni, Cu and Zn comparable to that observed for 250 μg/mL hCP-Ser (**Figure 2.6, Table 2.5**). For Mn and Zn, only trace quantities were observed in the treated medium regardless of supplementation, These Mn and Zn depletion profiles were expected for several reasons: (i) mCP is accepted to participate in withholding Mn(II) and Zn(II), which requires high-affinity binding of these metal ions; (ii) the concentration of mCP employed in this assay exceeds the total concentration of metal ions in the Tris:TSB medium; and (iii) we previously observed that 250 μg/mL hCP-Ser fully depletes Mn and Zn from Tris:TSB medium with and without Ca(II) and BME supplements.[31] The proteins also depleted Fe from the Tris:TSB medium, especially in the presence of the Ca(II) and BME supplements, albeit to a lesser degree than observed for Mn and Zn. These results are consistent with our prior studies of Fe depletion by hCP-Ser, which demonstrated that maximum Fe depletion occurs in the presence of Ca(II) ions and BME, and illuminated that the His_6 site of hCP-Ser binds Fe(II) with high affinity.[31] Depletion of Cu was also observed for all proteins, and the Ca(II) and BME supplements also afforded a slight

enhancement of the depletion of this metal ion, an observation that warrants future investigation. Depletion of Ni also occurred under all examined conditions. Although no Co depletion was observed, we reason that this result reflects the low Co content (≈30 nM) of the growth medium as well as the expected thermodynamic preference of mCP for Zn(II) over Co(II). We previously reported that hCP-Ser readily binds Co(II) at both the His_3Asp and His_6 sites and that Zn(II) is thermodynamically favored at both sites,[23] and we expect that mCP will exhibit similar Co(II)-binding properties.

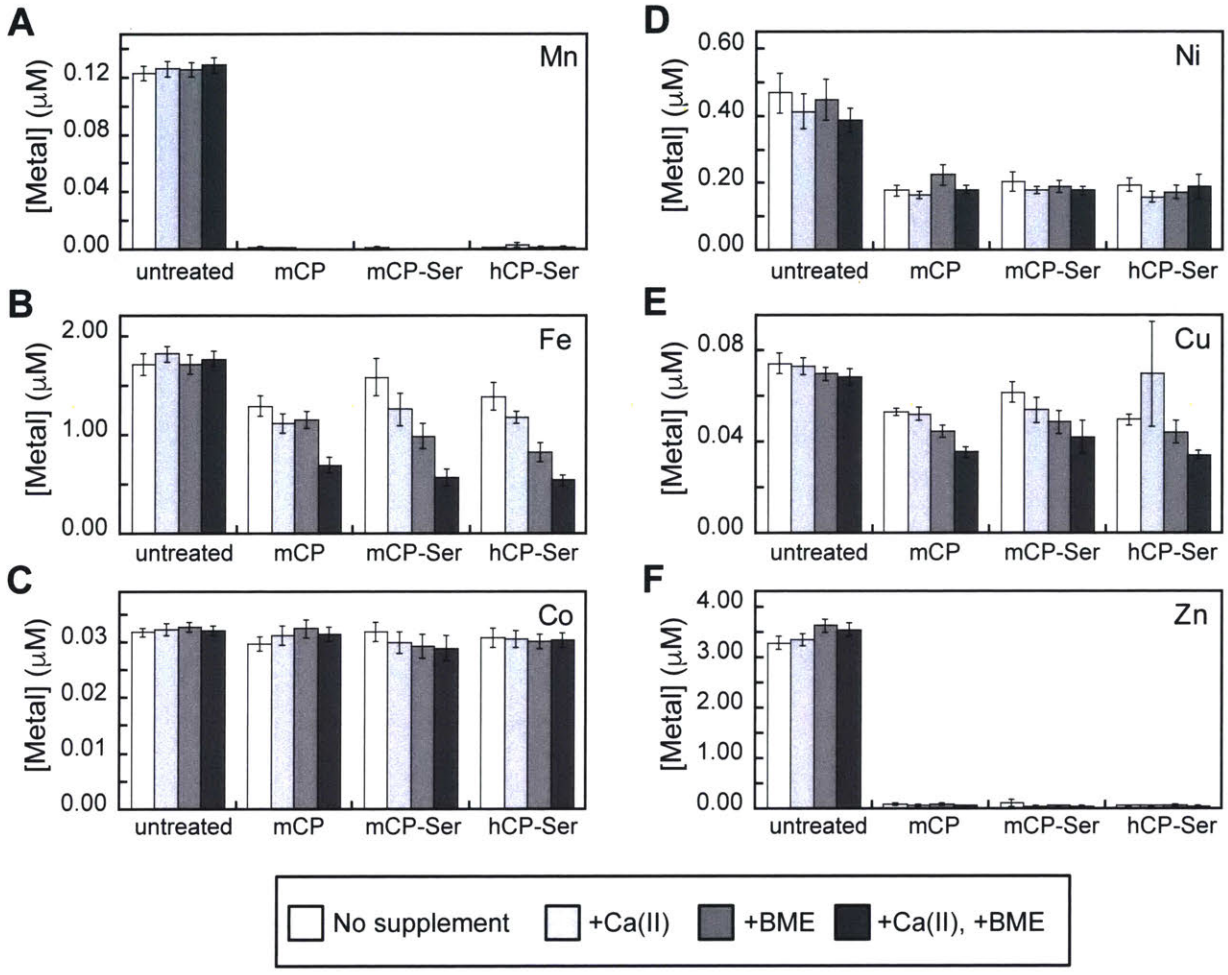

Figure 2.6. mCP depletes transition metal ions from Tris:TSB medium. (**A**) Mn depletion; (**B**) Fe depletion; (**C**) Co depletion; (**D**) Ni depletion; (**E**) Cu depletion; (**F**) Zn depletion. The medium was incubated with 250 μg/mL mCP, mCP-Ser, or hCP-Ser (20 h, 30 °C). Proteins were removed by spin filtration and the metal content of the filtrate was measured by ICP-MS (mean ± SEM, $n \geq 4$). The Tris:TSB medium contained no supplement (white bars), a 2-mM Ca(II) supplement (light grey bars), a 3-mM BME supplement (medium grey bars), or both 2-mM Ca(II) and 3-mM BME supplements (dark grey bars).

Table 2.5. Metal content (μM) of Tris:TSB medium with or without treatment with 250 μg/mL mCP, mCP-Ser, or hCP-Ser.[a]

Metal	Protein	n.s.[b]	SEM	Ca(II)	SEM	BME	SEM	Ca(II), BME	SEM
Mn	untreated	0.122	0.005	0.126	0.006	0.125	0.005	0.128	0.006
	mCP	0.002	0.000	0.001	0.000	0.001	0.000	0.000	0.000
	mCP-Ser	0.002	0.001	0.001	0.000	0.000	0.000	0.001	0.000
	hCP-Ser	0.001	0.000	0.003	0.002	0.002	0.001	0.001	0.001
Fe	untreated	1.717	0.106	1.824	0.079	1.712	0.097	1.768	0.082
	mCP	1.293	0.105	1.119	0.103	1.154	0.088	0.696	0.078
	mCP-Ser	1.586	0.184	1.260	0.164	0.990	0.125	0.571	0.082
	hCP-Ser	1.392	0.138	1.179	0.057	0.830	0.095	0.544	0.051
Co	untreated	0.032	0.001	0.032	0.001	0.033	0.001	0.032	0.001
	mCP	0.030	0.001	0.031	0.002	0.033	0.002	0.031	0.001
	mCP-Ser	0.032	0.002	0.030	0.002	0.029	0.002	0.029	0.002
	hCP-Ser	0.031	0.002	0.031	0.001	0.030	0.001	0.030	0.001
Ni	untreated	0.470	0.059	0.415	0.051	0.450	0.061	0.388	0.035
	mCP	0.178	0.015	0.166	0.011	0.226	0.030	0.181	0.013
	mCP-Ser	0.205	0.028	0.180	0.010	0.192	0.018	0.179	0.013
	hCP-Ser	0.196	0.020	0.160	0.016	0.173	0.020	0.191	0.035
Cu	untreated	0.074	0.004	0.073	0.004	0.070	0.003	0.068	0.003
	mCP	0.053	0.001	0.052	0.003	0.045	0.003	0.036	0.002
	mCP-Ser	0.062	0.005	0.054	0.005	0.049	0.005	0.042	0.007
	hCP-Ser	0.050	0.002	0.070	0.023	0.044	0.005	0.034	0.002
Zn	untreated	3.292	0.126	3.351	0.123	3.629	0.134	3.548	0.130
	mCP	0.089	0.023	0.079	0.018	0.100	0.022	0.069	0.012
	mCP-Ser	0.124	0.070	0.055	0.014	0.065	0.016	0.052	0.018
	hCP-Ser	0.064	0.011	0.067	0.015	0.075	0.018	0.048	0.014

[a]Metal content was determined by ICP-MS (mean ± SEM, $n \geq 4$).
[b] No supplement was added to the Tris:TSB medium.

These metal-depletion data indicate that mCP has the propensity to chelate a number of first-row transition metal ions with sufficient affinity to retain the bound metal during spin filtration, suggesting that this protein has the capacity to withhold these nutrients from micoorganisms. Moreover, depletion of Fe, and also Cu, by mCP and mCP-Ser is enhanced by the presence of both BME and Ca(II) ions. This result may stem from

a combination of an increase in transition metal affinities in the presence of excess Ca(II) ions (as observed for hCP) and redox speciation of the metal ions that is altered by the presence of a reducing agent to favor high-affinity binding (i.e. Fe(II) vs. Fe(III), as also observed for hCP). Future coordination chemistry studies of mCP will address these possibilities. Taken together, these data provide a foundation for elucidating the biological coordination chemistry of mCP and motivation for examining metals beyond Mn(II) and Zn(II) in future work.

2.4.5 mCP Exhibits Antimicrobial Activity

To provide a preliminary evaluation of the antimicrobial activity of mCP, we screened the protein (0–1000 μg/mL, 0–43 μM) against six bacterial strains that included two Gram-negative pathogens (*E. coli* CFT073 and *A. baumannii* ATCC 17961), three Gram-positive pathogens (*S. aureus* USA300 JE2, *S. epidermidis* NRS101, and *L. monocytogenes* ATCC 19115), and the Gram-positive probiotic *L. plantarum* WCFS1 (**Table 2.1**). We examined the growth inhibitory activity of mCP and mCP-Ser at 37 °C in AMA medium preparations that contained 68% Tris buffer and 32% growth medium (TSB, BHI or MRS depending on the strain, **Table 2.1**) in the absence and presence of a ≈2-mM Ca(II) supplement, which mimics extracellular Ca(II) levels.[46]

We monitored growth at 8-h (**Figure 2.7**) and 20-h (**Figure 2.8**) timepoints, and focus this analysis on the former dataset. Overall, mCP inhibited the growth of these six bacterial strains to varying degrees (**Figures 2.7A, 2.8A**). The ≈2-mM Ca(II) supplement afforded enhanced growth inhibition against *E. coli* CFT073 (8-h time point only), *A. baumannii* ATCC 17961, *L. plantarum* WCSF1, and to a lesser extent, *L. monocytogenes*

ATCC 19115. On the basis of the 8-h time point, two Gram-positive strains, *S. epidermidis* NRS101 and *L. monocytogenes* ATCC 19115, appear to be most susceptible to mCP because complete or almost complete growth inhibition occurred at 250 μg/mL mCP regardless of Ca(II) supplementation. mCP-Ser also exhibited antibacterial activity (**Figures 2.7B, 2.8B**). A comparison of the data for mCP and mCP-Ser affords several observations about the relative antimicrobial activity of these proteins: (i) in the absence of Ca(II), mCP-Ser generally displays lower growth inhibitory activity than mCP, (ii) the Ca(II)-induced enhancement of growth inhibitory activity is greater for mCP-Ser than for mCP, and (iii) several strains exhibit growth recovery at the 20-h timepoint when treated with mCP-Ser. These trends are especially pronounced for *S. epidermidis* NRS101, *L. monocytogenes* ATCC 19115, and *L. plantarum* WCSF1. These results may be a consequence of differing protein stability where one or more of the Cys→Ser mutations in the apo mCP-Ser heterodimer destabilize the protein relative to mCP and binding of Ca(II) ions is compensatory. It is also possible that mCP-Ser possesses lower transition metal affinities than mCP in the absence of Ca(II), which would account for the lower antibacterial activity.

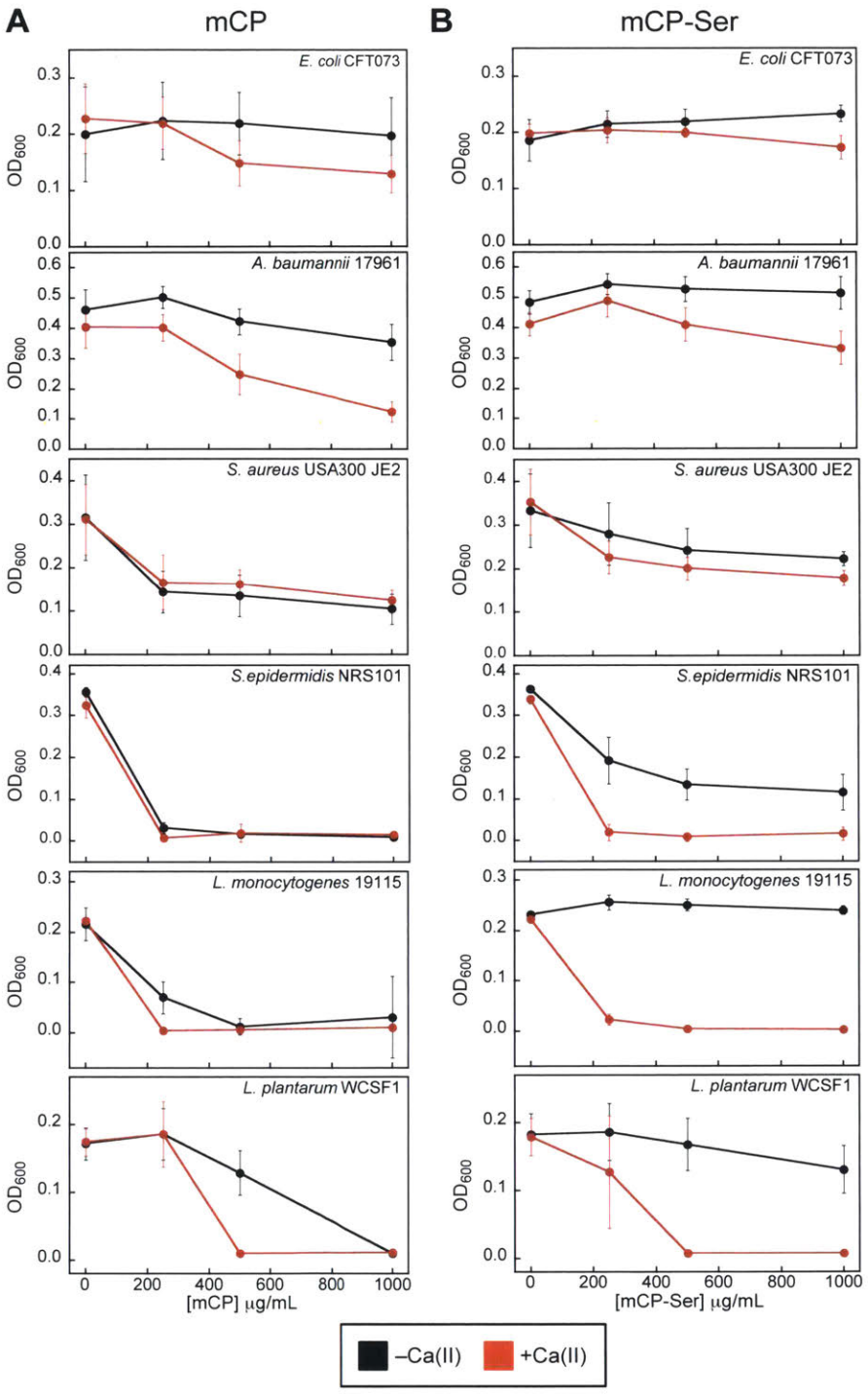

Figure 2.7. mCP inhibits growth of various bacterial species. (**A**) Growth inhibitory activity of mCP. (**B**) Growth inhibitory activity of mCP-Ser. Both proteins were assayed in the absence (black) and presence (red) of a 2-mM Ca(II) supplement in the AMA medium (Tris:TSB, T = 37 °C, 8 h) (mean ± SDM, $n \geq 3$).

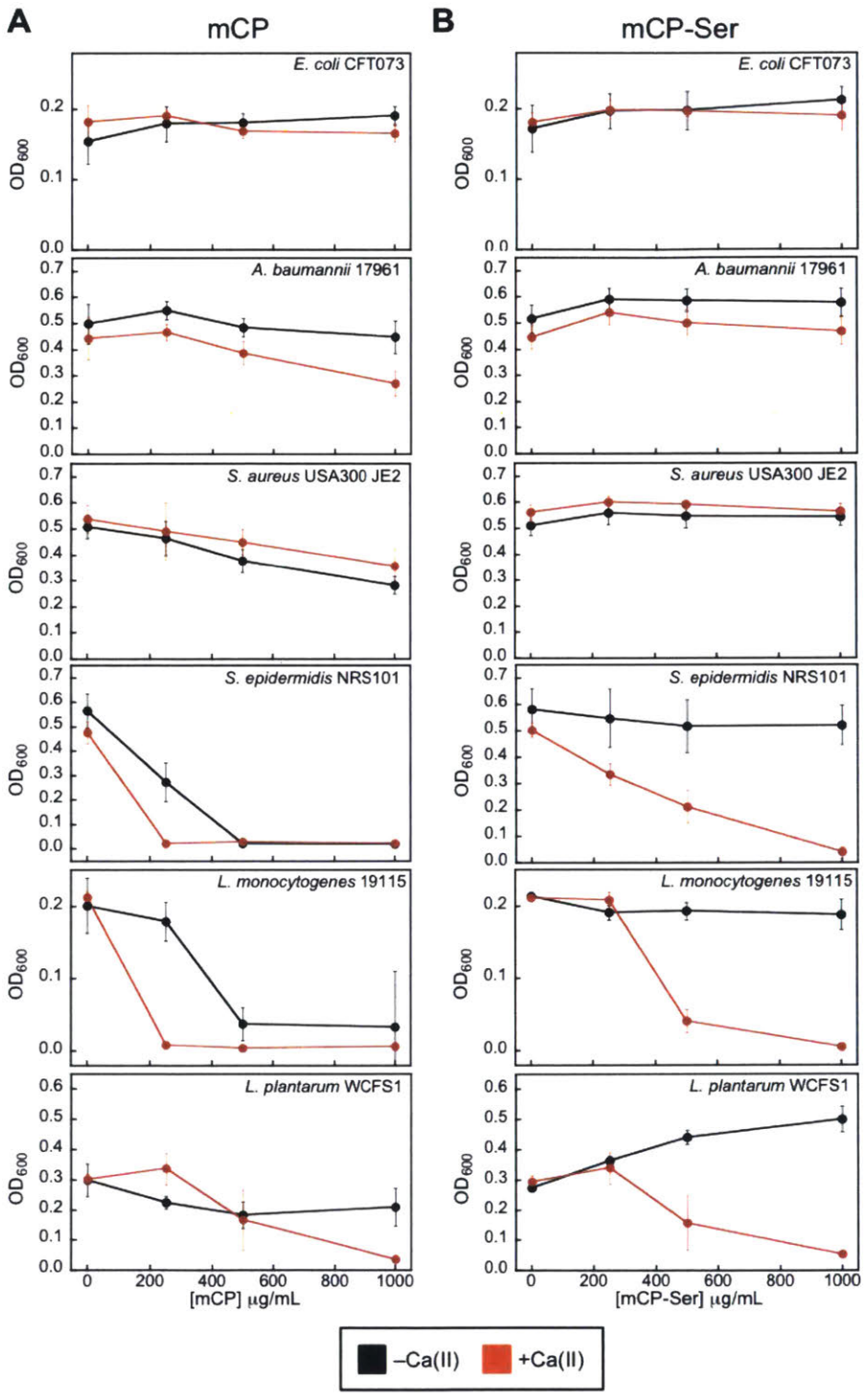

Figure 2.8. mCP inhibits growth of various bacterial species. (**A**) Growth inhibitory activity of mCP. (**B**) Growth inhibitory activity of mCP-Ser. Both proteins were assayed in the absence (black) and presence (red) of a 2-mM Ca(II) supplement in the AMA medium (Tris: TSB, T = 37 °C, 20 h) (mean ± SDM, $n \geq 3$).

Thus, we believe this initial study indicates that caution must be taken when employing mCP-Ser as a surrogate for the native protein. Prior studies of hCP and hCP-Ser reported that the Cys→Ser mutations have negligible effect on the growth inhibitory activity of the protein.[23]

2.5 Discussion

In this work, we report the purification and biochemical characterization of mCP, which provides a foundation for further studies of this protein. mCP can be readily obtained following overexpression of the mS100A8 and mS100A9 subunits in *E. coli* and reconstitution of the apo heterodimer, and in yields that will enable future biophysical and spectroscopic investigations of the protein. Preliminary characterization of mCP revealed that it has many comparable attributes to the human orthologue. Similar to hCP, Ca(II) ion binding causes two mCP heterodimers to self-associate and form a heterotetramer (**Figure 2.5**) and increases the stability of the protein to thermal denaturation (**Figure 2.4**). An initial evaluation of metal chelation by mCP demonstrates that it has the capacity to deplete multiple first-row transition metals ions – Mn, Fe, Ni, Cu, and Zn – from microbial growth medium, which is reminiscent of hCP (**Figure 2.6**). Moreover, this observation is in agreement with prior animal studies of infection, which indicate that mCP competes with microbes for Mn and Zn, as well as Cu.[7-10, 18] These data also suggest that mCP, like hCP, may contribute to the homeostasis of nutrient metals like Fe and Ni.[31, 35, 47] On the basis of the antibacterial activity assays presented in this work (**Figures 2.7, 2.8**), mCP appears to have broad-spectrum growth inhibitory activity. Both the metal-depletion and antibacterial activity assays indicate that Ca(II) ions modulate the functional properties of

mCP, enhancing transition metal affinities and growth inhibitory activity. These features are also reminiscent of hCP, and our prior investigations of hCP revealed that excess Ca(II) ions modulate its affinities for transition metal ions and antibacterial activity.[23, 30, 31]

This work also indicates some clear differences in the behavior of hCP and mCP that require further investigation as well as consideration in future experimental design and data interpretation. In particular, the current work reveals that, despite homology between the Ca(II)-binding loops in the S100A8 and S100A9 subunits of the human and murine polypeptides (**Figure 2.1**), mCP requires more equivalents of excess Ca(II) ions to fully tetramerize. The source of this disparity, and whether this decreased Ca(II) sensitivity has biological implications, is currently unknown and warrants examination. Extracellular Ca(II) ion concentrations are ≈2 mM,[46] and this work suggests that >200 equivalents of Ca(II) ions are required to fully tetramerize mCP. Thus, it is possible that full conversion to the heterotetramer is impaired at extracellular sites where the [Ca(II)] / [mCP] ratio is relatively low because mCP is abundant. We expect that further biophysical studies of mCP as well as *ex vivo* analyses of murine specimens will shed light on this matter.

We also examined the cysteine-null variant mCP-Ser. Because the hCP-Ser variant has been employed extensively in studies of the human orthologue, we reasoned that mCP-Ser could have comparable utility. Whereas both hS100A8 and mS100A8 have only one cysteine residue, which is conserved and located at position 42, the number and distribution of cysteine residues in the hS100A9 and mS100A9 differ. The human polypeptide contains only one cysteine at position 3, located two residues before an alternative translation start site defined by Met5. Neither Cys3 nor Met5 are found in

mS100A9. Rather, the murine polypeptide has three cysteine residues at positions 80, 91 and 111. mCP-Ser exhibited similar Ca(II)-dependent tetramerization and metal-depletion profiles to mCP. However, we routinely obtained lower yields of mCP-Ser from folding, observed that its stability to thermal denaturation was reduced, and found differences between mCP and mCP-Ser in the antibacterial assays where mCP-Ser often exhibited lower antibacterial activity and greater Ca(II) dependence than mCP (**Figures 2.7, 2.8**). Together, these observations indicate that one or more of the Cys→Ser mutations in mCP-Ser destabilize the protein and compromise its function to some degree.

In closing, mCP has played and will continue to play a prominent role in studies of the host response to microbial infection. The purification and biochemical characterization presented in this work provides a foundation for continued elucidation of the biological coordination chemistry of mCP and other biochemical investigations at the host/microbe interface. In particular, we anticipate that biochemical and biophysical evaluation of mCP will provide additional molecular level insights into current working models and metal withholding by the murine innate immune system.

2.6 Acknowledgements

We thank Dr. M. B. Brophy for preliminary studies of mCP. We gratefully acknowledge the NSF (CHE-1352132) and NIH (R01GM118695) for financial support. R. C. Hadley is a recipient of a R. R. Schrock Summer Fellowship. The ICP-MS instrument is housed in the MIT Center for Environmental Health Sciences Bioanalytical Core supported by NIH grant P30-ES002109. The MIT Biophysical Instrumentation Facility for the Study of Complex Macromolecular Systems is supported by NSF grant 0070319. The

staphylococcal strains were obtained from the Network on Antimicrobial Resistance in *Staphylococcus aureus* (NARSA) program supported under NIAID/NIH contract no. HHSN272200700055C.

2.7 References

1. Zimmer, D. B.; Eubanks, J. O.; Ramakrishnan, D.; Criscitiello, M. F. Evolution of the S100 family of calcium sensor proteins. *Cell Calcium* **2013,** *53*, 170-179.

2. Gifford, J. L.; Walsh, M. P.; Vogel, H. J. Structures and metal-ion-binding properties of the Ca^{2+}-binding helix-loop-helix EF-hand motifs. *Biochem. J.* **2007,** *405*, 199-221.

3. Zackular, J. P.; Chazin, W. J.; Skaar, E. P. Nutritional immunity: S100 proteins at the host-pathogen interface. *J. Biol. Chem.* **2015,** *290*, 18991-18998.

4. Cunden, L. S.; Nolan, E. M. Bioinorganic explorations of Zn(II) sequestration by human S100 host-defense proteins. *Biochemistry* **2018,** *57*, 1673-1680.

5. Zygiel, E. M.; Nolan, E. M. Transition metal sequestration by host-defense protein calprotectin. *Ann. Rev. Biochem.* **2018,** ASAP.

6. Hobbs, J. A. R.; May, R.; Tanousis, K.; McNeill, E.; Mathies, M.; Gebhardt, C.; Henderson, R.; Robinson, M. J.; Hogg, N. Myeloid cell function in MRP-14 (S100A9) null mice. *Mol. Cell. Biol.* **2003,** *23*, 2564-2576.

7. Corbin, B. D.; Seeley, E. H.; Raab, A.; Feldmann, J.; Miller, M. R.; Torres, V. J.; Anderson, K. L.; Dattilo, B. M.; Dunman, P. M.; Gerads, R.; Caprioli, R. M.; Nacken, W.; Chazin, W. J.; Skaar, E. P. Metal chelation and inhibition of bacterial growth in tissue abscesses. *Science* **2008,** *319*, 962-965.

8. Liu, J. Z.; Jellbauer, S.; Poe, A. J.; Ton, V.; Pesciaroli, M.; Kehl-Fie, T. E.; Restrepo, N. A.; Hosking, M. P.; Edwards, R. A.; Battistoni, A.; Pasquali, P.; Lane, T. E.; Chazin, W. J.; Vogl, T.; Roth, J.; Skaar, E. P.; Raffatellu, M. Zinc sequestration by the neutrophil protein calprotectin enhances *Salmonella* growth in the inflamed gut. *Cell Host Microbe* **2012,** *11*, 227-239.

9. Diaz-Ochoa, V. E.; Lam, D.; Lee, C. S.; Klaus, S.; Behnsen, J.; Liu, J. Z.; Chim, N.; Nuccio, S. P.; Rathi, S. G.; Mastroianni, J. R.; Edwards, R. A.; Jacobo, C. M.; Cerasi, M.; Battistoni, A.; Ouellette, A. J.; Goulding, C. W.; Chazin, W. J.; Skaar, E. P.; Raffatellu, M. *Salmonella* mitigates oxidative stress and thrives in the inflamed gut by evading calprotectin-mediated manganese sequestration. *Cell Host Microbe* **2016,** *19*, 814-825.

10. Hood, M. I.; Mortensen, B. L.; Moore, J. L.; Zhang, Y.; Kehl-Fie, T. E.; Sugitani, N.; Chazin, W. J.; Caprioli, R. M.; Skaar, E. P. Identification of an *Acinetobacter baumannii* zinc acquisition system that facilitates resistance to calprotectin-mediated zinc sequestration. *PLoS Pathog.* **2012,** *8*, e1003068.

11. Mortensen, B. L.; Rathi, S.; Chazin, W. J.; Skaar, E. P. *Acinetobacter baumannii* response to host-mediated zinc limitation requires the transcriptional regulator Zur. *J. Bacteriol.* **2014,** *196*, 2616-2626.

12. Juttukonda, L. J.; Chazin, W. J.; Skaar, E. P. *Acinetobacter baumannii* coordinates urea metabolism with metal import to resist host-mediated metal limitation. *mBio* **2016,** *7*, e01475-16.

13. Nairn, B. L.; Lonergan, Z. R.; Wang, J.; Braymer, J. J.; Zhang, Y.; Calcutt, M. W.; Lisher, J. P.; Gilston, B. A.; Chazin, W. J.; de Crecy-Lagard, V.; Giedroc, D. P.; Skaar, E.

P. The response of *Acinetobacter baumannii* to zinc starvation. *Cell Host Microbe* **2016,** *19*, 826-836.

14. Achouiti, A.; Vogl, T.; Endeman, H.; Mortensen, B. L.; Laterre, P. F.; Wittebole, X.; van Zoelen, M. A.; Zhang, Y.; Hoogerwerf, J. J.; Florquin, S.; Schultz, M. J.; Grutters, J. C.; Biesma, D. H.; Roth, J.; Skaar, E. P.; van 't Veer, C.; de Vos, A. F.; van der Poll, T. Myeloid-related protein-8/14 facilitates bacterial growth during pneumococcal pneumonia. *Thorax* **2014,** *69*, 1034-1042.

15. Gaddy, J. A.; Radin, J. N.; Loh, J. T.; Piazuelo, M. B.; Kehl-Fie, T. E.; Delgado, A. G.; Ilca, F. T.; Peek, R. M.; Cover, T. L.; Chazin, W. J.; Skaar, E. P.; Scott Algood, H. M. The host protein calprotectin modulates the *Helicobacter pylori cag* type IV secretion system via zinc sequestration. *PLoS Pathog.* **2014,** *10*, e1004450.

16. Clark, H. L.; Jhingran, A.; Sun, Y.; Vareechon, C.; de Jesus Carrion, S.; Skaar, E. P.; Chazin, W. J.; Calera, J. A.; Hohl, T. M.; Pearlman, E. Zinc and manganese chelation by neutrophil S100A8/A9 (calprotectin) limits extracellular *Aspergillus fumigatus* hyphal growth and corneal infection. *J. Immunol.* **2016,** *196*, 336-344.

17. Urban, C. F.; Ermert, D.; Schmid, M.; Abu-Abed, U.; Goosmann, C.; Nacken, W.; Brinkmann, V.; Jungblut, P. R.; Zychlinsky, A. Neutrophil extracellular traps contain calprotectin, a cytosolic protein complex involved in host defense against *Candida albicans*. *PLoS Pathog.* **2009,** *5*, e1000639.

18. Besold, A. N.; Gilston, B. A.; Radin, J. N.; Ramsoomair, C.; Culbertson, E. M.; Li, C. X.; Cormack, B. P.; Chazin, W. J.; Kehl-Fie, T. E.; Culotta, V. C. Role of calprotectin in withholding zinc and copper from *Candida albicans*. *Infect. Immun.* **2017,** *86*, e00779-17.

19. Juttukonda, L. J.; Berends, E. T. M.; Zackular, J. P.; Moore, J. L.; Stier, M. T.; Zhang, Y.; Schmitz, J. E.; Beavers, W. N.; Wijers, C. D.; Gilston, B. A.; Kehl-Fie, T. E.; Atkinson, J.; Washington, M. K.; Peebles, R. S.; Chazin, W. J.; Torres, V. J.; Caprioli, R. M.; Skaar, E. P. Dietary manganese promotes Staphylococcal infection of the heart. *Cell Host Microbe* **2017,** *22*, 531-542

20. Wakeman, C. A.; Moore, J. L.; Noto, M. J.; Zhang, Y.; Singleton, M. D.; Prentice, B. M.; Gilston, B. A.; Doster, R. S.; Gaddy, J. A.; Chazin, W. J.; Caprioli, R. M.; Skaar, E. P. The innate immune protein calprotectin promotes *Pseudomonas aeruginosa* and *Staphylococcus aureus* interaction. *Nat. Commun.* **2016,** *7*, 11951.

21. Korndörfer, I. P.; Brueckner, F.; Skerra, A. The crystal structure of the human $(S100A8/S100A9)_2$ heterotetramer, calprotectin, illustrates how conformational changes of interacting α-helices can determine specific association of two EF-hand proteins. *J. Mol. Biol.* **2007,** *370*, 887-898.

22. Hunter, M. J.; Chazin, W. J. High level expression and dimer characterization of the S100 EF-hand proteins, migration inhibitory factor-related proteins 8 and 14. *J. Biol. Chem.* **1998,** *273*, 12427-12435.

23. Brophy, M. B.; Hayden, J. A.; Nolan, E. M. Calcium ion gradients modulate the zinc affinity and antibacterial activity of human calprotectin. *J. Am. Chem. Soc.* **2012,** *134*, 18089-18100.

24. Damo, S. M.; Kehl-Fie, T. E.; Sugitani, N.; Holt, M. E.; Rathi, S.; Murphy, W. J.; Zhang, Y.; Betz, C.; Hench, L.; Fritz, G.; Skaar, E. P.; Chazin, W. J. Molecular basis for manganese sequestration by calprotectin and roles in the innate immune response to invading bacterial pathogens. *Proc. Natl. Acad. Sci.* **2013,** *110*, 3841-3846.

25. Gagnon, D. M.; Brophy, M. B.; Bowman, S. E.; Stich, T. A.; Drennan, C. L.; Britt, R. D.; Nolan, E. M. Manganese binding properties of human calprotectin under conditions of high and low calcium: X-ray crystallographic and advanced electron paramagnetic resonance spectroscopic analysis. *J. Am. Chem. Soc.* **2015,** *137*, 3004-3016.

26. Vogl, T.; Roth, J.; Sorg, C.; Hillenkamp, F.; Strupat, K. Calcium-induced noncovalently linked tetramers of MRP8 and MRP14 detected by ultraviolet matrix-assisted laser desorption/ionization mass spectrometry. *J. Am. Soc. Mass Spectrom.* **1999,** *10*, 1124-1130.

27. Strupat, K.; Rogniaux, H.; Van Dorsselaer, A.; Roth, J.; Vogl, T. Calcium-induced noncovalently linked tetramers of MRP8 and MRP14 are confirmed by electrospray ionization-mass analysis. *J. Am. Soc. Mass Spectrom.* **2000,** *11*, 780-788.

28. Vogl, T.; Leukert, N.; Barczyk, K.; Strupat, K.; Roth, J. Biophysical characterization of S100A8 and S100A9 in the absence and presence of bivalent cations. *Biochim. Biophys. Acta* **2006,** *1763*, 1298–1306.

29. Stephan, J. R.; Nolan, E. M. Calcium-induced tetramerization and zinc chelation shield human calprotectin from degradation by host and bacterial extracellular proteases. *Chem. Sci.* **2016,** *7*, 1962-1975.

30. Hayden, J. A.; Brophy, M. B.; Cunden, L. S.; Nolan, E. M. High-affinity manganese coordination by human calprotectin is calcium-dependent and requires the histidine-rich site formed at the dimer interface. *J. Am. Chem. Soc.* **2013,** *135*, 775-787.

31. Nakashige, T. G.; Zhang, B.; Krebs, C.; Nolan, E. M. Human calprotectin is an iron-sequestering host-defense protein. *Nat. Chem. Biol.* **2015,** *11*, 765-771.

32. Sohnle, P. G.; Collins-Lech, C.; Wiessner, J. H. Antimicrobial activity of an abundant calcium-binding protein in the cytoplasm of human neutrophils. *J. Infect. Dis.* **1991,** *163*, 187-192.

33. Sohnle, P. G.; Collins-Lech, C.; Wiessner, J. H. The zinc-reversible antimicrobial activity of neutrophil lysates and abscess fluid supernatants. *J. Infect. Dis.* **1991,** *164*, 137-142.

34. Clohessy, P. A.; Golden, B. E. Calprotectin-mediated zinc chelation as a biostatic mechanism in host-defense. *Scand. J. Immunol.* **1995,** *42*, 551-556.

35. Nakashige, T. G.; Zygiel, E. M.; Drennan, C. L.; Nolan, E. M. Nickel sequestration by the host-defense protein human calprotectin. *J. Am. Chem. Soc.* **2017,** *139*, 8828-8836.

36. Raftery, M. J.; Geczy, C. L. Identification of noncovalent dimeric complexes of the recombinant murine S100 protein CP10 by electrospray ionization mass spectrometry and chemical cross-linking. *J. Am. Soc. Mass Spectrom.* **1998,** *9*, 533-539.

37. Raftery, M. J.; Collinson, L.; Geczy, C. L. Overexpression, oxidative refolding, and zinc binding of recombinant forms of the murine S100 protein MRP14 (S100A9). *Protein Expr. Purif.* **1999,** *15*, 228-235.

38. Lackmann, M.; Cornish, C. J.; Simpson, R. J.; Moritz, R. L.; Geczy, C. L. Purification and structural analysis of a murine chemotactic cytokine (CP-10) with sequence homology to S100 proteins. *J. Biol. Chem.* **1992,** *267*, 7499-7504.

39. Raftery, M. J.; Harrison, C. A.; Alewood, P.; Jones, A.; Geczy, C. L. Isolation of the murine S100 protein MRP14 (14 kDa migration-inhibitory-factor-related protein) from

activated spleen cells: characterization of post-translational modifications and zinc binding. *Biochem. J.* **1996,** *316*, 285-293.

40. Kocher, M.; Kenny, P. A.; Farram, E.; Abdul Majid, K. B.; Finlay-Jones, J. J.; Geczy, C. L. Functional chemotactic factor CP-10 and MRP-14 are abundant in murine abscesses. *Infect. Immun.* **1996,** *64*, 1342-1350.

41. Mestas, J.; Hughes, C. C. W. Of mice and not men: differences between mouse and human immunology. *J. Immunol.* **2004,** *172*, 2731-2738.

42. Brophy, M. B.; Nakashige, T. G.; Gaillard, A.; Nolan, E. M. Contributions of the S100A9 C-terminal tail to high-affinity Mn(II) chelation by the host-defense protein human calprotectin. *J. Am. Chem. Soc.* **2013,** *135*, 17804-17817.

43. Nakashige, T. G.; Stephan, J. R.; Cunden, L. S.; Brophy, M. B.; Wommack, A. J.; Keegan, B. C.; Shearer, J. M.; Nolan, E. M. The hexahistidine motif of host-defense protein human calprotectin contributes to zinc withholding and its functional versatility. *J. Am. Chem. Soc.* **2016,** *138*, 12243-12251.

44. Cunden, L. S.; Gaillard, A.; Nolan, E. M. Calcium ions tune the zinc-sequestering properties and antimicrobial activity of human S100A12. *Chem. Sci.* **2016,** *7*, 1338-1348.

45. Cunden, L. S.; Brophy, M. B.; Rodriguez, G. E.; Flaxman, H. A.; Nolan, E. M. Biochemical and functional evaluation of the intramolecular disulfide bonds in the zinc-chelating antimicrobial protein human S100A7 (Psoriasin). *Biochemistry* **2017,** *56*, 5726-5738.

46. Brini, M.; Ottolini, D.; Cali, T.; Carafoli, E. Calcium in health and disease. *Met. Ions Life Sci.* **2013,** *13*, 81-137.

47. Nakashige, T. G.; Nolan, E. M. Human calprotectin affects the redox speciation of iron. *Metallomics* **2017,** *9*, 1086-1095.

Chapter 3: Murine Calprotectin Coordinates Mn(II) at a Hexahistidine Site with Ca(II)-dependent Affinity

This Chapter is adapted from *Inorg. Chem.* **2019**, *Just Accepted*.

3.1 Contributions

Dr. Derek Gagnon collected most of the EPR spectra and analyzed and plotted all of the EPR data. Dr. Andrew Ozarowski contributed to the collection and interpretation of the high-field EPR data.

3.2 Introduction

Transition metal ions are essential for many cellular processes including regulation, catalysis, and signaling.[1] During bacterial infection, the invading pathogen must obtain metal nutrients from the host. As a result, the competition for nutrient metal ions between host and pathogen is an important facet of the host-pathogen interaction.[1] In a process termed "nutritional immunity,"[1, 2] the host innate immune system deploys metal-sequestering proteins to lower available metal ion levels at infection sites in an effort to starve the invading pathogen.

Mn(II) sequestration is an important component of this host response to infection because many bacterial pathogens employ manganese-containing enzymes when colonizing the host.[3] Manganese-containing superoxide dismutases are expressed and utilized by bacterial pathogens to curb reactive oxygen species-mediated cell destruction.[3-8] Manganese is an important cofactor for enzymes involved in central metabolism, including class Ib ribonucleotide reductases, which produce deoxyribonucleotides from ribonucelotides.[9, 10] Additional metabolic enzymes, such as *Salmonella typhimurium* propionate kinase and *Escherichia coli* lactonase UlaG, have Mn(II)-dependent activity.[11, 12] The Mn(II)-dependent enzyme fructose 1,6-bisphosphatase II, involved in gluconeogenesis, is essential for virulence *in vivo* for the

intracellular pathogen *Francisella tularensis*.[13-15] Manganese enzymes also contribute to antibiotic resistance. In particular, the fosfomycin-inactivating enzyme FosB in *Staphylococcus aureus* and the ABC-F ATPase protein involved in antibiotic resistance in *Mycobacterium tuberculosis* both utilize Mn(II) cofactors.[16, 17] In order to obtain Mn(II), bacteria express ATP-binding cassette (ABC) transporters and natural resistance associated macrophage protein transporters (NRAMP, MntH in bacteria) that allow import of this nutrient. The importance of staphylococcal Mn(II) import systems MntABC and MntH has been highlighted in murine models of *S. aureus* infection.[18, 19] PsaABC, the Mn(II) import system in *Streptococcus pneumoniae*, is critical for infection in multiple model systems.[20] Furthermore, Mn(II) import systems are important for virulence in a number of other pathogens, including *Salmonella enterica* serovar Typhimurium, *Bacillus anthracis*, and *Enterococcus faecalus*.[21-23]

To date, the only known Mn(II)-sequestering host-defense protein is calprotectin (CP, S100A8/S100A9 oligomer, MRP8/MRP14 oligomer).[24] The role of CP in biology and infectious disease has been illuminated though many studies involving mouse models in which *S100A9*$^{-/-}$ (CP-deficient) mice are utilized.[25-30] In 2008, murine CP (mCP) was shown to reduce Mn(II) levels and limit *S. aureus* growth in murine liver abscesses.[26] This seminal work provided the first evidence for the ability of CP to sequester Mn(II) and inspired biochemical and biophysical investigations into the Mn(II)-binding properties of the protein.[8, 31-35] However, current understanding of the metal-binding properties of CP is almost exclusively based on evaluation of hCP, the human form of the protein, because this orthologue was the only one biochemically characterized until recently.[24]

hCP is a heterooligomer of the S100 proteins S100A8 (α subunit, 10.8 kDa) and S100A9 (β subunit, 13.2 kDa). Each subunit contains two Ca(II)-binding sites: one C-terminal canonical EF-hand and one N-terminal non-canonical EF-hand.[36] In the absence of Ca(II) ions, hCP exists as a heterodimer. Ca(II) binding to the EF-hand domains causes the self-association of two heterodimers to form a heterotetramer.[37] Each hCP heterodimer contains two distinct transition-metal-binding sites that form at the S100A8/S100A9 interface: a His_3Asp site (site 1) and a His_6 site (site 2). In the current working model, hCP is released from immune cells or epithelial cells at infection sites where it encounters high (~2 mM) extracellular Ca(II) levels and forms a heterotetramer.[37, 38] Tetramerization enhances the protease stability and transition-metal-ion affinities of hCP.[24] Biochemical, structural, and spectroscopic studies of Mn(II) coordination by hCP has provided a comprehensive molecular description of how the protein sequesters Mn(II).[31-35] Importantly, hCP employs a biologically unprecedented hexahistidine (His_6) motif to sequester Mn(II) and that the presence of excess Ca(II) ions lowers the apparent dissociation constant (K_d) by at least three orders of magnitude.[31-33,35] On the basis of all available data, Ca(II)-bound hCP coordinates Mn(II) with sub-nanomolar affinity at the His_6 site.[35] The His_3Asp site, in contrast, was found to have relatively low affinity for Mn(II) in the presence of Ca(II) ions (micromolar K_d assigned by room-temperature EPR spectroscopy); thus, it likely does not sequester Mn(II) in a physiological context.[31]

Given the utility and broad application of murine models in studying the biological function of CP, understanding the metal-binding properties of murine CP is important. Amino acid sequence alignment reveals similarities and differences between the human

and murine S100A8 and S100A9 subunits. The alignment indicates that the residues that compose sites 1 and 2 are conserved (**Figure 3.1A**), which suggests that hCP and mCP exhibit similar metal-binding properties and provides a working hypothesis that mCP employs a high-affinity His_6 motif to sequester divalent transition metal ions, including Mn(II). Nevertheless, hCP and mCP share ~56% amino acid identity, a lower value compared to the average of 85% amino acid identity between human and murine polypeptides.[39] This relatively large difference in primary structures suggests there may be some important structural and functional differences between the human and murine orthologues that warrant careful examination. Towards addressing the current knowledge gap about mCP, we recently reported initial biochemical characterization, which demonstrated that, similar to hCP, apo mCP exists as a mS100A8/mS100A9 heterodimer, and Ca(II) binding results in self-association to form a heterotetramer.[40] However, ~10-fold more Ca(II) equivalents were required to completely tetramerize mCP compared to hCP even though the two proteins exhibit similar Ca(II)-binding regions. This observation provided the first indication that the biophysical properties of hCP and mCP differ; the nature and extent of such differences requires further evaluation. Pertinent to the current study, our preliminary evaluation of the metal-binding ability of mCP demonstrated that mCP binds a number of transition metal ions, including Mn, present in a complex bacterial growth medium.[40]

In this work, we investigate the Mn(II)-binding properties of mCP. We report that mCP coordinates Mn(II) at a high-affinity His_6 site, displays Ca(II)-dependent Mn(II) affinity at this site, and that Mn(II) binding at the His_6 site confers tetramerization in the absence of Ca(II) ions. We also demonstrate that mCP can outcompete the solute-

binding proteins staphylococcal MntC and streptococcal PsaA for Mn(II) under conditions of high Ca(II). As expected based on prior animal studies, these Mn(II)-binding studies are consistent with a role of mCP in Mn(II) sequestration in the host-pathogen interaction. Furthermore, this study emphasizes an important similarity in the Mn(II)-binding capability between human and murine host-defense proteins that is a significant contributor during infection.

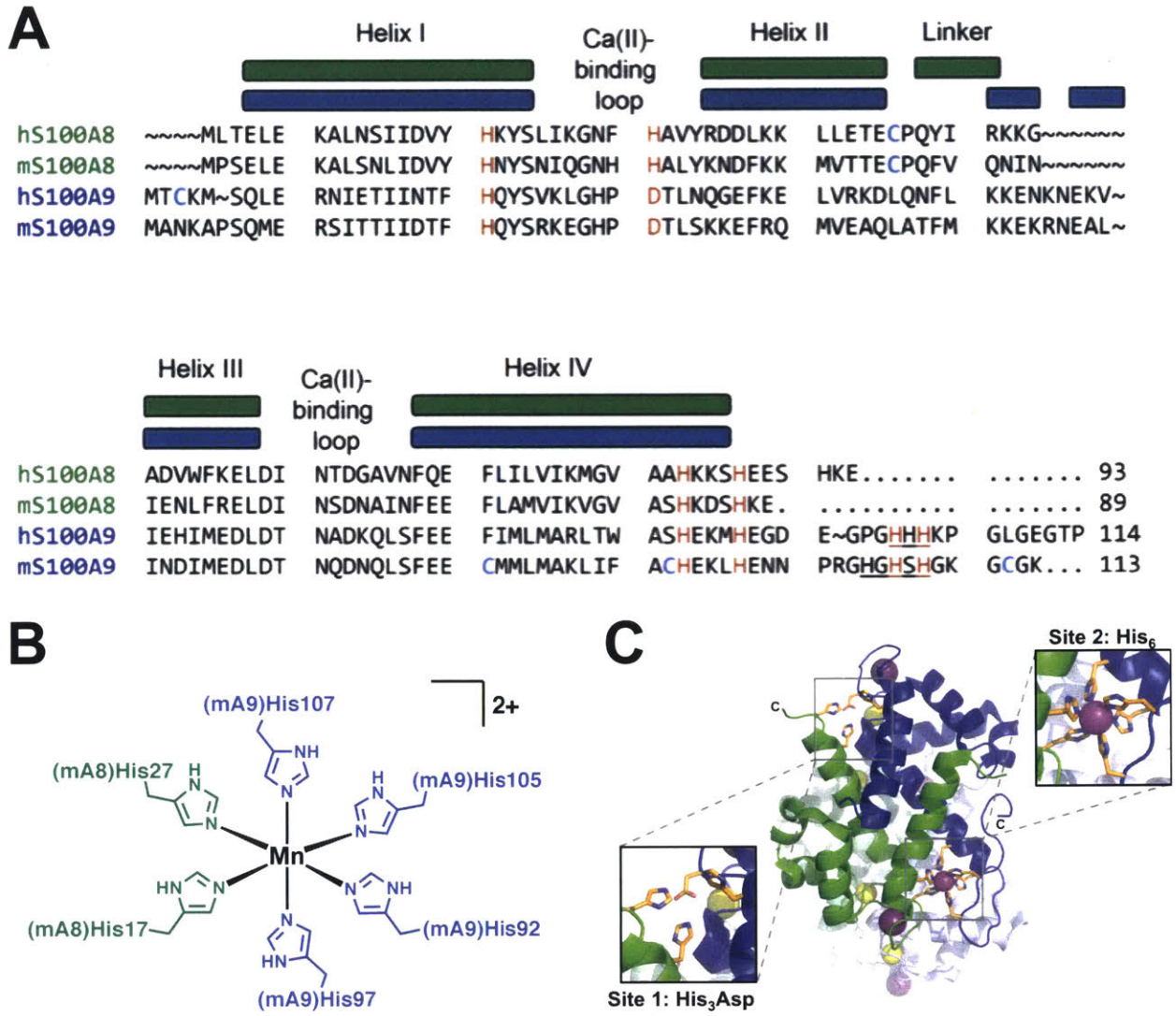

Figure 3.1. Overview of primary structure and putative His_6 metal-binding site of mCP. **(A)** Amino acid sequence alignment of human (h) and murine (m) S100A8 and S100A9 subunits of CP. The Ca(II)-binding regions are indicated, and the conserved transition-metal-binding residues are shown in red. Cysteine residues are shown in blue, and the S100A9 C-terminal tail regions containing His residues are underlined. The secondary structural elements represented are for the human subunits. **(B)** Predicted His_6 site of mCP based on sequence alignment of the human and murine S100A8 and S100A9 subunits. A coordinated Mn(II) ion is shown. (**C**) Crystal structure of the Mn(II)-, Ca(II)-, and Na(I)-bound human calprotectin heterotetramer (PDB: 4XJK).[33] One heterodimer shows the S100A8 subunit in green and the S100A9 subunit in blue, and the other heterodimer is colored gray. Metal ions are shown as spheres: Mn(II) is magenta, Ca(II) is yellow, and Na(I) is purple.

3.3 Experimental Section

3.3.1 General Materials and Methods

All chemicals were purchased from commercial suppliers and used as received. Milli-Q (18.2 MΩ·cm) water was used in the preparation of all buffers and metal ion solutions. Buffers used for biochemical and spectroscopic experiments were prepared from ULTROL grade HEPES (CalBiochem) and TraceSelect NaCl to limit metal ion contamination from buffer components. Buffers for analytical SEC were prepared with $CaCl_2 \cdot 2H_2O$ (>99.0%, MilliporeSigma). All buffers were filtered (0.2 μm) before use. Stock solutions of Ca(II) (1 M, 100 mL) were prepared from $CaCl_2 \cdot 2H_2O$ (>99.0%, MilliporeSigma) in acid-washed volumetric glassware and stored in polypropylene tubes. Stock solutions of Mn(II) (1 M, 100 mL) were prepared from $MnCl_2 \cdot 4H_2O$ (99.999%, Alfa Aesar) in acid-washed volumetric glassware and stored in polypropylene tubes. Working solutions of metal ions were prepared daily by dilution into MIlli-Q water and stored in polypropylene tubes. Protein aliquots were stored at -80 °C and thawed only once prior to use. All protein concentrations were determined using calculated extinction coefficients (https://web.expasy.org/protparam/). All CP concentrations are for the heterodimer form of mCP (mS100A8/mS100A9, ε_{280} = 5,960 M^{-1} cm^{-1}) or hCP-Ser (hS100A8/hS100A9 ε_{280} = 18,450 M^{-1} cm^{-1}). The solute-binding proteins MntC (ε_{280} = 35,870 M^{-1} cm^{-1}) and PsaA (ε_{280} = 35,870 M^{-1} cm^{-1}) are monomers and concentrations of these proteins are for the monomer.

3.3.2 Design of Synthetic Genes

The synthetic genes containing the nucleotide sequences of mS100A8 and mS100A9 and all variants were ligated into the *Nde*I and *Xho*I restriction sites of the pET41a vector, as described previously.[40] Synthetic genes for *mS100A8(H17A)(H27A)*, *mS100A8(H83A)(H87A)*, *mS100A9(H21A)(D31A)*, and *mS100A9(H92A)(H97A)* were codon-optimized for *Escherichia coli* expression, synthesized, and ligated into the *Nde*I and *Xho*I restriction sites of pET41a vectors by ATUM (formerly DNA2.0). Each plasmid was transformed into chemically-competent *E. coli* TOP10 cells (ThermoFisher), isolated using a miniprep kit (Qiagen), and analyzed by DNA sequencing (Quintara Biosciences). The pET41a vectors containing *mS100A8(H103A), mS100A9(H105A), mS1009(H107A), mS100A9(H103A)(H105A), mS100A9(H103A)(H107A),* and *mS100A9(H105A)(H107A)* genes were prepared by site-directed mutagenesis as described below.

E. coli optimized nucleotide sequence for ***Nde*I**-mS100A8(H17A)(H27A)-Stop-***Xho*I**:
CAT ATG CCG AGC GAA CTG GAG AAA GCA CTG AGC AAC CTG ATC GAC GTC TAC GCG AAC TAC AGC AAT ATT CAA GGT AAT CAT GCG GCT CTG TAC AAA AAT GAT TTC AAG AAG ATG GTT ACC ACG GAG TGC CCG CAG TTC GTG CAG AAT ATC AAC ATT GAA AAC CTG TTC CGT GAG CTG GAC ATC AAC TCC GAT AAT GCC ATT AAC TTT GAA GAG TTT TTG GCG ATG GTT ATC AAA GTG GGC GTC GCG AGC CAC AAG GAC TCT CAT AAA GAG **TAA** CTC GAG

Translated sequence for ***Nde*I**-mS100A8(H17A)(H27A)-Stop-***Xho*I**:
M P S E L E K A L S N L I D V Y A N Y S N I Q G N H A A L Y K N D F K K M V T T E C P Q F V Q N I N I E N L F R E L D I N S D N A I N F E E F L A M V I K V G V A S H K D S H K E Stop **L E**

E. coli optimized nucleotide sequence for ***Nde*I**-mS100A8(H83A)(H87A)-Stop-***Xho*I**:
CAT ATG CCG AGC GAA CTG GAG AAA GCA CTG AGC AAC CTG ATC GAC GTC TAC CAC AAC TAC AGC AAT ATT CAA GGT AAT CAT CAC GCT CTG TAC AAA AAT GAT TTC AAG AAG ATG GTT ACC ACG GAG TGC CCG CAG TTC GTG CAG AAT ATC AAC ATT GAA AAC CTG TTC CGT GAG CTG GAC ATC AAC TCC GAT

AAT GCC ATT AAC TTT GAA GAG TTT TTG GCG ATG GTT ATC AAA GTG GGC GTC GCG AGC GCG AAG GAC TCT GCG AAA GAG **TAA** CTC GAG

Translated sequence for ***Nde*I**-mS100A8(H83A)(H87A)-Stop-***Xho*I**:
M P S E L E K A L S N L I D V Y H N Y S N I Q G N H H A L Y K N D F K K M V T T E C P Q F V Q N I N I E N L F R E L D I N S D N A I N F E E F L A M V I K V G V A S A K D S A K E Stop **L E**

E. coli optimized nucleotide sequence for ***Nde*I**-mS100A9(H21A)(D31A)-Stop-***Xho*I**:
CAT ATG GCG AAC AAA GCA CCT AGC CAA ATG GAA CGC AGC ATC ACT ACT ATC ATC GAC ACT TTT GCG CAA TAC TCT CGT AAA GAG GGC CAC CCG GCG ACG CTG TCC AAG AAA GAG TTC CGC CAG ATG GTT GAG GCC CAG CTG GCG ACC TTT ATG AAG AAA GAA AAA CGT AAC GAG GCA CTG ATT AAC GAC ATT ATG GAA GAT CTG GAC ACC AAT CAA GAT AAT CAG CTG AGC TTC GAA GAG TGC ATG ATG CTG ATG GCG AAG TTG ATT TTC GCT TGC CAC GAG AAG CTG CAT GAA AAC AAT CCG CGT GGT CAT GGT CAC AGC CAC GGT AAG GGT TGT GGC AAA **TAA** CTC GAG

Translated sequence for ***Nde*I**-mS100A9(H21A)(D31A)-Stop-***Xho*I**:
M A N K A P S Q M E R S I T T I I D T F A Q Y S R K E G H P A T L S K K E F R Q M V E A Q L A T F M K K E K R N E A L I N D I M E D L D T N Q D N Q L S F E E C M M L M A K L I F A C H E K L H E N N P R G H G H S H G K G C G K Stop **L E**

E. coli optimized nucleotide sequence for ***Nde*I**-mS100A9(H92A)(H96A)-Stop-***Xho*I**:
CAT ATG GCG AAC AAA GCA CCT AGC CAA ATG GAA CGC AGC ATC ACT ACT ATC ATC GAC ACT TTT CAT CAA TAC TCT CGT AAA GAG GGC CAC CCG GAT ACG CTG TCC AAG AAA GAG TTC CGC CAG ATG GTT GAG GCC CAG CTG GCG ACC TTT ATG AAG AAA GAA AAA CGT AAC GAG GCA CTG ATT AAC GAC ATT ATG GAA GAT CTG GAC ACC AAT CAA GAT AAT CAG CTG AGC TTC GAA GAG TGC ATG ATG CTG ATG GCG AAG TTG ATT TTC GCT TGC GCG GAG AAG CTG GCG GAA AAC AAT CCG CGT GGT CAT GGT CAC AGC CAC GGT AAG GGT TGT GGC AAA **TAA** CTC GAG

Translated sequence for ***Nde*I**-mS100A9(H92A)(H96A)-Stop-***Xho*I**:
M A N K A P S Q M E R S I T T I I D T F H Q Y S R K E G H P D T L S K K E F R Q M V E A Q L A T F M K K E K R N E A L I N D I M E D L D T N Q D N Q L S F E E C M M L M A K L I F A C A E K L A E N N P R G H G H S H G K G C G K Stop **L E**

Mutations are highlighted in yellow. A *Nde*I restriction site was placed at the 5' end and a stop codon and a *Xho*I restriction site was placed at the 3' end (underlined above). Nucleotide sequences above are displayed from 5' to 3'.

3.3.3 Site-directed Mutagenesis

The His→Ala point mutations in the mS100A9 gene were prepared by site-directed mutagenesis using the primer pairs and templates listed in **Table 3.1.** The oligonucleotide primers were synthesized by Integrated DNA Technologies (Coralville, IA). A modified Quick-Change site-directed mutagenesis protocol was used to generate the variants using Pfu Turbo DNA polymerase (Agilent). The PCR protocol was 95 °C for 30 s; 95 °C for 30 s, 60–66 °C for 1 min, 68 °C for 12 min (25x); 4 °C hold temperature. *Dpn*I (New England Biolabs) was used to degrade the template plasmid. A 0.75-μL aliquot was added to the sample and incubated at 37 °C for 3 h. At 1.5 h into the incubation, a supplemental 0.75-μL aliquot of *Dpn*I was added. The remaining plasmid DNA was transformed into chemically-competent *E. coli* TOP10 cells and the resulting plasmids isolated using miniprep kit (Qiagen) and analyzed by DNA sequencing (Quintara Biosciences).

Table 3.1. Primers and templates for site-directed mutagenesis.[a]

Primer	Sequence	Template,[b] Temp.[c]
mA9(H103A)-1	5'-GAAAACAATCCGCGTGGT**GCT**GGTCACAGCCACGGTAAG-3'	*mA9*,
mA9(H103A)-2	5'-CTTACCGTGGCTGTGACC**AGC**ACCACGCGGATTGTTTTC-3'	60 °C
mA9(H105A)-1	5'-CAATCCGCGTGGTCATGGT**GCC**AGCCACGGTAAGGGTTGTG-3'	mA9,
mA9(H105A)-2	5'-CACAACCCTTACCGTGGCT**GGC**ACCATGACCACGCGGATTG-3'	61 °C
mA9(H107A)-1	5'-GGTCATGGTCACAGC**GCC**GGTAAGGGTTGTGGC-3'	mA9
mA9(H107A)-2	5'-GCCACAACCCTTACC**GGC**GCTGTGACCATGACC-3'	66 °C
mA9(H103A)(H105A)-1	5'-GAAAACAATCCGCGTGGT**GCT**GGTGCCAGCCACGGTAAG-3'	*mA9(H105A)*
mA9(H103A)(H105A)-2	5'-CTTACCGTGGCTGGCACC**AGC**ACCACGCGGATTGTTTTC-3'	63 °C
mA9(H103A)(H107A)-1	5'-GAAAACAATCCGCGTGGT**GCT**GGTCACAGCGCC-3'	*mA9(H107A)*
mA9(H103A)(H107A)-2	5'-GGCGCTGTGACC**AGC**ACCACGCGGATTGTTTTC-3'	63 °C
mA9(H105A)(H107A)-1	5'-GTGGTCATGGTGCCAGC**GCC**GGTAAGGGTTGTG-3'	*mA9(H105A)*
mA9(H105A)(H107A)-2	5'-CACAACCCTTACC**GGC**GCTGGCACCATGACCAC-3'	63 °C

[a] Bold codons indicate the mutation added. Underlined codons indicate a pre-existing mutation in the template plasmid relative to mS100A9. [b] Annealing temperature used in the PCR reaction.

3.3.4 Protein Overexpression and Purification

mCP and variants were overexpressed and purified as described previously.[40] The SBPs MntC and PsaA were overexpressed and purified as described previously.[35] hCP-Ser was also overexpressed and purified as described previously.[37] Globally ^{15}N-labeled mCP was prepared using reported procedures for hCP-Ser.[33] In brief, M9 minimal media (2 L) for overexpression was prepared with $^{15}NH_4Cl$ as the nitrogen source. The medium was sterilized and 1 L was added to each of two sterile 2-L baffled flasks. Immediately before use, 1 mL 1,000x vitamin mix (400 mg choline chloride, 500 mg folic acid, 1.1 g pantothenic acid, 500 mg nicotinamide, 500 mg myo-inositol, 500 mg pyridoxal·HCl, 500 mg thiamine·HCl, and 50 mg riboflavin in 15 mL of Milli-Q water)

was added to each flask along with a few flakes each of $FeCl_3$ (MilliporeSigma), biotin (Alfa Aesar), and thiamine-HCl (MilliporeSigma). Next, kanamycin was added to 50 μg/mL. A 20-mL aliquot of a saturated culture of BL21(DE3) cells containing either pET41a-*mS100A8* or pET41a-*mS100A9* was pelleted and resuspended in minimal media (25 mL). The centrifugation and resuspension steps were repeated again before the cell suspension were used to inoculate the culture media for overexpression. The overexpression was performed as described previously for mCP, with induction at OD_{600} = 0.6.[40] The ^{15}N-labeled protein was reconstituted and purified as described previously for mCP.[40] For all protein variants prepared, yields ranged from ≈14-60 mg / 2 L culture.

3.3.5 Analytical Size Exclusion Chromatography (SEC)

An ÄKTA Purifier FPLC system housed in a cold room (4 °C) and outfitted with a Superdex 75 10/300 GL SEC column was used for all analytical SEC. The running buffer was 75 mM HEPES, pH 7.0, 100 mM NaCl, 200 μM TCEP ± 25 mM Ca(II). Mn(II) (500 μM or 5 mM) was added to samples from a 1-M stock solution and the samples were incubated at room temperature for at least 15 min prior to SEC analysis. The column was calibrated with blue dextran and a low-molecular-weight protein mixture (GE Healthcare Life Sciences) consisting of ribonuclease A (13.7 kDa), carbonic anhydrase (29 kDa), ovalbumin (44 kDa), and conalbumin (75 kDa) prior to use. Proteins were buffer-exchanged (3x) into the running buffer using an Amicon spin filter (0.5 mL, 10 kDa MWCO). Samples (100 μM, 300 μL) were prepared and loaded into a 100-μL injection loop, and the FLPC system was programmed to inject 500 μL of sample onto the column. The samples were eluted over one column volume (24 mL) at

a flow rate of 0.5 mL/min. At least two independent replicates were performed for each experiment, and representative data from one experiment are shown. The protein concentration in the collected fractions was determined by absorbance at 280 nm in acid-washed quartz cuvettes using a Beckman DU 800 UV-Vis spectrophotometer equipped with a Peltier thermostat. To prepare ICP-MS samples for total Mn analyses, an aliquot (50 μL) of each fraction was diluted to 2 mL with 5% nitric acid (TraceSELECT, Fluka) and supplemented with 2 ppb Tb internal standard.

3.3.6 Liquid Chromatography-Mass Spectrometry (LC-MS)

An Agilent 6545 series Q-TOF LC-MS system with an Agilent Eclipse plus C18 with 2.1 X 50 mm and 1.8-μm particle size was used for all analyses. Each protein was diluted in Milli-Q water to a final concentration of ≈10 μM. A 5- or 10-μL protein aliquot was injected onto the column, and each sample was eluted using a gradient of 25–75% B over 10 min with a flow rate of 0.3 mL/min (solvent A: 0.1% formic acid in water; solvent B: 0.1% formic acid in acetonitrile). The spectra were deconvoluted using the maximum entropy algorithm in the MassHunter Bioconfirm software (Agilent).

3.3.7 Inductively-coupled Plasma Mass Spectrometry (ICP-MS)

The metal content of protein samples was determined using an Agilent 7900 ICP-MS with an autosampler housed in the Center for Environmental Health Sciences Bioanalytical Core Facility at MIT. The instrument was used in helium mode. Calibration standards were prepared from a serial dilution of the Environmental Standard calibration mixture (Agilent, part #5183-4688). Standards and samples were spiked with 2 ppb Tb

(100 ppb stock in 5% nitric acid) internal standard (Agilent, part # 5190-8590). Sample volumes of either 1.7 or 2.0 mL were employed.

3.3.8 Circular Dichroism Spectroscopy

Circular dichroism (CD) spectra were collected using a Jasco J-500 spectrometer housed in the Biophysical Instrumentation Facility at MIT. Proteins were buffer-exchanged into CD buffer (1 mM Tris-HCl, pH 7.5, 1 mM DTT) prior to analysis. For samples containing Ca(II), an aliquot was added to the sample from a 1 M Ca(II) stock solution to afford 3 mM Ca(II) in the sample. Samples (10 μM, 300 μL) were transferred to a Hellma quartz cuvette (1-mm pathlength) for analysis. Spectra were collected from 195 to 260 nm using continuous scan mode (50 nm/min) and 1 nm bandwidth. Data represent averages of triplicate baseline-subtracted scans.

3.3.9 Fluorescence Titrations

Zinpyr-1 (ZP1) was synthesized as described previously[41] and provided by Dr. Jacob Goldberg and Prof. Stephen J. Lippard. Stock solutions of ZP1 (~3 mM) were prepared in anhydrous DMSO, aliquoted, and stored at -20 °C. Each aliquot was thawed only once. Titrations were performed using 75 mM HEPES, 100 mM NaCl, pH 7.0 buffer. Mn(II) competition titrations between ZP1 and mCP (or variant) were performed as described previously for the hCP variants.[31] In brief, aliquots of protein were thawed and subsequently buffer-exchanged using 0.5-mL Amicon spin filters (10 kDa MWCO). For each titration, a 2-mL solution of titration buffer containing ZP1 (1 μM) and protein (4 μM) was prepared in a 1-cm path length nitric acid-washed quartz

cuvette. Ca(II) (1.2 mM) was added from a 1-M stock solution (2.4 μL). The mixture was titrated with Mn(II) (2 or 4 μL of a 500-μM Mn(II) solution in Milli-Q water). After each Mn(II) addition, the solution was gently mixed and incubated for ~10 min at room temperature and in the dark prior to recording the fluorescence emission. For the Ca(II) titration, protein (4 μM) and Mn(II) (4 μM) were pre-incubated for ~10 min prior to titration of Ca(II) (2-μL additions of either 20 mM or 250 mM Ca(II)) into the sample.

Emission spectra were collected on a Photon Technologies International QuantaMaster 40 fluorimeter outfitted with a continuous xenon source for excitation, autocalibrated QuadraScopic monochromators, a multimode PMT detector, and a circulating water bath maintained at 25 °C. This instrument was controlled by the FelixGX software package. The excitation wavelength was 490 nm. The emission spectra were collected and integrated over 500–650 nm.

3.3.10 EPR Spectroscopy

To prepare mCP samples for EPR spectroscopy, all protein samples were buffer-exchanged into 75 mM HEPES, 100 mM NaCl, pH 7.5. For X-band EPR spectroscopy, 200 μM protein was prepared with 180 μM Mn(II) in the absence or presence of 60 mM Ca(II). Samples (500 μL) were incubated for at least 15 min prior to being frozen in liquid nitrogen. Most protein samples were shipped in a liquid nitrogen dewar to CalEPR, UC Davis for analysis. For 388 GHz EPR spectroscopy, a sample (500 μL) of mCP (500 μM) was incubated with Ca(II) (50 mM) and Mn(II) (450 μM) for at least 15 min, transferred to a 1-mL LDPE vial (Fisher Scientific), frozen in liquid nitrogen, and shipped on dry ice to the National High Magnetic Field Laboratory (Tallahassee, FL) for

analysis. To evaluate the competition for Mn(II) between mCP and SBPs, mixed samples of SBP and mCP were prepared as described previously, with the exception that 60 mM Ca(II) was added for the +Ca(II) samples.[35] A 1:1 Mn(II):SBP sample (1 mM each) was prepared along with an mCP sample (1 mM) that contained Ca(II) (120 mM). Following ~15 min incubation, aliquots of each solution were mixed in a 1:1 ratio and allow to equilibrate for ~14 h at room temperature. These samples (170 μL) were subsequently frozen in liquid nitrogen and stored at -80 °C prior to analysis at MIT using instrumentation in the Department of Chemistry Instrumentation Facility.

At CalEPR, continuous wave (CW) X-band (ca. 9.38 GHz) EPR spectra were collected on a Bruker ELEXSYS E500 CW-EPR spectrometer with a super high QE (SHQE) resonator and an Oxford Instruments ESR900 liquid helium cryostat. Spectra were collected under slow-passage conditions so as not to distort the line shape. The spectrometer conversion time was set to 80 ms and a data point collected every ca. 0.3 mT with 0.5 mT modulation amplitude at 100 kHz. Spectra were collected at a temperature of 10 K.

At CalEPR, Q-band (ca. 34.1 GHz) spectra were collected on a Bruker ELEXSYS E580 X/Q-band pulse EPR spectrometer equipped with an Oxford Instrument CF935 liquid helium cryostat and a home-built probe.[42] Field sweeps were acquired using a 2-pulse Hahn echo sequence ($\pi/2 - \tau - \pi - \tau -$ echo) with a 2-step phase cycling program and data were collected every 0.3 mT. ^{15}N electron nuclear double resonance (ENDOR) spectra were collected using the Mims ENDOR sequence ($\pi/2 - \tau - \pi/2 - \pi_{RF} - \pi/2 - \tau -$ echo).[43] The 50-μs long π_{RF} pulse was amplified using an ENI A1000 amplifier providing 1 kW peak power. The shot repetition time was 1 ms at 10 K for all pulse sequences.

At CalEPR, D-band (ca. 130 GHz) spectra were collected on a home-built spectrometer described elsewhere.[44] Field sweeps were acquired with the 2-pulse Hahn echo sequence described above. The main coil field was set to 4.63 T ($g \approx 2$ for 130 GHz) and a separate sweep coil was used to sweep from −100 mT to +100 mT with data recorded every 0.1 mT. Scans were collected in the forward and reverse directions to verify that there were no passage effects. Field sweeps were calibrated against MgO with a Mn(II) impurity (>95% fused MgO, Aldrich) which has a g value of 2.00100(5) and ^{55}Mn hyperfine coupling constant of −243.6(5) MHz.[45, 46] The temperature was set to 10 K using an Oxford Instruments Spectrostat NMR cryostat.

At the National High Magnetic Field Lab, the transmission spectrometer was utilized to obtain a 388 GHz field sweep of Mn(II)-mCP in the presence of excess Ca(II). The temperature was 30 K with a modulation amplitude of 0.5 mT at 50 kHz, and downfield sweep rate 0.50 mT/s.

At MIT, X-band EPR spectra investigating the Mn(II) competition between mCP and SBPs was performed on a Bruker EMXplus spectrometer equipped with a ER4119HS resonator and a ColdEdge Technologies 4K waveguide cryogen-free cryostat. The spectrometer conversion time was set to 7.2 ms and a data point collected every ca. 0.1 mT with 0.5 mT modulation amplitude at 100 kHz. Spectra were collected at 10 K.

3.3.11 EPR Data Analysis

All spectra were simulated in Matlab R2017a (the Mathworks, Inc.) using the freely available EasySpin toolbox.[47] The EPR spectrum can be interpreted using the phenomenological Spin Hamiltonian below.

$$\hat{H} = \beta_e \hat{B} \cdot g \cdot \hat{S}/h + \sum_i \left(\hat{S} \cdot A_i \cdot \hat{I}_i - \beta_n g_{n,i} \hat{B} \cdot \hat{I}_i\right) + \hat{S} \cdot D \cdot \hat{S}$$

The terms in the Hamiltonian are the electron Zeeman interaction with an applied static magnetic field $\boldsymbol{B}$, the electron–nuclear hyperfine tensor $\boldsymbol{A_i}$, the nuclear Zeeman interaction, and the zero-field-splitting (ZFS) tensor $\boldsymbol{D}$ for the high-spin Mn(II) ion (S = 5/2). β_e and β_n are the Bohr magneton and nuclear, magneton respectively; g and g_n are the electron and nuclear *g* factors, respectively; h is the Planck constant.

3.4 Results and Discussion

3.4.1 Preparation and Biochemical Characterization of mCP Metal-binding Site Variants

We first designed protein variants to probe the amino acid residues in mS100A8 and mS100A9 predicted to be important for Mn(II) binding. Because the metal-binding site residues are conserved in hCP and mCP, we prepared and characterized variants with mutations that disrupted either the putative His_3Asp site (ΔHis_3Asp; mS100A8(H83A)(H87A)/mS100A9(H21A)(D31A)) or four residues of the putative His_6 site (ΔHis_4; mS100A8(H17A)(H27A)/mS100A9(H92A)(H97A)) (**Figure 3.1**, **Table 3.2**). The C-terminal tail of mS100A9 contains an HXHXH motif spanning residues 103-107. To evaluate whether these His residues contribute to Mn(II) binding, we prepared variants with one or two His→Ala mutations in this region (**Tables 3.1, 3.2, 3.3**). Following overexpression of each subunit in *E. coli* and reconstitution of the mCP

heterodimers according to a reported protocol,[40] the variants were characterized by inductively-coupled plasma mass spectrometry (ICP-MS), sodium docecyl sulfate polyacrylamide gel electrophoresis (SDS-PAGE), liquid chromatography-mass spectrometry (LC-MS), circular dichroism (CD) spectroscopy, and analytical size exclusion chromatography (SEC) (**Tables 3.4-3.7, Figures 3.2-3.4**). ICP-MS and SDS-PAGE analyses indicated that the proteins were isolated in the apo form (**Tables 3.5, 3.6**) and in high purity (**Figure 3.2**), respectively. LC-MS analysis demonstrated that the mS100A8 subunits displayed partial loss of the initiator methionine, whereas mS100A9 subunits lacked this residue (**Table 3.4**). Cleavage of Met1 is a common post-translational modification observed during heterologous overexpression in *E. coli*.[48] All variants afforded CD spectra consistent with an α-helical fold in the presence and absence of Ca(II) (**Figure 3.3**). Lastly, analytical SEC established that the purified proteins were isolated as heterodimers, as indicated by elution volumes of 12.0–12.1 mL (**Table 3.7, Figure 3.4**). In the presence of excess Ca(II) ions in the running buffer, the peak for each variant displayed a shift to a lower elution volume (11.3–11.4 mL), consistent with Ca(II)-induced tetramerization and our prior characterization of mCP **(Table 3.7, Figure 3.4)**.[40]

Table 3.2. Compositions of murine calprotectin (mCP) variants.

Protein	mS100A8 subunit	mS100A9 subunit
mCP	mS100A8	mS100A9
mCPΔHis$_3$Asp	mS100A8(H83A)(H87A)	mS100A9(H21A)(D31A)
mCPΔHis$_4$	mS100A8(H17A)(H27A)	mS100A9(H92A)(H97A)
mCP(H103A)	mS100A8	mS100A9(H103A)
mCP(H105A)	mS100A8	mS100A9(H105A)
mCP(H107A)	mS100A8	mS100A9(H107A)
mCP(H103A)(H105A)	mS100A8	mS100A9(H103A)(H105A)
mCP(H103A)(H107A)	mS100A8	mS100A9(H103A)(H107A)
mCP(H105A)(H107A)	mS100A8	mS100A9(H105A)(H107A)
^{15}N-mCP	^{15}N-mS100A8	^{15}N-mS100A9

Table 3.3. mS100A9 C-terminal tail variants.

mCP variants	tail residues (101-109)
mCP	RGHGHSHGK
(H103A)	RG**A**GHSHGK
(H105A)	RGHG**A**SHGK
(H107A)	RGHGHS**A**GK
(H103A)(H105A)	RG**A**G**A**SHGK
(H103A)(H107A)	RG**A**GHS**A**GK
(H105A)(H107A)	RGHG**A**S**A**GK

Table 3.4. Summary of results from protein mass spectrometry.[a]

Protein	mS100A8 subunit Calculated Mass ± ^{N}Met (Da)	Observed Mass (Da)[c]	mS100A9 subunit Calculated Mass ± ^{N}Met (Da)[b]	Observed Mass (Da)[c]
mCPΔHis$_3$Asp	10162.47	10161.12	12938.79	n. f.[e]
	10031.28 (-Met1)[d]	10031.10	12807.60 (-Met1)[d]	12807.23
mCPΔHis$_4$	10162.47	10162.11	12916.74	n.f.[e]
	10031.28 (-Met1)[d]	10031.08	12785.54 (-Met1)[d]	12784.77
mCP(H103A)	10294.59	10294.16	12982.80	n. f.[e]
	10163.40 (-Met1)[d]	10162.13	12851.61 (-Met1)[d]	12851.17
mCP(H105A)	10294.59	10293.15	12982.80	n. f.[e]
	10163.40 (-Met1)[d]	10163.13	12851.61 (-Met1)[d]	12851.19
mCP(H107A)	10294.59	10293.15	12982.80	n. f.[e]
	10163.40 (-Met1)[d]	10162.12	12851.61 (-Met1)[d]	12851.29
mCP(H103A)	10294.59	10294.16	12916.74	n. f.[e]
(H105A)	10163.40 (-Met1)[d]	10163.13	12785.54 (-Met1)[d]	12785.25
mCP(H103A)	10294.59	10294.16	12916.74	n. f.[e]
(H107A)	10163.40 (-Met1)[d]	10163.13	12785.54 (-Met1)[d]	12785.23
mCP(H105A)	10294.59	10294.16	12916.74	n. f.[e]
(H107A)	10163.40 (-Met1)[d]	10163.13	12785.54 (-Met1)[d]	12785.12
^{15}N-mCP	10416.65	10415.77	13213.64	n. f.[e]
	10284.46 (-Met1)[d]	10283.77	13081.45 (-Met1)[d]	13079.95

[a] A denaturing protocol on an Agilent Poroshell 300SB-C18 column over a 25–75% gradient of acetonitrile with 0.1 % formic acid was utilized for LC-MS. [b] Molecular weights were calculated by using the ProtParam tool found on the ExPASy site (http://web.expasy.org/protparam) with the exception of ^{15}N-mCP (http://sopnmr.ucsd.edu/biomol-tools.htm). [c] Masses were calculated with the Agilent MassHunter BioConfirm software package. [d] The N-terminal methionine can be cleaved during overexpression in *E. coli*. [e] Not found; the mass was not found following deconvolution of the raw data.

Table 3.5. Metal content of representative protein preparations.[a]

	mCP variant		
Metal	**mCP**[b] (24.0 μM)[c]	**ΔHis$_3$Asp** (6.0 μM)[c]	**ΔHis$_4$** (11.1 μM)[c]
[Mn] (μM)	0.002	0.001	0.002
equivalents[d]	0.000	0.000	0.000
[Fe] (μM)	0.098	0.012	0.072
equivalents[d]	0.004	0.002	0.007
[Co] (μM)	0.000	0.000	0.001
equivalents[d]	0.000	0.000	0.000
[Ni] (μM)	0.019	0.010	0.020
equivalents[d]	0.001	0.002	0.002
[Cu] (μM)	0.018	0.001	0.008
equivalents[d]	0.001	0.000	0.001
[Zn] (μM)	0.100	0.037	0.089
equivalents[d]	0.004	0.006	0.008

[a] Metal analysis (ICP-MS) was performed on purified proteins. [b] The concentration of protein in the ICP-MS sample. [c] Reported previously in Ref. 40 and included here for reference. [d] The equivalents of metal relative to the mCP heterodimer.

Table 3.6. Metal content of representative protein preparations continued.[a]

	mCP variant (mS100A9 C-terminal tail variants)					
Metal	**(H103A)** (10.5 μM)[b]	**(H105A)** (9.1 μM)[b]	**(H107A)** (15.1 μM)[b]	**(H103A) (H105A)** (19.3 μM)[b]	**(H103A) (H107A)** (15.7 μM)[b]	**(H105A) (H107A)** (20.6 μM)[b]
[Mn] (μM)	0.003	0.000	0.002	0.001	0.026	0.000
equivalents[c]	0.000	0.000	0.000	0.000	0.002	0.000
[Fe] (μM)	0.084	0.046	0.047	0.044	0.120	0.045
equivalents[c]	0.008	0.005	0.003	0.002	0.008	0.002
[Co] (μM)	0.000	0.000	0.000	0.000	0.000	0.000
equivalents[c]	0.000	0.000	0.000	0.000	0.000	0.000
[Ni] (μM)	0.012	0.012	0.010	0.014	0.008	0.008
equivalents[c]	0.001	0.001	0.001	0.001	0.000	0.000
[Cu] (μM)	0.011	0.011	0.009	0.004	0.007	0.008
equivalents[c]	0.001	0.001	0.001	0.000	0.000	0.000
[Zn] (μM)	0.117	0.078	0.146	0.071	0.054	0.041
equivalents[c]	0.011	0.009	0.010	0.004	0.003	0.002

[a] Metal analysis (ICP-MS) was performed on purified proteins. [b] The concentration of protein in the ICP-MS sample. [c]The equivalents of metal relative to the mCP heterodimer.

Table 3.7. Analytical SEC elution volume and calculated molecular weights of proteins.

Protein[a]	[Ca(II)] (mM)	[Mn(II)] (mM)	V_e (mL)[b]	MW (kDa)
Ribonuclease A[c]	0	0	13.5	13.7
Carbonic anhydrase[c]	0	0	11.8	29
Ovalbumin[c]	0	0	10.8	44
Conalbumin[c]	0	0	9.9	75
mCP	0	0	12.1	25.8
	0	1	11.5	34.0
	25	0.1	11.4	35.6
(500 μM protein)	0	5	11.4	35.6
ΔHis_3Asp	0	0	12.0	27.0
	25	0	11.3	37.3
	0	1	12.0	27.0
	25	0.1	11.3	37.3
(500 μM protein)	0	5	11.3	37.3
ΔHis_4	0	0	12.0	27.0
	25	0	11.6	32.5
	0	1	12.0	27.0
(H103A)	0	0	12.1	25.8
	25	0	11.4	35.6
	0	1	11.3	37.3
(H105A)	0	0	12.1	25.8
	25	0	11.5	34.0
	0	1	12.0	27.0
(H107A)	0	0	12.1	25.8
	25	0	11.4	35.6
	0	1	12.0	27.0
(H103A)(H105A)	0	0	12.0	27.0
	25	0	11.3	37.3
(H103A)(H107A)	0	0	12.0	27.0
	25	0	11.4	35.6
(H105A)(H107A)	0	0	12.0	27.0
	25	0	11.4	35.6

[a] The protein concentration was 100 μM, except where indicated otherwise. The running buffer was 75 mM HEPES, 100 mM NaCl, pH 7.0 ± 25 mM Ca(II) for mCP and variants. [b] The elution volume (V_e) corresponds to the maximum peak absorbance at 280 nm. [c] The listed molecular weights are the known molecular weights used to generate the calibration curve for the rest of the samples.

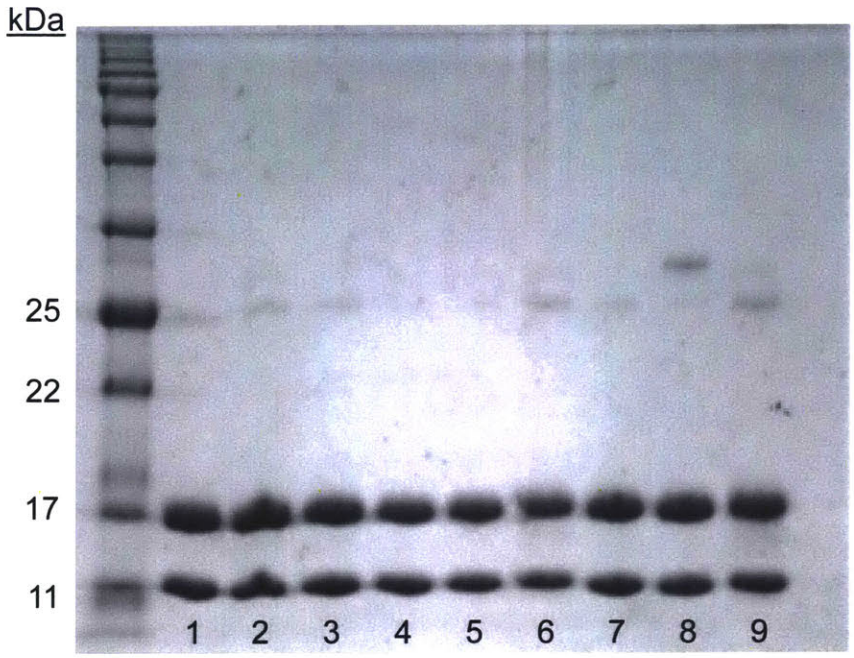

Figure 3.2. Purity of mCP variants by SDS-PAGE (15% Tris-glycine): (1) mCP(H103A), (2) mCP(H105A), (3) mCP(H107A), (4) mCP(H103A)(H105A), (5) mCP(H103A)(H107A), (6) mCP(H105A)(H107A), (7) mCPΔHis$_3$Asp, (8) mCPΔHis$_4$, (9) ^{15}N-mCP. The leftmost lane is a P7712S molecular weight ladder (New England Biolabs).

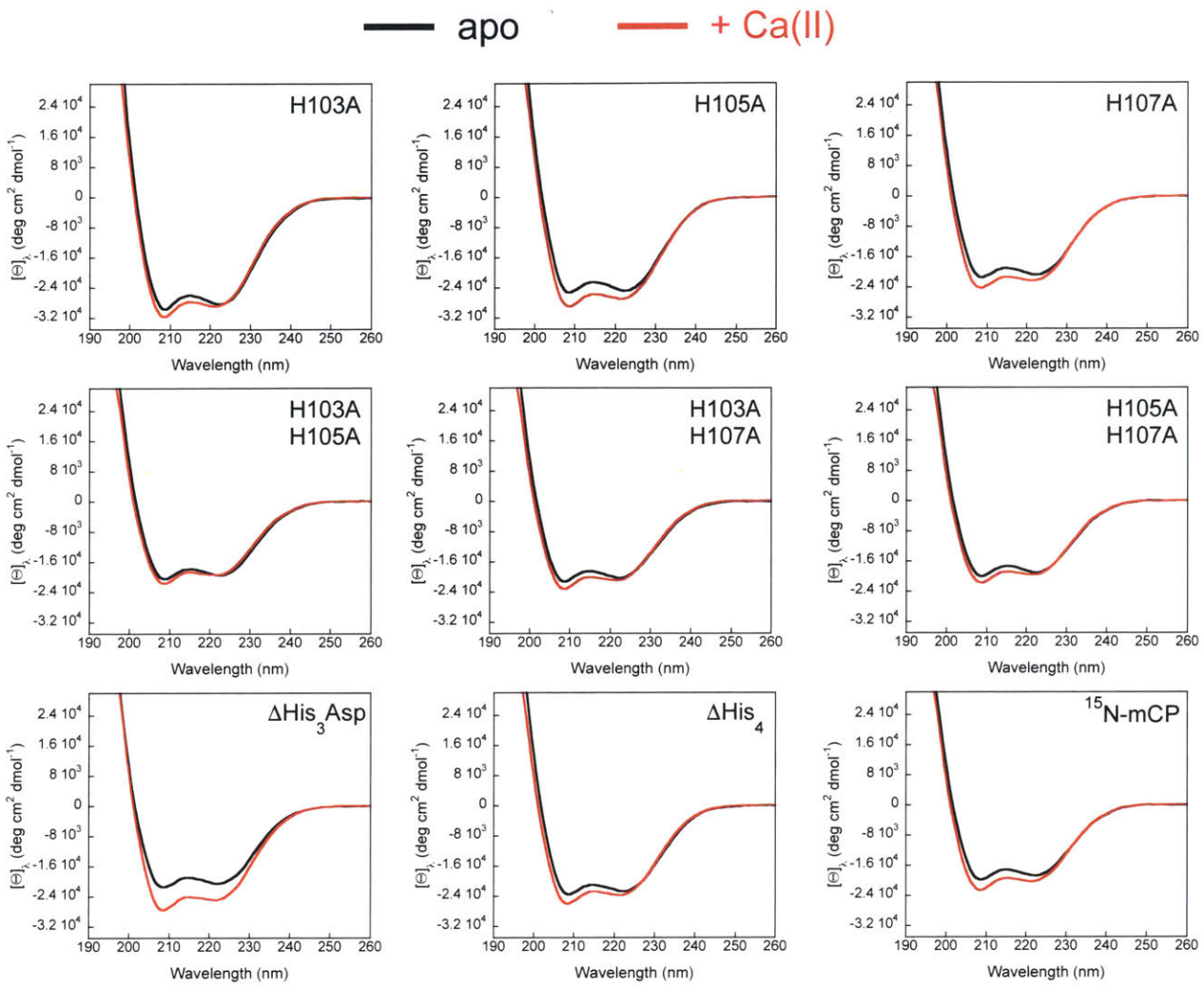

Figure 3.3. CD spectra of mCP variants (10 μM) in the absence (black) and presence (red) of 2 mM Ca(II) (1 mM Tris-HCl, 1 mM DTT, pH 7.5, 25 °C).

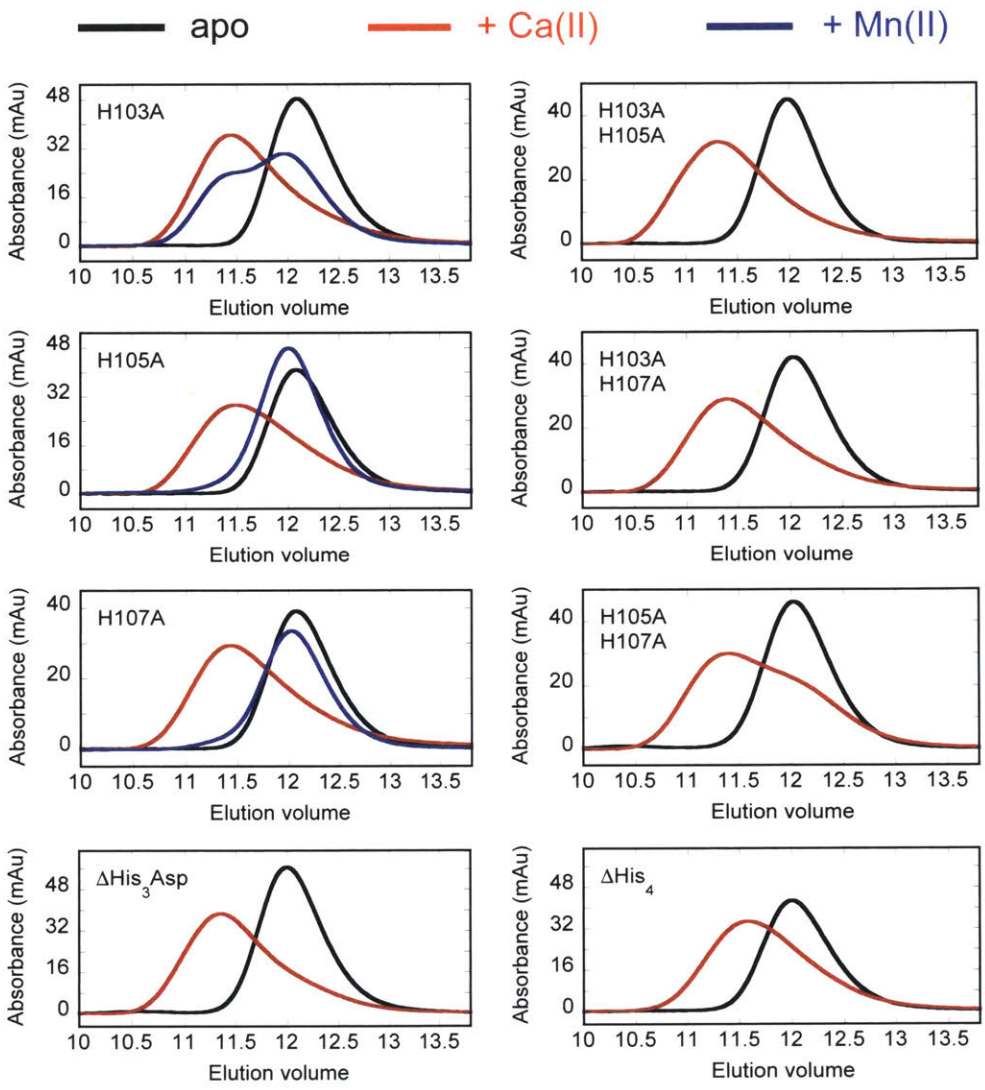

Figure 3.4. Analytical SEC chromatograms of mCP variants (100 μM) in 75 mM HEPES, 100 mM NaCl, pH 7.0, ± 25 mM Ca(II) in both the sample and running buffer. Single tail variants are also shown with 10 equiv Mn(II) in the sample and no Ca(II) added (blue traces) as a comparison. Absorbance at 280 nm was monitored. See Table 3.7 for tabulated elution volumes and calculated molecular weights.

3.4.2 Analytical Size-Exclusion Chromatography Uncovers the His_6 Site and Mn(II)-induced Tetramerization of mCP

Guided by our initial studies of Mn(II) binding to hCP,[31, 32] we first incubated mCP (100 μM) with 10 equiv. Mn(II) and analyzed the sample by SEC at pH 7.0. In the absence of Mn(II), mCP exhibits a single peak that elutes at 12.1 min. The presence of Mn(II) caused the peak to broaden and exhibit two local maxima at 11.5 and 11.8 min (**Figure 3.5A,B**). Quantitation of protein and Mn(II) concentrations in the fractions by optical absorption spectroscopy (A_{280}) and ICP-MS, respectively, revealed negligible Mn(II) in the apo sample, as expected. In contrast, ~1 equiv of Mn(II) was retained over the course of elution of the +Mn(II) sample. In the absence of Ca(II) ions, mCP coordinates Mn(II) with sufficiently high affinity to retain the metal during elution. The results also indicate that Mn(II) binding to mCP induces tetramerization, behavior previously observed for hCP.[31, 32]

We extended this experiment to examine the ability of the ΔHis_3Asp and ΔHis_4 variants to retain Mn(II). When we employed 100 μM protein and 10 equiv. Mn(II), both proteins displayed peak elution volumes consistent with dimers, and neither protein retained Mn(II) (**Figure 3.5C,D**). The result for ΔHis_4 was consistent with our working hypothesis that mCP uses a high-affinity His_6 site to coordinate Mn(II). In contrast, the results with ΔHis_3Asp were unexpected. Because Ca(II) ions enhanced the Mn(II) affinity of hCP, we questioned whether ΔHis_3Asp retains Mn(II) when excess Ca(II) is present. Thus, we examined samples of mCP and ΔHis_3Asp (100 μM) containing 1 equiv. Mn(II) using an elution buffer containing 25 mM Ca(II) (**Figure 3.5E,F**). Under these conditions, the peaks for both mCP and ΔHis_3Asp displayed a shift to a lower

elution volume, corresponding to tetramerization, and both proteins retained sub-stoichiometric Mn(II). Next, we repeated the SEC experiments with mCP and ΔHis_3Asp in the absence of Ca(II) ions using a 5-fold higher protein concentration (500 μM) and 10 equiv. Mn(II) (**Figure 3.5G,H**). Under these conditions, both proteins displayed comparable peak elution volume shifts consistent with nearly complete tetramerization, and both proteins retained Mn(II). Taken together, these results indicate that (i) Mn(II)-induced tetramerization of mCP exhibits protein-concentration dependence, (ii) mutation of the His_3Asp residues compromises the ability of the protein to retain Mn(II) at site 2 and self-associate to some degree, and (iii) the Mn(II) affinity is enhanced by Ca(II)-binding to the EF-hand domains.

Because the four residues of the putative His_6 site are essential for Mn(II) retention, we examined the contribution of H103, H105, and H107 in the mS100A9 C-terminal tail (**Figure 3.6**). For mCP(H103A), we observed a similar behavior as mCP with Mn(II) retention and partial tetramerization when the protein (100 μM) was incubated with 10 equiv. Mn(II) prior to elution from the SEC column (**Figure 3.6A**). In contrast, under these same experimental conditions, mCP(H105A) and mCP(H107A) eluted as dimers with minimal Mn(II) retained (**Figure 3.6B,C**). These results indicate that H105A and H107A are involved in Mn(II) coordination and that H103 does not participate in Mn(II) binding. Thus, these initial SEC experiments indicate that mCP employs a His_6 site composed of His17 and His27 of mS100A8 and His92, His97, His105 and His107 of mS100A9 to coordinate Mn(II). These residues are conserved in mCP and hCP. Moreover, this site is the high-affinity site and appears to display Ca(II)-dependent Mn(II) affinity.

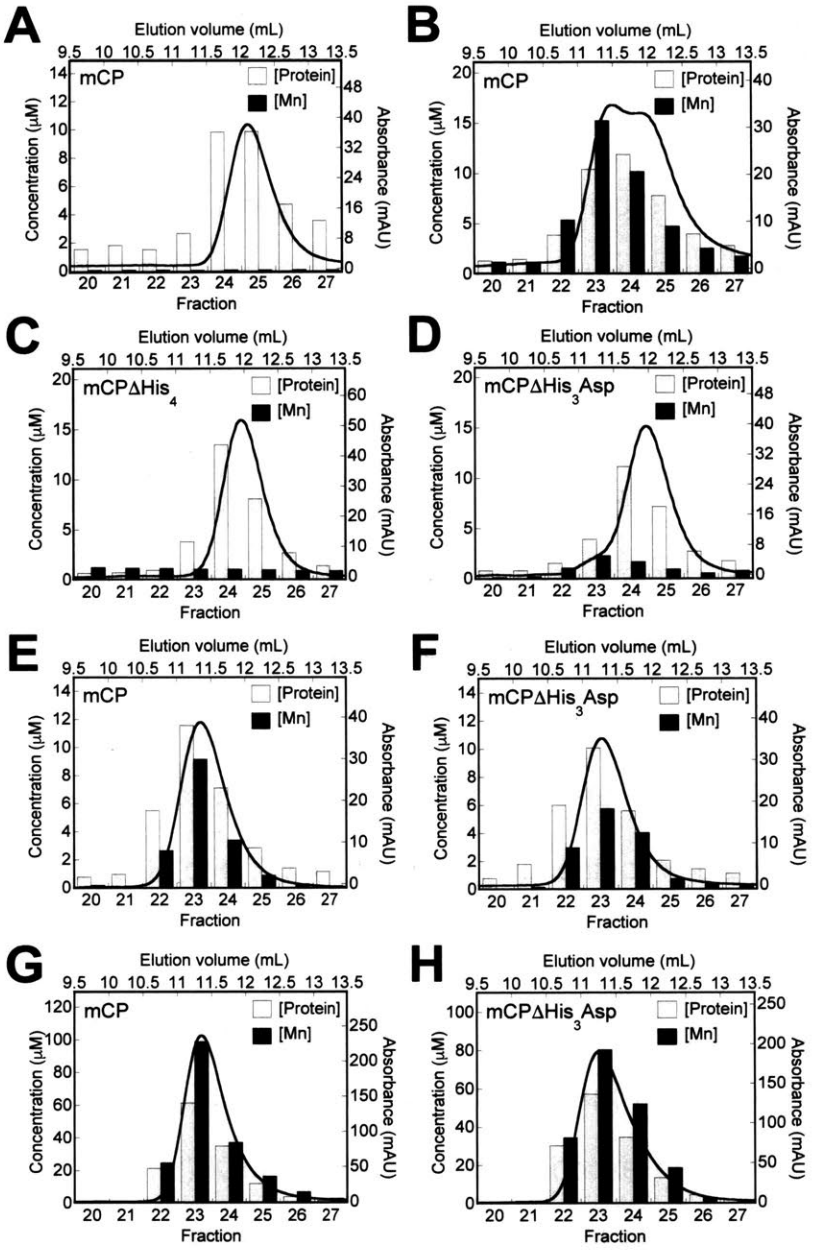

Figure 3.5. Representative data demonstrating Mn(II) retention by mCP and variants following SEC. Each plot shows a representative SEC chromatogram (black trace) and the quantification of protein and Mn(II) concentrations in the collected fractions (bars). For experiments in the absence of added Ca(II), the protein concentration was either 100 μM (**A-D**) or 500 μM (**G-H**). For experiments in the presence of 25 mM Ca(II), the protein concentration was 100 μM **(E-F**). The samples were incubated without (A) or with Mn(II) (B-H). For samples containing Mn(II), the Mn(II) concentration was 1 mM (B-D), 100 μM (D-E, +Ca(II) samples), or 5 mM (**G-H**). The elution buffer was 75 mM HEPES, 100 mM NaCl, 200 μM TCEP, pH 7.0 and T= 4 °C.

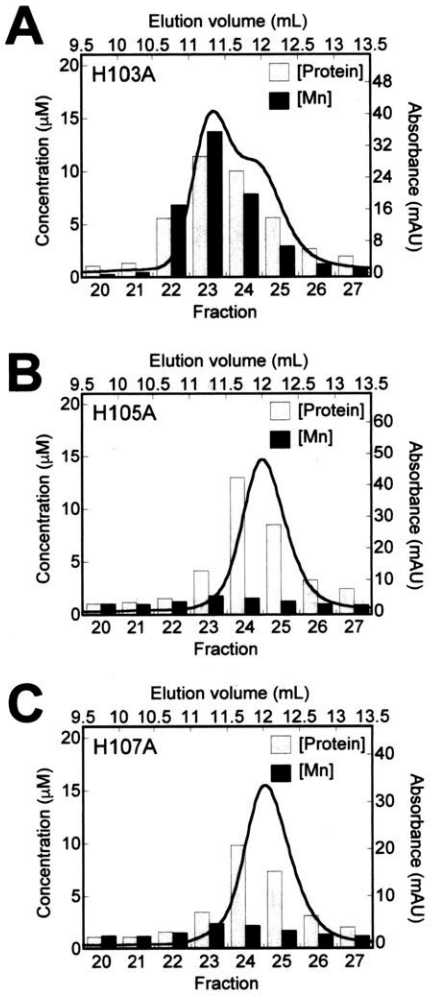

Figure 3.6. Representative data demonstrating Mn(II) retention by mCP C-terminal tail variants following SEC. Each plot shows a representative SEC chromatogram (black trace) and the quantification of protein and Mn(II) concentrations in the collected fractions (bars). The variants (100 μM) H103A (**A**), H105A (**B**), and H107A (**C**) were incubated with Mn(II) (1 mM) in the absence of added Ca(II). The elution buffer was 75 mM HEPES, 100 mM NaCl, 200 μM TCEP, pH 7.0 and T= 4 °C.

3.4.3 Mn(II) Competition Studies Demonstrate that Ca(II) Ions Enhance the Mn(II) affinity of mCP

On the basis of our prior studies of hCP which revealed that Ca(II) ions enhance the transition-metal affinities of the His_3Asp and His_6 sites,[37, 40] we hypothesized that mCP displays similar behavior. In our prior studies of hCP, we developed Zinpyr-1 (ZP1) competition assays to examine Ca(II)-dependent Mn(II) binding to the protein.[31, 32] ZP1 is a Ca(II)-independent fluorescent sensor with two di(2-picolyl)amine-based metal-binding sites that is quenched upon Mn(II) binding ($K_{d1,Mn(II)}$ = 550 nM).[49] When we combined ZP1 (1 μM), mCP (4 μM), and Mn(II) (5 μM), the fluorescence from ZP1 was quenched, indicating that Mn(II) bound to the probe and not mCP (**Figure 3.7**). This behavior is consistent with that of hCP.[31] Upon titration of Ca(II) into this solution, the fluorescence of ZP1 increased and reached its maximum emission once >200 equiv. Ca(II) relative to mCP was added. In agreement with previous reports, maximum ZP1 emission occurred following addition of ~20 equiv. Ca(II) to mixtures of ZP1, hCP-Ser, and Mn(II) (**Figure 3.7**).[31] These results show that (i) the Mn(II) affinity of mCP is Ca(II)-dependent, and (ii) that mCP is able to outcompete ZP1 for Mn(II) when excess Ca(II) is added, indicating that mCP binds Mn(II) with K_{d1} < 550 nM under these conditions. The observation that >200 equiv. Ca(II) is required to impart a full effect on modulating the Mn(II) affinity is consistent with our prior report that showed that >200 equiv. Ca(II) was necessary for full tetramerization of mCP.[40] We also note that the sigmoidal titration curve for mCP indicates cooperativity is at play, the origin and details of which are a subject for future work. Lastly, the Ca(II) responses of hCP and mCP clearly differ, which raises questions as to the implications of this difference for the working model of

CP action. Murine CP subunits are reported to exist at concentrations on the order of hundreds of micromolar at infection sites, whereas extracellular Ca(II) is ~2 mM.[38, 50]

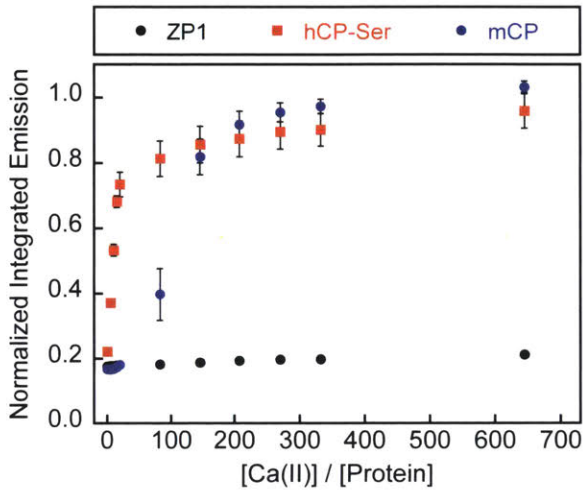

Figure 3.7. Titration of Ca(II) into a mixture of ZP1 (1 μM), hCP-Ser or mCP (4 μM), and Mn(II) (5 μM) monitored by fluorescence spectroscopy. The integrated emission was normalized to the integrated emission from the apo sensor (average ± SEM, n = 3). The buffer was 75 mM HEPES, 100 mM NaCl, 200 μM TCEP, pH 7.0 and T= 25°C.

3.4.4. Mn(II) Competition Studies Further Define the His_6 Site

We next evaluated how many equivalents of Mn(II) mCP binds with high affinity. We performed Mn(II) competition titrations between ZP1 (1 μM) and mCP (wild-type or mutant, 4 μM) in the presence of 300 equiv. Ca(II) (1.2 mM). Titration of Mn(II) into the ZP1/mCP/Ca(II) mixture resulted in no change of ZP1 fluorescence until a ~1:1 Mn(II):protein ratio was achieved, further demonstrating that mCP binds 1 equiv. Mn(II) with greater affinity than ZP1 (**Figure 3.8A**). The ΔHis_3Asp variant also outcompeted ZP1 for ~1 equiv. Mn(II), whereas the ΔHis_4 variant was unable to compete with ZP1 for this metal ion. Moreover, the mS100A9 C-terminal tail variants H105A and H107A afforded titration curves indicative of Mn(II) competition and reduced Mn(II) affinity

compared to mCP and ΔHis_3Asp (**Figure 3.8B**). The H103A variant, in contrast, outcompeted ZP1. Taken together, these results are in agreement with the observations from the SEC experiments and show that mCP coordinates one equivalent of Mn(II) with high affinity at the His_6 site that is completed by residues H105 and H107 of the mS100A9 C-terminal tail.

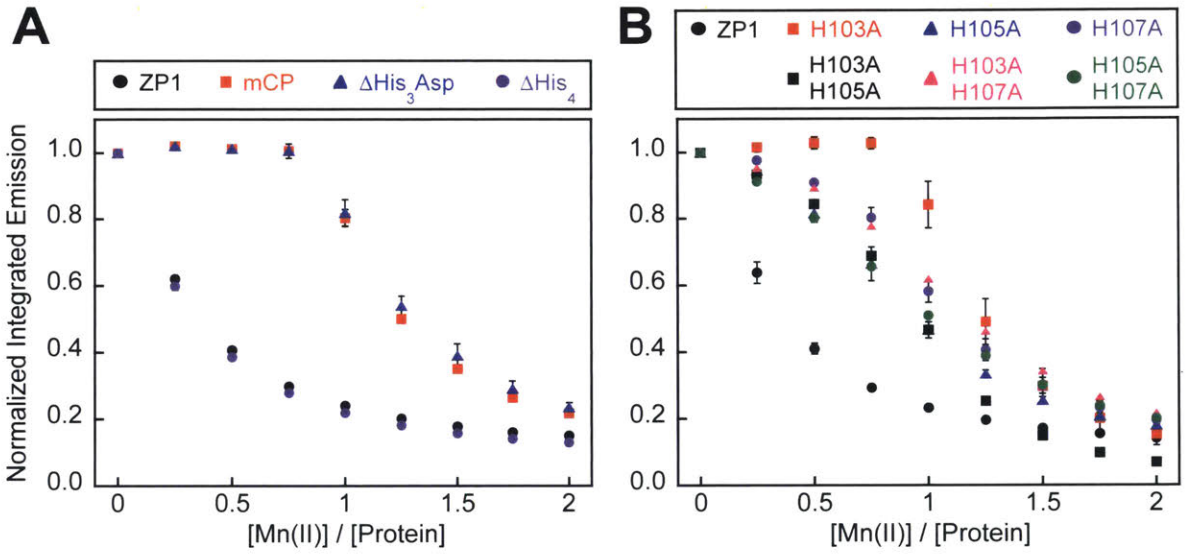

Figure 3.8. Titration of Mn(II) into a mixture of ZP1 (1 μM), mCP or variant (4 μM), and Ca(II) (1.2 mM) monitored by fluorescence spectroscopy. Data for mCP, ΔHis_3Asp and ΔHis_4 (**A**) and mS100A9 C-terminal tail variants (**B**). The integrated emission was normalized to the integrated emission from the apo sensor (average ± SEM, $n \geq 3$). The buffer was 75 mM HEPES, 100 mM NaCl, 200 μM TCEP, pH 7.0 and T= 25 °C. In the legend, "ZP1" refers to a sample containing ZP1 and no protein.

3.4.5 EPR Spectroscopy of Mn(II)-mCP

To further characterize the Mn(II)-His_6 site of mCP and describe its electronic structure, we applied multi-frequency EPR spectroscopic methods. First, we examined the X-band EPR spectra of Mn(II)-bound to mCP and several variants that included ΔHis_3Asp, H103A, H105A, and H107A analyzed in the biochemical experiments described above. We also studied mCP-Ser, an all Cys→Ser variant that we previously

reported (**Figure 3.9**).[40] Guided by our prior EPR spectroscopic evaluation of the human orthologue[31-33] and the Mn(II)-binding studies of mCP presented in this work, we prepared EPR samples containing 200 μM protein, 0.9 equiv. of Mn(II), and 300 equiv. Ca(II). Under these high Ca(II) conditions, we expect that all of the Mn(II) will be bound to the His_6 site with negligible free Mn(II) in solution.

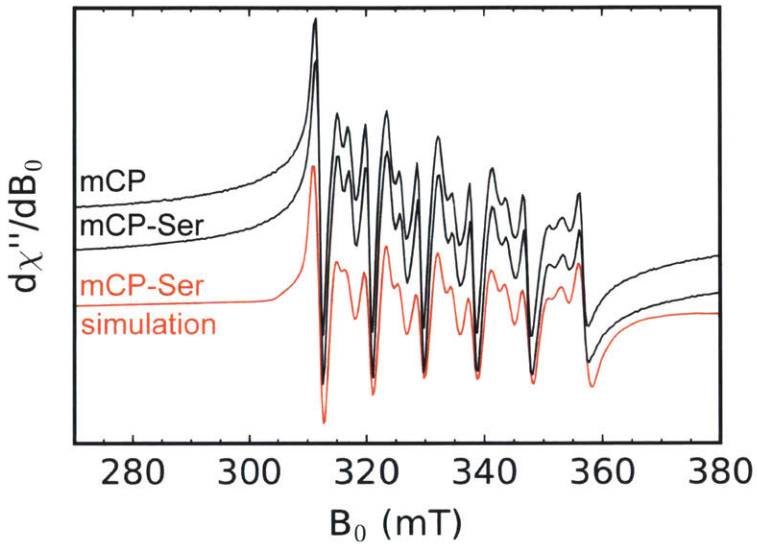

Figure 3.9. X-band EPR spectrum of Mn(II)-bound mCP and mCP-Ser in the presence of excess Ca(II) (180 μM Mn(II), 200 μM protein). The simulation of the mCP-Ser spectrum is shown in red. The buffer was 75 mM HEPES, 100 mM NaCl, pH 7.5.

The CW X-band EPR spectrum of Mn(II) bound to the His_6 site of mCP is typical for the high-spin d^5 Mn(II) ion (**Figure 3.10).**The isotropic *g*-value of 2.0008 is typical for the spherical symmetry of the electron distribution. The magnitude of the *g*-value is remarkably similar to the value of 2.001 that was determined for hCP-Ser.[33] The sextet features centered around g = 2.0008 arises from hyperfine interaction to the ^{55}Mn nucleus (I = 5/2, 100% abundance). This observed sextet arises from m_s transitions in

the "inner" m_s = ±1/2 Kramer's doublet. Hyperfine splitting in the "outer" Kramer's doublet (m_s = ±1/2 ↔ ±3/2 ↔ ±5/2) is rarely resolved in frozen spectra due to orientation-dependent broadening.[51, 52] The magnitude of this hyperfine interaction, 248 MHz, is nearly identical to the 247 MHz measured for hCP-Ser.[33, 53] In between each sextet pair are two additional transitions. These transitions arise from formally forbidden Δm_s ±1 and Δm_I ±1 transitions. Upon going to higher frequencies, the intensity of these transitions diminish, which further confirms their identities as forbidden transitions (**Figures 3.11, 3.12**). The intensity and positions of these transitions are indicative of the magnitude of the zero-field splitting (ZFS) parameters *D* and *E/D*. Simulations of the X-band EPR spectrum of the Mn(II)-bound mCP sample utilizing EasySpin afford values of 525 MHz and 0.30 for *D* and *E/D*, respectively (**Figure 3.10, red trace**). The low ZFS is indicative of a highly symmetric, octahedral coordination sphere. The values are remarkably similar to the simulated *D* and *E/D* values of 485 MHz and 0.30 determined for hCP-Ser.[33]

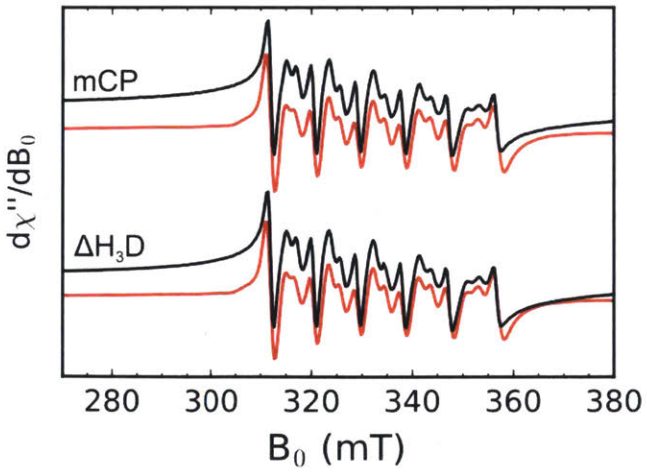

Figure 3.10. X-band EPR spectra (black) and simulations (red) for Mn(II) and Ca(II)-bound mCP and the ΔHis$_3$Asp variant (180 μM Mn(II), 200 μM protein, 60 mM Ca(II)). The buffer was 75 mM HEPES, 100 mM NaCl, pH 7.5.

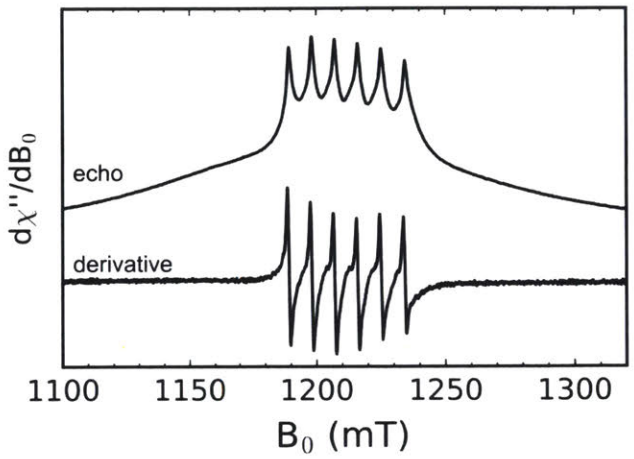

Figure 3.11. Echo detected Q-band field sweep of Mn(II)-bound mCP (180 μM Mn(II), 200 μM protein, 60 mM Ca(II)) in the presence of excess Ca(II). The lower trace is the derivative of the upper, echo detected data. The buffer was 75 mM HEPES, 100 mM NaCl, pH 7.5.

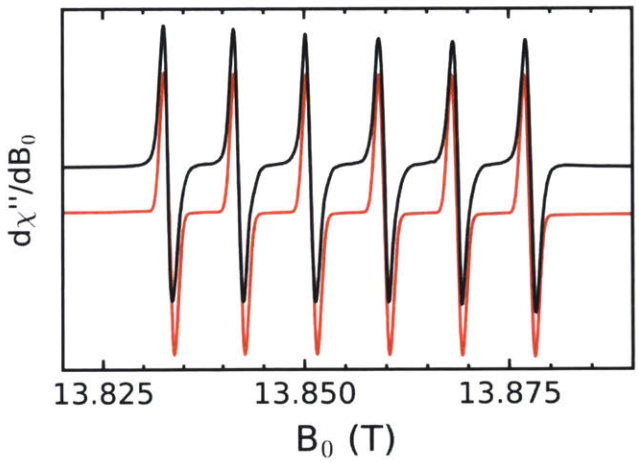

Figure 3.12. 388 GHz field sweep of Mn(II)-bound mCP in the presence of excess Ca(II) (black trace, 500 μM mCP, 450 μM Mn(II), 50 mM Ca(II)) and corresponding simulation (red trace). The buffer was 75 mM HEPES, 100 mM NaCl, pH 7.5. Temperature was 30 K, modulation amplitude of 0.5 mT at 50 kHz, and a sweep rate of 0.5 mT/s.

We employed the same protein/Mn(II)/Ca(II) ratio to prepare samples of the mCP variants and found that Mn(II)- and Ca(II)-bound ΔHis_3Asp exhibits the same EPR spectrum as mCP (**Figure 3.10**) and can be simulated using identical parameters (**Figure 3.10, red trace**), supporting the conclusion that Mn(II) is only bound at the His_6 site when the sample contains <1 equivalent of Mn(II). Moreover, the EPR spectrum of Mn(II)- and Ca(II)-bound mCP-Ser could also be simulated with the same parameters (**Figure 3.9**), indicating that the Cys→Ser mutations have negligible effect on Mn(II) binding by the His_6 site. We prepared EPR samples of the ΔHis_4 variant, but precipitation was observed during the sample preparation process so we did not analyze the samples. The mCP variants with mutations in the mS100A9 C-terminal tail afforded EPR spectra consistent with H105 and H107 completing the Mn(II)-His_6 coordination sphere (**Figure 3.13**). Variant H103A showed no change in the EPR spectrum and can be simulated using parameters identical to mCP (**Figure 3.13, red trace**). In contrast, the H105A and H107A variants show markedly perturbed EPR spectra (**Figure 3.13**). The large increase in the intensity of the forbidden transitions relative to the allowed transitions indicates that the symmetry of the Mn(II) site is lowered.

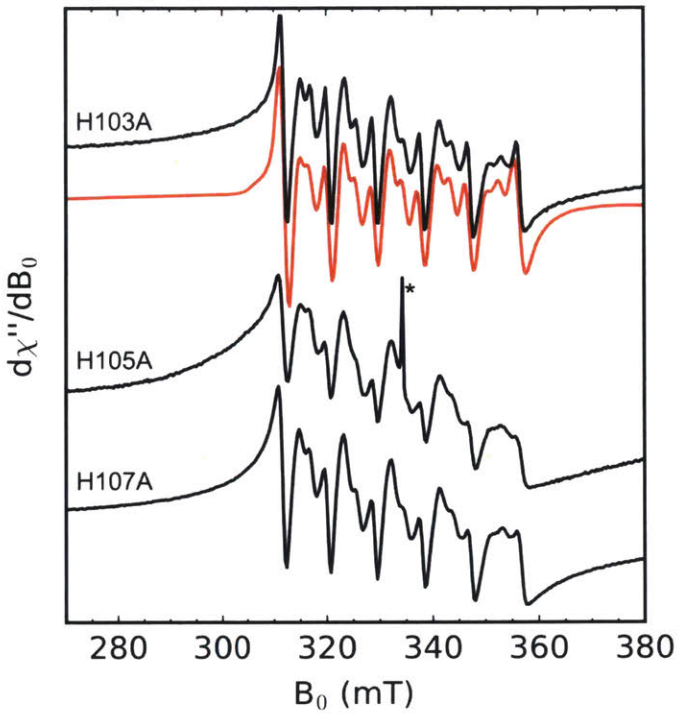

Figure 3.13. X-band EPR spectra (black) of Mn(II)- and Ca(II)-bound mCP variants H103A, H105A, and H107A (180 μM Mn(II), 200 μM protein, 60 mM Ca(II)). The red trace for H103A is a simulation using the parameters determined for Mn(II)- and Ca(II)-bound mCP. The peak marked by * is a background quartz radical. The buffer was 75 mM HEPES, 100 mM NaCl, pH 7.5.

To more quantitatively measure the interaction of the Mn(II) ion with the histidine residues of the His_6 site of mCP, we prepared globally ^{15}N-labeled protein (^{15}N-mCP) for electron nuclear double resonance (ENDOR) spectroscopy.[54-56] This sample contained ^{15}N-mCP (200 μM), 0.9 equiv Mn(II), and 300 equiv. Ca(II). The Mims ENDOR spectrum of Mn(II)- and Ca(II)-bound ^{15}N-mCP displays two sets of resonances centered at the ^{15}N Larmor frequency (**Figure 3.14**). The broader doublet (labeled A in **Figure 3.14**) is assigned to the proximal nitrogen atoms of the histidine imidazoles (Nε2, based on structures of Mn(II)-bound hCP-Ser).[33, 34] The splitting of the peaks is caused by a tau-dependent blind spot confirmed by collecting the spectrum with different tau values (**Figure 3.15**). This doublet can be simulated with a hyperfine tensor of [3.3 3.6 6.0]

MHz and a_{iso} of 4.3 MHz. The isotropic hyperfine coupling (a_{iso}) is nearly identical to the 4.36 MHz measured for the Nε2 nitrogen of hCP-Ser.[33] The second, narrower doublet corresponding to B in **Figure 3.14** is assigned to the distal nitrogen of the histidine imidazole (Nδ1). This doublet can be simulated with an isotropic hyperfine coupling constant of 0.25 MHz. Consistent with the CW results comparing mCP with hCP-Ser, this value is nearly identical to the 0.24 MHz measured for hCP-Ser. [33]

A comparison of these EPR spectroscopic data for Mn(II)- and Ca(II)-bound mCP with those previously analyzed for the human orthologue reveals that the electronic structure of the Mn(II) ion coordinated to the His_6 site is remarkably similar in both proteins. In particular, the ^{55}Mn hyperfine, ZFS, and *g*-values parameters for Mn(II)- and Ca(II)-bound mCP are nearly identical to the parameters published for hCP-Ser utilizing samples prepared such that only the His_6 site is occupied with Mn(II).[33]

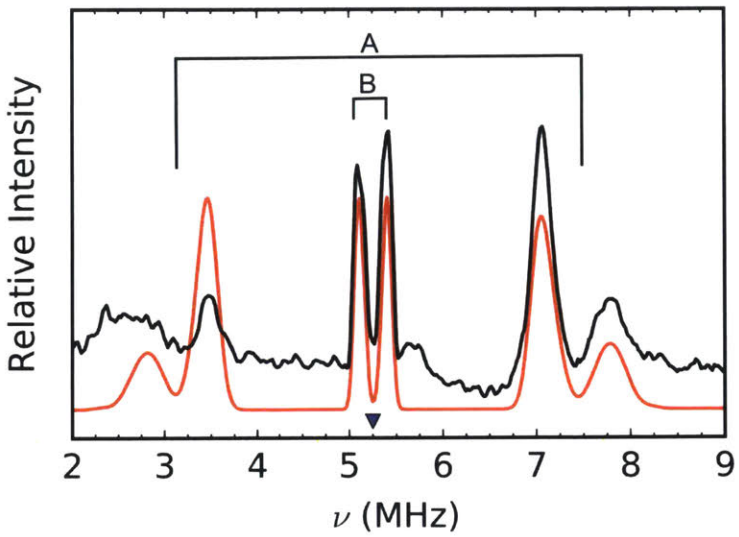

Figure 3.14. ^{15}N-Mims ENDOR of Mn(II)- and Ca(II)-bound to globally labeled ^{15}N-mCP (180 μM Mn(II), 200 μM protein, 60 mM Ca(II)). The red trace is a simulation. The τ value is 700 ns. Additional τ values can be found in **Figure 3.15**. A and B indicate the two sets of resonances centered at the ^{15}N Larmor frequency. The inverted triangle indicates the ^{15}N Larmor frequency. The buffer was 75 mM HEPES, 100 mM NaCl, pH 7.5.

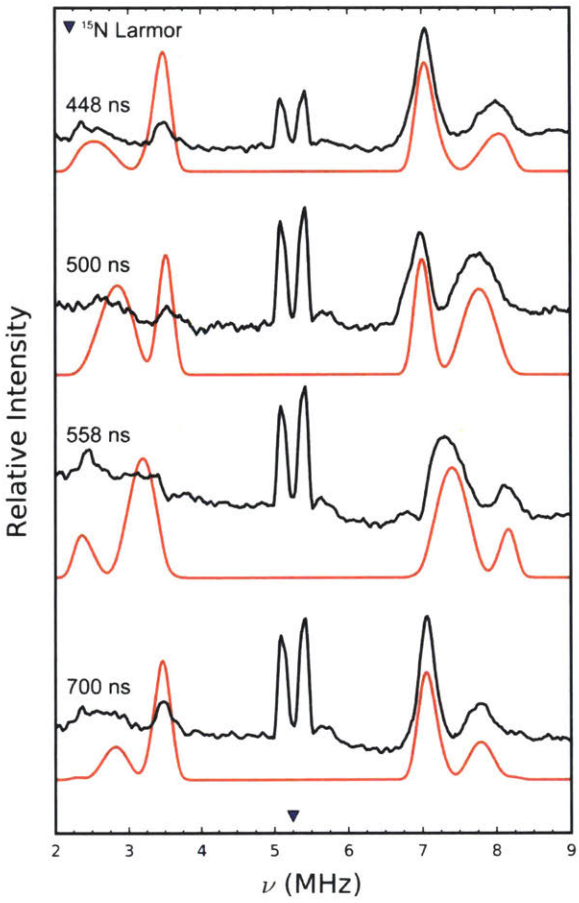

Figure 3.15. ^{15}N-Mims ENDOR of globally ^{15}N-labeled Mn(II)- and Ca(II)-bound mCP (180 μM Mn(II), 200 μM protein, 60 mM Ca(II)). The red traces are simulations The numbers correspond to the τ value in ns. The inverted triangle indicates the ^{15}N Larmor frequency. The buffer was 75 mM HEPES, 100 mM NaCl, pH 7.5.

3.4.6 mCP Can Outcompete MntC and PsaA for Mn(II)

The bacterial pathogens *S. aureus* and *S. pneumoniae* employ the ABC-transport systems MntABC and PsaABC, respectively, to import Mn(II).[57, 58] In our previous work on hCP, we demonstrated that in the presence of high Ca(II) concentrations, hCP-Ser can outcompete the two bacterial solute-binding proteins (SBPs), MntC and PsaA, which are thought to be responsible for sequestering extracelluar Mn(II).[35] This work is presented in Chapter 4 of this thesis. To evaluate whether mCP exhibits similar behavior, we prepared samples containing a 1:1:1 ratio of

mCP, SBP, and Mn(II) (500 μM each) in the absence and presence of 120 equiv. Ca(II) and evaluated the Mn(II) speciation in the samples by X-band EPR spectroscopy. As described in Chapter 4, the EPR spectroscopic signatures of Mn(II)-bound hCP-Ser and the Mn(II)-bound SBPs are distinct.[35] In contrast to the six-line feature centered at ca. g = 2 for Mn(II)-bound hCP-Ser, the Mn(II)-bound SBPs present a broad, relatively featureless spectrum at ca. g = 2 and sharp spectral features in the g ~ 4.5 region.[35] Similar to our observations for hCP-Ser described in Chapter 4, this assay demonstrates that mCP outcompetes MntC and PsaA for Mn(II) under conditions of excess Ca(II) but not in the absence of this cation (**Figure 3.16**). Based on the reported $K_{d,Mn(II)}$ values of MntC and PsaA ($K_{d,Mn(II)}$ ~ 4 nM[59] and ≤10 nM[60], respectively) these observations indicate that Ca(II)-bound mCP binds Mn(II) with a sub-nanomolar K_d value. We also note that these results support prior biological work; in a murine model of *S. aureus* infection, deletion of the pathogen's Mn(II) import machinery, including *mntC*, was detrimental to infection in wild-type mice expressing mCP.[18, 19]

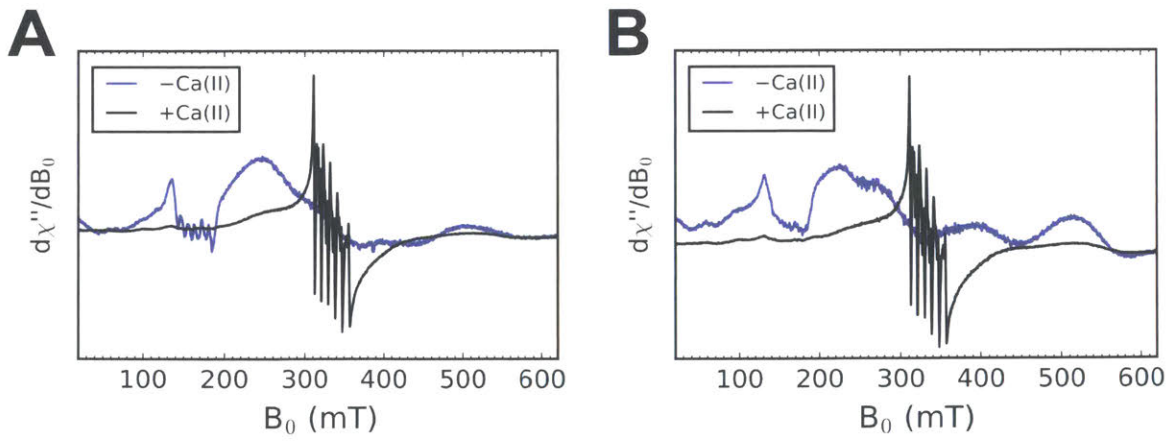

Figure 3.16. X-band EPR spectra of 500 μM mCP, 500 μM Mn(II), and 500 μM either MntC (**A**) or PsaA (**B**) without or with 60 mM Ca(II) following incubation for ~14 hours at room temperature. The buffer was 75 mM HEPES, 100 mM NaCl, pH 7.5.

3.4.7 Comparisons of hCP and mCP

These studies examine the molecular basis of Mn(II) sequestration by mCP. This work is important because CP is the only known Mn(II)-sequestering host-defense protein. Moreover, the vast majority of biochemical and biophysical characterization reported to date has focused on the human orthologue, whereas the understanding of the biological function of CP is derived from murine infection models.[4] This current biochemical and EPR spectroscopic investigation demonstrates that the Mn(II)-binding properties of mCP are remarkably similar to those of hCP. In particular, both proteins bind one equivalent of Mn(II) with high affinity at a His_6 site that is formed by four His residues that reside at the mS100A8/mS100A9 dimer interface and two His residues in an HXH motif of the mS100A9 C-terminal tail. The EPR spectroscopic analyses reveal that Mn(II) binding to mCP occurs in a highly symmetric coordination sphere characterized by very similar EPR spectroscopy parameters to those determined previously for hCP. Moreover, both proteins show enhanced Mn(II) affinities in the presence of excess Ca(II) ions, Mn(II)-induced tetramerization, and the ability to outcompete two bacterial SBPs for this metal ion.

Despite these similarities, there are also notable differences in the Mn(II)-binding properties of hCP and mCP. In particular, how Ca(II) modulates the biophysical properties of the two proteins differs; mCP requires ~10-fold more Ca(II) than hCP to exhibit complete conversion to the heterotetramer and fully enhanced Mn(II) affinity. Ca(II) ions are an important part of the working model for the extracellular function of CP in metal-withholding because Ca(II) binding induces tetramerization, enhance metal affinities, and protect CP from proteolytic degradation.[24] Further biophysical and

biological work is needed to illuminate both the origin and impact of the differing Ca(II) sensitivities in the tetramerization of hCP and mCP. The higher Ca(II) requirement of mCP suggests that it may exhibit different speciation in the extracellular space where the Ca(II) concentration is ~2 mM,[38] possibly with a higher proportion of heterodimers compared to hCP. Along similar lines, we also observed reduced tetramerization of mCP in the presence of excess Mn(II) compared to prior studies of hCP, further underscoring the fact that there are differences in oligomerization behavior between these orthologues. Taken together, these observations suggest that local and/or global differences in protein structures and/or dynamics exist. How these properties account for the differing attributes observed in this study and are affected by the coordination of divalent cations warrants future study.

In closing, the investigations presented herein provide a foundation for understanding the molecular basis for Mn(II) sequestration by mCP in murine models of infection as well as further examining the coordination chemistry and function of the His_6 site of this protein. The work experimentally demonstrates a conserved hexahistidine metal-binding motif that both mice and humans utilize in the metal-withholding innate immune response. Whether this feature is present in a wider range of CP orthologues remains to be investigated. Ultimately, this work emphasizes the importance of investigating and appreciating both the similarities and differences in human and murine host-defense strategies.

3.5 Acknowledgements

We gratefully acknowledge NIH grants R01GM118695 (E.M.N.) and 1R35GM126961 (R.D.B) for financial support. The ICP-MS is housed in the MIT Center for Environmental Health Sciences Bioanalytical Core, which is supported by NIH grant P30-ES002109. The MIT Biophysical Instrumentation Facility for the Study of Complex Macromolecular Systems is supported by NSF grant 0070319. A portion of this work was performed at the National High Magnetic Field Laboratory, which is supported by the National Science Foundation Cooperative Agreement No. DMR-1644779 and the State of Florida. The Q-TOF mass spectrometer is housed in the MIT Department of Chemistry Instrumentation Facility.

3.6 References

1. Hood, M. I.; Skaar, E. P. Nutritional immunity: transition metals at the pathogen–host interface. *Nat. Rev. Microbiol.* **2012,** *10*, 525-537.

2. Weinberg, E. D. Nutritional immunity: Host's attempt to withhold iron from microbial invaders. *J. Am. Med. Assoc.* **1975,** *231*, 39–41.

3. Juttukonda, L. J.; Skaar, E. P. Manganese homeostasis and utilization in pathogenic bacteria. *Mol. Microbiol.* **2015,** *97*, 216-228.

4. Brophy, M. B.; Nolan, E. M. Manganese and microbial pathogenesis: sequestration by the mammalian immune system and utilization by microorganisms. *ACS Chem. Biol.* **2015,** *10*, 641-651.

5. Kelliher, J. L.; Kehl-Fie, T. E. Competition for manganese at the host–pathogen interface. *Prog. Mol. Biol. Transl. Sci.* **2016,** *142*, 1-25.

6. Papp-Wallace, K. M.; Maguire, M. E. Manganese transport and the role of manganese in virulence. *Annu. Rev. Microbiol.* **2006,** *60*, 187-209.

7. Garcia, Y. M.; Barwinska-Sendra, A.; Tarrant, E.; Skaar, E. P.; Waldron, K. J.; Kehl-Fie, T. E. A superoxide dismutase capable of functioning with iron or manganese promotes the resistance of *Staphylococcus aureus* to calprotectin and nutritional immunity. *PLoS Pathog.* **2017,** *13*, e1006125.

8. Kehl-Fie, T. E.; Chitayat, S.; Hood, M. I.; Damo, S.; Restrepo, N.; Garcia, C.; Munro, K. A.; Chazin, W. J.; Skaar, E. P. Nutrient metal sequestration by calprotectin inhibits bacterial superoxide defense, enhancing neutrophil killing of *Staphylococcus aureus*. *Cell Host Microbe.* **2011,** *10*, 158-164.

9. Makhlynets, O.; Boal, A. K.; Rhodes, D. V.; Kitten, T.; Rosenzweig, A. C.; Stubbe, J. *Streptococcus sanguinis* class Ib ribonucleotide reductase: high activity with both iron and manganese cofactors and structural insights. *J. Biol. Chem.* **2014,** *289*, 6259-6272.

10. Rhodes, D. V.; Crump, K. E.; Makhlynets, O.; Snyder, M.; Ge, X.; Xu, P.; Stubbe, J.; Kitten, T. Genetic characterization and role in virulence of the ribonucleotide reductases of *Streptococcus sanguinis*. *J. Biol. Chem.* **2014,** *289*, 6273-6287.

11. Chittori, S.; Simanshu, D. K.; Banerjee, S.; Murthy, A. M. V.; Mathivanan, S.; Savithri, H. S.; Murthy, M. R. Mechanistic features of *Salmonella typhimurium* propionate kinase (TdcD): insights from kinetic and crystallographic studies. *Biochim. Biophys. Acta* **2013,** *1834*, 2036-2044.

12. Garces, F.; Fernández, F. J.; Montellà, C.; Penya-Soler, E.; Prohens, R.; Aguilar, J.; Baldomà, L.; Coll, M.; Badia, J.; Vega, M. C. Molecular architecture of the Mn^{2+}-

dependent lactonase UlaG reveals an RNase-like metallo-beta-lactamase fold and a novel quaternary structure. *J. Mol. Biol.* **2010,** *398*, 715-729.

13. Brissac, T.; Ziveri, J.; Ramond, E.; Tros, F.; Kock, S.; Dupuis, M.; Brillet, M.; Barel, M.; Peyriga, L.; Cahoreau, E.; Charbit, A. Gluconeogenesis, an essential metabolic pathway for pathogenic *Francisella*. *Mol. Microbiol.* **2015,** *98*, 518-534.

14. Gutka, H. J.; Wolf, N. M.; Bondoc, J. M. G.; Movahedzadeh, F. Enzymatic characterization of fructose 1,6-bisphosphatase II from *Francisella tularensis*, an essential enzyme for pathogenesis. *Appl. Biochem. Biotechnol.* **2017,** *183*, 1439-1454.

15. Kadzhaev, K.; Zingmark, C.; Golovliov, I.; Bolanowski, M.; Shen, H.; Conlan, W.; Sjöstedt, A. Identification of genes contributing to the virulence of *Francisella tularensis* SCHU S4 in a mouse intradermal infection model. *PLoS One.* **2009,** *4*, e5463.

16. Daniel, J.; Abraham, L.; Martin, A.; Pablo, X.; Reyes, S. Rv2477c is an antibiotic-sensitive manganese-dependent ABC-F ATPase in *Mycobacterium tuberculosis*. *Biochem. Biophys. Res. Commun.* **2018,** *495*, 35-40.

17. Thompson, M. K.; Keithly, M. E.; Goodman, M. C.; Hammer, N. D.; Cook, P. D.; Jagessar, K. L.; Harp, J.; Skaar, E. P.; Armstrong, R. N. Structure and function of the genomically encoded fosfomycin resistance enzyme, FosB, from *Staphylococcus aureus*. *Biochemistry.* **2014,** *53*, 755-765.

18. Kehl-Fie, T. E.; Zhang, Y.; Moore, J. L.; Farrand, A. J.; Hood, M. I.; Rathi, S.; Chazin, W. J.; Caprioli, R. M.; Skaar, E. P. MntABC and MntH contribute to systemic *Staphylococcus aureus* infection by competing with calprotectin for nutrient manganese. *Infect. Immun.* **2013,** *81*, 3395-3405.

19. Handke, L. D.; Gribenko, A. V.; Timofeyeva, Y.; Scully, I. L.; Anderson, A. S. MntC-dependent manganese transport Is essential for *Staphylococcus aureus* oxidative stress resistance and virulence. *mSphere* **2018,** *3*, e0036-18.

20. Marra, A.; Lawson, S.; Asundi, J. S.; Brigham, D.; Hromockyj, A. E. *In vivo* characterization of the psa genes from *Streptococcus pneumoniae* in multiple models of infection. *Microbiology.* **2002,** *148*, 1483-1491.

21. Diaz-Ochoa, V. E.; Lam, D.; Lee, C. S.; Klaus, S.; Behnsen, J.; Liu, J. Z.; Chim, N.; Nuccio, S. P.; Rathi, S. G.; Mastroianni, J. R.; Edwards, R. A.; Jacobo, C. M.; Cerasi, M.; Battistoni, A.; Ouellette, A. J.; Goulding, C. W.; Chazin, W. J.; Skaar, E. P.; Raffatellu, M. *Salmonella* mitigates oxidative stress and thrives in the inflamed gut by evading calprotectin-mediated manganese sequestration. *Cell Host Microbe.* **2016,** *19*, 814-825.

22. Gat, O.; Mendelson, I.; Chitlaru, T.; Ariel, N.; Altboum, Z.; Levy, H.; Weiss, S.; Grosfeld, H.; Cohen, S.; Shafferman, A. The solute-binding component of a putative Mn(II) ABC transporter (MntA) is a novel *Bacillus anthracis* virulence determinant. *Mol. Microbiol.* **2005,** *58*, 533-551.

23. Colomer-Winter, C.; Flores-Mireles, A. L.; Baker, S. P.; Frank, K. L.; Lynch, A. J. L.; Hultgren, S. J.; Kitten, T.; Lemos, J. A. Manganese acquisition is essential for virulence of *Enterococcus faecalis*. *PLoS Pathog.* **2018,** *14*, e1007102.

24. Zygiel, E. M.; Nolan, E. M. Transition metal sequestration by host-defense protein calprotectin. *Ann. Rev. Biochem.* **2018,** *87*, 621-643.

25. Hobbs, J. A. R.; May, R.; Tanousis, K.; McNeill, E.; Mathies, M.; Gebhardt, C.; Henderson, R.; Robinson, M. J.; Hogg, N. Myeloid cell function in MRP-14 (S100A9) null mice. *Mol. Cell. Biol.* **2003,** *23*, 2564-2576.

26. Corbin, B. D.; Seeley, E. H.; Raab, A.; Feldmann, J.; Miller, M. R.; Torres, V. J.; Anderson, K. L.; Dattilo, B. M.; Dunman, P. M.; Gerads, R.; Caprioli, R. M.; Nacken, W.; Chazin, W. J.; Skaar, E. P. Metal chelation and inhibition of bacterial growth in tissue abscesses. *Science.* **2008,** *319*, 962-965.

27. Liu, J. Z.; Jellbauer, S.; Poe, A. J.; Ton, V.; Pesciaroli, M.; Kehl-Fie, T. E.; Restrepo, N. A.; Hosking, M. P.; Edwards, R. A.; Battistoni, A.; Pasquali, P.; Lane, T. E.; Chazin, W. J.; Vogl, T.; Roth, J.; Skaar, E. P.; Raffatellu, M. Zinc sequestration by the neutrophil protein calprotectin enhances *Salmonella* growth in the inflamed gut. *Cell Host Microbe.* **2012,** *11*, 227-239.

28. Hood, M. I.; Mortensen, B. L.; Moore, J. L.; Zhang, Y.; Kehl-Fie, T. E.; Sugitani, N.; Chazin, W. J.; Caprioli, R. M.; Skaar, E. P. Identification of an *Acinetobacter baumannii* zinc acquisition system that facilitates resistance to calprotectin-mediated zinc sequestration. *PLoS Pathog.* **2012,** *8*, e1003068.

29. Clark, H. L.; Jhingran, A.; Sun, Y.; Vareechon, C.; de Jesus Carrion, S.; Skaar, E. P.; Chazin, W. J.; Calera, J. A.; Hohl, T. M.; Pearlman, E. Zinc and manganese chelation by neutrophil S100A8/A9 (calprotectin) limits extracellular *Aspergillus fumigatus* hyphal growth and corneal infection. *J. Immunol.* **2016,** *196*, 336-344.

30. Juttukonda, L. J.; Berends, E. T. M.; Zackular, J. P.; Moore, J. L.; Stier, M. T.; Zhang, Y.; Schmitz, J. E.; Beavers, W. N.; Wijers, C. D.; Gilston, B. A.; Kehl-Fie, T. E.; Atkinson, J.; Washington, M. K.; Peebles, R. S.; Chazin, W. J.; Torres, V. J.; Caprioli, R.

M.; Skaar, E. P. Dietary manganese promotes staphylococcal infection of the heart. *Cell Host Microbe.* **2017,** *22*, 531-542

31. Hayden, J. A.; Brophy, M. B.; Cunden, L. S.; Nolan, E. M. High-affinity manganese coordination by human calprotectin is calcium-dependent and requires the histidine-rich site formed at the dimer interface. *J. Am. Chem. Soc.* **2013,** *135*, 775-787.

32. Brophy, M. B.; Nakashige, T. G.; Gaillard, A.; Nolan, E. M. Contributions of the S100A9 C-terminal tail to high-affinity Mn(II) chelation by the host-defense protein human calprotectin. *J. Am. Chem. Soc.* **2013,** *135*, 17804-17817.

33. Gagnon, D. M.; Brophy, M. B.; Bowman, S. E. J.; Stich, T. A.; Drennan, C. L.; Britt, R. D.; Nolan, E. M. Manganese binding properties of human calprotectin under conditions of high and low calcium: X-ray crystallographic and advanced electron paramagnetic resonance spectroscopic analysis. *J. Am. Chem. Soc.* **2015,** *137*, 3004-3016.

34. Damo, S. M.; Kehl-Fie, T. E.; Sugitani, N.; Holt, M. E.; Rathi, S.; Murphy, W. J.; Zhang, Y.; Betz, C.; Hench, L.; Fritz, G.; Skaar, E. P.; Chazin, W. J. Molecular basis for manganese sequestration by calprotectin and roles in the innate immune response to invading bacterial pathogens. *Proc. Natl. Acad. Sci.* **2013,** *110*, 3841-3846.

35. Hadley, R. C.; Gagnon, D. M.; Brophy, M. B.; Gu, Y.; Nakashige, T. G.; Britt, R. D.; Nolan, E. M. Biochemical and spectroscopic observation of Mn(II) sequestration from bacterial Mn(II) transport machinery by calprotectin. *J. Am. Chem. Soc.* **2018,** *140*, 110-113.

36. Gifford, J. L.; Walsh, M. P.; Vogel, H. J. Structures and metal-ion-binding properties of the Ca^{2+}-binding helix-loop-helix EF-hand motifs. *Biochem. J.* **2007,** *405*, 199-221.

37. Brophy, M. B.; Hayden, J. A.; Nolan, E. M. Calcium ion gradients modulate the zinc affinity and antibacterial activity of human calprotectin. *J. Am. Chem. Soc.* **2012,** *134*, 18089-18100.

38. Brini, M.; Ottolini, D.; Cali, T.; Carafoli, E. Calcium in health and disease. *Met. Ions Life Sci.* **2013,** *13*, 81-137.

39. Makałowski, W.; Zhang, J.; Boguski, M. S. Comparative analysis of 1196 orthologous mouse and human full-length mRNA and protein sequences. *Genome Res.* **1996,** *6*, 846-857.

40. Hadley, R. C.; Gu, Y.; Nolan, E. M. Initial biochemical and functional evaluation of murine calprotectin reveals Ca(II)-dependence and its ability to chelate multiple nutrient transition metal ions. *Biochemistry* **2018,** *57*, 2846-2856.

41. Walkup, G. K.; Burdette, S. C.; Lippard, S. J.; Tsien, R. Y. A new cell-permeable fluorescent probe for Zn^{2+}. *J. Am. Chem. Soc.* **2000,** *122*, 5644-5645.

42. Forrer, J.; Garcia-Rubio, I.; Schuhmam, R.; Tschaggelar, R.; Harmer, J. Cryogenic Q-band (35 GHz) probehead featuring large excitation microwave fields for pulse and continuous wave electron paramagnetic resonance spectroscopy: performance and applications. *J. Magn. Reson.* **2008,** *190*, 280-291.

43. Mims, W. B. Pulsed endor experiments. *Proc. R. Soc. Math. Phys. Eng. Sci.* **1965,** *283*, 452-457.

44. Oyala, P. H.; Ravichandran, K. R.; Funk, M. A.; Stucky, P. A.; Stich, T. A.; Drennan, C. L.; Britt, R. D.; Stubbe, J. Biophysical characterization of fluorotyrosine probes site-specifically incorporated into enzymes: *E. coli* ribonucleotide reductase as an example. *J. Am. Chem. Soc.* **2016,** *138*, 7951-7964.

45. Stoll, S.; Gunn, A.; Brynda, M.; Sughrue, W.; Kohler, A. C.; Ozarowski, A.; Fisher, A. J.; Lagarias, J. C.; Britt, R. D. Structure of the biliverdin radical intermediate in phycocyanobilin:ferredoxin oxidoreductase identified by high-field EPR and DFT. *J. Am. Chem. Soc.* **2009,** *131*, 1986-1995.

46. Stoll, S.; Ozarowski, A.; Britt, R. D.; Angerhofer, A. Atomic hydrogen as high-precision field standard for high-field EPR. *J. Magn. Reson.* **2010,** *207*, 158-163.

47. Stoll, S.; Schweiger, A. EasySpin, a comprehensive software package for spectral simulation and analysis in EPR. *J. Magn. Reson.* **2006,** *178*, 42-55.

48. Bradshaw, R. A.; Brickey, W. W.; Walker, K. W. N-Terminal processing: the methionine aminopeptidase and N. *Trends Biochem. Sci.* **1998,** *23*, 263-267.

49. You, Y.; Tomat, E.; Hwang, K.; Atanasijevic, T.; Nam, W.; Jasanoff, A. P.; Lippard, S. J. Manganese displacement from Zinpyr-1 allows zinc detection by fluorescence microscopy and magnetic resonance imaging. *Chem. Commun.* **2010,** *46*, 4139-4141.

50. Kocher, M.; Kenny, P. A.; Farram, E.; Abdul Majid, K. B.; Finlay-Jones, J. J.; Geczy, C. L. Functional chemotactic factor CP-10 and MRP-14 are abundant in murine abscesses. *Infect. Immun.* **1996,** *64*, 1342-1350.

51. Duboc, C.; Phoeung, T.; Zein, S.; Pécaut, J.; Collomb, M.-N.; Neese, F. Origin of the zero-field splitting in mononuclear octahedral dihalide Mn^{II} complexes: an

investigation by multifrequency high-field electron paramagnetic resonance and density functional theory. *Inorg. Chem.* **2007,** *46*, 4905-4916.

52. Duboc, C.; Collomb, M.-N.; Neese, F. Understanding the zero-field splitting of mononuclear manganese(II) complexes from combined EPR spectroscopy and quantum chemistry. *Appl. Magn. Reson.* **2010,** *37*, 229-245.

53. Un, S. Structure and nature of manganese(II) imidazole complexes in frozen aqueous solutions. *Inorg. Chem.* **2013,** *52*, 3803-3813.

54. Mims, W. B.; Peisach, J. The nuclear modulation effect in electron spin echoes for complexes of Cu^{2+} and imidazole with ^{14}N and ^{15}N. *J. Chem. Phys.* **1978,** *69*, 4921-4930.

55. Zweier, J.; Aisen, P.; Peisach, J.; Mims, W. B. Pulsed electron paramagnetic resonance studies of the copper complexes of transferrin. *J. Biol. Chem.* **1979,** *254*, 3512-3515.

56. Deligiannakis, Y.; Louloudi, M.; Hadjiliadis, N. Electron spin echo envelope modulation (ESEEM) spectroscopy as a tool to investigate the coordination environment of metal centers. *Coord. Chem. Rev.* **2000,** *204*, 1-112.

57. Horsburgh, M. J.; Wharton, S. J.; Cox, A. G.; Ingham, E.; Peacock, S.; Foster, S. J. MntR modulates expression of the PerR regulon and superoxide resistance in *Staphylococcus aureus* through control of manganese uptake. *Mol. Microbiol.* **2002,** *44*, 1269-1286.

58. Dintilhac, A.; Alloing, G.; Granadel, C.; Claverys, J.-P. Competence and virulence of *Streptococcus pneumoniae*: Adc and PsaA mutants exhibit a requirement for Zn and

Mn resulting from inactivation of putative ABC metal permeases. *Mol. Microbiol.* **1997,** *25*, 727-739.

59. Gribenko, A.; Mosyak, L.; Ghosh, S.; Parris, K.; Svenson, K.; Moran, J.; Chu, L.; Li, S.; Liu, T.; Woods, V. L., Jr.; Jansen, K. U.; Green, B. A.; Anderson, A. S.; Matsuka, Y. V. Three-dimensional structure and biophysical characterization of *Staphylococcus aureus* cell surface antigen-manganese transporter MntC. *J. Mol. Biol.* **2013,** *425*, 3429-3445.

60. McDevitt, C. A.; Ogunniyi, A. D.; Valkov, E.; Lawrence, M. C.; Kobe, B.; McEwan, A. G.; Paton, J. C. A molecular mechanism for bacterial susceptibility to zinc. *PLoS Pathog.* **2011,** *7*, e1002357.

Chapter 4: Biochemical and Spectroscopic Observation of Mn(II) Sequestration from Bacterial Mn(II) Transport Machinery by Calprotectin

This Chapter was adapted from *J. Am. Chem. Soc.* **2018**, 140 (1), 110–113.

4.1 Contributions

Dr. Derek Gagnon collected and analyzed the EPR data presented in this Chapter. Dr. Megan Brophy did the cloning and initial purification of MntC and PsaA, and performed initial Mn(II) competition spectroscopic studies. Ms. Vicky (Yu) Gu optimized the purification and demetallation procedures for PsaA. Dr. Toshiki Nakashige performed the Biotin-CP control experiments, including the antimicrobial activity assays, analytical SEC studies, and metal-binding experiments.

4.2 Introduction

Transition metal ions are essential nutrients for all organisms. In the context of the host/pathogen interaction, microbes must acquire nutrient metals from the host environment. In response to invading pathogens, the mammalian innate immune system launches a metal-withholding response, often termed "nutritional immunity," to restrict the availability of essential metal nutrients.[1, 2] Human calprotectin (CP) is a metal-chelating protein that contributes to this innate immune response. CP harbors two transition-metal-ion binding sites: a His_3Asp motif and a His_6 site.[3] While the His_3Asp site coordinates Zn(II) with high affinity, CP can employ the unusual hexahistidine site to sequester a number of divalent first-row transition metals, including Mn(II).[4-10] In the presence of excess Ca(II), the protein binds Ca(II) and forms a heterotetrameric species.[4] Ca(II) binding causes enhanced transition metal affinities, including for Mn(II).[3] The molecular characterization of Mn(II) sequestration by CP revealed that Mn(II) is encapsulated at the His_6 site in a nearly-octahedral coordination environment.[5, 9]

The ability of CP to affect Mn(II) availability was first recognized during studies of murine tissue abscesses infected with the Gram-positive opportunistic human pathogen *Staphylococcus aureus*[11] and later examined for the Gram-negative gastrointestinal pathogen *Salmonella enterica* serovar Typhimurium.[12] CP was suggested to compete with *S. aureus* for Mn(II) and the competition was dependent upon the presence of the bacterial Mn transport systems.[13] *S. aureus* employs the ATP-binding cassette transport system MntABC when battling with CP for Mn(II).[11, 13] MntC is the SBP that scavenges Mn(II) from the extracellular space. Following Mn(II) capture, MntC delivers the Mn(II) ion to MntAB, which transports the divalent cation across the cell membrane to the cytoplasm. Structural and solution studies of MntC revealed that Mn(II) is coordinated in a $His_2AspGlu$ motif with an affinity in the low nanomolar range.[14]

Although less is known about the competition between CP and *S. pneumoniae* for nutrient metals, a recent study showed that CP inhibits the growth of *S. pneumoniae*.[15] *S. pneumoniae* expresses the ATP-binding cassette transporter PsaABC for Mn(II) acquisition, which is important for virulence.[16-19] Like MntC in *S. aureus*, PsaA is the SBP that scavenges Mn(II) from the extracellular space and brings the ion to PsaBC for cytoplasmic delivery. Mn(II) is coordinated by PsaA in a $His_2AspGlu$ motif.[20]

Most reported studies that consider the interplay between CP and bacterial metal transport systems are at the cellular or organismal level and typically begin with a comparison of the growth inhibitory activity of CP against wild-type bacteria and knock-out strains that lack a component of the metal transport machinery under investigation.[11-13, 15, 19] Biochemical and biophysical methods provide complementary approaches for investigating metal competition at the host/pathogen interface that can afford direct

assessment of the metal-ion speciation during competition between microbial and host proteins for metal ions. To provide molecular understanding of the tug-of-war between CP and microbes for Mn(II), herein we employ biochemical and electron paramagnetic resonance (EPR) spectroscopic methods to evaluate metal competition between human CP and the SBPs MntC and PsaA.[14, 20] The results demonstrate that CP outcompetes both SBPs for Mn(II) under conditions of high Ca(II), as found in the extracellular environment.

4.3 Experimental

4.3.1 General Materials and Methods

Buffers used for titrations, EPR sample preparation, and pull-down assays were prepared in nitric acid-washed volumetric glassware using ULTROL grade HEPES (Calbiochem), TraceSelect NaCl (Sigma), and Milli-Q water (18.2 M·cm, 0.22-μm filter). TraceSelect NaOH (Sigma) was used to adjust the buffer pH. Stock solutions of Ca(II) (1 M, 100 mL) and Mn(II) (1 M, 100 mL) were prepared from 99.999% $CaCl_2$ (Sigma) and 99.999% $MnCl_2$ (Alfa Aesar), respectively, and Milli-Q water using acid-washed volumetric glassware and the solutions were stored in polypropylene tubes. Working solutions of metal solutions were prepared by serial dilution of the stock solutions in Milli-Q water immediately prior to each experiment. Zinpyr-1 (ZP1) was synthesized as described elsewhere (kindly provided by Dr. Jacob Goldberg and Prof. Stephen J. Lippard).[21] Stock solutions of ZP1 (≈3 mM) were prepared in DMSO and stored in aliquots (≈15 μL) at -20 °C. The concentration of each stock solution was determined using the reported extinction coefficient of apo ZP1 (A_{515} = 79,500 $M^{-1}cm^{-1}$).[21] Aliquots of ZP1 were

thawed only once, immediately prior to use, and the solutions were handled in the dark. Oligonucleotide primers were synthesized by Integrated DNA Technologies (Coralville, IA) and used as received (standard desalting protocol). *Staphylococcus aureus* USA300 JE2 was obtained from the Network on Antimicrobial Resistance in *Staphylococcus aureus* (NARSA, BEI Resources). The CP protein used in this work is human CP-Ser, which is the heterooligomer of S100A8(C42S) and S100A9(C3S).[4] CP-Ser is referred to as "CP" in the text. It was overexpressed and purified as described previously.[4] Protein concentration was determined using the calculated extinction coefficient for the S100A8(C42S)/S100A9(C3S) heterodimer (A_{280} = 18,450 $M^{-1}cm^{-1}$, calculated using the ProParam tool available at http://web.expasy.org/protparam/). All B-CP and CP protein concentrations are for the heterodimer.

4.3.2 Preparation of Biotin-CP (B-CP)

B-CP was prepared by conjugating biotin polyethyleneoxide iodoacetamide (BPEOIA, Sigma) to the Cys3 thiol moiety of the S100A9 subunit of CP(C42S) (the heterooligomer of S100A8(C42S) and native S100A9) using the procedure previously described for a biotinylated CP ΔHis_3Asp variant.[10] The Ca(II)-dependent oligomerization properties of the protein were evaluated by analytical size-exclusion chromatography (SEC) using a reported procedure.[4, 10]

4.3.3 Cloning, Overexpression and Purification of MntC

The Wizard Genomic DNA Purification Kit (Promega, manufacturer protocol) was used to isolate genomic DNA from *S. aureus* USA300 JE2. A portion of the *mntC* gene

that lacks the sequence for the N-terminal lipid anchor (*mntC*$^{19\text{-}309}$) was PCR amplified from *S. aureus* USA300 JE2 genomic DNA using the forward primer 5'-ggaatccatatgggtactggtggtaaacaaag-3' (*Nde*I restriction site underlined) and reverse primer 5'-gatcctcgag**tta**tttcatgcttccgtgtac-3' (*Xho*I restriction site underlined, stop codon bold). Polymerase chain reactions were performed using Pfu Turbo DNA polymerase (Stratagene). The amplified *mntC* gene sequence was digested with *Nde*I and *Xho*I (New England Biolabs), purified by 1% agarose gel electrophoresis, and subsequently isolated with the GE Illustra PCR and Gel Band Purification Kit. The resulting gene was ligated into the *Nde*I and *Xho*I sites of pET41a using T4 DNA ligase (New England Biolabs). Following the ligation reaction, the vector was transformed into chemically competent *Escherichia coli* TOP10 cells and isolated using a miniprep kit (Qiagen). The identity of the resulting pET41a-*mntC* construct was verified by DNA sequencing (MIT Biopolymers). The plasmid pET41a-*mntC* was transformed into chemically competent *E. coli* BL21(DE3). Freezer stocks were prepared by combining a 1:1 ratio of an overnight culture (LB, 50 μg/mL kanamycin, 37 °C, 9 h, 150 rpm) and sterile 50% glycerol, and flash freezing the mixture in liquid nitrogen. Cell stocks were stored at -80 °C. For protein overexpression, 40 mL of LB containing 50 μg/mL kanamycin was inoculated from a freezer stock and grown overnight with shaking (37 °C, 150 rpm, 12-16 h). This overnight culture was diluted 1:100 into 1 L of LB medium containing 50 μg/mL kanamycin, and the resulting culture was incubated with shaking (37 °C, 150 rpm). At OD_{600} ≈0.6, protein expression was induced by addition of 500 μM IPTG (1 mL of a 0.5 M stock solution in water). The culture was grown for another ≈3.5 h at which time the cells were pelleted by

centrifugation (3,000 rpm, 20 min, 4 °C), frozen in liquid nitrogen, and stored at -80 °C. Cell pellets weighed ≈2.5 g / L of culture.

A cell pellet obtained from 1 L of culture was thawed on ice. Lysis buffer A (50 mM MES, pH 6.5, 100 mM NaCl, 1 mM EDTA, 0.5% Triton X-100) was stored at 4 °C and supplemented with 1 mM PMSF (Amresco, prepared immediately before use by dissolving 21 mg in ≈1 mL EtOH) immediately prior to use. The pellet was suspended in 60 mL of cold lysis buffer A, and transferred to an ice-cold stainless steel beaker, and lysed on ice by sonication by using a Branson sonicator (30 sec pulse on, 10 sec pulse off, 2.5 min, 40% amplitude). The lysate was then centrifuged (10 min, 14,000 rpm, 4 °C) and the supernatant was transferred to a glass beaker on ice. The resulting cell pellet was resuspended in 60 mL of lysis buffer A and the sonication and centrifugation process was repeated with this material. The combined supernatants were moved to a 4 °C room and treated with 60% ammonium sulfate (Sigma) for ≈1 h with stirring. This procedure resulted in the precipitation of contaminating proteins. The mixture was centrifuged (20 min, 14,000 rpm, 4 °C) and vacuum filtered. The filtrate (≈130 mL) was transferred to dialysis tubing (Spectra/Por 3,500 kDa MWCO) and dialyzed against 4 L of 20 mM HEPES, pH 7.0 at 4 °C (2 x ≈12-24 h).

The dialyzed protein solution was centrifuged (10 min, 14,000 rpm, 4 °C) and filtered (0.2 μm filter). A GE ÄKTA Purifier housed in a 4 °C room was employed for ion exchange and size exclusion chromatographic purification. MntC was first purified by cation exchange chromatography using a MonoS 10/100 cation exchange column with elution buffers composed of 20 mM HEPES, pH 7.0, without (buffer A) or with (buffer B) 1 M NaCl. MntC was eluted with a gradient of 0–30% buffer B over 15 column volumes

at a 2 mL/min flow rate. MntC-containing fractions (identified by SDS-PAGE) were combined, concentrated to ≈10 mL by centrifugation (3,700 rpm, 4 °C) using a 15-mL spin filter (Pall, 10 kDa MWCO) and loaded onto a HiLoad 26/600 Superdex-75 gel filtration column pre-equilibrated with 20 mM HEPES, pH 7.0, 200 mM NaCl. MntC was eluted from the column using a flow rate of 1 mL/min. Fractions containing MntC were combined, transferred to dialysis tubing (Spectra/Por, 3,500 kDa MWCO), and dialyzed against 4 L of de-metalating buffer (100 mM acetic acid, 20 mM EDTA, pH 3.7) at room temperature (2 x ≈12 h). MntC was then dialyzed once (≈12 h, 4 °C) against 4 L of storage buffer (20 mM HEPES, 200 mM NaCl, pH 7.0) and subsequently filtered (0.2-μm syringe filter; this step is optional), concentrated by centrifugation (3,700 rpm, 4 °C) using a 15-mL spin filter (Pall, 10 kDa MWCO), aliquoted, flash frozen in liquid nitrogen, and stored at -80 °C. Typical yields of MntC were ≈30 mg / L culture.

4.3.4 Cloning, Overexpression and Purification of PsaA

A fragment of *Streptococcus pneumoniae* D39 genomic DNA containing the *psaA* gene was provided by Professor David P. Giedroc (Indiana University). The NCBI reference sequence NC_011072.1 was used to design primers for amplification of a portion of the *psaA* gene that lacks the sequence for the N-terminal lipid anchor ($PsaA^{21-309}$). The forward primer 5'-ggaatccatatggctagcggaaaaaaagatac-3' (*Nde*I restriction site underlined) and the reverse primer (5'-gatcctcgag**tta**ttttgccaatccttcag-3' (*Xho*I restriction site underlined, stop codon in bold) were used to PCR amplify *psaA* as described above for *mntC*. The gene was ligated into the *Nde*I and *Xho*I sites of pET41a using T4 DNA ligase. Following the ligation reaction, the vector was transformed into chemically-

competent *Escherichia coli* TOP10 cells and isolated using a miniprep kit (Qiagen). The identity of the resulting pET41a-*psaA* construct was verified by DNA sequencing (MIT Biopolymers). The plasmid pET41a-*psaA* was transformed into chemically competent *E. coli* BL21(DE3). Freezer stocks were prepared by combining a 1:1 ratio of an overnight culture (LB, 50 μg/mL kanamycin, 37 °C, 9 h, 150 rpm) and sterile 50% glycerol, and flash freezing the mixture in liquid nitrogen. Cell stocks were stored at -80 °C. For protein overexpression, 50 mL of LB containing 50 μg/mL kanamycin was inoculated from a freezer stock and grown overnight with shaking (37 °C, 150 rpm, 12-16 h). This overnight culture was diluted 1:100 into 2 L of LB medium containing 50 μg/mL kanamycin, and the resulting culture was incubated with shaking (37 °C, 150 rpm). Once the cultures reached OD_{600} ≈0.6, overexpression of PsaA was induced with 100 μM IPTG. The cultures were incubated at 37 °C and 150 rpm for an additional ≈3.5 h, and the cells were pelleted by centrifugation (3,000 rpm, 20 min, 4 °C). Cell pellets were frozen in liquid nitrogen and stored at -80 °C. Cell pellets weighed ≈4.6 g / 2 L culture.

A cell pellet from 2 L of culture was thawed on ice. PMSF (1 mM, prepared immediately before use by dissolving 17.4 mg in ≈1 mL EtOH) was added to ≈100 mL of lysis buffer B (50 mM Tris-HCl, pH 8.0, 100 mM NaCl, 1 mM EDTA, 0.5% Triton X-100) immediately before use. The pellet was suspended in 50 mL lysis buffer B and lysed by sonication with a Branson sonicator (30 sec pulse on, 10 sec pulse off, 2.5 min, 40% amplitude). The lysate was then centrifuged (10 min, 14,000 rpm, 4 °C) and the PsaA-containing supernatant was transferred to a glass beaker on ice. The lysis process was repeated on the remaining pellet with a second 50-mL aliquot of lysis buffer B. The

supernatant fractions were combined and dialyzed (Spectra/Por 3,500 kDa MWCO) in 4 L of 20 mM HEPES, pH 8.0 at 4 °C (3 x ≈12-24 h).

The dialyzed protein solution was centrifuged (10 min, 14,000 rpm, 4 °C) and filtered (0.2 μm). A GE ÄKTA Purifier housed in a 4 °C room was employed for ion exchange and size exclusion chromatographic purification. PsaA was first purified by anion exchange chromatography. A MonoQ 10/100 anion–exchange column was used with elution buffers composed of 20 mM HEPES, pH 8.0 without (buffer A) or with (buffer B) 1 M NaCl. PsaA was eluted with 0–30% buffer B over 15 column volumes with a flow rate of 2 mL/min. When purified from a 2-L culture, PsaA eluted as a broad peak that contained apo and Zn(II)-bound PsaA. During optimization of this protocol when PsaA was purified on a smaller scale (200-mL culture), two base-line separated peaks eluted that corresponded to apo and Zn(II)-bound PsaA (as determined by ICP-MS analysis), respectively. All of the PsaA-containing fractions were combined, concentrated to ≈10 mL, and loaded onto a Hiload 26/600 Superdex-75 gel filtration column pre-equilibrated with 75 mM HEPES, 100 mM NaCl, pH 7.5. The fractions containing PsaA were transferred to a dialysis bag (Spectra/Pro 3,500 kDa MWCO) and dialyzed in 4 L of de-metalating buffer (100 mM acetic acid, 20 mM EDTA, pH 3.7) at room temperature (2 x ≈12-24 h). The PsaA solution was then dialyzed (Spectra/Por 3,500 kDa MWCO) once against the storage buffer (20 mM HEPES, 100 mM NaCl, pH 7.5) in a 4 °C cold room (≈12 h) before it was filtered (0.2 μm filter), concentrated by centrifugation (Pall, 15-mL spin filter, 10 kDa MWCO) aliquoted, frozen in liquid nitrogen, and stored at -80 °C. The yield of protein was typically ≈100 mg / 2 L of culture.

4.3.5 Buffer Exchange of MntC and PsaA

For all experiments presented in this work, the purified SBPs were buffer-exchanged six times using 0.5-mL Amicon spin filters. During initial experiments, we found evidence for EDTA contamination in the protein samples when less thorough buffer exchange was performed. For instance, in one case, Mn(II) competition titrations with ZP1 showed that the protein sample outcompeted ZP1 for >4 equiv. of Mn(II) when only three rounds of buffer exchange were performed, whereas the SBP outcompeted ZP1 for 1 equiv. of Mn(II) with six rounds of buffer exchange.

4.3.6 Circular Dichroism Spectroscopy.

A Jasco J-1500 circular dichroism spectrometer housed in the Biophysical Instrumentation Facility at MIT was used for all measurements. Proteins were thawed on ice and buffer-exchanged into 1 mM Tris-HCl, pH 7.5 using 10 kDa MWCO Amicon spin concentrators. CD samples (300 μL) were prepared using 10-41 μM protein with and without 1.0 equiv of Mn(II). Samples were transferred to a nitric acid-washed Hellma quartz cuvette (1-mm path length) for data collection. CD spectra were recorded from 195 to 260 nm using continuous scan mode (50 nm/min) and a 1-nm bandwidth. All data represent averages of three replicate baseline-subtracted scans, where the baseline scan was obtained from the buffer.

4.3.7 Liquid-Chromatography Mass-Spectrometry (LC-MS)

An Agilent 1290 series LC system with an Agilent Jetstream ESI source and Agilent 6230 TOF system was utilized for protein mass spectrometry. An Agilent Poroshell

300SB-C18 column (5-μm particle size) was used for gradient elution (60–85% B over 13 min at 0.2 mL/min) with 0.1% formic acid in water (solvent A) and 0.1% formic acid in acetonitrile (solvent B). Protein samples were thawed and diluted in Milli-Q water to a final concentration of ≈30-40 μM, and 10 μL was injected. The Agilent MassHunter Workstation Data Acquisition Software was used with the Agilent MassHunter Qualitative Analysis program for analysis.

4.3.8 Metal Analysis by Inductively-Coupled Plasma Mass Spectrometry (ICP-MS)

An Agilent 7900 instrument outfitted with an auto-sampler housed in the Center for Environmental Health Sciences (CEHS) Bioanalytical Core Facility at MIT was employed for all ICP-MS. Metal ion concentrations were analyzed in He mode. The spectrometer was calibrated immediately prior to each sample analysis using an Environmental Calibration Standard mix (Agilent) serially diluted in ≈3% nitric acid. All standards and samples were spiked with internal standard (2 ppb Tb, Agilent) to monitor for sample effects. For analysis of the metal content in PsaA and MntC, samples were prepared by diluting a protein stock solution ≥35-fold in ≈3% nitric acid to afford a final concentration of 7-20 μM. For analysis of the metal content in samples obtained from the B-CP pull-down assay (*vide infra*), 200 μL of B-CP assay flow-through was diluted with 1.2 mL of ≈3% nitric acid, and 28 μL of Tb internal standard (2 ppb) was added. In all cases, ICP-MS samples were centrifuged (10 min, 13,000 rpm, 4 °C) as a precaution to remove any particulates or precipitated material prior to analysis.

4.3.9 Mn(II) Competition Titrations with ZP1

Mn(II) competition titrations between the fluorescent metal sensor ZP1 and either MntC or PsaA were performed as described previously for CP variants.[6] In brief, aliquots of MntC and PsaA were thawed and subsequently buffer-exchanged into titration buffer (75 mM HEPES, 100 mM NaCl, pH 7.0) using 0.5-mL Amicon spin filters (10 kDa MWCO). For each titration, a 2-mL solution of titration buffer containing ZP1 (1 μM) and either MntC (4 μM) or PsaA (4 μM) was prepared in a 1-cm path length nitric acid-washed quartz cuvette. The mixture was titrated with Mn(II) (2 or 4 μL of a 500-μM Mn(II) solution in Milli-Q water). After each Mn(II) addition, the solution was gently mixed and incubated for ≥4 min at room temperature prior to recording the fluorescence emission. Emission spectra were collected on a Photon Technologies International QuantaMaster 40 fluorimeter outfitted with a continuous xenon source for excitation, autocalibrated QuadraScopic monochromators, a multimode PMT detector, and a circulating water bath maintained at 25 °C. This instrument was controlled by the FelixGX software package. The excitation wavelength was 490 nm. The emission spectra were collected and integrated over 500-650 nm.

4.3.10 Mn(II) Competition Assay Monitored by B-CP Pull-Down

To examine Mn(II) competition between CP and either MntC or PsaA, 300-μL solutions containing 20 μM MntC or PsaA, 20 μM B-CP, and 18 μM Mn(II) were prepared with or without 400 μM Ca(II) in plastic microcentrifuge tubes (75 mM HEPES, pH 7.5, 100 mM NaCl). In each case, Mn(II) was added last and the solutions were gently mixed by using a pipetman, capped, and incubated at room temperature for 10 h, at which time

pull-down with streptavidin resin was performed. Immediately prior to use, streptavidin resin (Thermo Scientific, 200 μL) was transferred to a spin-X centrifuge tube with a 0.22-μm cellulose acetate filter (Corning) and washed. To wash the resin, 500 μL of buffer (75 mM HEPES, pH 7.5, 100 mM NaCl) was added, the sample was centrifuged (2 min, 13,000 rpm, 4 °C), and the flow-through was discarded. The resin was washed three times in this manner before application of the protein mixture. The samples (300 μL) were transferred to the filters containing the washed resin, and the filters were capped and mixed by inversion on a tube rotator for 45 min at room temperature. The samples were then centrifuged (3 min, 13,000 rpm, 4 °C) to separate the B-CP-containing resin and SBP-containing flow-through. Aliquots (200 μL) of the flow-through were prepared for ICP-MS as described above. The flow-through was also analyzed by SDS-PAGE. Samples for which the pull-down was not performed were prepared for ICP-MS analysis in the same manner to measure the total Mn concentration in the starting mixtures.

4.3.11 EPR Sample Preparation of Mn(II)-MntC, Mn(II)-PsaA

MntC and PsaA were buffer-exchanged into 75 mM HEPES, 100 mM NaCl, pH 7.5. Protein concentrations were determined by absorbance at 280 nm (ε_{280} = 35,870 M^{-1} cm^{-1} for MntC and PsaA, calculated using the ProParam tool available at http://web.expasy.org/protparam/). To prepare 0.75:1 Mn(II)-MntC and Mn(II)-PsaA samples, 750 μM Mn(II) (1.6 μL from a 100 mM working solution in Milli-Q water) was added to MntC or PsaA (1 mM protein, 210 μL). The samples were incubated for 15 min before a 200-μL portion was transferred to an SQ EPR tube (≈4x3 mm OD x ID) and frozen in liquid nitrogen. We also examined the effect of PEG-200 on the Mn(II) EPR

spectra of Mn(II)-MntC and Mn(II)-PsaA. Samples without PEG-200 contained 750 μM Mn(II) and 1 mM SBP (75 mM HEPES, 100 mM NaCl, pH 7.5). Samples with 20% PEG-200 contain 750 μM Mn(II) and 1 mM SBP for the Mn(II)-PsaA sample or 500 μM Mn(II) and 1.1 mM protein for the Mn(II)-MntC sample (75 mM HEPES, 100 mM NaCl, pH 7.5, 20% PEG-200 (v/v)). A comparison of the Mn(II) EPR spectra of samples prepared with and without PEG-200 showed that the presence of PEG-200 affected the signal for each protein (**Figure 4.1**). As a result, all EPR spectroscopy studies were performed without PEG in the sample. The samples were shipped to the University of California Davis in a liquid-nitrogen cooled shipping dewar for EPR spectroscopic analysis.

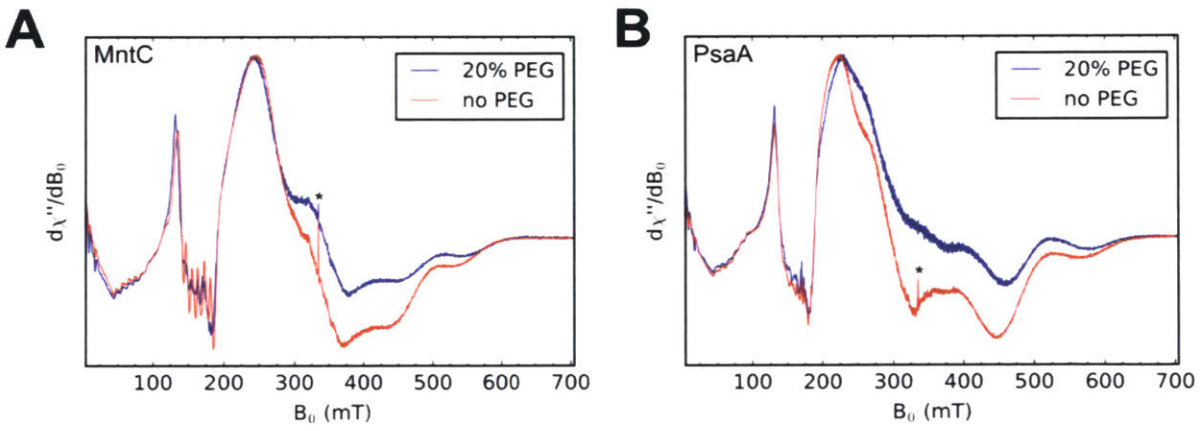

Figure 4.1. X-band CW EPR spectra of Mn(II)-MntC (**A**) and Mn(II)-PsaA (**B**) with and without 20% (v/v) PEG-200 in the sample. Samples without PEG-200 contain 750 μM Mn(II) and 1 mM protein (75 mM HEPES, 100 mM NaCl, pH 7.5). Samples with 20% PEG-200 contain 500 μM Mn(II) and 1.1 mM protein for Mn(II)-MntC or 750 μM Mn(II) and 1.0 mM protein for Mn(I)-PsaA (75 mM HEPES, 100 mM NaCl, pH 7.5, 20% PEG-200 (v/v)). The asterisk denotes a quartz background signal. Spectrometer settings: ν_{mw} = 9.4 GHz, 0.5 mT modulation amplitude at 100 kHz, power = 200 μW, temperature = 10 K.

4.3.12 Mn(II) Transfer Assay Monitored by EPR Spectroscopy

To investigate Mn(II) transfer from Mn(II)-MntC or Mn(II)-PsaA to CP-Ser, end-point and time-course experiments were performed. For the end-point experiments, solutions of CP-Ser (1 mM) were prepared with or without 10 equivalents of Ca(II) (10 mM from a 1-M stock solution) in 75 mM HEPES, 100 mM NaCl, pH 7.5. This Ca(II):CP-Ser ratio was selected on the basis of prior EPR spectroscopic investigations of Mn(II)-CP.[4] Solutions containing 1 mM SBP and 1 mM Mn(II) were prepared in 75 mM HEPES, 100 mM NaCl, pH 7.5 and incubated for 15 min at room temperature. Subsequently, a 90 μL portion of the CP-Ser solution was added to 90 μL of the Mn(II)-SBP solution, which afforded 180-μL mixture containing 500 μM CP-Ser, 500 Mn(II)-SBP with or without 5 mM Ca(II). The solutions were gently mixed with a pipetman and incubated for 10 h at room temperature. Then, 170 μL of each solution was transferred to a PQ EPR tube (Wilmad-706-PQ-9.50; 3.8 x 2.8 mm OD x ID) and frozen in liquid nitrogen. This experiment was performed twice and representative spectra from one trial are presented. No discernible spectral differences were detected between the two trials.

For the time course experiments, solutions (≈1.5 mL) containing 1 mM CP-Ser and 10 mM Ca(II) were was prepared in 75 mM HEPES, 100 mM NaCl, pH 7.5 as described above. Solutions (360 μL) containing 1 mM SBP and 1 mM Mn(II) were prepared in 75 mM HEPES, 100 mM NaCl, pH 7.5 and incubated for 15 min at room temperature. A 360-μL portion of the CP-Ser solution was then added to the Mn(II)-SBP solution to afford a 720-μL mixture containing 500 μM CP-Ser, 500 μM Mn(II)-SBP, and 5 mM Ca(II). The solution was mixed for ≈10 sec with a pipetman and a 170-μL aliquot was transferred to a PQ EPR tube. At t = 30 sec after addition of the CP-Ser solution, this sample was frozen

in liquid nitrogen. The remaining assay solution was incubated at room temperature, and additional 170-μL aliquots were taken, transferred to PQ EPR tubes, and frozen in liquid nitrogen at t = 5, 10, and 30 min. In each case, freezing of an EPR sample began at the indicated time point and took ≈40 seconds to freeze completely. The samples were shipped to the University of California Davis in a liquid-nitrogen cooled shipping dewar for EPR spectroscopic analysis. Following optimization, this time course experiment was performed in duplicate and spectra from one representative trial are presented. No discernible spectral differences were detected between the two trials.

4.3.13 EPR Spectroscopy

All low-temperature continuous-wave (CW) electron paramagnetic resonance (EPR) spectra were collected on a Bruker E500 spectrometer equipped with a super-high QE (SHQE) resonator and an Oxford Instruments ESR900 cryostat. A data point was collected every 0.34 mT (1 mT = 10 G) with a conversion time of 80 ms and 0.5 mT of field modulation at 100 kHz. The microwave power was 200 μW and the frequency was 9.4 GHz. All spectra presented were collected under slow passage conditions at 10 K.

4.3.14 Antimicrobial Activity Assay

The growth inhibitory activity of B-CP against *Escherichia coli* ATCC 25922 was evaluated using a reported protocol.[4] The antimicrobial activity assay medium was a 32:68 (v/v) mixture of tryptic soy broth (TSB) and antimicrobial assay buffer (20 mM Tris-HCl, 100 mM NaCl, pH 7.5 supplemented with 3 mM Ca(II) and 5 mM β-mercaptoethanol).

4.4 Results

4.4.1 Preparation and Characterization of MntC and PsaA

In an effort to achieve a molecular picture of Mn(II) competition between CP and SBPs, we overexpressed and purified MntC and PsaA. Guided by reported studies of these proteins, we prepared MntC and PsaA that lack the N-terminal lipid anchors and obtained soluble proteins during overexpression.[14, 20, 22-24] We overexpressed and purified each SBP without an affinity tag using ion exchange chromatography followed by size exclusion chromatography. For MntC, the lysate was treated with ammonium sulfate to precipitate contaminating proteins prior to column purification. Both MntC and PsaA purifications afforded the proteins in high yield and purity, and properly folded, as evidenced by liquid-chromatography mass spectrometry (LCMS), SDS-PAGE, and circular dichroism (CD) spectroscopy (**Table 4.1, Figures 4.2, 4.3**). The SBPs were found to accumulate bound metals during purification, so a demetallation step was employed post-purification to remove contaminating metal ions (**Table 4.2**), which afforded MntC and PsaA with notably low metal content (**Table 4.3**). Mn(II) competition titrations with the metal-ion sensor ZP1 indicated that both SBPs outcompete ZP1 ($K_{d,Mn(II)}$ = 550 nM)[25] for 1 equiv of Mn(II) in the absence and presence of excess Ca(II) (**Figure 4.4**), which confirmed that each SBP was obtained predominantly in the apo form and binds 1 equiv of Mn(II) with high affinity.

Table 4.1. Summary of Results from Protein Mass Spectrometry.[a]

Protein	Calculated Mass ± ^{N}Met (Da)[b]	Observed Mass (Da)[c]
MntC$^{19-309}$	32967.33	n.f.[e]
	32836.13 (-Met1) [d]	32837.99
PsaA$^{21-309}$	32596.75	n.f.[e]
	32465.55 (-Met1) [d]	32466.17
B-CP (S100A8(C42S) subunit)	10,818.4	10,818.93
B-CP (biotinylated S100A9 subunit)	13,525.3 (-Met1) [d]	13,525.64

[a] A denaturing protocol on an Agilent Poroshell 300SB-C18 column over a 60-85% gradient of acetonitrile in 0.1 % formic acid was utilized for LC-MS. [b] Molecular weights were calculated by using the ProtParam tool found on the ExPASy site (http://web.expasy.org/protparam). [c] Masses were calculated with the Agilent MassHunter BioConfirm software package. [d] The N-terminal methionine can be cleaved during overexpression in *E. coli*. [e] Not found; the mass was not found following deconvolution of the raw data.

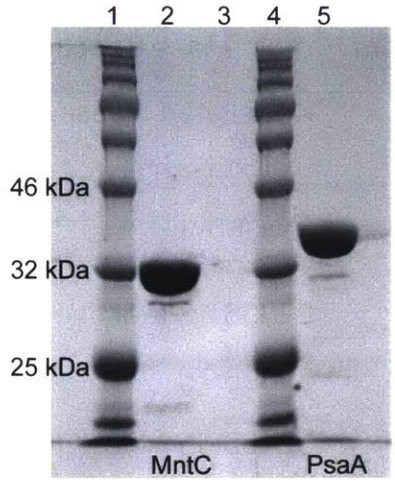

Figure 4.2. SDS-PAGE gel (12% Tris-glycine) of purified MntC and PsaA. Lanes: (1) ladder P7712S (New England Biolabs), (2) MntC, (3) empty lane, (4) ladder P7712S (New England Biolabs), (5) PsaA. The SBPs were overexpressed as MntC$^{19\text{-}309}$ (32.8 kDa) and PsaA$^{21\text{-}309}$ (32.5 kDa) to obtain soluble protein. The N-terminal region of each full-length protein contains a hydrophobic lipid anchor.

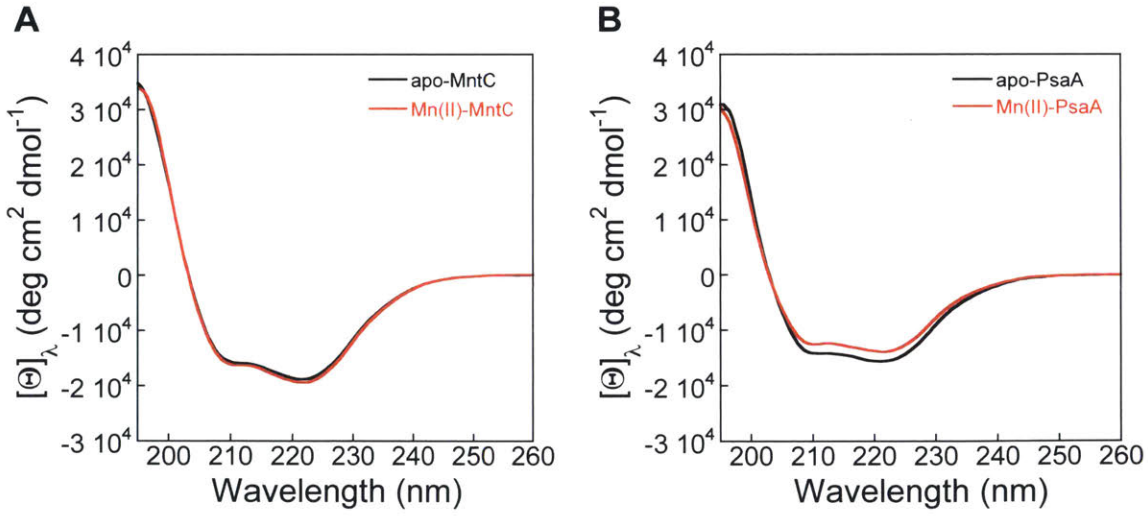

Figure 4.3. Circular dichroism spectra of 10 μM MntC and 41 μM PsaA with no metal added (black) or 1 equivalent of Mn(II) added (red) in 1 mM Tris-HCl, pH 7.5.

Table 4.2. Metal content of SBP samples at stages during representative protein purifications.

Metal	*MntC Purification Steps*			*PsaA Purification Steps*		
	Dialysis[a] (4.9 μM)	Post-IEX[b] (5.4 μM)	Post-SEC[c] (4.9 μM)	Dialysis[a] (12.4 μM)	Post-IEX[b] (6.7 μM)	Post-SEC[c] (n.d.[d])
[Mn] (μM)	0.029	0.067	0.064	0.059	0.101	*n.d.*[d]
equivalents[e]	0.006	0.012	0.013	0.005	0.015	*n.d.*[d].
[Fe] (μM)	0.324	0.223	0.150	0.574	0.939	*n.d.*[d].
equivalents[e]	0.066	0.041	0.031	0.046	0.141	*n.d.*[d].
[Co] (μM)	0.001	0.001	0.001	0.001	0.001	*n.d.*[d].
equivalents[e]	0.000	0.000	0.000	0.000	0.000	*n.d.*[d].
[Ni] (μM)	0.112	0.108	0.101	0.021	0.002	*n.d.*[d].
equivalents[e]	0.023	0.02	0.021	0.002	0.003	*n.d.*[d].
[Cu] (μM)	0.008	0.006	0.007	0.008	0.008	*n.d.*[d].
equivalents[e]	0.002	0.001	0.001	0.001	0.001	*n.d.*[d].
[Zn] (μM)	0.169	0.878	0.872	0.718	2.19	*n.d.*[d].
equivalents[e]	0.034	0.163	0.178	0.058	0.329	*n.d.*[d].

[a] Metal analysis (ICP-MS) was performed after lysis and dialysis into the ion-exchange chromatography (IEX) buffer before column purification. [b] Metal analysis (ICP-MS) was performed after IEX. [c] Metal analysis (ICP-MS) was performed size-exclusion chromatography (SEC). [d] Not determined. [e] Equivalents of metal compared to the protein concentration.

Table 4.3. Metal content of representative purified SBPs.[a]

Metal	Protein	
	MntC (8 μM)	PsaA (19.5 μM)
[Mn] (μM)	0.004	0.011
equivalents[b]	0.001	0.001
[Fe] (μM)	0.096	0.167
equivalents[b]	0.012	0.009
[Co] (μM)	0.0004	0.0003
equivalents[b]	0.000	0.000
[Ni] (μM)	0.036	0.102
equivalents[b]	0.004	0.005
[Cu] (μM)	0.005	0.006
equivalents[b]	0.001	0.000
[Zn] (μM)	0.184	0.137
equivalents[b]	0.023	0.007

[a] Metal content was determined by ICP-MS. [b] Equivalents of metal compared to the protein concentration.

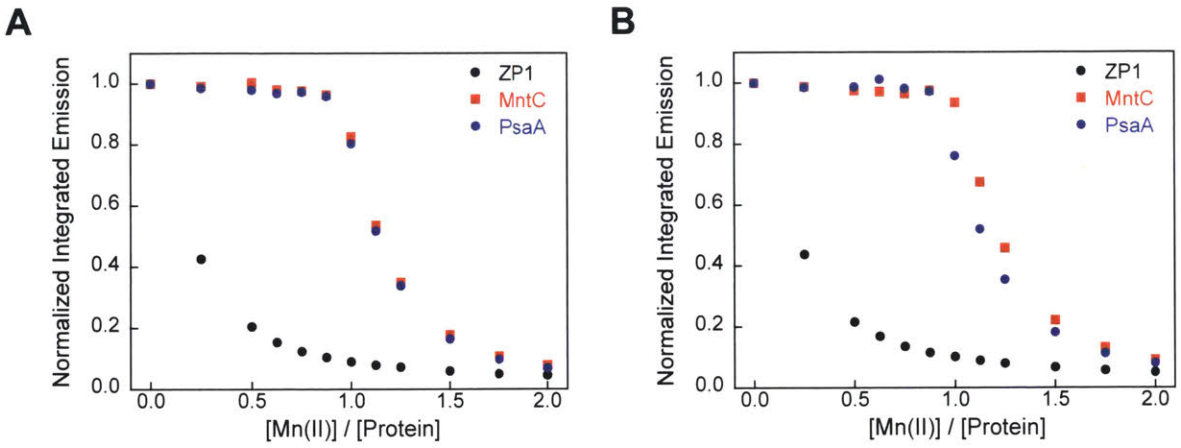

Figure 4.4. Representative Mn(II) competition titrations of ZP1 (1 μM) and MntC (4 μM) or PsaA (4 μM) in 75 mM HEPES, 100 mM NaCl, pH 7.0 in the absence (**A**) and presence (**B**) of 400 μM Ca(II). Black circles: titration of ZP1 with Mn(II) in the absence of a SBP; red squares: titration of ZP1 and MntC with Mn(II); blue circles: titration of ZP1 and PsaA with Mn(II). For ZP1, the reported apparent $K_{d1,Mn(II)}$ is 550 nM at pH 7.0.[25]

4.4.2 Biotin-CP and SBP Mn Competition Assay

To evaluate the competition for Mn(II) between CP and the SBPs, we first designed a pull-down assay for evaluating Mn(II) speciation between the SBPs and CP. We prepared biotinylated CP (B-CP), which has a biotin moiety covalently attached to Cys3 of S100A9, and established that it displays Ca(II)-dependent heterotetramerization, antibacterial activity comparable to the unmodified protein, and coordinates Mn(II), Fe(II) and Zn(II) with the expected stoichiometries (**Figures 4.5, 4.6**). Next, we prepared solutions containing 18 μM Mn(II), 20 μM SBP, and 20 μM B-CP in the absence and presence of 400 μM Ca(II) at pH 7.5. We selected a 10-h time point for this preliminary experiment because we lacked information about the timescale required for the mixture to reach equilibrium. Following removal of B-CP with streptavidin resin (**Figure 4.7**), we analyzed the Mn(II) content of the solution by inductively-coupled plasma mass spectrometry (ICP-MS) (**Figure 4.8**). In the absence of Ca(II), >80% of Mn(II) remained

in solution, presumably bound by the SBP. In the presence of Ca(II), <4% of Mn(II) remained in solution, indicating that B-CP outcompeted the SBPs for Mn(II) and the pull-down removed Mn(II) from solution. These data provide evidence that the Ca(II)-bound, high-affinity form of CP coordinates Mn(II) with greater affinity than MntC or PsaA. This Ca(II)-bound CP species is expected to exist in the extracellular space where Ca(II) concentrations are ≈2 mM.[26, 27]

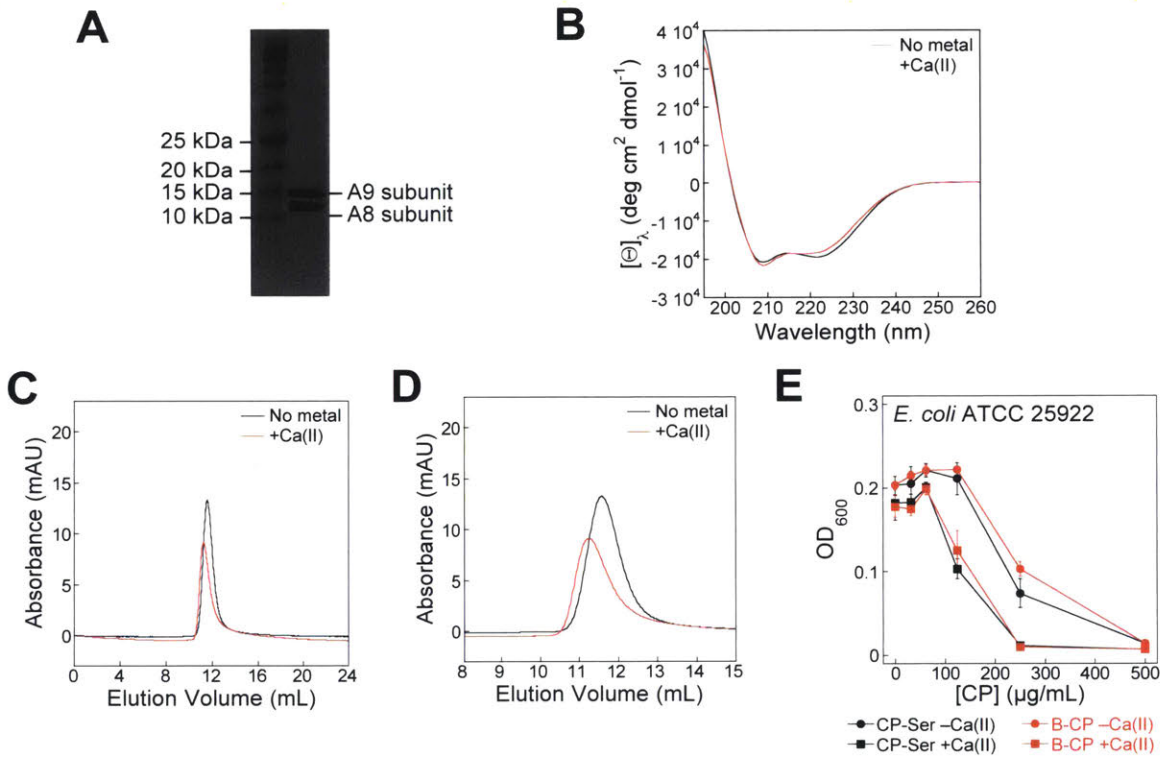

Figure 4.5. Characterization of B-CP. (**A**) SDS-PAGE gel (15% Tris-glycine) of purified B-CP with the P7704 protein ladder (New England BioLabs). (**B**) Circular dichroism spectra of 10 μM B-CP in the absence and presence of 2 mM Ca(II) in 1.0 mM Tris-HCl, pH 7.5. (**C**) Analytical SEC of 20 μM B-CP in the absence and presence of 2 mM Ca(II) in 75 mM HEPES, 100 mM NaCl, pH 7.0. B-CP elutes at ≈11.7 mL (–Ca(II)) and ≈11.1 mL (+Ca(II)), and these peak elution volumes correspond to the αβ heterodimer and $\alpha_2\beta_2$ heterotetramer, respectively.[4, 10] (**D**) Zoom-in view of analytical SEC chromatograms presented in panel D. (**E**) Antimicrobial activity of CP-Ser (positive control) and B-CP against *E. coli* ATCC 25922. The mean OD_{600} values and SEM are shown (n = 3; t = 20 h, T = 30 °C, 150 rpm).

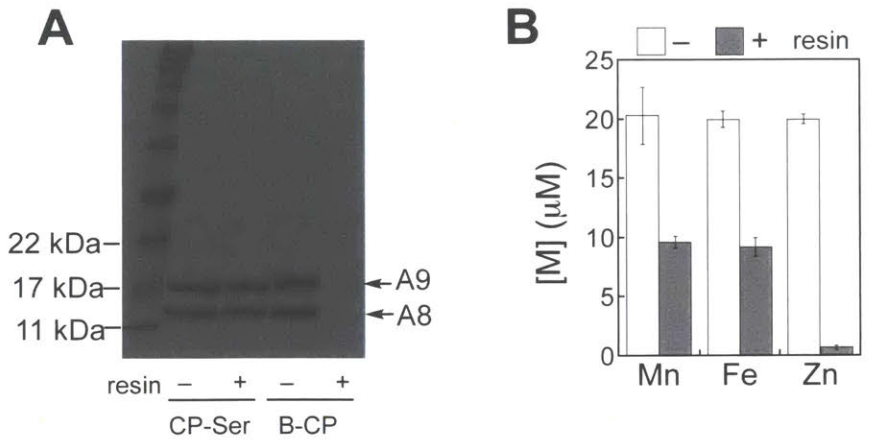

Figure 4.6. B-CP binds to streptavidin agarose resin and complexes transition metals. (**A**) SDS-PAGE gel (15% Tris-glycine) of 10 μM CP-Ser and B-CP in 75 mM HEPES, 100 mM NaCl, pH 7.0 before and after pull-down with streptavidin agrose resin. (**B**) B-CP (10 μM) was pre-incubated with 20 μM Mn(II), 20 μM Fe(II) or 20 μM Zn(II) and each mixture was treated with streptavidin agarose resin (75 mM HEPES, 100 mM NaCl, pH 7.0, 2 mM Ca(II)). The metal content of each solution was measured before (light gray bars) and after (dark gray bars) pull-down with streptavidin agarose resin by ICP-MS.

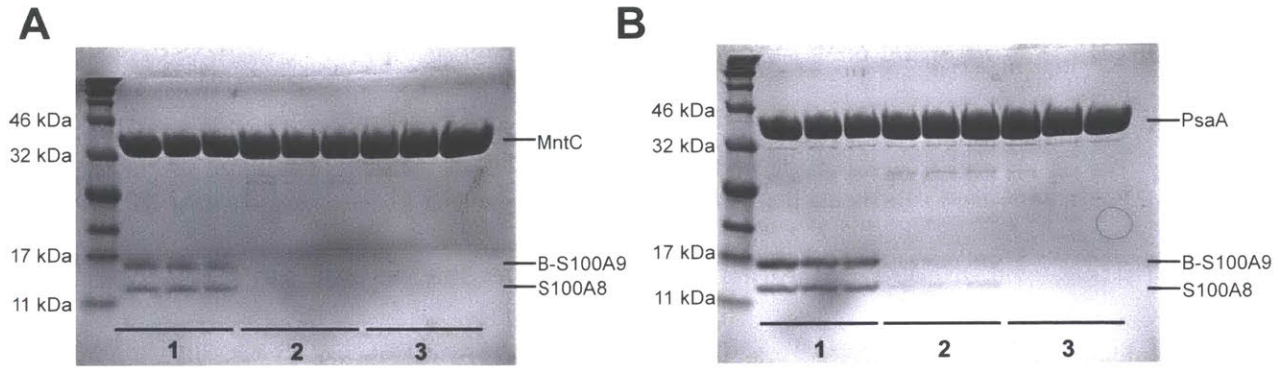

Figure 4.7. SDS-PAGE (15% Tris-glycine) analysis of B-CP pull-down assays. (**A**) The gel corresponds to the competition between MntC and B-CP for Mn(II). (**B**) The gel corresponds to the competition between PsaA and B-CP for Mn(II). The samples labeled as 1-3 are from mixtures of B-CP, SBP and Mn(II) (1) prior to pull-down, (2) the soluble portion after pull-down with streptavidin agarose resin for experiments performed without added Ca(II), and (3) the soluble portion after pull-down with streptavidin agarose resin for experiments performed in the presence of added Ca(II). The three lanes per type of sample correspond to three independent replicates. The results from metal analysis are presented in Figure 4.8.

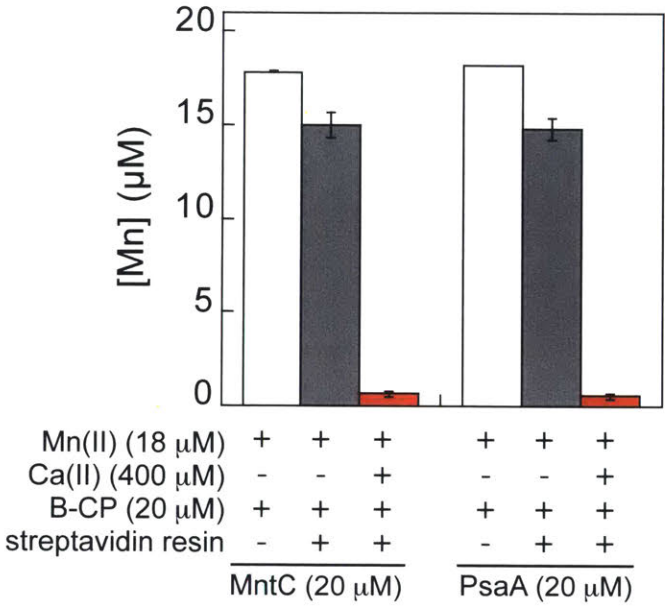

Figure 4.8. Concentration of Mn(II) in solution determined by ICP-MS following pull-down of mixtures containing B-CP, MntC or PsaA, and Mn(II) with or without Ca(II) (75 mM HEPES, 100 mM NaCl, pH 7.5). The mixtures were incubated for 10 h at room temperature before pull-down.

4.4.3 Electron Paramagnetic Resonance (EPR) Spectroscopy of the Mn(II)-SBPs

Because removal of B-CP from solution by streptavidin resin takes minutes, we limited application of this assay to the end-point analysis. Moreover, we sought to directly observe and discriminate between Mn(II) bound to CP versus the SBPs in the same assay mixture at varying time points. Low-temperature EPR spectroscopy is ideally suited for this purpose because previous structural studies demonstrated that the Mn(II)-binding sites of CP and the SBPs have notably distinct coordination environments and degrees of symmetry. The high-affinity Mn(II)-His_6 site of CP shows a nearly idealized octahedral coordination geometry.[5, 6, 9] Prior EPR spectroscopy of this site revealed a six-line pattern centered at $g = 2$ (≈335 mT) with a low zero-field splitting (ZFS) of 485 MHz ($E/D = 0.30$) for [5, 6]the Mn(II) ion ($S = 5/2$), consistent with a highly symmetric site.[5, 6] A crystal structure

of MntC indicates that it coordinates Mn(II) at a 5-coordinate N_2O_3 motif composed of two His, one bidentate Glu, and one Asp residue.[14] A crystal structure of Mn(II)-PsaA shows that it binds Mn(II) with the same residues as MntC, but the site has been described as tetrahedral where the Glu and Asp residues are reported to be monodentate ligands.[20, 24, 27] On the basis of this characterization, we expected that the Mn(II) EPR spectra of these proteins would exhibit larger ZFS than Mn(II)-CP.[28-31] We therefore reasoned that the different Mn(II) coordination environments in CP and the SBPs would result in readily distinguishable low-temperature Mn(II) EPR spectroscopic signatures,[28] providing spectral discrimination between Mn(II)-CP and Mn(II)-SBP in a sample.

We prepared samples containing 1 mM SBP and 750 μM Mn(II) (75 mM HEPES, 100 mM NaCl, pH 7.5). Both of the Mn(II)-SBP spectra (**Figure 4.9**) indicate a high-spin Mn(II) ion (S = 5/2) with a large ZFS that is of comparable magnitude to the microwave quanta at X-band (≈9.4 GHz).[29, 30, 32, 33] The large ZFS (D > 3 GHz) leads to these systems not being in the "high field" regime at X-band, which is met when the electron Zeeman is the dominant term in the spin Hamiltonian and results in broad spectra that span >600 mT at X-band.[31] Multi-frequency EPR studies are needed to further evaluate the electronic structure of the Mn(II) ions coordinated by MntC and PsaA; however, the current spectra provide suitable handles for monitoring Mn(II) competition between these proteins and CP. In contrast to the Mn(II)-PsaA EPR spectrum in Figure 4.9, a previously reported Mn(II)-PsaA spectrum showed 6-line Mn(II) EPR features at g = 2 (≈335 mT),[34] which likely arose from aqueous Mn(II) contamination. As anticipated, the EPR spectra

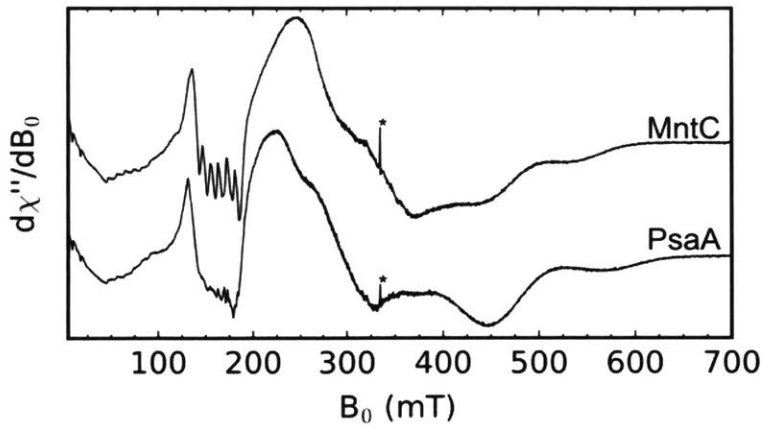

Figure 4.9. X-band CW EPR spectra of Mn(II) (750 μM) bound to SBPs (1 mM) (75 mM HEPES, 100 mM NaCl, pH 7.5). The asterisk denotes a quartz background radical.

of the Mn(II)-SBPs are markedly different than those of Mn(II)-CP or aqueous Mn(II), allowing simultaneous monitoring of Mn(II)-bound CP and MntC or PsaA (**Figure 4.10**). The sharp spectral features in the g = 4.5 region (≈150 mT) of the Mn(II)-SBP spectra do not overlap with the Mn(II)-CP signals in the g = 2 region (≈335 mT).

4.4.4 CP and SBP Competition for Mn(II) Monitored by EPR Spectroscopy

Thus, to examine Mn(II) speciation between CP and the SBPs by EPR spectroscopy, we prepared samples containing a 1:1:1 ratio of Mn(II), CP, and SBP (500 μM each) in the absence and presence of 5 mM Ca(II) at pH 7.5 and incubated them for 10 h at room temperature. In the samples without added Ca(II), we observed a distinct low-field feature around g = 4.5 (≈150 mT, **Figure 4.11A,C**; black spectra) that corresponds to Mn(II)-MntC or Mn(II)-PsaA and a weak Mn(II)-CP signal centered at g = 2 (≈335 mT, **Figure 4.11B,D**; black spectra). In the presence of excess Ca(II), a strong Mn(II)-CP signal (**Figure 4.11B,D**; red spectra) and a negligible Mn(II)-SBP signal (**Figure 4.11A,C**; red spectra) occur, indicating that Ca(II)-bound CP outcompetes both

SBPs for Mn(II). These results are consistent with the pull-down assays performed in the absence and presence of Ca(II) (**Figure 4.8**). This work also provides further information about the Mn(II) affinity of CP. Prior studies indicated that the His_6 site coordinates Mn(II) with $K_{d,Mn(II)} \leq 10$ nM when Ca(II) ions are present.[27] The current results indicate that this value is in the sub-nanomolar range based on the reported $K_{d,Mn(II)}$ values of MntC ($K_d \approx 4$ nM)[14] and PsaA ($K_d < 10$ nM).[20]

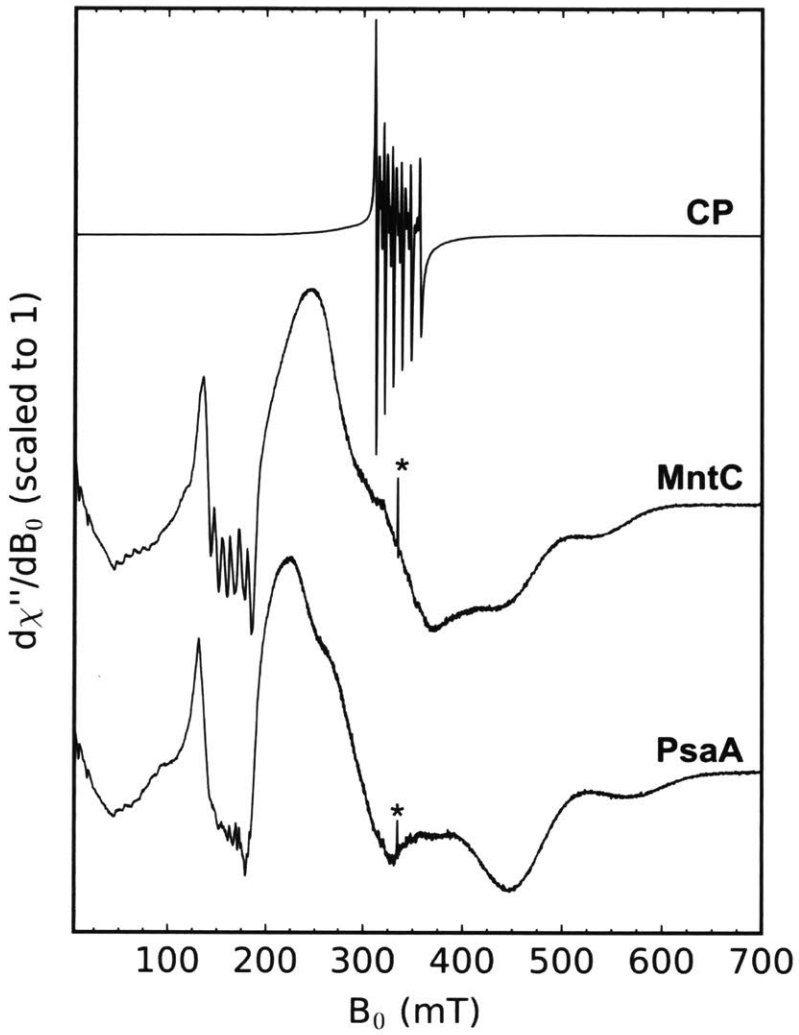

Figure 4.10. Comparison of X-band Mn(II) EPR spectra of Mn(II)-bound CP-Ser in the presence of 10 equivalents of Ca(II), Mn(II)-bound MntC, and Mn(II)-bound PsaA (75 mM HEPES, 100 mM NaCl, pH 7.5). The asterisk denotes a quartz background radical. For the Mn(II)-CP-Ser spectrum, the sample contained 600 μM CP-Ser, 500 μM Mn(II), and 6 mM Ca(II). Spectrometer settings: ν_{mw} = 9.4 GHz, 0.5 mT modulation amplitude at 100 kHz, power = 200 μW, temperature = 10 K.

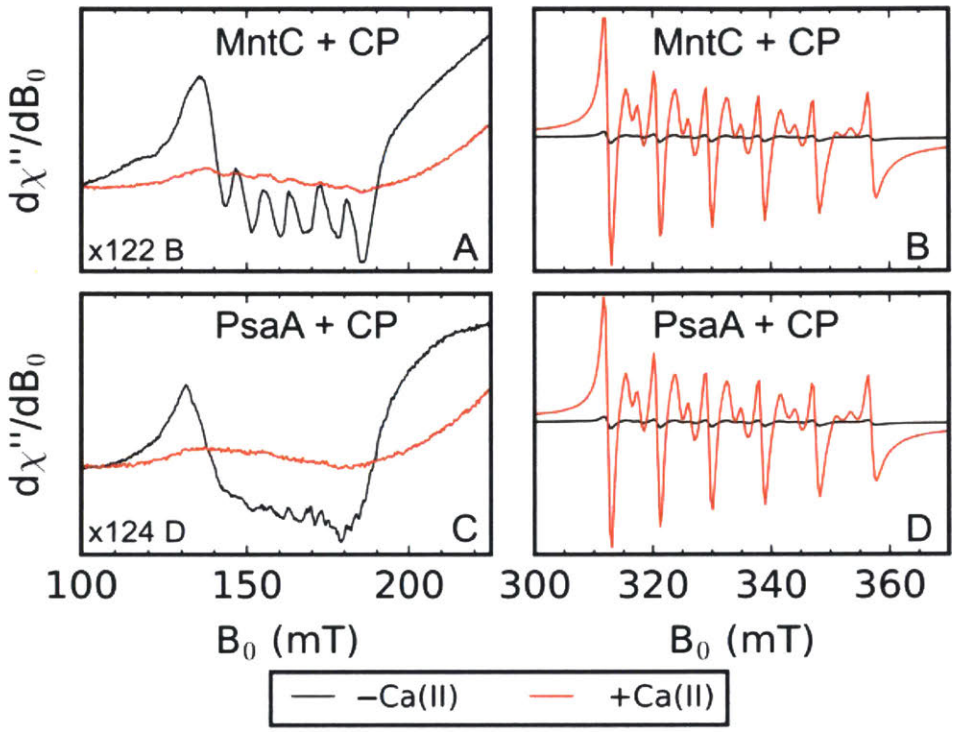

Figure 4.11. X-band CW EPR spectra of 1:1:1 mixtures of Mn(II):CP-Ser:SBP incubated for 10 h at room temperature in the absence (black) or presence (red) of 5 mM Ca(II) (75 mM HEPES, 100 mM NaCl, pH 7.5). Each sample contained 500 μM Mn(II), 500 μM SBP, and 500 μM CP-Ser after mixing. Panels A and B contain the same Mn(II) spectra of the samples containing CP-Ser and MntC, and panels C and D contain the same Mn(II) spectra of the samples containing CP-Ser and PsaA. Panels A and C are scaled differently from B and D along the y-axis to make the low-field, g = 4.5, features of each Mn(II)-SBP more apparent relative to the mid-field features, g = 2, of Mn(II)-CP-Ser.

4.4.5 Timescale of CP and SBP Competition for Mn(II) Monitored by EPR Spectroscopy

Next, to probe the timescale for the sequestration of Mn(II) from each SBP by CP-Ser, we performed experiments where a solution containing 1 mM CP-Ser and 10 mM Ca(II) was added to an equal volume of a solution containing 1 mM Mn(II)-SBP. Aliquots of this mixture were frozen at varying time points and analyzed by EPR spectroscopy

(**Figure 4.12**). This assay revealed a time-dependent decrease in the Mn(II)-MntC or Mn(II)-PsaA signal (**Figure 4.12A,C**), and a corresponding increase in the Mn(II)-CP-Ser signal (**Figure 4.12B,D**). The greatest changes in signal intensity, marking movement of the Mn(II) ion from each SBP to CP-Ser, occurred in the first 10 min of the time course. This short timescale is striking and highlights the remarkable ability of the His_6 site of CP-Ser to capture and retain labile divalent transition metals.

4.5 Conclusion

In closing, to our knowledge, this work affords the first direct analysis of metal speciation between CP and a metal-capturing SBP. These experiments demonstrate that the Ca(II)-bound, high-affinity form of CP rapidly outcompetes MntC and PsaA, two SBPs used by Gram-positive pathogens for Mn(II) acquisition. This work informs the current model of how CP contributes to extracellular metal withholding at the host/pathogen interface. It also provides an important benchmark for future studies of this system and other microbial metal transporters. For instance, whether the Mn(II) sequestration process is facilitated by an interaction between CP and the SBPs, or is contact-independent, requires elucidation. Our current model focuses on how Ca(II) ions markedly enhance Mn(II) sequestration by CP; however, we recognize that high Ca(II) levels may affect the

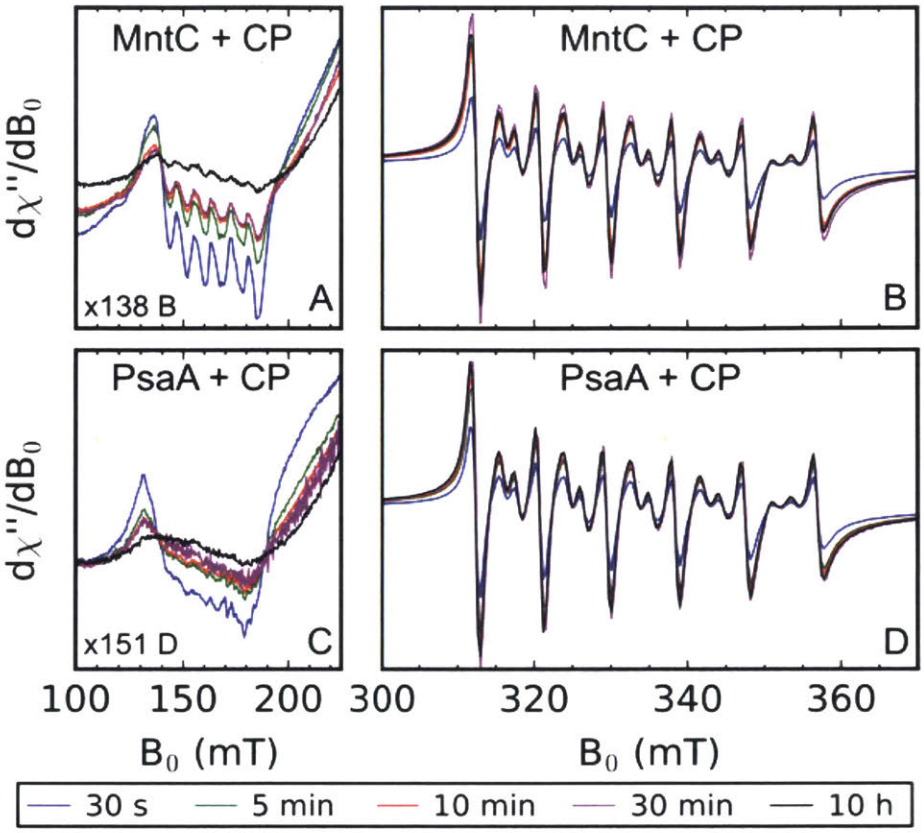

Figure 4.12. X-band CW EPR spectra showing the time-dependent loss of Mn(II) from Mn(II)-SBPs and formation of Mn(II)-CP-Ser. The starting mixture contained Mn(II)-SBP (500 μM), CP-Ser (500 μM), and 5 mM Ca(II) (75 mM HEPES, 100 mM NaCl, pH 7.5). See Figure 4.11 caption for description of panels A-D.

metal-binding thermodynamics and kinetics of the SBPs and thereby contribute in another manner. Thus, further fundamental investigation of Mn(II) binding by these SBPs in solution is another avenue for future inquiry. From the standpoint of metal-withholding in the complex biological milieu, the His_6 site of CP is functionally versatile and allows CP to sequester multiple divalent first-row transition metals that include Fe(II) and Zn(II). MntC and PsaA also bind multiple transition metal ions, which is another variable that warrants consideration. It will be important to decipher how the presence of other, abundant nutrient metals affects the interplay between CP and the SBPs considered in

this work. Lastly, we expect that investigations of metal competition between CP and fully reconstituted ABC transporter systems will be informative.

4.6 Acknowledgements

This work was supported by the NIH (R01GM118695 to E.M.N and R01GM104543 to R.D.B). R. C. Hadley is a recipient of the R. R. Schrock Graduate Fellowship, and T. G. Nakashige is a recipient of a NSF graduate fellowship. The MIT Biophysical Instrumentation Facility for the Study of Complex Macromolecular Systems is supported by NSF grant 0070319. The MIT CEHS Bioanalytical Core is supported by NIH grant P30-ES002109. We thank Prof. D. P. Giedroc for his comments on the manuscript reporting this study, and Prof. Giedroc and Dr. J. Lisher for contributing a *S. pneumoniae* D39 genomic DNA fragment containing the *psaA* sequence, and J. R. Stephan and E. M. Zygiel for assistance with protein purifications. *S. aureus* USA300 JE2 was obtained from the Network on Antimicrobial Resistance Against *Staphylococcus aureus* (NARSA) program supported under NIAID/NIH contract no. HHSN272200700055C.

4.7 References

1. Weinberg, E. D. Nutritional immunity: Host's attempt to withhold iron from microbial invaders. *J. Am. Med. Assoc.* **1975,** *231*, 39–41.

2. Hood, M. I.; Skaar, E. P. Nutritional immunity: transition metals at the pathogen-host interface. *Nat. Rev. Microbiol.* **2012,** *10*, 525-537.

3. Zygiel, E. M.; Nolan, E. M. Transition metal sequestration by host-defense protein calprotectin. *Ann. Rev. Biochem.* **2018,** *87*, 621-643.

4. Brophy, M. B.; Hayden, J. A.; Nolan, E. M. Calcium ion gradients modulate the zinc affinity and antibacterial activity of human calprotectin. *J. Am. Chem. Soc.* **2012,** *134*, 18089-18100.

5. Gagnon, D. M.; Brophy, M. B.; Bowman, S. E.; Stich, T. A.; Drennan, C. L.; Britt, R. D.; Nolan, E. M. Manganese binding properties of human calprotectin under conditions of high and low calcium: X-ray crystallographic and advanced electron paramagnetic resonance spectroscopic analysis. *J. Am. Chem. Soc.* **2015,** *137*, 3004-3016.

6. Hayden, J. A.; Brophy, M. B.; Cunden, L. S.; Nolan, E. M. High-affinity manganese coordination by human calprotectin is calcium-dependent and requires the histidine-rich site formed at the dimer interface. *J. Am. Chem. Soc.* **2013,** *135*, 775-787.

7. Nakashige, T. G.; Stephan, J. R.; Cunden, L. S.; Brophy, M. B.; Wommack, A. J.; Keegan, B. C.; Shearer, J. M.; Nolan, E. M. The hexahistidine motif of host-defense protein human calprotectin contributes to zinc withholding and its functional versatility. *J. Am. Chem. Soc.* **2016,** *138*, 12243-12251.

8. Nakashige, T. G.; Zhang, B.; Krebs, C.; Nolan, E. M. Human calprotectin is an iron-sequestering host-defense protein. *Nat. Chem. Biol.* **2015,** *11*, 765-771.

9. Damo, S. M.; Kehl-Fie, T. E.; Sugitani, N.; Holt, M. E.; Rathi, S.; Murphy, W. J.; Zhang, Y.; Betz, C.; Hench, L.; Fritz, G.; Skaar, E. P.; Chazin, W. J. Molecular basis for manganese sequestration by calprotectin and roles in the innate immune response to invading bacterial pathogens. *PNAS.* **2013,** *110*, 3841-3846.

10. Nakashige, T. G.; Zygiel, E. M.; Drennan, C. L.; Nolan, E. M. Nickel sequestration by the host-defense protein human calprotectin. *J. Am. Chem. Soc.* **2017,** *139*, 8828-8836.

11. Corbin, B. D.; Seeley, E. H.; Raab, A.; Feldmann, J.; Miller, M. R.; Torres, V. J.; Anderson, K. L.; Dattilo, B. M.; Dunman, P. M.; Gerads, R.; Caprioli, R. M.; Nacken, W.; Chazin, W. J.; Skaar, E. P. Metal chelation and inhibition of bacterial growth in tissue abscesses. *Science.* **2008,** *319,* 962-965.

12. Diaz-Ochoa, V. E.; Lam, D.; Lee, C. S.; Klaus, S.; Behnsen, J.; Liu, J. Z.; Chim, N.; Nuccio, S. P.; Rathi, S. G.; Mastroianni, J. R.; Edwards, R. A.; Jacobo, C. M.; Cerasi, M.; Battistoni, A.; Ouellette, A. J.; Goulding, C. W.; Chazin, W. J.; Skaar, E. P.; Raffatellu, M. *Salmonella* mitigates oxidative stress and thrives in the inflamed gut by evading calprotectin-mediated manganese sequestration. *Cell Host Microbe.* **2016,** *19,* 814-825.

13. Kehl-Fie, T. E.; Zhang, Y.; Moore, J. L.; Farrand, A. J.; Hood, M. I.; Rathi, S.; Chazin, W. J.; Caprioli, R. M.; Skaar, E. P. MntABC and MntH contribute to systemic *Staphylococcus aureus* infection by competing with calprotectin for nutrient manganese. *Infect. Immun.* **2013,** *81,* 3395-3405.

14. Gribenko, A.; Mosyak, L.; Ghosh, S.; Parris, K.; Svenson, K.; Moran, J.; Chu, L.; Li, S.; Liu, T.; Woods, V. L., Jr.; Jansen, K. U.; Green, B. A.; Anderson, A. S.; Matsuka, Y. V. Three-dimensional structure and biophysical characterization of *Staphylococcus aureus* cell surface antigen-manganese transporter MntC. *J. Mol. Biol.* **2013,** *425,* 3429-3445.

15. Makthal, N.; Nguyen, K.; Do, H.; Gavagan, M.; Chandrangsu, P.; Helmann, J. D.; Olsen, R. J.; Kumaraswami, M. A Critical Role of Zinc Importer AdcABC in Group A Streptococcus-Host Interactions During Infection and Its Implications for Vaccine Development. *EBioMedicine.* **2017,**

16. Ogunniyi, A. D.; Mahdi, L. K.; Jennings, M. P.; McEwan, A. G.; McDevitt, C. A.; Van der Hoek, M. B.; Bagley, C. J.; Hoffmann, P.; Gould, K. A.; Paton, J. C. Central role of manganese in regulation of stress responses, physiology, and metabolism in *Streptococcus pneumoniae*. *J. Bacteriol.* **2010,** *192*, 4489-4497.

17. Rajam, G.; Anderton, J.; Carlone, G.; Sampson, J.; Ades, E. Pneumococcal Surface Adhesin A (PsaA): A Review. *Crit. Rev. Microbiol.* **2008,** *34*, 131-142.

18. Eijkelkamp, B. A.; Morey, J. R.; Ween, M. P.; Ong, C. L.; McEwan, A. G.; Paton, J. C.; McDevitt, C. A. Extracellular zinc competitively inhibits manganese uptake and compromises oxidative stress management in Streptococcus pneumoniae. *PLoS One.* **2014,** *9*, e89427.

19. Marra, A.; Lawson, S.; Asundi, J. S.; Brigham, D.; Hromockyj, A. E. *In vivo* characterization of the *psa* genes from *Streptococcus pneumoniae* in multiple models of infection. *Microbiology.* **2002,** *148*, 1483-1491.

20. McDevitt, C. A.; Ogunniyi, A. D.; Valkov, E.; Lawrence, M. C.; Kobe, B.; McEwan, A. G.; Paton, J. C. A molecular mechanism for bacterial susceptibility to zinc. *PLoS Pathog.* **2011,** *7*, e1002357.

21. Walkup, G. K.; Burdette, S. C.; Lippard, S. J.; Tsien, R. Y. A new cell-permeable fluorescent probe for Zn2+. *J. Am. Chem. Soc.* **2000,** *122*, 5644-5645.

22. Anderson, A. S.; Scully, I. L.; Timofeyeva, Y.; Murphy, E.; McNeil, L. K.; Mininni, T.; Nunez, L.; Carriere, M.; Singer, C.; Dilts, D. A.; Jansen, K. U. *Staphylococcus aureus* manganese transport protein C is a highly conserved cell surface protein that elicits protective immunity against S. aureus and *Staphylococcus epidermidis*. *J. Infect. Dis.* **2012,** *205*, 1688-96.

23. Salazar, N.; Castiblanco-Valencia, M. M.; Silva, L. B. d.; Castro, Í. A. d.; Monaris, D.; Masuda, H. P.; Barbosa, A. S.; Arêas, A. P. M. *Staphylococcus aureus* Manganese Transport Protein C (MntC) Is an Extracellular Matrix- and Plasminogen-Binding Protein. *PLoS One.* **2014,** *9*, e112730.

24. Counago, R. M.; Ween, M. P.; Begg, S. L.; Bajaj, M.; Zuegg, J.; O'Mara, M. L.; Cooper, M. A.; McEwan, A. G.; Paton, J. C.; Kobe, B.; McDevitt, C. A. Imperfect coordination chemistry facilitates metal ion release in the Psa permease. *Nat. Chem. Biol.* **2014,** *10*, 35-41.

25. You, Y.; Tomat, E.; Hwang, K.; Atanasijevic, T.; Nam, W.; Jasanoff, A. P.; Lippard, S. J. Manganese displacement from Zinpyr-1 allows zinc detection by fluorescence microscopy and magnetic resonance imaging. *Chem. Commun.* **2010,** *46*, 4139-4141.

26. Brini, M.; Ottolini, D.; Cali, T.; Carafoli, E. Calcium in health and disease. *Met. Ions Life Sci.* **2013,** *13*, 81-137.

27. Brophy, M. B.; Nolan, E. M. Manganese and microbial pathogenesis: sequestration by the Mammalian immune system and utilization by microorganisms. *ACS Chem. Biol.* **2015,** *10*, 641-651.

28. Stich, T. A.; Lahiri, S.; Yeagle, G.; Dicus, M.; Brynda, M.; Gunn, A.; Aznar, C.; DeRose, V. J.; Britt, R. D. Multifrequency Pulsed EPR Studies of Biologically Relevant Manganese(II) Complexes. *Appl. Magn. Reson.* **2007,** *31*, 321-341.

29. Walsby, C. J.; Telser, J.; Rigsby, R. E.; Armstrong, R. N.; Hoffman, B. M. Enzyme Control of Small-Molecule Coordination in FosA as Revealed by 31P Pulsed ENDOR and ESE-EPR. *J. Am. Chem. Soc.* **2005,** *127*, 8310-8319.

30. Whittaker, J. W.; Whittaker, M. M. Active site spectral studies on manganese superoxide dismutase. *J. Am. Chem. Soc.* **1991,** *113*, 5528-5540.

31. Vance, C. K.; Miller, A. F. Novel insights into the basis for Escherichia coli superoxide dismutase's metal ion specificity from Mn-substituted FeSOD and its very high E(m). *Biochemistry* **2001,** *40*, 13079-87.

32. Un, S.; Tabares, L. C.; Cortez, N.; Hiraoka, B. Y.; Yamakura, F. Manganese(II) Zero-Field Interaction in Cambialistic and Manganese Superoxide Dismutases and Its Relationship to the Structure of the Metal Binding Site. *J. Am. Chem. Soc.* **2004,** *126*, 2720-2726.

33. Tabares, L. C.; Cortez, N.; Agalidis, I.; Un, S. Temperature-Dependent Coordination in *E. coli* Manganese Superoxide Dismutase. *J. Am. Chem. Soc.* **2005,** *127*, 6039-6047.

34. Li, N.; Yang, X. Y.; Guo, Z.; Zhang, J.; Cao, K.; Han, J.; Zhang, G.; Liu, L.; Sun, X.; He, Q. Y. Varied metal-binding properties of lipoprotein PsaA in *Streptococcus pneumoniae*. *J. Biol. Inorg. Chem.* **2014,** *19*, 829-838.

Appendix A: High–field EPR Spectroscopic Characterization of Mn(II) Bound to the Bacterial Solute-binding Proteins MntC and PsaA

This Chapter is adapted from a manuscript *Submitted*.

A.1 Contributions

Dr. Derek Gagnon analyzed and plotted all EPR spectra. Dr. Andrew Ozarowski contributed to the data collection and analysis.

A.2 Introduction

Transition metal ions are essential nutrients for all organisms.[1-2] In the context of bacterial infection, the invading microbe must acquire metal nutrients required for growth and virulence from the host.[2] These pathogens have evolved several mechanisms to scavenge and import metal ions that include the biosynthesis and deployment of metallophores and the expression of high-affinity metal uptake proteins.[2] In this work, we employ high-field electron paramagnetic resonance (EPR) spectroscopy to evaluate the metal-binding properties of two transport proteins that function in the acquisition of Mn(II), a nutrient that is required for high levels of virulence in diverse bacterial pathogens.[3-5]

Staphylococcus aureus and *Streptococcus pneumoniae* are Gram-positive bacterial pathogens of significant clinical concern because they cause a variety of life-threatening infections.[6-7] Both organisms employ ATP-binding cassette (ABC) transporters to acquire Mn(II) from the host.[8-9] These transport systems consist of a membrane-anchored solute-binding protein (SBP) that scavenges Mn(II) from the extracellular environment, a transmembrane permease, and an ATPase located on the cytoplasmic side of the cell membrane.[10] The Mn(II) ABC transporters for *S. aureus* and *S. pneumoniae* are MntABC and PsaABC, respectively. MntC and PsaA are the SBPs that capture Mn(II) and deliver it to the transmembrane permeases of each uptake system.[11-13]

How MntC and PsaA coordinate Mn(II) and deliver it to their respective permease has not been fully elucidated. Reported crystal structures of Mn(II)-MntC (2.2-Å resolution)[14] and Mn(II)-PsaA (2.7-Å resolution)[15] show Mn(II) bound by a $His_2AspGlu$ coordination sphere in both proteins (**Figure A.1**). The crystallographic Mn(II)-MntC site was described as 5-coordinate where His50, His123, Oε1 of Glu189, and both Oδ1 and Oδ2 of Asp264 coordinate the metal ion (**Figure A.1B**).[14] However, the metal–ligand distances determined crystallographically range from 2.1–2.8 Å and do not preclude the possibility of other coordination geometries (**Figure A.1**). In addition, the metal content of the crystallized protein is ambiguous because the protein in solution contained low amounts of various metal ions according to inductively-coupled mass spectrometry and anomalous diffraction data was not reported, which ca be employed to confirm the identity of the bound metal. As a result, the Mn(II) coordination sphere of MntC is not well-defined and requires further examination. The crystallographic Mn(II)-PsaA site was described as 4-coordinate where His67, His139, Oε1 of Glu205 and Oδ1 of Asp280 bind the Mn(II) ion (**Figure A.1D,E**).[15] Nevertheless, the metal-ligand distances determined from this crystal structure range from 2.1–2.4 Å,[15] and the possibility that the bound Mn(II) ion has a higher coordination number cannot be ruled out based on this structural model.[5] In an effort to gain further insight into these systems, we recently examined the Mn(II) sites of MntC and PsaA by X-band (≈9 GHz) EPR spectroscopy.[16] These studies revealed broad spectra resulting from the high magnitude of the zero-field splitting (|D|) relative to the spectrometer frequency ($|D|/h\nu$ ≈30%).[16] As a consequence, the Spin Hamiltonian parameters could not be accurately determined.

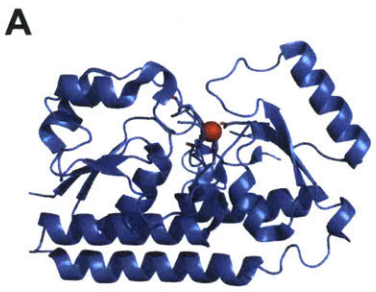

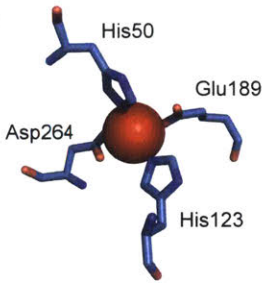

C

Residue	M-L distance (Å)
His50	2.1 Å
His123	2.1 Å
Glu189 Oε1	2.3 Å
Glu189 Oε2	2.8 Å
Asp264 Oδ1	2.2 Å
Asp264 Oδ2	2.3 Å

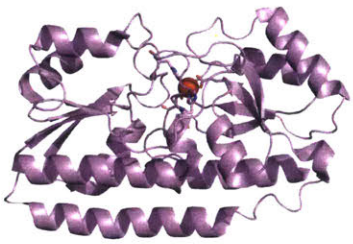

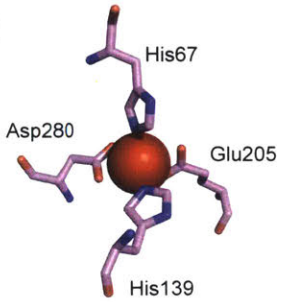

F

Residue	M-L distance (Å)
His67	2.1 Å
His139	2.1 Å
Glu205 Oε1	2.1 Å
Glu205 Oε2	2.4 Å
Asp280 Oδ1	2.1 Å
Asp280 Oδ2	2.4 Å

Figure A.1. Crystal structures, zoom-in view of the metal-binding sites, and metal-ligand distances of Mn(II)-MntC (A,B,C) and Mn(II)-PsaA (D,E,F). The Mn(II) ion is shown as a red sphere (PDB: 4K3V and 3ZTT). Ligand numbering in MntC corresponds to a truncated form of the protein.[14]

In this work, we further investigate the electronic structure of Mn(II)-MntC and Mn(II)-PsaA in the "high-field regime" where $|D| << h\nu$ by employing high field (>3 T) and high frequency (>90 GHz) EPR spectroscopy. In this regime, the spectra become simplified and simulation of the data can afford values for the Spin Hamiltonian parameters. The spectral data and simulations indicate that MntC and PsaA both bind Mn(II) in a similar tetrahedral or trigonal prismatic coordination environment consistent with the primary coordination sphere defined by the $His_2AspGlu$ motifs observed crystallographically.[14-15, 17]

A.3 Experimental and Theoretical Methods

A.3.1 Sample Preparation

MntC and PsaA were overexpressed, purified, demetalated, and stored as described previously.[16] All EPR samples were buffer exchanged into 75 mM HEPES, 100 mM NaCl, pH 7.5 that was prepared using high-purity buffer reagents as described elsewhere.[16] For D-band analyses (130 GHz) of the Mn(II)-SBPs, samples of SBP (1 mM) were incubated with Mn(II) (750 μM) for ≈15 min before an approximately 15-μL aliquot was transferred to a D-band tube (0.50 x 0.60 mm ID x OD quartz capillary tubing supplied by Vitrocom) and frozen in liquid nitrogen. These samples were prepared at MIT and shipped to the CalEPR facility at University of California, Davis in a liquid nitrogen dewar. For high frequency (388 GHz) analyses, MntC (1.2 mM) was incubated with Mn(II) (900 μM) for ~15 min before a 500 μL aliquot was transferred to a 1 mL LDPE sample vial (Fischer) and frozen in liquid nitrogen. PsaA (2.4 mM) was incubated with Mn(II) (1.8 mM) for ~15 min before 500 μL was transferred to a 1 mL LDPE sample vial (Fischer) and frozen in liquid nitrogen. These samples were shipped to the National High Magnetic Field Laboratory (NHMFL) Electron Magnetic Resonance facility on dry ice.

A.3.2 EPR Measurements

Pulse spectra at 130 GHz were collected at the University of California, Davis CalEPR facility utilizing a D band (130 GHz) spectrometer described previously.[18] Spectra were collected at 15 K, with a 20 ns $\pi/2$ pulse length, a τ value of 300 ns, and 1 ms repetition time. The field axis was calibrated by collecting a spectrum of Mn(II) impurity

in MgO (>95% fused MgO, Aldrich). The Mn(II) in MgO signal has a *g* value of 2.00100(5) and ^{55}Mn hyperfine of -243.6(5) MHz.[19-20]

Spectra collected at the NHMFL were collected utilizing a spectrometer described previously.[21] The field was calibrated with an internal sample standard of H-atom trapped in an octaisobutylsilsesquioxane nanocage with a *g* value of 2.00294(3) and hyperfine of 1413.7(1) MHz.[19] Spectra were collected at multiple temperatures with different modulation amplitudes to enhance the intensity of different m_s transitions.

The field calibration with both the external Mn(II) impurity in MgO and internal H-atom standards was carried out during post-processing of the data. Briefly, the general procedure involved manually aligning a simulation of the standard with the experimental data of the field standard by both an initial visual inspection and a subsequent mathematical process. Example inputs for simulations of the standards are included below. For the Mn(II) impurity in MgO standard, the lowest field hyperfine peak was selected for the initial alignment. After initial visual alignment, the fine adjustment was carried out by calculating the field difference between simulated and experimental field positions for the maximum intensity of the first hyperfine line. We found that this procedure afforded a satisfactory result where all six hyperfine lines of the Mn(II) impurity in MgO lined up. The calculated offset was then used as a field offset factor for the experimental data prior to simulation. The internal hydrogen atom standard required an entirely visual-inspection alignment of the simulation and experimental data due to distortions of the line shape caused by passage and modulation effects during data collection.

A.3.3 EPR Theory and Simulations

The EPR spectrum of the d^5 Mn(II) (S = 5/2) ion can be interpreted using the phenomenological spin Hamiltonian given below.[22-23]

$$\hat{H} = \frac{\beta_e}{h} B \cdot g \cdot \hat{S} + a_{iso} \hat{S} \cdot \hat{I} + D\left(\hat{S}_z^2 - S\,(S+1)/3\right) + E\left(\hat{S}_x^2 - \hat{S}_y^2\right)$$

Where β_e is the Bohr magneton, B is the magnetic field, g is the electron g-value, S the electron spin, h is the Planck constant, a_{iso} is the isotropicand hyperfine interaction with the ^{55}Mn (I = 5/2, 100% abundance) nucleus, I is the nuclear spin, D and E are the axial and rhombic zero-field splitting values, respectively. The ratio E/D is reported to indicate the rhombicity of the zero-field splitting tensor. When the coordinate frame is choen correctly, the values of E/D range from 0 (perfectly axial) to 1/3 (maximally rhombic). All spectra were simulated using the freely available EasySpin (v5.2.24) toolbox for MATLAB R2017a (The Mathworks, Inc.).[24]

The ^{55}Mn hyperfine values and g-values were determined from simulations of the data collected at temperatures ≥10 K and assessed by visual inspection. The zero-field splitting values D and E were determined by simulating the data collected at temperatures ≤5 K We found that the relative peak intensities of simulations at high fields and low temperature (≤5 K) were sensitive to the temperature employed in the simulation. In order to improve the agreement between thesimulation and experimental data, it necessary to set the simulation temperature 2 K higher than the temperature reported by the spectrometer to achieve the correct relative intensities of the different transitions. The simulation temperature is not expected to affect the measured zero-field splitting parameters, but it affects the relative peak intensities in the simulations. The 388 GHz and 400 GHz Mn(II)-MntC spectra collected at 3 K were simulated using a temperature

of 5 K. The 388 GHz Mn(II)-PsaA spectra collected at 5 K was simulated using a temperature of 7 K. We note that the recorded spectrometer temperature is not from a temperature probe located at the sample, and that there may be heating of the sample induced by the field modulation in the experiment. A 300 *D* and *E* strain of 300 MHz was used to help the simulation lineshape better match the linewidths of the experimental data.

A.3.4 Simulation Parameters for Field Standards

% Sys is a structure containing the spin system inputted into EasySpin's pepper function

% Exp is a structure containing experimental inputs for the simulation

The reader is encouraged to visit the EasySpin documentation online at http://easyspin.org/easyspin/documentation/ for further information.

Mn(II) Impurity in MgO for Simulation at D Band:

```
Sys.S = 5/2;
Sys.lw = 0.6; % mT
Sys.g = 2.001;
Sys = nucspinadd(Sys,'55Mn',-243.6); % hyperfine in MHz
D = -50; % MHz
Sys.D = [D 0.0*D];

[xsim,ysim] = pepper(Sys,Exp);
```

H-atom Standard:

```
Sys.S = 1/2;
Sys.g = 2.00294;
Sys.lw = 0.5; % mT
Sys.Nucs = '1H';
Sys.A = 1413.7; % MHz

[xsim_H,ysim_H] = pepper(Sys,Exp);
```

A.3.5 EasySpin Phenomenological Line Width Inputs Used in Simulations

Figure A.2. MntC and PsaA, Sys.lw = [1.0 1.0]
Figure A.3. Sys.lw = [0.7 1.0]
Figure A.4. Sys.lw = [0.7 1.8]
Figure A.5. Sys.lw = [0.7 0.5]
Figure A.6. Sys.lw = [0.7 1.0]
Figure A.7. Sys.lw = [0.7 0.8]
Figure A.8. Sys.lw = [1.0 1.5]

A.4 Results and Discussion

The EPR spectra of Mn(II)-MntC and Mn(II)-PsaA feature a six-line pattern at $g \cong 2.001$ (4.64 T at 130 GHz, 13.86 T at 388 GHz) that arises from the transition between $m_s = \pm 1/2$ electron spin manifolds and their hyperfine couplings to the ^{55}Mn nucleus ($I = 5/2$, 100% abundance) (**Figures A.2-A.5**). Surrounding this central sextet is a broad envelope of transitions belonging to the $m_s = \pm 3/2$ and $m_s = \pm 5/2$ manifolds where the ZFS and strain in those elements results in relatively featureless spectra with no resolved ^{55}Mn hyperfine couplings.[33] Simulation of the spectra in the sextet region affords ^{55}Mn isotropic hyperfine values of 241 and 236 MHz for Mn(II)-MntC and Mn(II)-PsaA, respectively (**Table A.1**). The relatively low ^{55}Mn hyperfine constant values indicate a more covalent interaction of the $S = 5/2$ Mn(II) ion with its ligands in the binding site of the protein compared to hexa-aqua Mn(II), for which the ^{55}Mn hyperfine value is ≈265 MHz.[22] This more covalent interaction combined with the electrostatic interaction from the negatively charged carboxylate groups of the $His_2AspGlu$ binding site likely contributes to tight binding of the Mn(II) ion ($K_{d,Mn(II)} \leq 10$ nM)[14-15] observed for these two proteins. The simulation also affords isotropic g-values of 2.0011 and 2.0007 for MntC and PsaA, respectively. The isotropic nature of g and the ^{55}Mn hyperfine is expected from the

spherically symmetrical unpaired electron spin density of the high spin ($S = 5/2$) d^5 ground state of the Mn(II) ion with no low-lying excited states.

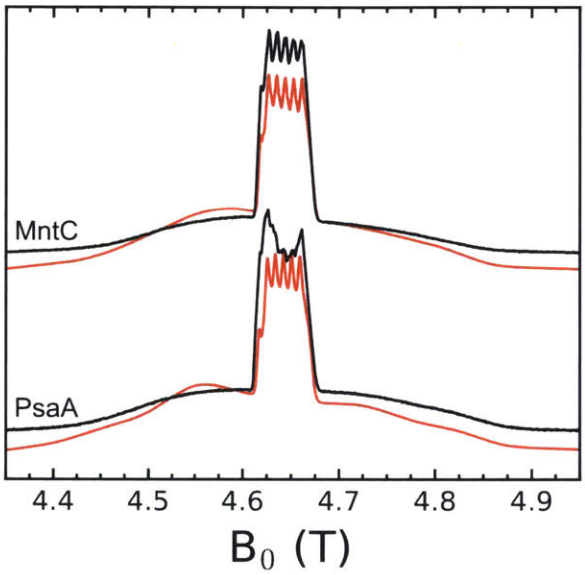

Figure A.2. 2p echo detected field sweep of Mn(II)-MntC and Mn(II)-PsaA at 130 GHz (75 mM HEPES, 100 mM NaCl, pH 7.5). The black trace is the experimental data and the red trace is a simulation with the parameters listed in Table A.1. Experimental settings: spectrometer frequency 130 GHz, 1 ms rep time, 20 ns $\pi/2$ pulse length, τ = 300 ns, T = 15 K. The Mn(II)-PsaA appears to have a contaminant around ≈4.630-4.66 T that partially obscures the sextet.

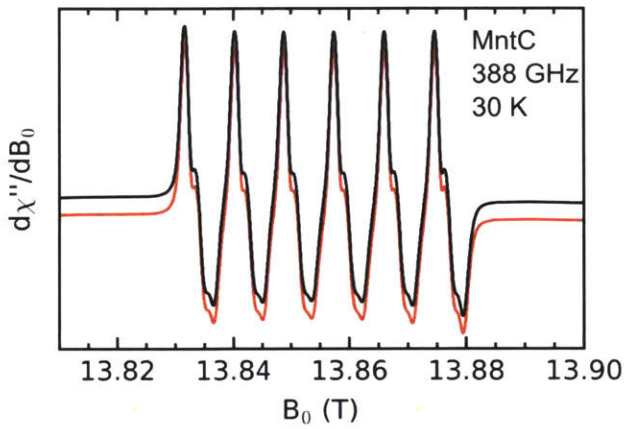

Figure A.3. High-field/frequency CW EPR spectrum of Mn(II)-MntC at 388 GHz (75 mM HEPES, 100 mM NaCl, pH 7.5). The black trace is the experimental data and the red trace is a simulation with the parameters listed in Table A.1. Experimental settings: spectrometer frequency 388 GHz, 0.5 mT modulation amplitude at 50 kHz, T = 30 K.

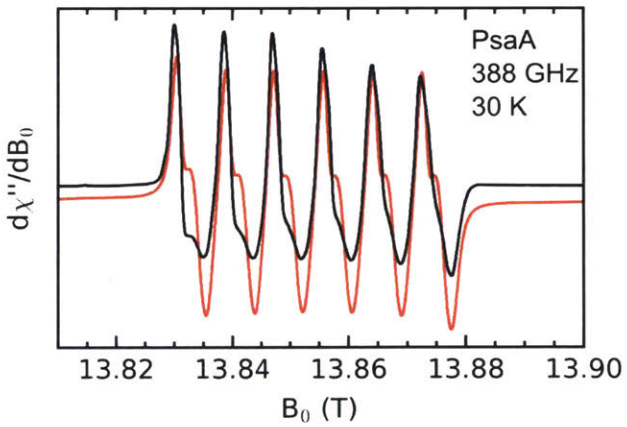

Figure A.4. High-field/frequency CW EPR spectrum of Mn(II)-PsaA at 388 GHz (75 mM HEPES, 100 mM NaCl, pH 7.5). The black trace is the experimental data and the red trace is a simulation with the parameters listed in Table A.1. Experimental settings: spectrometer frequency 388 GHz, 0.5 mT modulation amplitude at 50 kHz, T = 30 K.

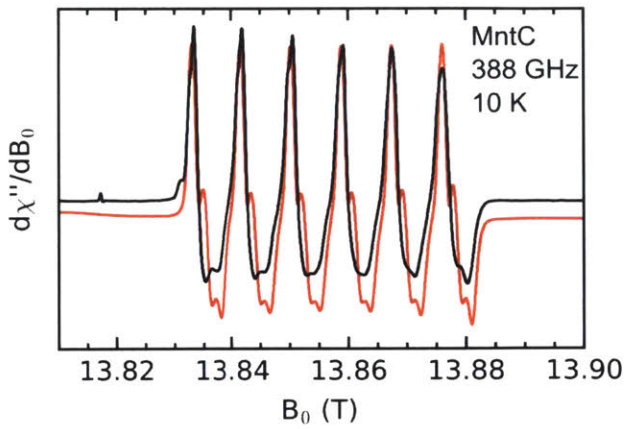

Figure A.5. High-field/frequency CW EPR spectrum of Mn(II)-MntC at 388 GHz (75 mM HEPES, 100 mM NaCl, pH 7.5). Experimental settings: spectrometer frequency 388 GHz, 0.5 mT modulation amplitude at 50 kHz, T = 10 K.

The zero-field splitting parameters *D* and *E/D* are best measured in the high frequency/field spectra. At these high fields, and at low temperatures (<6 K), the lower Zeeman energy m_s −5/2 and −3/2 levels become preferentially populated, leading to an increased intensity of the m_s −5/2↔−3/2 and −3/2↔−1/2 transitions relative to the other transitions (**Figures A.6-A.8**). Simulation affords values for *D* (*E/D*) of +2.72 GHz (0.177) and +2.87 GHz (0.122) for Mn(II)-MntC and Mn(II)-PsaA, respectively (**Table A.1**). The ability to determine the magnitude and sign of *D* from high-field EPR spectroscopy allows comparisons to other spectroscopically and structurally characterized systems. The values of |*D*| determined for Mn(II)-MntC and Mn(II)-PsaA are intermediate between the relatively high values reported for the 5-coordinate superoxide dismutases (SODs) and the remarkably low values reported for the nearly idealized octahedral Mn(II)-bound human and murine calprotectin (**Table A.1**).[26, 31-32] Moreover, the sign of *D* is positive for the Mn(II)-SBPs and negative, when reported, for MnSOD.[25] Taken together, these comparisons suggest that the Mn(II)-SBP sites are neither 5-coordinate nor highly symmetrical 6-coordinate species. Moreover, the zero-field splitting parameters for the

Mn(II)-SBPs show the greatest similarity to the 6-coordinate Mn(II) sites displayed in OxDc site II and the bacterial reaction center from *Rhodobacter spheroides*.[27-28] Thus, it is possible that the Mn(II)-SBP sites are trigonal prismatic. However, we note that caution must be taken when using the magnitude of the Mn(II) zero-field splitting parameter *D* to infer coordination geometry. The comparison should only be done with similar ligand types since the identity of the ligands can influence the zero-field splitting.[34-36] We also note that there is a paucity of zero-field splitting parameters determined for known tetrahedral Mn(II) complexes reported in the literature. To the best of our knowledge, this work is currently limited to Mn(II) complexes containing halide ligands,[37] which are inappropriate comparisons for the Mn(II)-SBPs because halide ligands affect the ZFS.[35-36, 38] Thus, we are unable to determine how similar or different the Mn(II) zero-field splitting parameter values of the Mn(II)-SBPs are to known tetrahedral Mn(II) species. Nevertheless, both Mn(II)-MntC and Mn(II)-PsaA exhibit similar spectroscopic parameters, which suggests that these two Mn(II) sites exhibit more similar coordination environments than indicated by interpretations of the Mn(II)-MntC (5-coordinate)[14] and Mn(II)-PsaA (4-coordinate)[15] crystal structures.

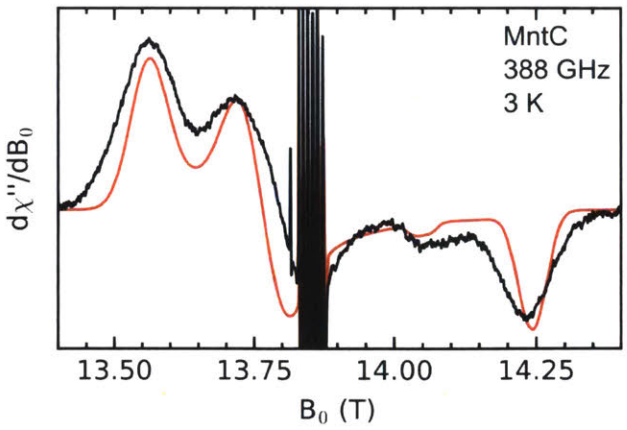

Figure A.6. High-field/frequency CW EPR spectrum of Mn(II)-MntC at T = 3 K, conditions where the spectrum is dominated by the −5/2↔−3/2 and −3/2↔−1/2 transitions (75 mM HEPES, 100 mM NaCl, pH 7.5). Experimental settings: spectrometer frequency 388 GHz, 2.5 mT modulation amplitude at 50 kHz, T = 3 K.

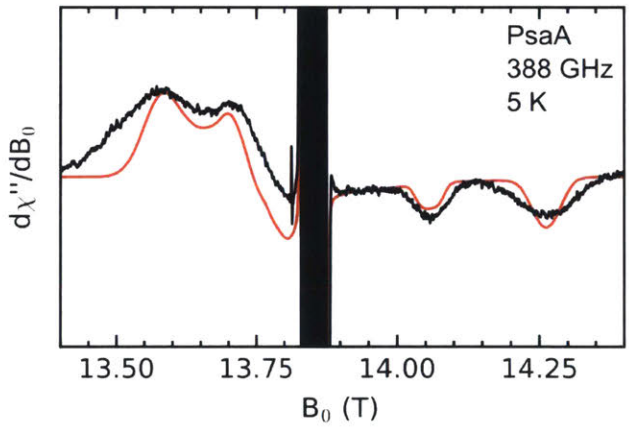

Figure A.7. High-field/frequency CW EPR spectrum of Mn(II)-PsaA at T = 3 K, conditions where the spectrum is dominated by the −5/2↔−3/2 and −3/2↔−1/2 transitions (75 mM HEPES, 100 mM NaCl, pH 7.5). Experimental settings: spectrometer frequency 388 GHz, .4 mT modulation amplitude at 50 kHz, T = 5 K.

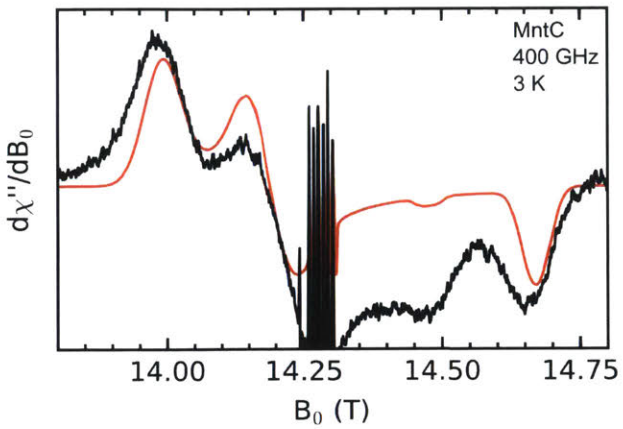

Figure A.8. High-field/frequency CW EPR spectrum of Mn(II)-MntC at 400 GHz and T = 3 K, conditions where the spectrum is dominated by the −5/2↔−3/2 and −3/2↔−1/2 transitions (75 mM HEPES, 100 mM NaCl, pH 7.5). Experimental settings: spectrometer frequency 400 GHz, 2.5 mT modulation amplitude at 50 kHz, T = 3 K.

Table A.1. Table of Spectroscopic Parameters for Mn(II) Bound to Various Proteins

Mn(II)-bound protein	*D* (GHz) [a]	|*E*| (GHz)	|*E/D*|	^{55}Mn a_{iso} (MHz)	Coordination motif [b]	ref
MntC	+2.720	0.480	0.177	241	N_2O_2 or N_2O_4	this work
PsaA	+2.870	0.350	0.122	236	N_2O_2 or N_2O_4	this work
Dr MnSOD [c]	–10.490	0.779	0.074	244	N_3O_2	25
Ec MnSOD [d]	10.640	0.853	0.080	230	N_3O_2	26
Ec MnSOD + 0.1 M azide [d]	1.390	0.270	0.194	245	N_4O_2	26
Mn(II) photosynthetic reaction center from *R. spheroides*	3.328	0.749	0.225	n.d. [f]	N_4O_2	27
OxDc site I [e]	1.200	0.250	0.208	253	N_3O_3	28
OxDc site II [e]	2.700	0.675	0.250	250	N_3O_3	28
concanavalin A	0.645	0.071	0.010	259	N_1O_5	29
Mnx [f]	1.080	0.356	0.329	n.d. [f]	N_1O_5	30
human calprotectin	0.485	0.146	0.30	247	N_6	31
murine calportectin	0.525	0.158	0.30	248	N_6	32
$[Mn(H_2O)_6]^{2+}$ [g]	0.430-0.610	0-0.183	0-0.30	≈265	O_6	22

[a] The sign of *D* is unknown unless reported with a + or – sign. [b] Nitrogen ligands are backbone amides, histidines, or azide. Oxygen ligands are carboxylate groups or water derived. [c] MnSOD of *Deinococcus radiodurans*. [d] MnSOD of *Escherichia coli*. [e] Oxalate decarboxylase of *Bacillus subtilis*. [f] Multi-copper oxidase of *Bacillis* sp. PL-12 with substrate Mn(II) bound. [g] The zero-field splitting parameters and ^{55}Mn hyperfine for $[Mn(H_2O)_6]^{2+}$ depend on the ionic strength, buffer, and glassing agent as detailed in ref. 22. [h] n.d. = not determined.

A.5 Conclusion

The high similarity in the Spin Hamiltonian parameters determined for Mn(II)-MntC and Mn(II)-PsaA suggests that the Mn(II) coordination spheres of these two SBPs are nearly identical in solution. Based on comparisons to previously characterized Mn(II) proteins, the current data may suggest that the Mn(II) sites of both proteins are not five coordinate; however, more information on Mn(II) complexes of known coordination geometries is needed to further substantiate this possibility and ascertain whether the SBPs coordinate Mn(II) in a tetrahedral or trigonal prismatic manner. Thus, we reason that both SBPs release and deliver Mn(II) to their respective permeases in a similar manner. Indeed, elucidating the molecular mechanism by which the fully reconstituted transport systems MntABC and PsaABC capture Mn(II) with high affinity and deliver the ion to the bacterial cytoplasm is an important and intriguing avenue for future investigation.

A.6 Acknowledgments

We gratefully acknowledge financial support from the National Institute of Health grants R35GM126961 (R.D.B) and R01GM118695 (E.M.N.). The work performed at the National High Magnetic Field Laboratory is supported by the National Science Foundation Cooperative Agreement No. DMR-1644779 and the State of Florida.

A.7 References

1. Waldron, K. J.; Rutherford, J. C.; Ford, D.; Robinson, N. J., Metalloproteins and metal sensing. *Nature* **2009,** *460*, 823-830.

2. Hood, M. I.; Skaar, E. P., Nutritional immunity: transition metals at the pathogen–host interface. *Nat. Rev. Microbiol.* **2012,** *10* (8), 525-537.

3. Papp-Wallace, K. M.; Maguire, M. E., Manganese transport and the role of manganese in virulence. *Annu. Rev. Microbiol.* **2006,** *60*, 187-209.

4. Juttukonda, L. J.; Skaar, E. P., Manganese homeostasis and utilization in pathogenic bacteria. *Mol. Microbiol.* **2015,** *97* (2), 216-228.

5. Brophy, M. B.; Nolan, E. M., Manganese and microbial pathogenesis: sequestration by the Mammalian immune system and utilization by microorganisms. *ACS Chem. Biol.* **2015,** *10* (3), 641-651.

6. Kobayashi, S. D.; Malachowa, N.; DeLeo, F. R., Pathogenesis of *Staphylococcus aureus* abscesses. *Am. J. Pathol.* **2015,** *185* (6), 1518-1527.

7. Kim, L.; McGee, L.; Tomczyk, S.; Beall, B., Biological and epidemiological features of antibiotic-resistant *Streptococcus pneumoniae* in re- and post-conjugate vaccine eras: a United States perspective. *Clin. Microbiol. Rev.* **2016,** *29* (3), 525-552.

8. Horsburgh, M. J.; Wharton, S. J.; Cox, A. G.; Ingham, E.; Peacock, S.; Foster, S. J., MntR modulates expression of the PerR regulon and superoxide resistance in *Staphylococcus aureus* through control of manganese uptake. *Mol. Microbiol.* **2002,** *44* (5), 1269-1286.

9. Dintilhac, A.; Alloing, G.; Granadel, C.; Claverys, J.-P., Competence and virulence of *Streptococcus pneumoniae*: Adc and PsaA mutants exhibit a requirement for Zn and Mn resulting from inactivation of putative ABC metal permeases. *Mol. Microbiol.* **1997,** *25* (4), 727-739.

10. Ma, Z.; Jacobsen, F. E.; Giedroc, D. P., Coordination chemistry of bacterial metal transport and sensing. *Chem. Rev.* **2009,** *109*, 4644-4681.

11. Rajam, G.; Anderton, J. M.; Carlone, G. M.; Sampson, J. S.; Ades, E. W., Pneumococcal surface adhesin A (PsaA): a review. *Crit. Rev. Microbiol.* **2008,** *34*, 131-142.

12. Gribenko, A. V.; Liberator, P.; Anderson, A. S.; Matsuka, Y. V.; Mosyak, L., Cell surface antigen – manganese-binding protein MntC from *Staphylococcus aureus*. In *Encyclopedia of Inorganic and Bioinorganic Chemistry*, John Wiley & Sons, Ltd: 2015.

13. Eijkelkamp, B. A.; McDevitt, C. A.; Kitten, T., Manganese uptake and streptococcal virulence. *Biometals.* **2015,** *28* (3), 491-508.

14. Gribenko, A.; Mosyak, L.; Ghosh, S.; Parris, K.; Svenson, K.; Moran, J.; Chu, L.; Li, S.; Liu, T.; Woods, V. L., Jr.; Jansen, K. U.; Green, B. A.; Anderson, A. S.; Matsuka, Y. V., Three-dimensional structure and biophysical characterization of *Staphylococcus aureus* cell surface antigen–manganese transporter MntC. *J. Mol. Biol.* **2013,** *425* (18), 3429-3445.

15. McDevitt, C. A.; Ogunniyi, A. D.; Valkov, E.; Lawrence, M. C.; Kobe, B.; McEwan, A. G.; Paton, J. C., A molecular mechanism for bacterial susceptibility to zinc. *PLoS Pathog.* **2011,** *7* (11), e1002357.

16. Hadley, R. C.; Gagnon, D. M.; Brophy, M. B.; Gu, Y.; Nakashige, T. G.; Britt, R. D.; Nolan, E. M., Biochemical and spectroscopic observation of Mn(II) sequestration from bacterial Mn(II) transport machinery by calprotectin. *J. Am. Chem. Soc.* **2018,** *140* (1), 110-113.

17. Lawrence, M. C.; Pilling, P. A.; Epa, V. C.; Berry, A. M.; Ogunniyi, A. O.; Paton, J. C., The crystal structure of pneumococcal surface antigen PsaA reveals a metal-binding site and a novel structure for a putative ABC-type binding protein. *Structure* **1998,** *6* (12), 1553-1561.

18. Oyala, P. H.; Ravichandran, K. R.; Funk, M. A.; Stucky, P. A.; Stich, T. A.; Drennan, C. L.; Britt, R. D.; Stubbe, J., Biophysical characterization of fluorotyrosine probes site-specifically incorporated into enzymes: *E. coli* ribonucleotide reductase as an example. *J. Am. Chem. Soc.* **2016,** *138* (25), 7951-7964.

19. Stoll, S.; Ozarowski, A.; Britt, R. D.; Angerhofer, A., Atomic hydrogen as high-precision field standard for high-field EPR. *J. Magn. Reson.* **2010,** *207* (1), 158-163.

20. Burghaus, O.; Rohrer, M.; Götzinger, T.; Plato, M.; Möbius, K., A novel high-field/high-frequency EPR and ENDOR spectrometer operating at 3 mm wavelength. *Meas. Sci. Technol.* **1992,** *3*, Meeting 765-774.

21. Hassan, A. K.; Pardi, L. A.; Krzystek, J.; Sienkiewicz, A.; Goy, P.; Rohrer, M.; Brunel, L.-C., Ultrawide band multifrequency high-field EMR technique: a methodology for increasing spectroscopic information. *J. Magn. Reson.* **2000,** *142* (2), 300-312.

22. Stich, T. A.; Lahiri, S.; Yeagle, G.; Dicus, M.; Brynda, M.; Gunn, A.; Aznar, C.; DeRose, V. J.; Britt, R. D., Multifrequency pulsed EPR studies of biologically relevant manganese(II) complexes. *Appl. Magn. Reson.* **2007,** *31*, 321-341.

23. Weil, J. A.; Bolton, J. R., *Electron paramagnetic resonance: elementary theory and practical applications*. 2 ed.; Wiley-Interscience: Hoboken, N. J., 2007.

24. Stoll, S.; Schweiger, A., EasySpin, a comprehensive software package for spectral simulation and analysis in EPR. *J. Magn. Reson.* **2006,** *178* (1), 42-55.

25. Sharma, A.; Gaidamakova, E. K.; Grichenko, O.; Matrosova, V. Y.; Hoeke, V.; Klimenkova, P.; Conze, I. H.; Volpe, R. P.; Tkavc, R.; Gostinčar, C.; Gunde-Cimerman, N.; DiRuggiero, J.; Shuryak, I.; Ozarowski, A.; Hoffman, B. M.; Daly, M. J., Across the tree of life, radiation resistance is governed by antioxidant Mn^{2+}, gauged by paramagnetic resonance. . *Proc. Natl. Acad. Sci. U. S. A.* **2017,** *114* (44), E9253-E9260.

26. Un, S.; Dorlet, P.; Voyard, G.; Tabares, L. C.; Cortez, N., High-field EPR characterization of manganese reconstituted superoxide dismutase from *Rhodobacter capsulatus*. *J. Am. Chem. Soc.* **2001,** *123* (41), 10123-10124.

27. Tabares, L. C.; Cortez, N.; Agalidis, I.; Un, S., Temperature-dependent coordination in *E. coli* manganese superoxide dismutase. *J. Am. Chem. Soc.* **2005,** *127* (16), 6039-6047.

28. Angerhofer, A.; Moomaw, E. W.; García-Rubio, I.; Ozarowski, A.; Krzystek, J.; Weber, R. T.; Richards, N. G. J., Multifrequency EPR studies on the Mn(II) centers of oxalate decarboxylase. *J. Phys. Chem. B.* **2007,** *111* (19), 5043-5046.

29. Meirovitch, E.; Luz, Z.; Kalb, A. J., Electron spin resonance spectroscopy of aqueous solutions of concanavalin A. *J. Am. Chem. Soc.* **1974,** *96* (24), 7542-7546.

30. Tao, L.; Stich, T. A.; Butterfield, C. N.; Romano, C. A.; Spiro, T. G.; Tebo, B. M.; Casey, W. H.; Britt, R. D., Mn(II) binding and subsequent oxidation by the multicopper oxidase MnxG investigated by electron paramagnetic resonance spectroscopy. *J. Am. Chem. Soc.* **2015,** *137* (33), 10563-10575.

31. Gagnon, D. M.; Brophy, M. B.; Bowman, S. E. J.; Stich, T. A.; Drennan, C. L.; Britt, R. D.; Nolan, E. M., Manganese binding properties of human calprotectin under conditions

of high and low calcium: X-ray crystallographic and advanced electron paramagnetic resonance spectroscopic analysis. *J. Am. Chem. Soc.* **2015,** *137* (8), 3004-3016.

32. Hadley, R. C.; Gagnon, D. M.; Ozarowski, A.; Britt, R. D.; Nolan, E. M., Murine calprotectin coordinates Mn(II) at a hexahistidine site with Ca(II)-dependent affinity. **2019,** (Submitted for publication).

33. Reed, G. H.; Markham, G. D., EPR of Mn(II) complexes with enzymes and other proteins. In *Biological Magnetic Resonance*, Berliner, L. J.; Reuben, J., Eds. Plenum Press: New York, 1984; Vol. 6, pp 73-142.

34. Walsby, C. J.; Telser, J.; Rigsby, R. E.; Armstrong, R. N.; Hoffman, B. M., Enzyme control of small-molecule coordination in FosA as revealed by ^{31}P pulsed ENDOR and ESE-EPR. *J. Am. Chem. Soc.* **2005,** *127* (23), 8310-8319.

35. Duboc, C.; Phoeung, T.; Zein, S.; Pécaut, J.; Collomb, M.-N.; Neese, F., Origin of the zero-field splitting in mononuclear octahedral dihalide Mn^{II} complexes: an investigation by multifrequency high-field electron paramagnetic resonance and density functional theory. *Inorg. Chem.* **2007,** *46* (12), 4905-4916.

36. Duboc, C.; Collomb, M.-N.; Neese, F., Understanding the zero-field splitting of mononuclear manganese(II) complexes from combined EPR spectroscopy and quantum chemistry. *Appl. Magn. Reson.* **2010,** *37*, 229-245.

37. Wood, R. M.; Stucker, D. M.; Jones, L. M.; Lynch, W. B.; Misra, S. K.; Freed, J. H., An EPR study of some highly distorted tetrahedral manganese(II) complexes at high magnetic fields. *Inorg. Chem.* **1999,** *38* (23), 5384-5388.

38. Zein, S.; Duboc, C.; Lubitz, W.; Neese, F., A systematic density functional study of the zero-field splitting in Mn(II) coordination compounds. *Inorg. Chem.* **2008,** *47* (1), 134-142.

Appendix B: Preparation and Iron Redox Speciation Study of the Fe(II)-binding Antimicrobial Protein Calprotectin

This Appendix was adapted from *Meth. Mol. Biol.* **2019**, 1929, 397-415.

B.1. Introduction

Calprotectin (CP, S100A8/S100A9 heterooligomer) is a member of the S100 family of Ca(II)-binding proteins and a topic of interest in the metal homeostasis community because of its contributions to the metal-withholding innate immune response, which is often termed nutritional immunity.[1, 2] CP is a cytoplasmic protein produced by neutrophils, macrophages, monocytes, and epithelial cells. It is released at sites of infection and, in the extracellular space, the protein sequesters essential nutrient metal ions to limit microbial growth. Our current understanding of its metal-sequestering function largely comes from mouse models of infectious disease,[3-8] including studies that involve a $S100A9^{-/-}$ or CP knockout mouse,[9] and molecular characterization of the recombinant human protein.[10-20] A recombinant expression and purification of murine CP was recently reported, which provides a foundation for future evaluation of this orthologue.[21]

Biochemical, biophysical and structural studies of human CP (hCP) demonstrated that the protein is a heterooligomer of S100A8 and S100A9.[10, 11, 22, 23] Each subunit possesses two EF-hand Ca(II)-binding sites: a canonical C-terminal EF-hand and a non-canonical N-terminal EF-hand.[24] In the absence of Ca(II) and transition metal ions, hCP is a heterodimer.[10] Two transition-metal-binding sites form at the dimer interface.[11, 12, 25] Site 1 is a His_3Asp motif composed of (A8)His83, (A8)His87, (A9)His20 and (A9)Asp30.[11] Site 2 is a His_6 motif composed of (A8)His17, (A8)His27, (A9)His91, (A9)His95, (A9)His103 and (A9)His105.[13-15] The His_6 site of hCP has gained significant attention in recent years because it can sequester a range of divalent first-row transition metal ions including Mn(II), Fe(II), Zn(II) and Ni(II).[1, 14-17, 19, 20] Like the human protein, murine CP (mCP) is also a heterooligomer of S100A8 and S100A9, and each subunit contains a

canonical C-terminal EF-hand and a non-canonical N-terminal EF-hand domain. Amino acid sequence alignment of the human and murine S100A8 and S100A9 polypeptides indicates that the His_3Asp and His_6 sites are conserved.[21]

Early studies of hCP revealed that Ca(II) binding causes two heterodimers to self-associate and form a heterotetramer.[22, 23] In addition to this change in quaternary structure, Ca(II) binding enhances the transition metal affinities, antimicrobial activity, and proteolytic stability of hCP.[1, 12, 26] Initial biochemical evaluation of mCP revealed that Ca(II) binding also causes this orthologue to form heterotetramers[21], and further investigations are required to decipher whether Ca(II) ions modulate other structural and functional properties of the protein. The studies of hCP provide the basis for a working model where CP senses the high extracellular Ca(II) concentration (≈2 mM) at an infection site and becomes a tetramer with high transition metal affinities.[1, 12]

In this chapter, we first present the overexpression and purification protocols for mCP and hCP-Ser, a cysteine-null variant [(S100A8(C42S)/S100A9(C3S)], which has been used extensively in biochemical, biophysical and structural studies of the human orthologue. These protocols are based on published work,[12, 21] provide each protein as the apo heterodimer, and can be used for preparing native hCP as well as other mCP and hCP-Ser variants with single or multiple point mutations. Because the His_6 site of hCP was recently shown to sequester Fe(II) and the protein was found to affect the redox speciation of Fe in aerobic solution,[18, 19] we also provide a protocol for an Fe speciation assay that we first designed and utilized to study hCP-Ser.[18, 19] Herein, we extend this assay to mCP and report that this protein also shifts the redox speciation of Fe from Fe(III) to Fe(II) under aerobic conditions.

B.2. Materials

1. All chemicals are purchased from commercial suppliers and used as received.
2. All solutions are prepared using Milli-Q water (18.2 MΩ•cm, 22-μm filter).
3. Protein concentrations are determined using the calculated extinction coefficients of the S100A8/S100A9 (calprotectin) homodimer (Protparam: ε_{280} = 5960 M^{-1} cm^{-1} for mCP (mS100A8/mS100A9), 18,450 $M^{-1}cm^{-1}$ for hCP (hS100A8/hS100A9) and hCP-Ser (hS100A8(C42S)/hS100A9(C3S)). All concentrations reported are for the homodimer.

B.2.1 Preparation of Expression Plasmids

1. The synthetic genes for each protein subunit (mS100A8, mS100A9, hS100A8, hS100A9) are optimized for *Escherichia coli* codon usage and obtained from ATUM (formerly DNA2.0). These genes, as well as procedures for site-directed mutagenesis to obtain genes encoding hS100A8(C42S) and hS100A9(C3S), are described in the literature.[12, 21]
2. The pET41a expression vector is obtained from Invitrogen.
3. The genes are inserted into the *Nde*I and *Xho*I restriction sites of pET41a, which affords the untagged, full-length proteins with no additional amino acids after IPTG-induced overexpression.[12, 21]
4. The pET41a plasmids containing mS100A8, mS100A9, hS100A8(C42S), and hS100A9(C3S) are transformed into chemically-competent *E. coli* BL21(DE3) cells for overexpression.

5. Cell stocks of *E. coli* BL21(DE3) cells are prepared by growing the cells in LB to saturation, diluting 1:1 into a 50 % glycerol solution, freezing the resulting cells in liquid nitrogen, and storing the cells at -80 °C.

Protein	Abbreviation	Subunits	Expression plasmid	Ref*
Human calprotectin	hCP	hS100A8 hS100A9	pET41a-*hS100A8* pET41a-*hS100A9*	12 12
Human calprotectin Cys→Ser variant	hCP-Ser	hS100A8(C42S) hS100A9(C3S)	pET41a-*hS100A8(C42S)* pET41a-*hS100A9(C3S)*	12 12
Murine calprotectin	mCP	mS100A8 mS100A9	pET41a-*mS100A8* pET41a-*mS100A9*	21 21

* The original names for the plasmids containing the human S100A8 and S100A9 genes did not include "*h*" to designate "human."

B.2.2 Commercial Materials and Preparation of Reagents

1. To reduce metal ion contamination, plastic spatulas are used to transfer reagents.[1]
2. Stock solutions of metal ions and sodium citrate (100 mM) are prepared in nitric acid-washed volumetric glassware and transferred to polypropylene tubes for storage. [1]
3. Stock solutions of Fe(III) (100 mM) are prepared from ≥99.99% trace metals basis anhydrous $FeCl_3$, Milli-Q water, and trace metals basis 37% HCl.[2]
4. Stock solutions of Ca(II) (1 M) are prepared from 99.999% $CaCl_2$ and Milli-Q water.
5. Other reagents utilized in this protocol are listed below:

Purpose	Reagent	Supplier
Protein overexpression and purification	Luria-Bertani (LB)	Beston Dickinson
	Kanamycin sulfate	VWR
	Isopropyl β-D-1-thiogalactopyranoside (IPTG)	BACHEM
	99.5 % 4-(2-hydroxyethyl)-1-piperazineethanesulfonic acid (HEPES)	MilliporeSigma
	Sodium chloride	MilliporeSigma
	Sodium hydroxide	Macron
	Triton X-100	EMD
	Ethylenediaminetetraacetic acid disodium salt dihydrate (EDTA)	VWR
	Phenylmethylsulfonyl fluoride (PMSF)	VWR
	Dithiothreitol (DTT)	VWR
	Guanidinium hydrochloride (GuHCl)	MilliporeSigma
	Ammonium sulfate	MilliporeSigma
	Chelex resin	Bio-Rad
Fe speciation assay	Ultrol grade HEPES (free acid)	Calbiochem
	TraceSELECT sodium chloride	MilliporeSigma
	37% Hydrochloric acid (HCl), trace metals basis	MilliporeSigma
	≥99.5% sodium citrate tribasic dihydrate	MilliporeSigma
	99.99% anhydrous ferric chloride	MilliporeSigma
	≥99.0% sodium ascorbate	MilliporeSigma
	≥99.5% trichloroacetic acid (TCA)	MilliporeSigma
	≥99.99% Ammonium acetate	MilliporeSigma
	97% 3-(2-Pyridyl)-5,6-diphenyl-1,2,4-triazine-*p,p'*-disulfonic acid monosodium salt hydrate (ferrozine)	MilliporeSigma

B.2.3 Ferrozine Preparation

For the Fe speciation assay, ferrozine is used to determine the Fe(II) content of solutions via detection of the $[Fe(ferrozine)_3]^{4-}$ complex by optical absorption spectroscopy.[18, 27, 28]

1. Stock solutions (≈100 mM, 20 mL) of ferrozine are prepared in Milli-Q water, aliquoted into 800-μL portions, and stored at -80 °C.

2. Each aliquot is thawed only once and subsequently diluted to the working concentration of 6.17 mM (10 mL) in 0.1 M HCl immediately before use.

B.2.4 Buffers for Protein Purification and the Iron Speciation Assay

Buffers employed for the purification of mCP and CP-Ser are prepared as indicated below with Milli-Q water and are subsequently filtered (0.2 μm) and stored at 4 °C. For buffers used in the preparation of mCP or hCP, DTT (5 mM final concentration) is added to all buffers immediately before use because these proteins contain cysteine residues.[3] The Fe speciation assay buffer is prepared from high purity reagents (see Section B.2.2) in acid-washed volumetric glassware and subsequently transferred to a polypropylene container.[1]

Buffer (1 L)	Composition
lysis buffer A:	50 mM Tris, 100 mM NaCl, 1 mM EDTA, 0.5 % Triton X-100, 1 mM PMSF*, pH 8.0
lysis buffer B:	50 mM Tris, 100 mM NaCl, 4 M GuHCl, pH 8.0
dialysis buffer:	20 mM HEPES, pH 8.0
MonoQ buffer A:	20 mM HEPES, pH 8.0
MonoQ buffer B:	20 mM HEPES, 1 M NaCl, pH 8.0
S75 buffer:	20 mM Tris, 100 mM NaCl, pH 8.0
Fe speciation assay buffer:	75 mM HEPES, 100 mM NaCl, 2 mM Ca(II)**, pH 7.0

*PMSF is added immediately before use. It is dissolved in anhydrous ethanol before use or a stock solution can be stored at -20 °C.
**Ca(II) (80 μL of a 1-M stock solution) is added to 40 mL of the buffer before use.

B.2.5 Equipment for Protein Purification

1. An ÄKTA purifier (GE Life Sciences) housed in a 4 °C room and equipped with a 150-mL Superloop (GE Life Sciences) is employed for chromatographic purification.
2. Both human and murine CP orthologues are purified in two chromatographic steps: anion exchange chromatography using a MonoQ 10/100 GL column (GE Life Sciences) is performed first, followed by size exclusion chromatography using a Superdex 75 10/300 GL column (GE Life Sciences).

B.2.6 Equipment for Optical Absorption Spectroscopy

1. A Beckman Coulter DU 800 spectrophotometer thermostatted at 25 °C with a Peltier temperature controller is used for optical absorption spectroscopy.
2. Plastic cuvettes (1-cm pathlength, polystyrene, VWR) are employed for optical absorption measurements during the Fe speciation assay. New cuvettes are used for each measurement. Acid-washed quartz cuvettes can also be used for these measurements.
3. Plastic cuvettes (1-cm pathlength, polystyrene, VWR) are used for monitoring the bacterial culture optical density at 600 nm (OD_{600}, absorption at 600 nm).
4. Observed OD_{600} values of bacterial cultures are given throughout this protocol as benchmarks; however, these values will vary from instrument to instrument.

B.3. Methods

The methods for protein overexpression and purification described in this section are based on published procedures[12, 21] and can be employed to produce human and murine CP variants obtained by site-directed mutagenesis.

B.3.1 Protein Preparation

The protein purification procedures are described for overexpression carried out using a 1 L culture for each subunit. Typical yields are ≈60 mg / 2 L culture for CP-Ser and ≈45 mg / 2 L culture for mCP.

Day 1: Preparation for protein overexpression

1. Prepare and autoclave Luria-bertani (LB) medium for protein overexpression according to the manufacturer's instructions. Prepare 1 L LB medium in a 2-L

baffled flask for each S100 subunit to be overexpressed. Cool the autoclaved medium and place the flasks in a 37 °C incubater-shaker or warm room overnight.

2. Prepare 50 mg/mL kanamycin by dissolving kanamycin sulfate in Milli-Q water. Filter the solution (0.2-μm syringe filter), collecting the filtrate in a polypropylene centrifuge tube, and store the solution at -20 °C. The pET41a vector contains a kanamycin resistance cassette.
3. Prepare 0.5 M IPTG by dissolving IPTG in Milli-Q water. Filter the solution (0.2-μm syringe filter), collect the filtrate in a polypropylene centrifuge tube, and store at -20 °C. Protein expression will be induced by IPTG addition on Day 2.
4. Prepare starter cultures of *E. coli* BL21(DE3) containing the desired pET41a expression plasmids. To a sterile 250-mL baffled flask, add 30 mL of LB and 50 μg/mL kanamycin. Inoculate the medium from a freezer stock (Section A.2.1) of the *E. coli* overexpression strain or from a single colony that was grown on an agar plate. Incubate the cultures (37 °C, 150 rpm) for ≈16 h.

Day 2: Overexpression of S100A8 and S100A9 subunits

5. Measure the OD_{600} of the overnight culture, which should be >1.5.
6. Add 50 μg/mL kanamycin (final concentration, 1 mL of a 50 mg/mL stock solution in Milli-Q water) into the 2-L baffled flask containing 1 L of LB medium and dilute a 10-mL volume (1:100 dilution) of the overnight culture into the medium. Place the resulting culture in an incubator-shaker (37 °C, 150 rpm).
7. Monitor the OD_{600}.

8. When OD_{600} ≈0.6-0.7, add 125 μM IPTG (250 μL of 0.5 M IPTG stock solution) to the culture.
9. Incubate the culture (37 °C, 150 rpm) for and additional 3.5-4 h after induction. At this time, measure the OD_{600} of the culture, which should be >1.5.
10. Harvest the cells by centrifugation (2246 g, 15 min, 4 °C), discard the supernatant, and transfer the cell pellet to a sterile 50-mL polypropylene centrifuge tube. Flash freeze the pellet in liquid nitrogen and store at -80 °C until use.

This procedure typically yields ≈2 g cells / 1 L culture (wet weight) for each subunit, which can be stored at -80 °C for over four months without an impact on protein yield. The overexpression can be evaluated by SDS-PAGE analysis (Coomassie stain) of the pre- and post-induction cell samples (whole cell lysate) using a 15% tricine gel (**Figure B.1**). Successful overexpression of the S100A8 subunit should show an intense band at ≈11 kDa in the post-induction sample, corresponding to the S100A8 monomer. Successful overexpression of the S100A9 subunit should show an intense band at ≈13 kDa, corresponding to the S100A9 monomer. These overexpression conditions result in insoluble hS100A8, hS100A8(C42S), hS100A9, hS100A9(C3S), and mS100A8, and soluble mS100A9.

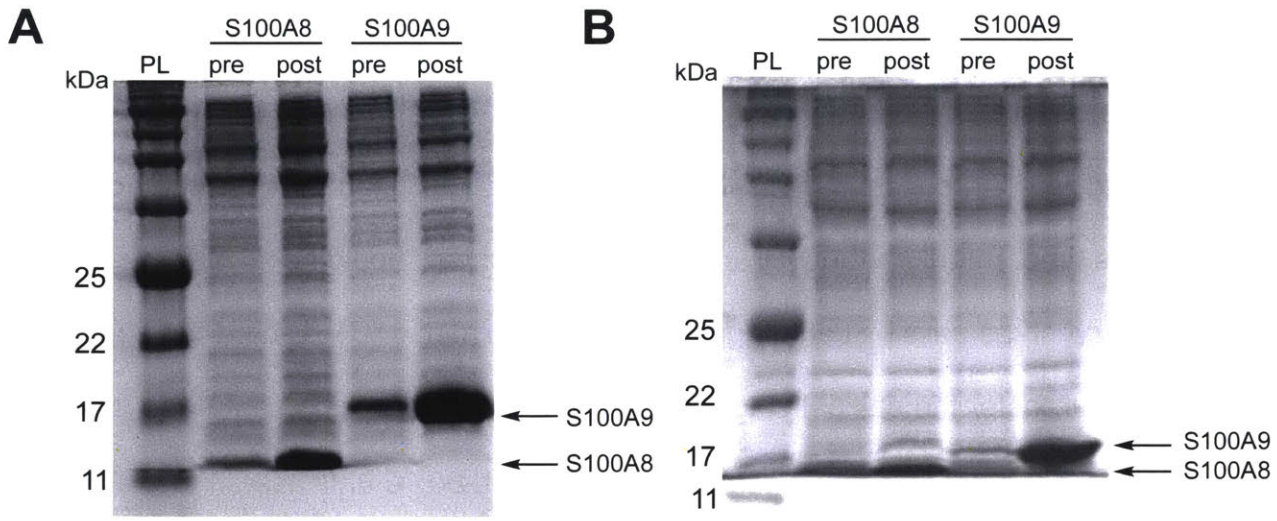

Figure B.1. Representative 15% Tris-glycine SDS-PAGE gel of whole cell lysate of *E. coli* BL21(DE3) obtained from the overexpression of the S100A8 and S100A9 subunits of mCP (**A**) and hCP-Ser (**B**). Samples pre- and post-induction with IPTG are shown. The samples were prepared using the B-PER reagent (Thermo Fisher Scientific, manufacturer protocol). The protein ladder (PL) is p7712S (New England Biolabs).

Day 3: Lysis and refolding of mCP

The following steps should be carried out at 4 °C and buffers should be equilibrated and stored at 4 °C (in a cold room) or on ice.

11. Thaw one mS100A8 and one mS100A9 cell pellet, each from a 1-L overexpression culture, on ice.
12. Add 116 mg DTT to 150 mL of lysis buffer A and stir to dissolve and afford a final concentration of 5 mM.[4] Keep lysis buffer A on ice or in a 4 °C room.
13. Suspend each cell pellet in 30 mL of lysis buffer A containing 5 mM DTT. Once the cell pellets are fully suspended, combine the suspensions to yield a 60-mL mixture containing both mS100A8 and mS100A9.
14. Transfer the combined suspension to a stainless steel beaker on ice. Lyse the cells by sonication on ice (40% amplitude, 2.5 min, 30 s on, 10 s off).

15. Centrifuge the mixture (22,000 g, 4 °C, 10 min). Transfer the supernatant, which contains soluble mS100A9, to a glass beaker on ice.
16. Repeat steps 13-15 for a total of two times. Keep the final pellets (containing insoluble mS100A8) on ice and combine the supernatant from each round (containing soluble mS100A9) in a glass beaker on ice.
17. To precipitate contaminating proteins from the combined supernatant containing soluble mS100A9, add ≈45 g of ammonium sulfate to the solution (≈120 mL) in one portion and stir rapidly for ≈1 h at 4 °C. This quantity of ammonium sulfate affords a final concentration of 60% ammonium sulfate.
18. Centrifuge the mixture obtained from step 17 (22,000 g, 4 °C, 20 min). Vacuum filter (Büchner funnel) and collect the filtrate on ice. The filtrate contains soluble mS100A9.
19. Add ≈38 g of ammonium sulfate to the combined filtrate in one portion to increase the ammonium sulfate concentration to 100%. Stir the mixture at 4 °C for ≈1 h to precipitate mS100A9.
20. Centrifuge the mixture obtained in step 19 (22,000 g, 4 °C, 20 min). Vacuum filter (Büchner funnel) and collect the precipitate, which contains mS100A9.
21. Add 77 mg DTT to 100 mL lysis buffer B,[4] stir to dissolve, and keep the buffer on ice. Resuspend the mS100A8 pellets (step 16) and the mS100A9 precipitate (step 20) together in this solution by using a tissue homogenizer or by gently stirring the mixture with a stir bar at 4 °C.
22. Transfer the suspension to a stainless steel beaker and sonicate for 5 min (40% amplitude, 30 s on, 10 s off) on ice.

23. Centrifuge the mixture (22,000 g, 4 °C, 10 min). Transfer the supernatant to a dialysis bag (3500 MWCO) and dialyze against 3 x 4L of dialysis buffer containing 5 mM DTT at 4 °C for at least 12 h each.[4]

Day 3: Lysis and refolding of hCP-Ser

The following steps should be carried out at 4 °C and buffers should be equilibrated and stored at 4 °C (in a cold room) or on ice.

24. Thaw one hS100A8(C42S) and one hS100A9(C3S) cell pellet, each from a 1-L overexpression culture, on ice.
25. Keep 200 mL of lysis buffer A on ice or in a 4 °C room. Suspend each cell pellet in 30 mL (60 mL total) lysis buffer A. Once the cell pellets are fully suspended, combine the suspensions to yield a 60-mL mixture containing both hS100A8(C42S) and hS100A9(C3S).
26. Transfer the mixture to a stainless steel beaker on ice. Lyse the cells by sonication (40% amplitude, 2.5 min, 30 s on, 10 s off).
27. Centrifuge the crude lysate (22,000 g, 4 °C, 10 min). Discard the supernatant. The pellet contains the hS100A8(C42S) and hS100A9(C3S) subunits.
28. Repeat steps 25-27 for a total of three times.
29. Suspend the resulting cell pellets together in 100 mL lysis buffer B using a tissue homogenizer or by gently stirring the mixture with a stir bar at 4 °C.
30. Transfer the solution to a steel beaker on ice and sonicate for 5 min (40% amplitude, 30 s on, 10 s off).

31. Centrifuge the mixture (22,000 g, 4 °C, 10 min). Transfer the supernatant to a dialysis bag (3500 MWCO) and dialyze against 3 x 4 L of dialysis buffer at 4 °C for at least 12 h each.

Days 4 and 5: Change dialysis buffer

32. Change the dialysis buffer. If it is an mCP dialysis, add 5 mM DTT to the new dialysis buffer (3.1 g to 1 L dialysis buffer).

After dialysis, the refolded protein is purified by AEC and SEC – see Day 6.

33. The day before the chromatography steps, pre-equilibrate the S75 column with 1 column volume (CV) of S75 buffer.

Day 6: Protein purification of mCP and hCP-Ser

Over the course of the refolding process described above, some insoluble aggregates form and accumulate at the bottom of the dialysis bag as a white precipitate.

34. Centrifuge the dialysate to pellet the precipitate (22,000 g, 4°C, 10 min). Decant and vacuum filter the supernatant using a 0.2-µm bottle-top filter and collect the filtrate in a polypropylene bottle stored on ice.
35. Load the filtrate (≈110 mL; dialysis can cause some increase in the volume) solution onto the Superloop.
36. Equilibrate the MonoQ column with 2 CV Milli-Q water, 2 CV MonoQ buffer A, 2 CV MonoQ buffer B, 2 CV MonoQ buffer A. Use a flow rate of 2 mL/min. Include 5 mM DTT in the MonoQ A and B buffers when purifying a cysteine-containing protein.[4]

37. Load the column with the protein solution and elute at 2 mL/min using MonoQ buffer A and a gradient of:

    a. 0–15 % MonoQ buffer B over 15 CV for mCP (**Figure B.2A,C**)

    OR

    b. 0–30% MonoQ buffer B over 30 CV for hCP-Ser (**Figure B.2B,D**)

    Monitor protein elution at 280 nm and collect 5-mL fractions. SDS-PAGE analysis of the fractions is used to determine which fractions contain the CP heterodimer, which is evidenced by the presence of both the S100A8 and S100A9 subunits in about equal abundance on the gel (**Figure B.2**). We typically perform two or three monoQ runs for a protein purification on this scale. The column is equilibrated (step 36) between runs.

38. Combine fractions containing both mS100A8 and mS100A9 (**Figure B.2**) and concentrate the protein by centrifugation to ≈10 mL using an Amicon spin filter (10 kDa MWCO) and centrifuging (3210 g, ≈25 min, 4 °C).

39. Load all of the concentrated protein onto the Superloop.

40. Elute the heterodimer over 1 CV on the pre-equilibrated S75 column at a flow rate of 1 mL/min using S75 buffer (**Figure B.3**). Include 5 mM DTT in the S75 buffer when purifying a cysteine-containing protein.[4]

41. Collect the fractions containing CP and dialyze for at least 12 h in 1 L S75 buffer containing ≈10 g Chelex at 4 °C. Include 5 mM DTT in this buffer when purifying a cysteine-containing protein.[4]

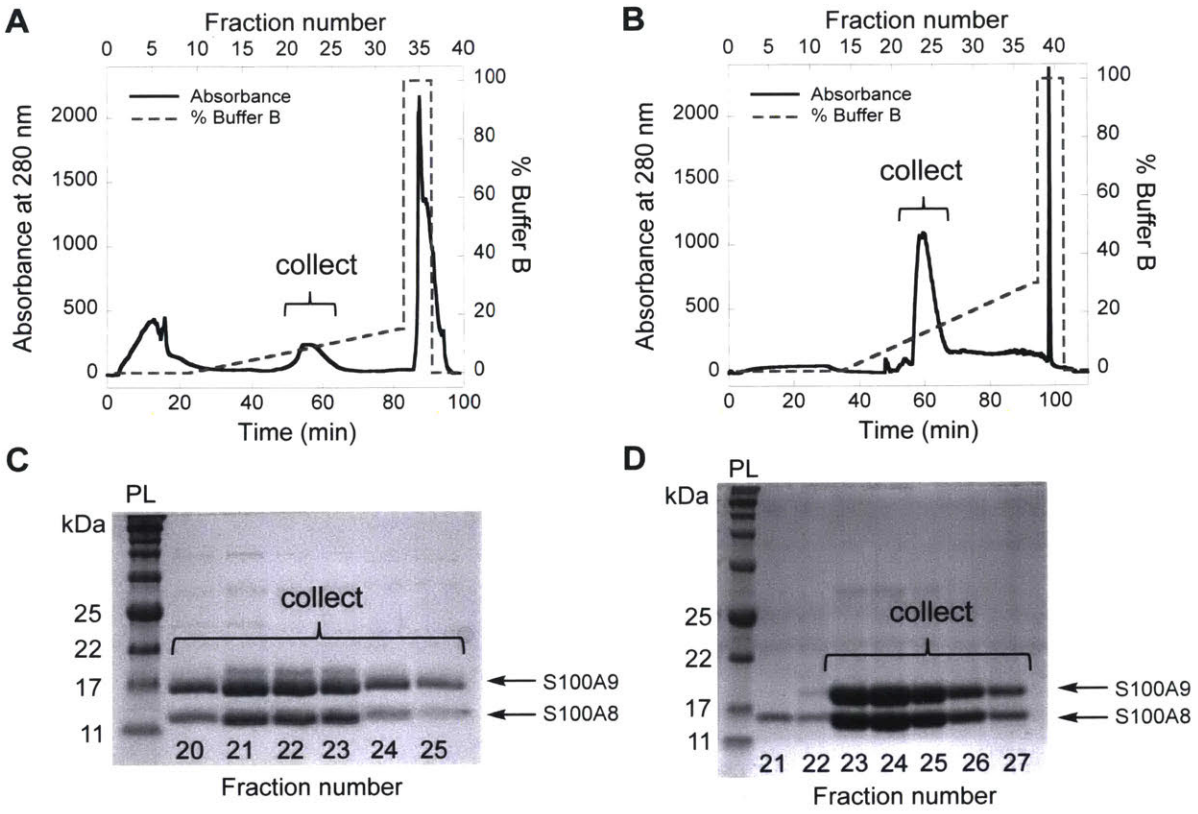

Figure B.2. Purification of mCP (**A, C**) and CP-Ser (**B, D**) by anion exchange chromatography using a MonoQ column. Elution profiles (**A, B**) and corresponding 15% Tris-glycine SDS-PAGE gels of the fractions (**C, D**), indicating the fractions collected for subsequent purification. The protein ladder (PL) is p7712S (New England Biolabs).

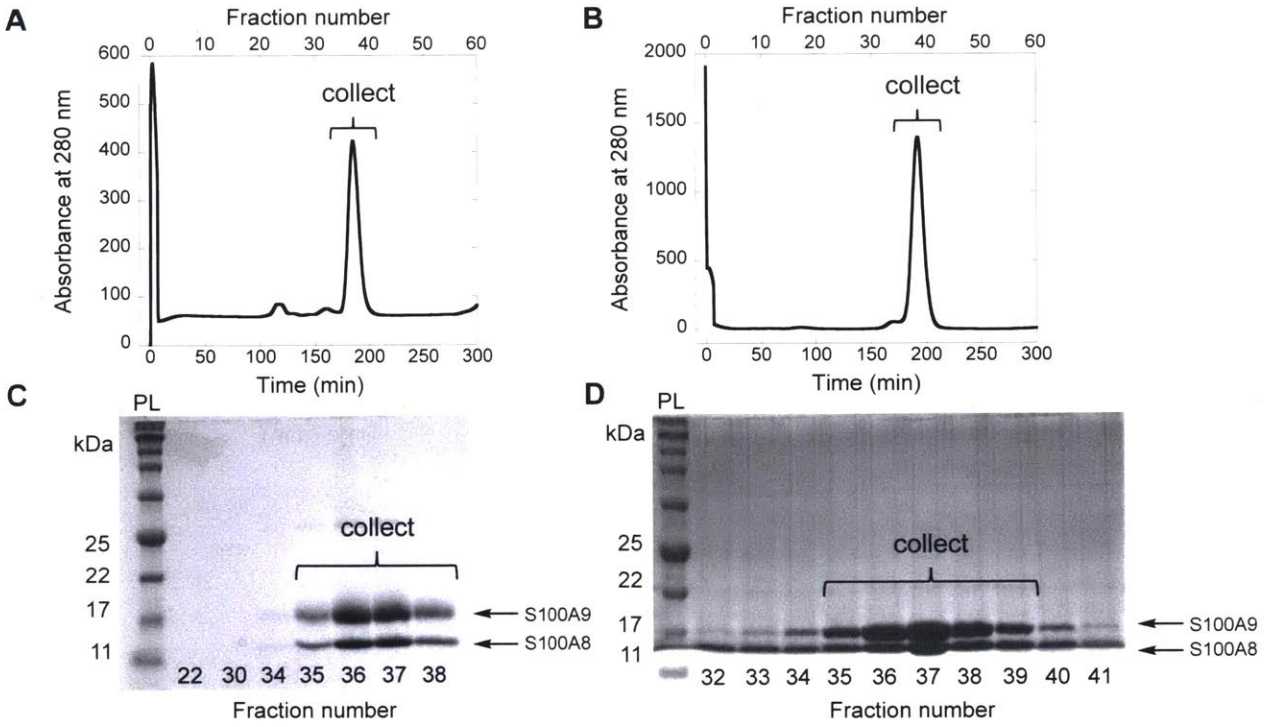

Figure B.3. Purification of mCP (**A, C**) and CP-Ser (**B, D**) by size exclusion chromatography using a S75 column. Elution profiles (**A, B**) and corresponding 15% Tris-glycine SDS-PAGE gels of the fractions (**C, D**), indicating fractions collected for subsequent dialysis. The protein ladder (PL) is p7712s (New England Biolabs).

Day 7: Protein Storage

42. Concentrate the protein solution to >500 μM (≈3 mL). Aliquot the protein into microcentrifuge tubes, freeze the protein aliquots in liquid nitrogen, and store at -80 °C.

B.3.2 Biochemical Characterization of Calprotectin

Following the purification of human or murine CP, we recommend employing standard biochemical techniques to evaluate the integrity of the purified protein.[12] These methods include SDS-PAGE (**Figure B.4**) to ascertain purity, analytical size exclusion

chromatography to monitor oligomeric state, and metal analysis by inductively-coupled plasma mass spectrometry (ICP-MS). The experimental conditions for these procedures, as well as circular dichroism spectroscopy, are found in *references 12 and 21.*

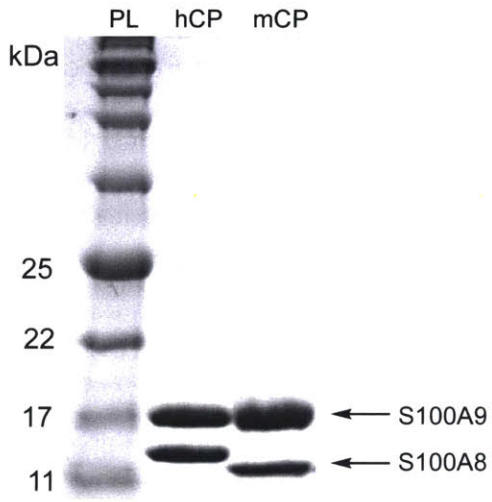

Figure B.4. Representative 15% Tris-glycine SDS-PAGE gel of purified hCP-Ser (hCP) and mCP. The protein ladder (PL) is p7712S (New England Biolabs).

B.3.3 Fe Speciation Assay Using Ferrozine

The Fe speciation assay allows quantification of Fe(II) as well as total Fe content in solutions containing this metal ion. The protocol described below is modified from prior reports.[18, 27, 28]

Day 1: Preparation of samples

1. Combine 1 mL of the 100 mM $FeCl_3$ stock solution (Section A.2.2) with l mL of the 100 mM sodium citrate stock solution (Section A.2.2) to afford a 50 mM Fe(III)-citrate solution (2 mL).
2. Dilute l mL of the 50 mM Fe(III)-citrate solution with 9 mL Milli-Q water to afford a 5 mM Fe(III)-citrate solution (10 mL).

3. Buffer-exchange mCP and hCP-Ser into the Fe speciation assay buffer (4x, 500 μL spin filter).[5]
4. Prepare 5-mL samples of 30 μM Fe(III)-citrate and 20 μM protein in 15-mL polypropylene tubes by diluting the 5 mM Fe(III)-citrate solution (step 2) and the buffer-exchanged protein (step 3) into the Fe speciation assay buffer. Cap the tubes and incubate in an incubator shaker (30 °C, 150 rpm).
5. Prepare Fe standards for a standard curve. Dilute the 50 mM Fe(III)-citrate stock solution (step 1) with Fe speciation assay buffer to afford 10-mL aliquots of 32 μM and 25 μM Fe(III)-citrate. Serially dilute the 32 μM Fe(III)-citrate solution (1:1 dilution series) with Fe speciation assay buffer to prepare standards containing 16, 8, 4, and 2 μM Fe(III)-citrate. Another standard used to generate the calibration curve is buffer with no added Fe.

Day 1: Fe speciation assay of calibration standards

6. Before initiating the assay, set a heating block to 95 °C and turn on the optical absorption spectrophotometer.
7. Prepare 0.4 M TCA and 1.3 M ammonium acetate solutions in Milli-Q water (or thaw a solution prepared the same day and stored at -20 °C).[6]
8. Thaw an aliquot of 100 mM ferrozine.
9. Prepare 0.2 M HCl (10 mL) in a 15-mL polypropylene tube by diluting 166.6 μL of 37% HCl into 10 mL of Milli-Q water.[7]

10. Prepare 40 mL 1.5 mM sodium ascorbate in 0.2 M HCl. Dilute 667 μL 37% HCl into 40 mL of Milli-Q water and add 12 mg sodium ascorbate. This solution must be prepared immediately before use.[6,7]
11. Prepare 6.17 mM ferrozine in 0.1 M HCl. Dilute 83.3 μL 37% HCl and 617 μL 100 mM ferrozine into 10 mL of Milli-Q water in a 15-mL polypropylene centrifuge tube.[6,7]
12. Transfer 200 μL of each standard solution to a separate 1.7-mL microcentrifuge tube. The total Fe content of these standards will be quantified. Ascorbate will be added to each sample to reduce all Fe(III) to Fe(II) before absorption of the Fe(II)-ferrozine complex is measured by optical absorption spectroscopy. Label each these tubes with an **A**.
13. Add 200 μL of 1.5 mM ascorbate solution to each tube labeled **A**.
14. Add 200 μL of 0.4 M TCA to each tube labeled **A**.
15. Vortex each tube labeled **A** for 10 s.
16. Heat all tubes labeled **A** for 5 min at 95 °C.
17. Centrifuge all tubes labeled **A** (15,000 g, 5 min, 4 °C).
18. Transfer 300 μL of each supernatant to a new microcentrifuge tube.
19. Add 400 μL of 1.3 M ammonium acetate to each tube.
20. Add 100 μL of 6.17 mM ferrozine in 0.1 M HCl to each tube. Vortex to mix.
21. Transfer 500 μL of each solution to disposable semi-micro polystyrene cuvettes.
22. Blank the optical absorption spectrometer using Milli-Q water and collect the optical absorption spectrum of each solution (**Figure B.5A**).

23. Plot A_{562} vs [Fe_{total}] of the calibration standards and apply a linear regression to generate a calibration curve (**Figure B.5B**).

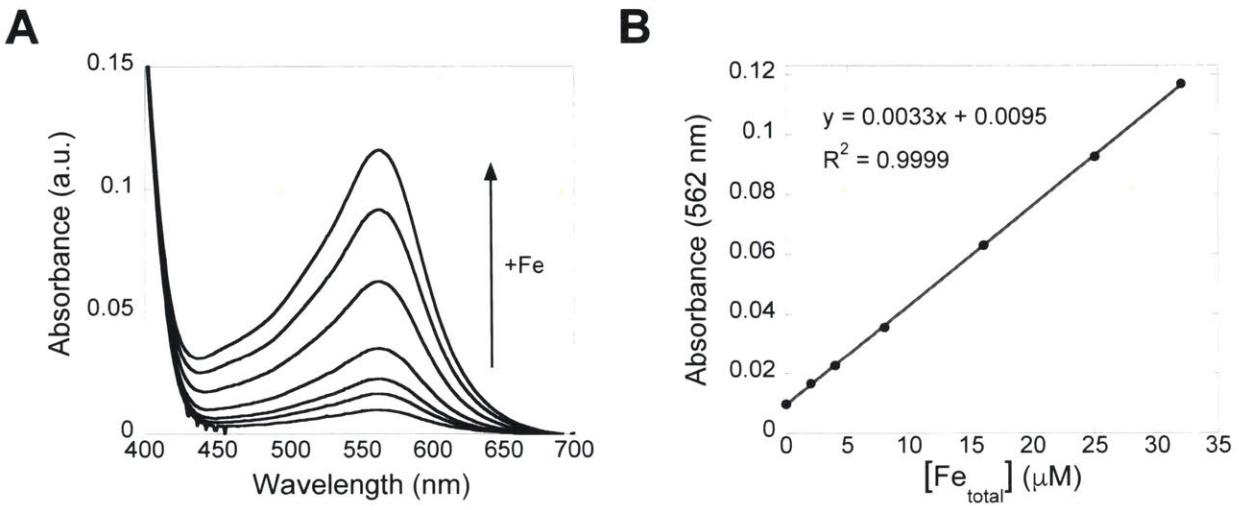

Figure B.5. Absorbance profile (**A**) of Fe standards in Fe speciation assay buffer (0, 2, 4, 8, 16, 25, and 32 μM total Fe). A calibration curve is generated by plotting A_{562} vs. [Fe_{total}] and applying a linear regression fit (**B**).

Days 1-4: Fe speciation assay of protein samples

This assay is conducted at 0, 24, 48, and 72 h after the protein assay setup.

24. On each day, complete steps 6-11 from *Fe speciation assay of calibration standards*, above.
25. Immediately after preparing the protein samples, and on each day after, add 200 μL of each sample to <u>each</u> of two microcentrifuge tubes, labeled **A** and **B**, respectively. Samples labeled **A** will be treated with an ascorbate solution to reduce all Fe to Fe(II) and quantity total Fe. Samples labeled **B** will not be treated with ascorbate to quantify Fe(II).
26. Add 200 μL of 0.2 M HCl to all tubes labeled **B**.

27. Add 200 μL of 1.5 mM ascorbate solution to all tubes labeled **A**.
28. Add 200 μL of 0.4 M TCA to all tubes labeled **A** and **B**.
29. Vortex each tube for 10 s.
30. Heat all tubes for 5 min at 95 °C.
31. Centrifuge all tubes (15,000 g, 5 min, 4 °C). A small, white protein pellet is observed in the bottom of the tubes containing protein.
32. Transfer 300 μL of the supernatant to new microcentrifuge tubes.
33. Add 400 μL of 1.3 M ammonium acetate to each tube.
34. Add 100 μL of 6.17 mM ferrozine in 0.1 M HCl to each tube. Vortex to mix.
35. Transfer 500 μL of each solution to disposable semi-micro polystyrene cuvettes.
36. Blank the optical absorption spectrometer using Milli-Q water and collect the optical absorption spectrum of each solution 400-700 nm (**Figure B.6A,B**). Record the absorbance of the Fe(II)-ferrozine complex in each solution at 562 nm.
37. Use the calibration curve to determine the [Fe(II)] and [Fe_{total}] in the mCP and CP-Ser samples. Subtract the measured [Fe(II)] from the [Fe_{total}] to determine the [Fe(III)]. Plot the concentrations of Fe(II), Fe(III), and total Fe for the samples over days 0-3 (**Figure B.7**).[8]

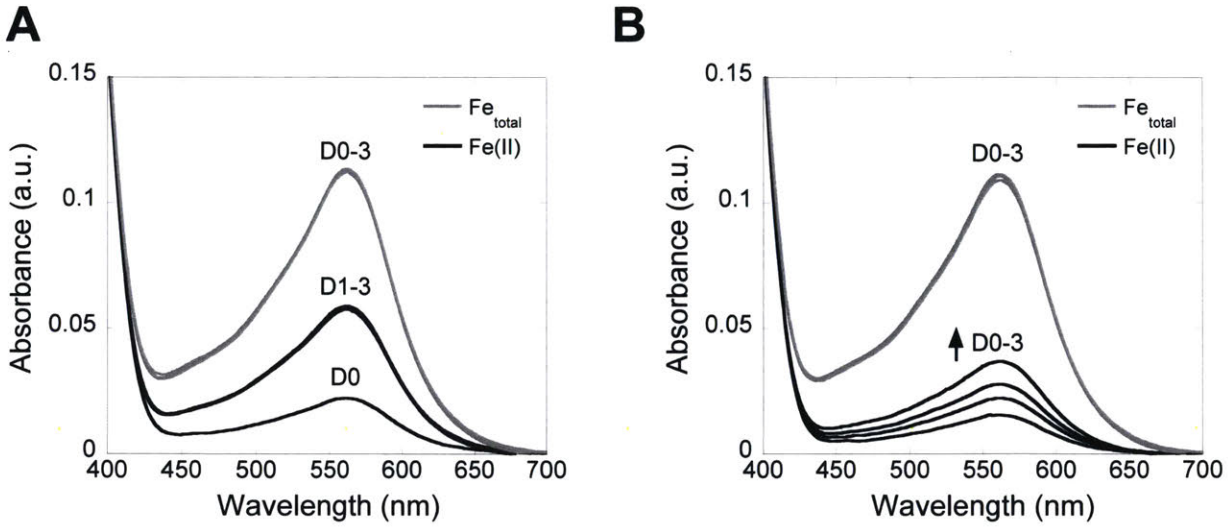

Figure B.6. Absorbance profiles of mCP (**A**) and hCP-Ser (**B**) samples analyzed by the Fe speciation assay. Spectra obtained for the Fe_{total} quantification samples (tubes labeled A, gray traces) and the Fe(II) quantification samples (tubes labeled B, black traces) over days 0-3 (D0-3) are shown.

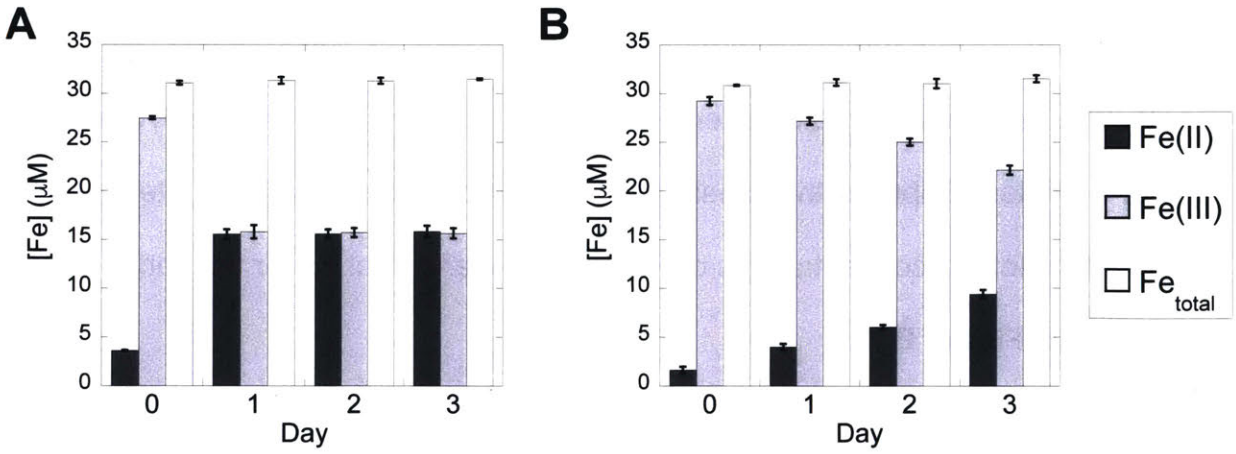

Figure B.7. Bar plots showing the concentrations of Fe(II), Fe(III), and total Fe in solutions containing mCP (**A**) and hCP-Ser (**B**) quantified on days 0-3 using the Fe speciation assay (average ± SDM, n = 3).

B.4. Notes

1. Both human and murine CP coordinate transition metal ions with high affinity. Thus, precautions must be taken to reduce metal contamination when working with these proteins and to ensure the apo heterodimers are obtained from the purification. Because calcium ions affect the quaternary structure and transition metal affinities of CP, precautions must be taken to avoid calcium contaminations during the preparation of the apo heterodimer. After column purification, the protein is dialyzed in buffer containing Chelex resin to limit metal ion contamination. Additionally, for solution studies such as the Fe speciation assay, high purity reagents are employed and precautions are taken to avoid metal ion contamination. These precautions include the use of plastic spatulas to transfer reagents, the exclusive use of Milli-Q water, and the use of acid-washed glassware for the preparation of buffer and metal ion solutions. Because metal ions can leach from glassware, solutions are transferred to polypropylene containers for long-term storage.
2. Anhydrous $FeCl_3$ is purchased in an ampule and is hygroscopic. Upon opening the ampule, the powder should be weighed and the stock solution prepared immediately.
3. If the protein contains one or more cysteine residues, 5 mM DTT is included in all buffers used for protein purification.[12, 13, 21] This modification is employed for purifying hCP, which contains two cysteine residues, as well as variants of mCP, and should be applicable for variants that have cysteine residues incorporated at non-native positions by site-directed mutagenesis. It is important to determine

whether DTT in the storage buffer must be removed prior to an experiment. Note that DTT can affect the redox speciation of metal ions like Fe and Cu.

4. DTT is not infinitely stable and thus buffer containing DTT should not be stored for extended periods of time. We recommend storing buffers without DTT and adding DTT powder to buffers immediately before use.
5. To set up the Fe speciation assay, proteins are buffer-exchanged into the Fe speciation assay buffer. Remember that mCP is stored in buffer that contains 5 mM DTT, and this reducing agent must be removed before setting up the Fe speciation assay.
6. We strongly recommend that the TCA, ammonium acetate, and sodium ascorbate reagents used in the ferrozine assay are prepared immediately before use. Ferrozine solutions can be stored at -80 °C and thawed daily for use in the assay.
7. We strongly recommend using high purity reagents for the iron speciation assay, including trace metals basis HCl solution, to avoid metal contamination. In particular, we have found that use of lower purity HCl compromises the Fe speciation assay.
8. We recommend using at least 30 μM total Fe concentration in the assay. This concentration will provide absorbance values > 0.1 a.u. when measuring the total iron content of the solution with a 1-cm pathlength cuvette.

B.5 Acknowledgments

Our current studies of calprotectin are supported by the National Science Foundation (CHE-1352132) and the National Institutes of Health (R01GM118695 and R01GM126376).

B.6 References

1. Zygiel, E. M.; Nolan, E. M. Transition metal sequestration by host-defense protein calprotectin. *Ann. Rev. Biochem.* **2018,** *87*, 621-643.

2. Hood, M. I.; Skaar, E. P. Nutritional immunity: transition metals at the pathogen-host interface. *Nat. Rev. Microbiol.* **2012,** *10*, 525-537.

3. Clark, H. L.; Jhingran, A.; Sun, Y.; Vareechon, C.; de Jesus Carrion, S.; Skaar, E. P.; Chazin, W. J.; Calera, J. A.; Hohl, T. M.; Pearlman, E. Zinc and manganese chelation by neutrophil S100A8/A9 (calprotectin) limits extracellular *Aspergillus fumigatus* hyphal growth and corneal infection. *J. Immunol.* **2016,** *196*, 336-344.

4. De Jong, H. K.; Achouiti, A.; Koh, G. C.; Parry, C. M.; Baker, S.; Faiz, M. A.; van Dissel, J. T.; Vollaard, A. M.; van Leeuwen, E. M.; Roelofs, J. J.; de Vos, A. F.; Roth, J.; van der Poll, T.; Vogl, T.; Wiersinga, W. J. Expression and function of S100A8/A9 (calprotectin) in human typhoid fever and the murine *Salmonella* model. *PLoS Negl. Trop. Dis.* **2015,** *9*, e0003663.

5. Hood, M. I.; Mortensen, B. L.; Moore, J. L.; Zhang, Y.; Kehl-Fie, T. E.; Sugitani, N.; Chazin, W. J.; Caprioli, R. M.; Skaar, E. P. Identification of an *Acinetobacter baumannii* zinc acquisition system that facilitates resistance to calprotectin-mediated zinc sequestration. *PLoS Pathog.* **2012,** *8*, e1003068.

6. Liu, J. Z.; Jellbauer, S.; Poe, A. J.; Ton, V.; Pesciaroli, M.; Kehl-Fie, T. E.; Restrepo, N. A.; Hosking, M. P.; Edwards, R. A.; Battistoni, A.; Pasquali, P.; Lane, T. E.; Chazin, W. J.; Vogl, T.; Roth, J.; Skaar, E. P.; Raffatellu, M. Zinc sequestration by the neutrophil protein calprotectin enhances *Salmonella* growth in the inflamed gut. *Cell Host Microbe* **2012,** *11*, 227-239.

7. Wakeman, C. A.; Moore, J. L.; Noto, M. J.; Zhang, Y.; Singleton, M. D.; Prentice, B. M.; Gilston, B. A.; Doster, R. S.; Gaddy, J. A.; Chazin, W. J.; Caprioli, R. M.; Skaar, E. P. The innate immune protein calprotectin promotes *Pseudomonas aeruginosa* and *Staphylococcus aureus* interaction. *Nat. Commun.* **2016,** *7*, 11951.

8. Corbin, B. D.; Seeley, E. H.; Raab, A.; Feldmann, J.; Miller, M. R.; Torres, V. J.; Anderson, K. L.; Dattilo, B. M.; Dunman, P. M.; Gerads, R.; Caprioli, R. M.; Nacken, W.; Chazin, W. J.; Skaar, E. P. Metal chelation and inhibition of bacterial growth in tissue abscesses. *Science* **2008,** *319*, 962-965.

9. Hobbs, J. A. R.; May, R.; Tanousis, K.; McNeill, E.; Mathies, M.; Gebhardt, C.; Henderson, R.; Robinson, M. J.; Hogg, N. Myeloid cell function in MRP-14 (S100A9) null mice. *Mol. Cell. Biol.* **2003,** *23*, 2564-2576.

10. Hunter, M. J.; Chazin, W. J. High level expression and dimer characterization of the S100 EF-hand proteins, migration inhibitory factor-related proteins 8 and 14. *J. Biol. Chem.* **1998,** *273*, 12427-12435.

11. Korndörfer, I. P.; Brueckner, F.; Skerra, A. The crystal structure of the human $(S100A8/S100A9)_2$ heterotetramer, calprotectin, illustrates how conformational changes of interacting α-helices can determine specific association of two EF-hand proteins. *J. Mol. Biol.* **2007,** *370*, 887-898.

12. Brophy, M. B.; Hayden, J. A.; Nolan, E. M. Calcium ion gradients modulate the zinc affinity and antibacterial activity of human calprotectin. *J. Am. Chem. Soc.* **2012,** *134*, 18089-18100.

13. Brophy, M. B.; Nakashige, T. G.; Gaillard, A.; Nolan, E. M. Contributions of the S100A9 C-terminal tail to high-affinity Mn(II) chelation by the host-defense protein human calprotectin. *J. Am. Chem. Soc.* **2013,** *135*, 17804-17817.

14. Damo, S. M.; Kehl-Fie, T. E.; Sugitani, N.; Holt, M. E.; Rathi, S.; Murphy, W. J.; Zhang, Y.; Betz, C.; Hench, L.; Fritz, G.; Skaar, E. P.; Chazin, W. J. Molecular basis for manganese sequestration by calprotectin and roles in the innate immune response to invading bacterial pathogens. *Proc. Natl. Acad. Sci.* **2013,** *110*, 3841-3846.

15. Gagnon, D. M.; Brophy, M. B.; Bowman, S. E.; Stich, T. A.; Drennan, C. L.; Britt, R. D.; Nolan, E. M. Manganese binding properties of human calprotectin under conditions of high and low calcium: X-ray crystallographic and advanced electron paramagnetic resonance spectroscopic analysis. *J. Am. Chem. Soc.* **2015,** *137*, 3004-3016.

16. Hayden, J. A.; Brophy, M. B.; Cunden, L. S.; Nolan, E. M. High-affinity manganese coordination by human calprotectin is calcium-dependent and requires the histidine-rich site formed at the dimer interface. *J. Am. Chem. Soc.* **2013,** *135*, 775-787.

17. Nakashige, T. G.; Stephan, J. R.; Cunden, L. S.; Brophy, M. B.; Wommack, A. J.; Keegan, B. C.; Shearer, J. M.; Nolan, E. M. The hexahistidine motif of host-defense protein human calprotectin contributes to zinc withholding and its functional versatility. *J. Am. Chem. Soc.* **2016,** *138*, 12243-12251.

18. Nakashige, T. G.; Nolan, E. M. Human calprotectin affects the redox speciation of iron. *Metallomics* **2017,** *9*, 1086-1095.

19. Nakashige, T. G.; Zhang, B.; Krebs, C.; Nolan, E. M. Human calprotectin is an iron-sequestering host-defense protein. *Nat. Chem. Biol.* **2015,** *11*, 765-771.

20. Nakashige, T. G.; Zygiel, E. M.; Drennan, C. L.; Nolan, E. M. Nickel sequestration by the host-defense protein human calprotectin. *J. Am. Chem. Soc.* **2017,** *139*, 8828-8836.

21. Hadley, R. C.; Gu, Y.; Nolan, E. M. Initial Biochemical and Functional Evaluation of Murine Calprotectin Reveals Ca(II)-Dependence and Its Ability to Chelate Multiple Nutrient Transition Metal Ions. *Biochemistry* **2018,** *57*, 2846-2856.

22. Vogl, T.; Roth, J.; Sorg, C.; Hillenkamp, F.; Strupat, K. Calcium-induced noncovalently linked tetramers of MRP8 and MRP14 detected by ultraviolet matrix-assisted laser desorption/ionization mass spectrometry. *J. Am. Soc. Mass Spectrom.* **1999,** *10*, 1124-1130.

23. Strupat, K.; Rogniaux, H.; Van Dorsselaer, A.; Roth, J.; Vogl, T. Calcium-induced noncovalently linked tetramers of MRP8 and MRP14 are confirmed by electrospray ionization-mass analysis. *J. Am. Soc. Mass Spectrom.* **2000,** *11*, 780-788.

24. Gifford, J. L.; Walsh, M. P.; Vogel, H. J. Structures and metal-ion-binding properties of the Ca^{2+}-binding helix-loop-helix EF-hand motifs. *Biochem. J.* **2007,** *405*, 199-221.

25. Kehl-Fie, T. E.; Chitayat, S.; Hood, M. I.; Damo, S.; Restrepo, N.; Garcia, C.; Munro, K. A.; Chazin, W. J.; Skaar, E. P. Nutrient metal sequestration by calprotectin inhibits bacterial superoxide defense, enhancing neutrophil killing of *Staphylococcus aureus*. *Cell Host Microbe.* **2011,** *10*, 158-164.

26. Stephan, J. R.; Nolan, E. M. Calcium-induced tetramerization and zinc chelation shield human calprotectin from degradation by host and bacterial extracellular proteases. *Chem. Sci.* **2016,** *7*, 1962-1975.

27. Stookey, L. L. Ferrozine- A New Spectrophotometric Reagent for Iron. *Anal. Chem.* **1970,** *42*, 779-781.

28. Carter, P. Spectrophotometric Determination of Serum Iron at the Submicrogram Level with a New Reagent (Ferrozine). *Anal. Biochem. 40*, 450-458.

Biographical Note

Rose C. Hadley was raised in New Boston, New Hampshire by parents Shirley M. F. Hadley and Harlan L. Hadley. She attended Goffstown Area High School followed by the University of New Hampshire, Durham where she earned B.S. degrees is Chemistry and Neuroscience. While an undergraduate student, she performed research in the labs of Professor Roy P. Planalp and Professor Rick H. Cote studying the metal-dependent properties of phosphodiesterases. Rose then enrolled in the Chemistry Ph.D. program at the Massachusetts Institute of Technology in 2014, where she worked in the lab of Professor Elizabeth M. Nolan and studied the biochemical and Mn(II)-binding properties of murine calprotectin as well as the competition for Mn(II) between calprotectin and the Mn(II)-transporting solute-binding proteins MntC (*Staphylococcus aureus*) and PsaA (*Streptococcus pneumoniae*). Following graduation, she plans to pursue post-doctoral studies in the lab of Professor Amy C. Rosenzweig at Northwestern University.

Rose C. Hadley

Education

Ph.D. Chemistry — Massachusetts Institute of Technology
2014-2019 — Advisor: Professor Elizabeth M. Nolan

B.S. Chemistry — University of New Hampshire
B.S. Neuroscience — Advisor: Professor Roy P. Planalp
2010-2014

Publications

1. Gagnon, D. M.; Hadley, R. C.; Ozarowski, A.; Nolan, E. M.; Britt, R. D. High–field EPR spectroscopic characterization of Mn(II) bound to the bacterial solute-binding proteins MntC and PsaA. **2019**, *Submitted*.

2. Hadley, R. C.; Gagnon, D. M.; Ozarowski, A.; Britt, R. D.; Nolan. E. M. Murine calprotectin coordinates Mn(II) at a hexahistidine site with Ca(II)-dependent affinity. *Inorg. Chem.* **2019**, *Just Accepted*.

3. Hadley, R. C.; Nolan, E. M. Preparation and iron redox speciation study of the Fe(II)-binding antimicrobial protein calprotectin. *Meth. Mol. Biol.* **2019**, 1929, 397-415.

4. Hadley, R. C.; Gu, Y.; Nolan, E. M. Initial biochemical and functional evaluation of murine calprotectin reveals Ca(II)-dependence and its ability to chelate multiple nutrient transition metal ions. *Biochemistry* **2018**, 57, 2846–2856.

5. Hadley, R. C.; Gagnon, D. M.; Brophy, M. B.; Gu, Y.; Nakashige, T. G.; Britt, R. D.; Nolan, E. M. Biochemical and spectroscopic observation of Mn(II) sequestration from bacterial Mn(II) transport machinery by calprotectin. *J. Am. Chem. Soc.* **2018**, 140, 110–113.

6. Neumann, W.; Hadley, R. C.; Nolan, E. M. Transition metals at the host–pathogen interface: how Neisseria exploit human metalloproteins for acquiring iron and zinc. *Essays Biochem.* **2017**, 61, 211-223.